Anilox Cell Geometries For Printable Electronics and Flexible Packaging

By
Sakulrat Foulston

Submitted to the Swansea University in fulfilment of the requirements for the Degree of Engineering Doctorate

Swansea University
2020

Abstract

Flexography is a major high-volume printing process used extensively for flexible packaging. The heart of flexographic press is the anilox roll, which meters the flow of ink to the image carrier (plate) by virtue of the engraved cells on the surface. The anilox was original engraved mechanically using a stylus to peck at the surface. This limited the size and profile of the engraved cells. However, laser engraving has enabled much more control with a variety of shapes and aspect ratios. Much has been claimed by the manufacturers for these new designs – improved ink transfer, higher volumes of ink transfer and better half tone reproduction – on the basis of industrial field trials. The objective of the research reported in this thesis has been to quantify the ink release from the anilox to the plate for both traditional cell profiles and the open channel designs.

Previously, the ink release was mostly determined by examining the optical density of the print products. The optical density is a qualitative indicator of the ink release from anilox cells. These studies were limited to closed anilox cells with a low ink viscosity, as typically used for graphic prints. This study explores an extended range of anilox cell shapes, including open channel geometries, and the ink viscosities. The ink released from the anilox cells has been be directly measuring and quantified.

Experiments were performed printing directly to glass and on flexible packaging at a commercial printers to establish the current industry position. A laboratory scale printability tester was then used to study ink release using three inks: UV Cyan, Carbon and Silver. These represented a link to the graphic experiments in previous published studies, while the Carbon and Silver were highly viscoelastic functional inks used in printed electronics. Four cell geometries were used: laser engraved closed cells, extended hexagonal and wavy channels together with mechanically engraved conventional closed pyramid cells. The laser engraved anilox afforded the opportunity to vary key parameters of cell width, depth, profile and volume. A brief exploration of print speed was also undertaken with exemplar anilox of each cell type. The main study considered ink transfer to a 100% solid plate, as this would allow the ink release to be studied without influence of the plate distorting into the cells thereby extracting more ink. A limited study was then undertaken with a half tone plate to establish the impacted on ink transfer.

The amount of ink transferred was highly dependent on the absolute volume of cells, i.e. the amount of ink available on the anilox. The anilox cells with wider, shallower and smaller depth-to-width ratio released a higher proportion of the ink. The ink's physical characteristics of viscoelasticity and extensional

viscosity also determine the proportion of ink transferred.

The anilox hexagonal closed cells (typically used in the flexographic printing process) performed best with the low viscosity ink. The information gaining from this study would aid in the design of anilox cell geometries and development of ink characteristics to enhance its capability for functional print applications such as printable electronics.

The anilox wavy channels released the greatest proportion of the ink with high viscosity, elastic modulus, and filament breakup time. The anilox wavy channel has the potential to be used for the functional print as it increased the release of paste-like ink. Additionally, it improved the ink lay-down. The anilox engraving technique affected the ink release. The anilox cells, which were engraved by the laser technique, gave greater ink release comparing to the anilox cells, which were engraved by the mechanically engraving technique. The increase of the dot coverage increased the ink release out of the anilox cells because of the increase of the receiving area. However, the increase of the ink release plateaued after the dot coverage of 50% for UV Silver because of its large filament breakup time.

The characteristics of ink influenced the ink release out of the anilox cells. Unlike previous work which examined only the ink viscosity, this studied included ink elastic modulus and filament breakup. The ink with high viscosity and elastic modulus, but small filament breakup time gave greatest ink release for all anilox shapes.

When the printing speed increased, it decreased the ink release due to two factors; reduction of engagement time between the anilox cells and the plate (reducing time for ink to transfer) and enlargement of the filament extension rate (reducing the amount of ink transfer). The decrease of ink release was affected by the ink characteristics and the anilox cells shapes. The decrease of ink release was significant when UV Cyan ink (small viscosity and elastic modulus) was used with the anilox open cells and wavy channels. Contrarily, the decrease of ink release was insignificant when UV Carbon and Silver inks (large viscosity and elastic modulus) was used with the anilox open cells and wavy channels.

The experimental data was analysed and the critical parameters in releasing the ink of the anilox cells were identified. The depth of anilox cell was the most critical parameter; the shallower cell depth released a higher proportion of the ink. The ratio of depth-to-width was the second most important parameter in determining the ink release. The smaller depth-to-width ratio released more ink. The width of anilox cell could not be used as a parameter predicting the ink

release because the wider anilox cell did not always release the higher proportion of the ink.

Declarations

I declare this work has not previously been accepted in substance for any degree and is not being concurrently submitted in candidature for any degree.

Signed.....(Candidate)

Date.....13th August, 2020.....

I declared that this thesis is the result of my own investigations, except where otherwise stated. Other sources are acknowledged by footnotes giving explicit references. A bibliography is appended.

Signed.....(Candidate)

Date.....13th August, 2020.....

I hereby give consent for my thesis, if accepted, to be available for photocopying and for inter-library loan, and for the title and summary to be made available to outside organisations.

Signed.....(Candidate)

Date.....13th August, 2020.....

Acknowledgement

Firstly, I would like to thank my heavenly Father and my Lord and Saviour Christ Jesus, who is being good and faithful to me.

Secondly, I would like to thank Professor Tim Claypole and Professor David Gethin for giving me the opportunity to study and work for this project. I would like to thank them for the guidance, advice and all the support given to me throughout my studies. I would like to thank everyone at Welsh Centre of Printing and Coating (WCPC). I would like to give special thanks to Dr David Beynon, who has trained, taught, and supported me everything I needed to complete the studies. Mrs Christine Hammett, who has been taking care of me and everyone of us at the office; I am very grateful for her kindness. I am thankful for Dr Davide Deganello, Dr Christopher Phillip, Dr Simon and Dr Anya Hamblyn, Dr Zari Tehrani, Dr Tatyana Korochkina, Dr Ben Clifford, Dr Tim Mortensen, Dr Tamara Tomašegović, Dr Matthew Everett, Dr Miles Morgan, Dr David Shaw, Dr Youmna Mouhamad, Mr Glyn Davies, Dr John Lau, and the rest at WCPC for their help, support and friendship.

Thirdly, I would like to thank M2A team, especially Mrs. Rebecca White who has been kind helping and sorting out things for us tirelessly throughout the years.

Finally, I would like to thank my families and friends for all the support and encouragement.

This work is part-funded by the European Social Fund (ESF) through the European Union's Convergence programme administered by the Welsh Government and International Centre for Manufacture by Print (icmPrint). I would like to thank the organizations, without them it would not be possible.

Contents

List of Figures

List of Tables

Abbrevations

A/ B	Constants of the fluids
ANN	Artificial Neural Network approach
BCM	Billion Cubic Micrometre
CFD	Computational Fluid Dynamic
CI	Central Impression
CP	Cone Plate
cPs	Centipoise
^{O}C	Degree Celcius
D	Dimension
D	Deformed Diameter
D0	Original Diameter
DI	DeIonized
Ds	Optical Density of the substrate
Dsa	Optical Density of the solid print
Dt	Optical Density of the halftone
F	Force
HD	High Definition
HDI	High Definition Ink
HDP	High Definition Plate
LED	Light Emitting Diode
LPCM	Line Per Centimetre
LPI	Line Per Inch
OPP	Orientated PolyPropylene
PS	Print Speed
SD	Standard flexo process
SDI	Standard Ink
SDP	Standard Plate
T	The absolute temperature
UV	UltraViolet
VOF	Volume of Fluid
XSA	Channel Anilox Roll
θ	Contact Angle
α	Contact Angle
ηE	Extensional viscosity
γ^{lv}	Liquid/Surface free energy
μm	Micrometre
Υ	Shear rate
η	Shear viscosity
γ^{sl}	Solid/Liquid interfacial free energy
γ^{sv}	Solid/Surface free energy
δ	Surface tension

Chapter 1

Introduction

1.1 Introduction

Printing is a high volume, precision manufacturing process capable of accurately, selectively covering and curing as many as 15 ink layers up to speeds of 600m/minute. Printing has had to adopt new materials and technologies to improve economic performance and meet the increasingly strict environmental legislation. Flexographic printing is primarily used for flexible packaging which was 43% overall printing market in 2016. Flexographic printing packaging sector generated approximately $150 billion in 2015. The total revenue of global packaging was approximately $840 billion and is expected to grow at approximately 3.5% per year through to 2020 and revenue to approach of $1 trillion per year [Flexographic Technical Association, 2018].

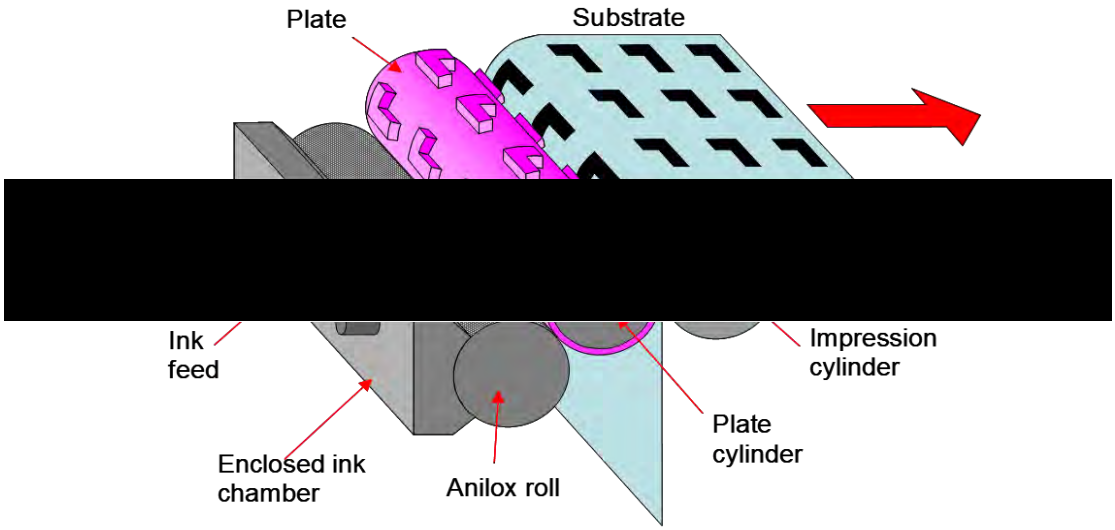

Figure 1.1: The main components of flexographic printing technique [Source: Simon Hamblyn]

In flexographic printing the image is carried on the raised areas of a digitally exposed photopolymer plate which transfers the inks selectively to the substrate (**Figure 1.1**). The anilox is an engraved cylinder at the heart of the process

that meters the transfer of ink to the surface of the plate. Advances in producing the anilox rolls, printing plate and ink has facilitated the current high print quality. Additionally, its ability to print at the high speed makes it possible for the printer to rapidly increase production when requires.

Flexography is more effective cost than other printing techniques for volume printing of packaging, such as gravure. The price of printing plate is lower than the gravure engraved roll. The print image can be changed quickly, as the time to make a flexo plate is far less than the time taken to engrave and chrome a gravure cylinder. This decreases the interruption of production and keeps production cost low. The flexographic printing process is also capable of printing continuous fine lines required for printed electronics and sensors.

At the heart of the flexographic printing process is the anilox, an engraved roll that meters the supply of ink through the system. Advances in laser engraving technology has enabled more flexibility in the shape of the cells, which has led to alternative geometries to the previous standard pyramid cell achieved with mechanical engraving. These new geometries are claimed by the suppliers to improve the print process by increasing the ink transferred. However, there is little scientific evidence to support these claims. The focus of this research has been to understand the effect of these new anilox cell geometries on ink release from the cell and hence determine the actual metering capacity of the cylinder. It also considers the interaction with inks, including the more structured inks used for printed electronics, and process parameters such as speed, as these will have a direct impact on the deposited ink film thickness. The ink film thickness affects the quality of the graphic images on the packaging, or the functional attributes, for example the conductivity, in the case of printed functional devices, such as electronics.

1.2 Flexography Printing Process

Main components of the flexo process are composed of the ink supply unit, the anilox roll, the printing plate and the impression roll (**Figure 1.1**). The enclosed chambered doctor blade system is commonly used in the ink supply unit as it reduces solvent evaporation compared with open tray systems reducing the variation in viscosity. The viscosity of ink can be more easily maintained during the printing process by the addition of solvent.

The anilox engraved cells receives the ink within the chamber and meters the supply of ink based upon their specified cell volume. The excess ink is wiped off by the doctor blade. The ink is then transferred to the printing plate and finally reaches the substrate, which is supported by the impression cylinder.

The ink is metered onto the flexographic plate by the anilox roll. The amount of ink available is determined by the volume of the anilox cells per unit area. The doctor blade ensures the ink is only carried forward in the engraving. The flexographic plate engages with anilox, distorting into the cell to collect the ink. (**Figure 1.2**). As the press rotates the plate is pulled away from the anilox, drawing the ink out of the cells. This process includes internal flow within the cells, which will be impacted by the cell geometry as well as the volume. It also will be influenced by the plate, both its elastic properties and the image, as smaller features will not be as effectively supported as large solid areas in bridging the cells and in some cases small features will dip directly into the cells. The ink is also subject to extension during the separation and visco elastic flow within the cell geometry. The plate continues to rotate and engages with the substrate to transfer the image.

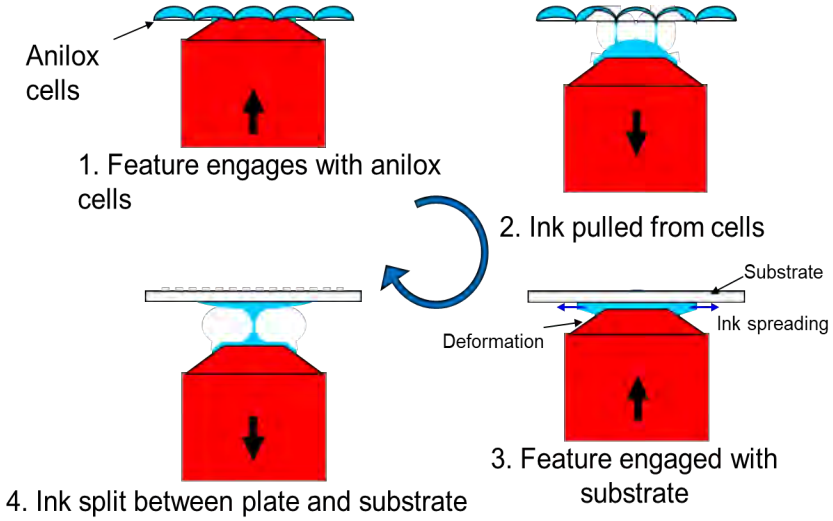

Figure 1.2: Schematic of the ink transfer in flexographic printing process

To achieve the desired print quality, it is important to select the right combination of anilox roll, printing plate and ink. These interact with the process parameters including image, speed, engagement pressures and substrate type. The general practice in the printing industry to select these based on experience and fingerprinting trials. These three components are considered in more detail in the next sections.

1.2.1 Anilox Roll

The anilox surface is engraved to create the cells to meter the ink supply (**Figure 1.3**). Each anilox roll is specified in terms of cell volume per surface area of the anilox where the amount of ink is determined by the engraved geometry. The cell volume is constrained by the numbers of anilox cells per inch, cell width, cell depth and cell shape. The advance in laser engraving technology has improved the precision of cell volume and has provided the

opportunity to engrave different cell geometry. The anilox roll is considered to be at the heart of the flexographic printing process because of its attribute of carrying the ink, which determines the ink film thickness and influences the print quality.

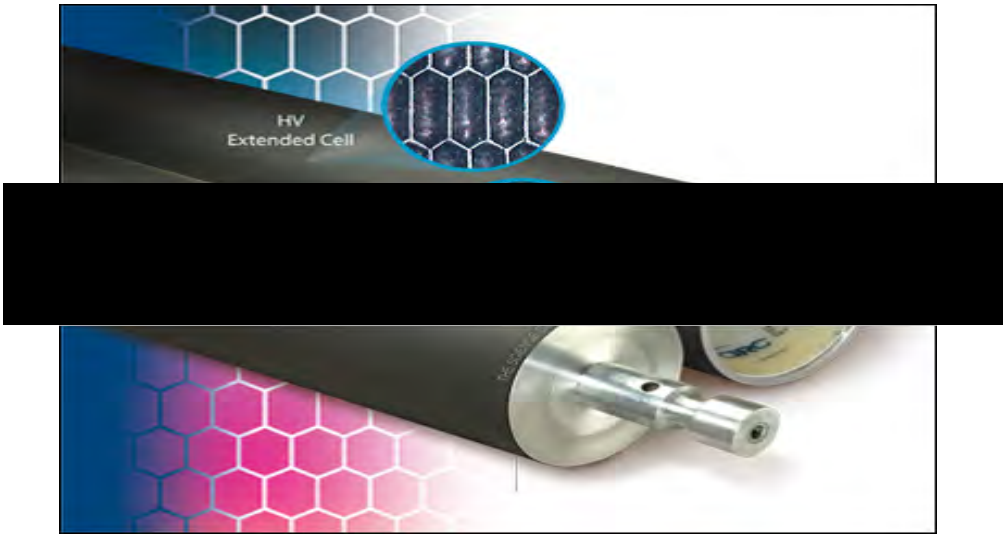

Figure 1.3: The anilox engraved cells [Correct-Touch Graphic Arts, 2017]

1.2.2 Anilox Cell Parameters

Anilox cell geometry is generally defined by cell volume, screen count (or line count), shapes, depth, and width or opening (**Figure 1.4**).

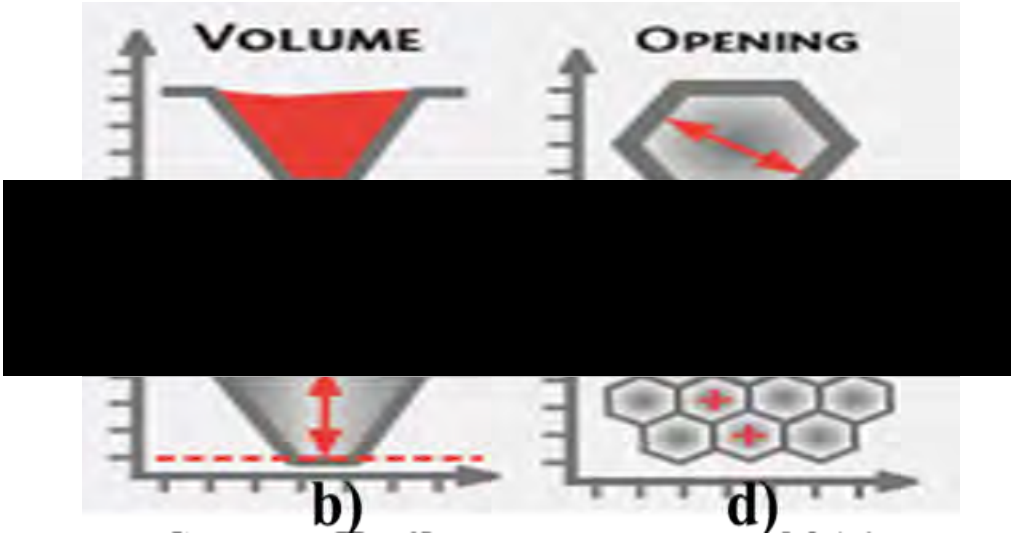

Figure 1.4: Anilox cell parameters [source: troika-systems.com, 2014]

The cell volume determines the capacity of the anilox cells to receive the ink from the ink chamber. The anilox cell volume is constrained by its screen count,

cell shape, cell opening, and cell depth. The higher the anilox cell volume, the more ink it can receive from the ink chamber.

The anilox cell depth is measured from the top to the bottom of the cell (**Figure 1.4b**). When the other parameters are kept constant, the deeper cells increase the anilox cell volume.

The cell opening or width is defined by the length across the top opening of the cell (**Figure 1.4c**). The anilox screen count is the number of anilox cells along the engraved angle per specify length (**Figure 1.4d**). Generally, it is defined in either line per inch (LPI) or line per centimetre (LPCM) unit. The higher the screen count number, the smaller the cell opening (width) become.

1.2.3 Anilox Engraving

The engraving technique influences the print quality because it forms the shape, which determines the ink volume and the ink release [Cherry, 2007]. Anilox rolls can be produced by three main engraving techniques: mechanically, electromechanical, and laser. The mechanically engraving used a mill, which has a male pattern (**Figure 1.5**), to generate the anilox cells.

Figure 1.5: Mechanically engraving mill [Source: apex-groupofcompanies.com, 2018]

The electromechanically engraved technique uses a diamond shaped tip for engraving (**Figure 1.6**). The anilox cell shape obtained using this technique is the pyramid shape with either a pointed or flat bottom.

Figure 1.6: Electromechanically engraving [source: pamarco.com, 2018]

The quadratic channel (QCH) has a cell shape with the cell angle of 90^o and a channel connects to its neighbouring cells (**Figure 1.7**). This geometry is claimed to allow the ink to smoothly flow and improve the ink laydown [Pamarco.com, 2015].

Figure 1.7: The quadratic channel shape

The laser technology is also used to engrave anilox cells. The Carbon dioxide (CO_2) laser was introduced after 1980 followed by the Yttrium Aluminium Garnet (YAG). The latest engraving laser is based on fibre optic technology.

The early development of the CO_2 laser had the energy of 400-800 Watts. It used a single pulse to engrave an anilox cell. It could engrave less than 500LPI with limited volume capacity. Later, when the energy was increased to 1,000 Watts and coupled with the split beam technology; the range of cell volume was increased because of the increase of cell depth. The engraving speed was also increased substantially to approximately 10,000-15,000 cells/second. The Ablative YAG laser imparts low thermal energy and initially the anilox screen

count could be engraved up to 1,000LPI.

The evolution of anilox cell shape using different types of lasers can be seen in **Figure 1.8**. The anilox cells produced by CO_2 laser generated more residual or recast than Multi hit YAG laser because CO_2 laser used more power but fewer pulses. This made the anilox cells produced by CO_2 laser narrower. The anilox cells produced by the YAG laser generated smoother cells and less surface roughness. Additionally, its low thermal energy could widen the anilox cells as the YAG laser technology [Flexoexchange.com, 2014].

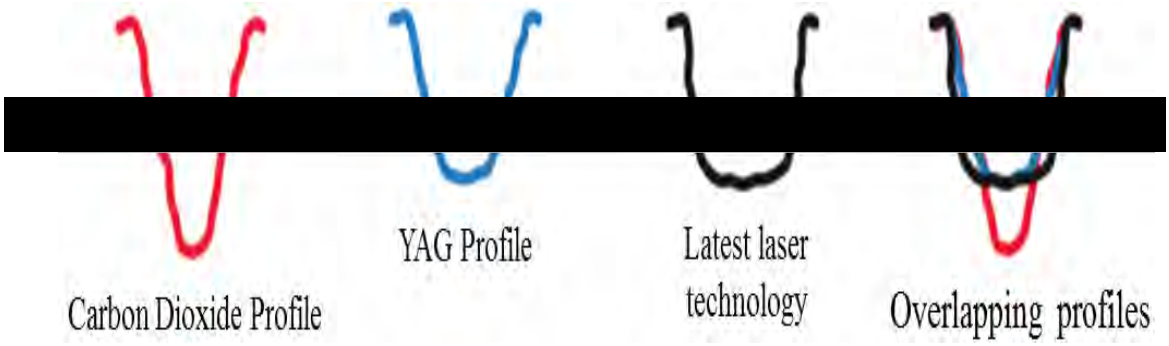

Figure 1.8: Comparison of cell shape profiles of laser technology [Harperimage.com, 2014]

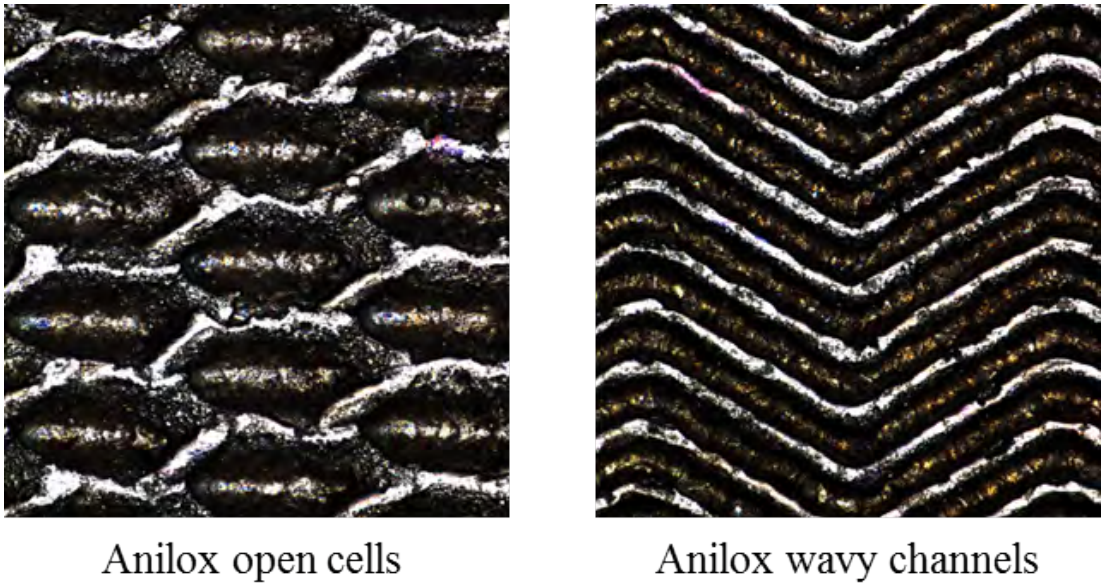

Figure 1.9: The example of the anilox open cells and wavy channel engraving

Thermal fibre optic YAG laser increased the screen count up to over 1,800LPIat up to 60,000 cells per second [Pamarco, 2015]. It enabled cells with steeper sides and increased depth, providing the opportunity to explore cell shape. Laser technology offers more choices for the anilox cell geometries. Additional to the

conventional hexagonal closed cells, the open-cell (where the height of the wall reduced and the boundary was open to the neighbouring cell) or channelled engraved cells (the wall completely removed) to be produced. The example of the anilox open cells and wavy channel engraving is shown in **Figure 1.9**. These new developments of anilox cell geometries are recommended by the manufacturers to increase the ink flow [Harperimage.com, 2014], however there is no scientific evidence to support this claim. The effect of anilox cell shapes on ink release is examined in chapter 5, 6 and 7.

1.2.4 Printing Plate

The printing plate carries the image to be printed. The image is formed as a relief by exposing a photopolymer material to the UV light and the printed image is raised above the non-printed area (**Figure 1.10**). The printing plate receives the ink from the anilox cells, and then transfers the image to the substrate. The images can be solid area or tonal patches of dot area covering a range from 0.5 to 100%. There are four main parameters critical to the plate: thickness or calliper, relief, floor or thickness of the photopolymer base layer, and hardness. The ratio of 40:60 is typically maintained for the plate relief and floor. [Scrimgeour, 2017].

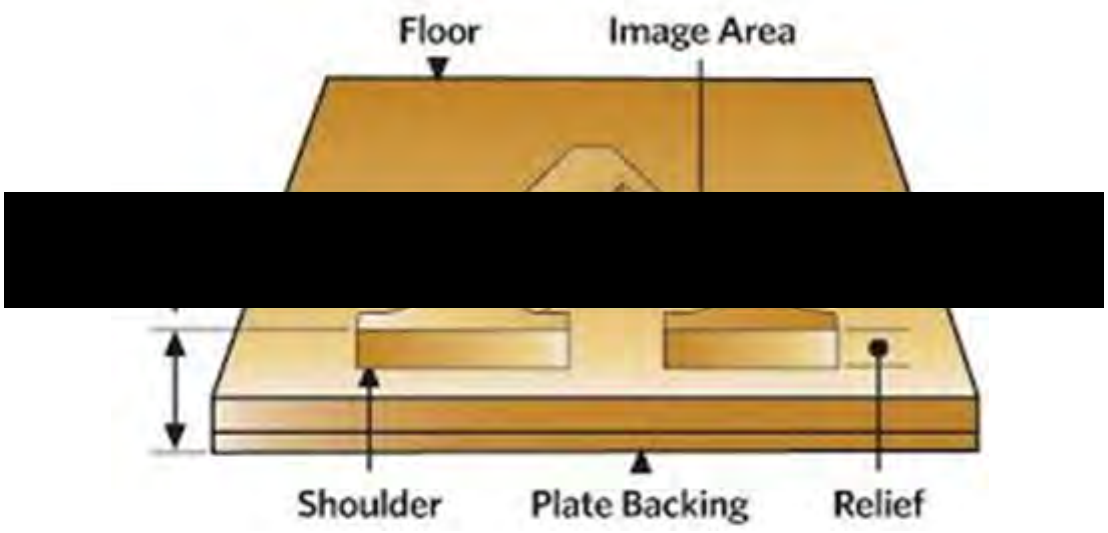

Figure 1.10: The Flexo printing plate [Source: packageprinting.com]

Tonal images are used in graphics printing where images are separated into tones to facilitate a colour rendition. Fine lines represent a 2 dimensional version of the half tone dot with related performance and are used extensively in functional printing, such as for RFID. The solid feature is used for the print of a mono colour or features to realise functional devices.

For the solid plate, the thickness and the hardness of the material are the main

attributes. However, for the tonal patch plate, the physical and optical dot sizes are of interest because the plate dot can be deformed when it engaged with the anilox cells during the printing process. The size of dot on the plate can influence the ink volume received from the anilox cells.

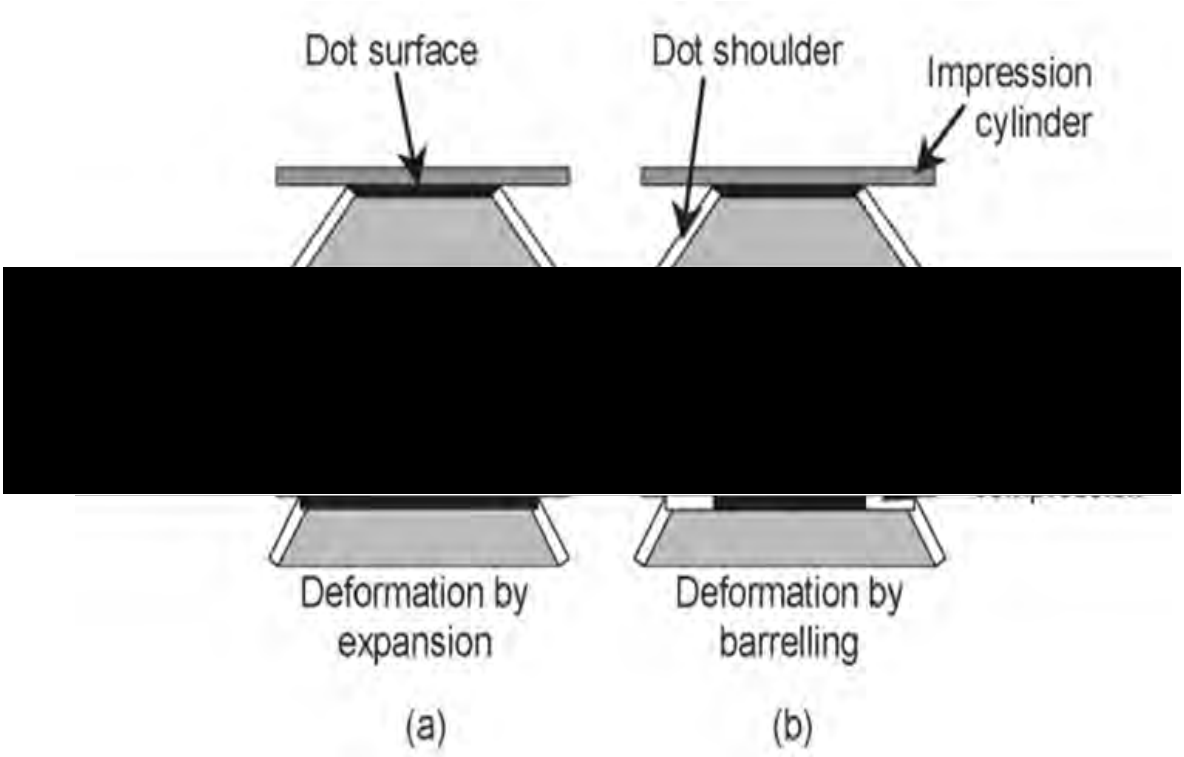

Figure 1.11: The effect of the barrelling an expanding to the plate dot [Bould, Claypole, and Bohan, 2004]

Bould (2001) investigated the effect of the plate thickness to the tone gain by increasing the plate thickness from 1.14mm to 1.70mm. There was only 0.6% decrease of tone gain. Therefore, only the physical and optical attributes of the plate were further examined. The thickness and hardness of the printing plate were kept constant throughout the investigations. The physical dot area coverage of the printing plate was measured using the white light interferometry or microscope. The physical dot area coverage of the printed substrate was measured using the same techniques. It can be larger than the physical dot area coverage of the printing plate, because when the printing plate is compressed and engaged with the impression roll, the printing plate is expanded and increases the size of the dot. Addition to the expansion of plate, the dot shoulder barrels under compression. When the dot contacts the substrate, the print shows as if the dot shoulder barrelling is a part of the dot surface printed on the substrate. This results in the printed dot is larger than the original size. The dot expansion and barrelling mechanisms are shown in **Figure 1.11** [Bould, Claypole and Bohan, 2004].

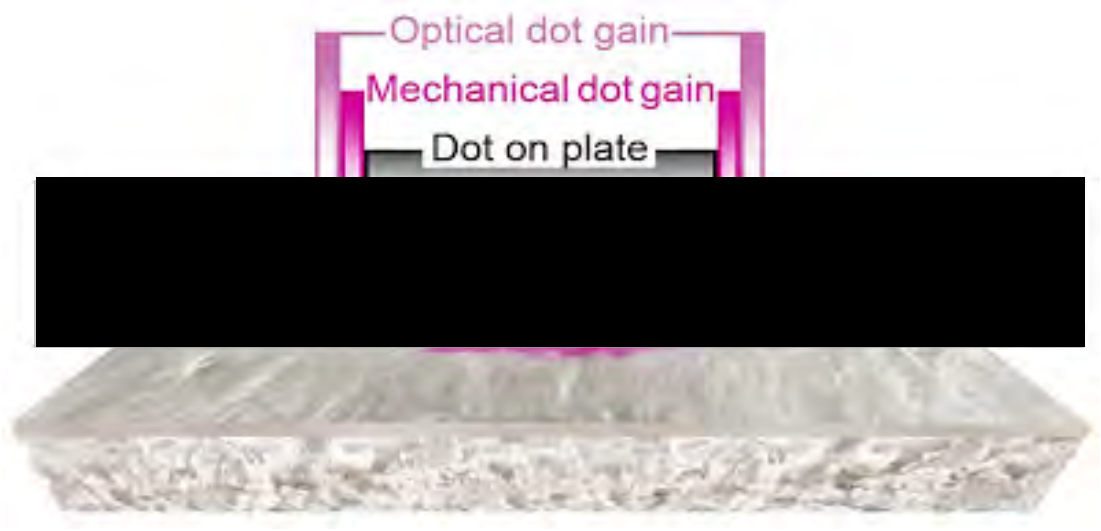

Figure 1.12: The optical dot gain [Pritchard, 2017]

Figure 1.12 shows the size of the dot on the plate, the mechanical and optical dot gain [Pritchard, 2017].

The difference between the physical dot area of the dot on the printing plate and the physical dot area of the dot on the printed substrate is called ***"the mechanical dot gain"***. The difference between the physical dot area and the optical dot area of the dot on the printed substrate is called ***"the optical dot gain"***. The optical dot area coverage is larger than the physical dot area coverage because the light which enters the substrate adjacent to the perimeter is scattered back under the dot, increasing the amount of light which is absorbed.

The greatest tone gain incurs in the mid-tone area because the effect of dot barrelling increases as the dot perimeter increases with the dot coverage, but after the mid-tone area the effect of dot barrelling decreases as the dot perimeter could not increase further after it reaches the neighbour dots, and additionally the dot expansion significantly decreases at higher coverages [Bould, 2001].

The light reflection or the thickness of the dot using the spectrophotometer is translated into ***"the optical density"***. The thicker the dot is, the greater the optical density. Therefore, the optical density is used as a parameter to compare the amount of the ink on the substrate. Additionally, the optical density is used to determine the optical dot area coverage by using the Murray-Davies equation as shown below [Lychock, 1995].

$$\frac{1 - 10^{\wedge -Dt}}{1 - 10^{\wedge -Ds}} \times 100$$

where: **Dt** is the **density** of the **tint** or halftone
Ds is the **density** of the **solid**

Note : **Dt** and **Ds** are **always** measured **minus paper**

Hamblyn (2004) investigated the effect of plate to the ink release from the anilox cells. The ink volume was assumed to be 50% released from the anilox cells. The printed dot volumes increased as the dot area coverage on the plate increased. However, in terms of the ink transfer ratio, the ratio of ink transferred volume to the plate was greater in the small dot size because the dot size was small and could enter the anilox cells. This made the small dots carried excess ink to the substrate [Hamblyn, 2004].

The printing plate can influence the print quality, however the focus of the investigations is on how the printing plate affects the extraction of the ink out of the anilox cells.

1.2.5 Inks

The ink is the final ingredient to achieve the desired print quality. The ink transfer depends on the wettability i.e. the ability of ink to adhere and spread out to the plate or substrate. The amount of ink transferred determines the ink film thickness, which relates to the desirable functions in the printable electronics, or the colour required in the image. The ink comprises four components; pigments, resins, solvents, and additives [nzic.org.nz, 2018]. There are three main types of the printing inks categorised by the carriers; water, solvents, and UV. Water based and solvent based inks rely on evaporation to cure, whereas the UV-based ink has to be exposed by UV light to cure and adhere to the substrates. As there is no evaporation the volume remains constant. Therefore, it is best suited for the ink transfer investigation because there is no need to compensate for solvent loss, i.e. the volume printed is the volume which was released from the anilox, transferred to the plate and then to the substrate.

1.2.5.1 Shear Viscosity

The ink shear viscosity is a main characteristic to determine whether the ink will flow during printing process. [Mai, Pekarovicova and Fleming, 2007]. Viscosity is the resistance of the liquid to flow. The shear viscosity of a Newtonian material is independent of the shear rate i.e. the change of the shear rate does not change the shear viscosity of Newtonian material. The viscosity of non-Newtonian material can significantly change with shear rate. When the shear viscosity decreases because of the shear rate increase, it is called "shear-thinning" behaviour of the material. When the shear viscosity increases because of the shear rate increase, it is called "shear-thickening" [Barnes, Hutton and Walters, 1989].

1.2.5.2 Viscoelasticity

The viscoelastic material shows both viscous (liquid-like) and elastic (solid-like) properties. The solid-like material displays the ability of the material to return to its initial state when the stress or force is removed as long as the stress does not exceed the elastic limit. Whilst, the liquid-like material starts deforming as soon as the stress is applied, and the deformation is permanent [Malvernpanalytical.com, 2019].

Generally, the viscoelastic of the ink is measured to determine its response to the shear stress: if it is solid-like or liquid-like over a range of shear stress. If it is liquid-like, the ink will flow at the small initial shear stress. If it is solid-like, the ink will flow at a greater shear stress. This will help the printer determining the printing setup. For example, if the ink is solid-like, the ink will be required to be shear during the filling ink process prior to printing on the substrate. The viscoelastic measurement will provide information on the elastic modulus of the ink which can be used to predict the filament breakup behaviour of the ink.

1.2.5.3 Extensional Viscosity

The extensional viscosity is the viscosity during the extensional flow i.e. the resistance of the liquid to extension flow. It is a function of the extensional strain rate as the shear viscosity is a function of shear rate. For Newtonian material, the ratio of the extensional viscosity to the shear viscosity is three times. The ratio is called "Trouton ratio" [Barnes, Hutton, Walters, 1989]. However, the ratio of the extensional viscosity to the shear viscosity of the non-Newtonian material is greater than Newtonian material due to its large strain hardening [Chellamuthu, 2010]. The extensional viscosity is of interest due to the formation of ink film filament during the printing process [Khandavalli and Rothstein, 2017]. Most of extensional viscosity studies are limited to the low viscous liquids of Newtonian and viscoelastic polymer materials. There is no study of extensional viscosity of the functional inks.

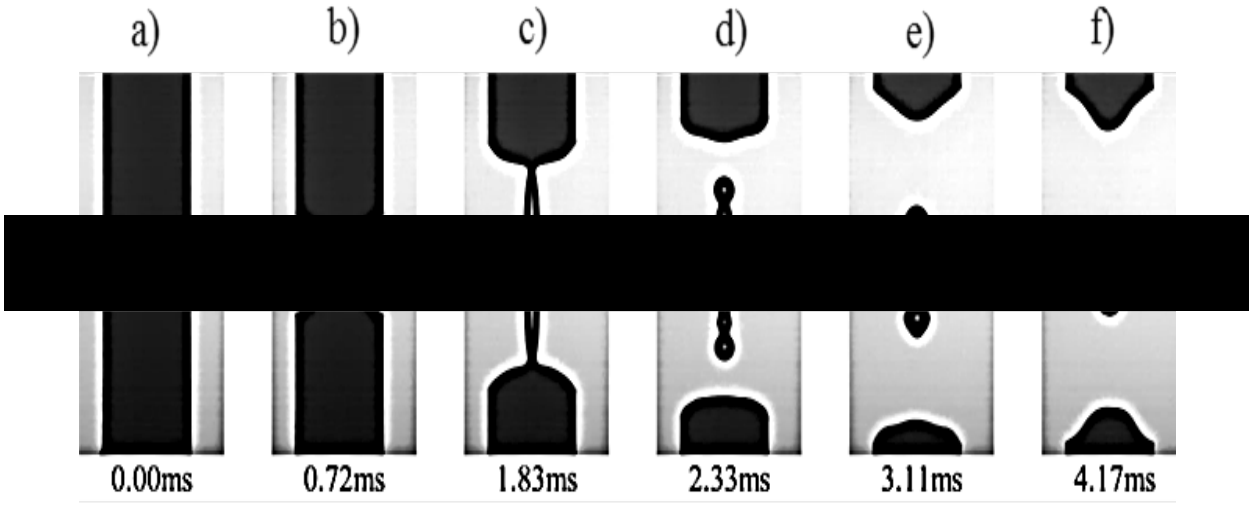

Figure 1.13: The filament breakup of a low viscosity Newtonian [Mackley et al., 2017]

Figure 1.13 shows the filament breakup of a low viscosity Newtonian Phosphate Buffer Solution (Dubelco's PBS) with a viscosity of 1.03 mPa. s with surface tension of 69.5 mN/m. At the initial deformation, the filament took form of a symmetric "wineglass" appearance (b). The filament breakup happened during the deformation as the piston moving (c). The "end pinching" of the liquid also occurred (d) [Mackley et al., 2017].

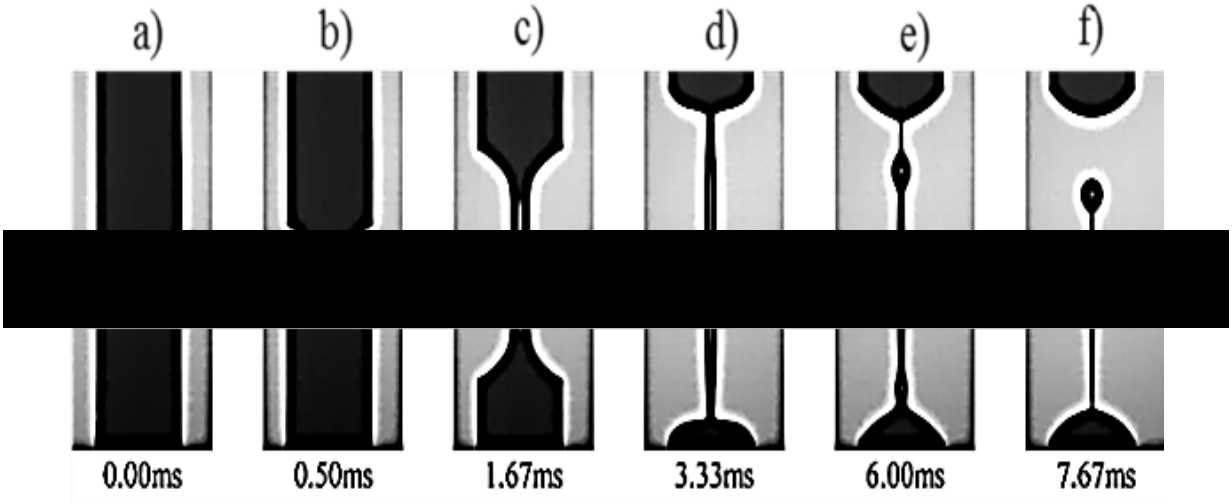

Figure 1.14: The filament breakup of low viscosity viscoelastic polymer solution [Mackley et al., 2017]

Figure 1.14 shows the filament breakup of low viscosity viscoelastic polymer solution of a 1% by weight solution of polystyrene (molecular weight of 110,000) in diethyl phthalate (which had viscosity of 15.3mPa.s and surface tension of 37mN/m). Similar to Newtonian filament breakup, at the initial deformation,

the filament took form of wine glass thinning process (b). However, the more stable and longer filament was formed (c-e), and the filament breakup occurred after the stop of the piston movement (f). Its end pinching was much less than the low viscosity Newtonian Phosphate Buffer Solution [Mackley et al., 2017].

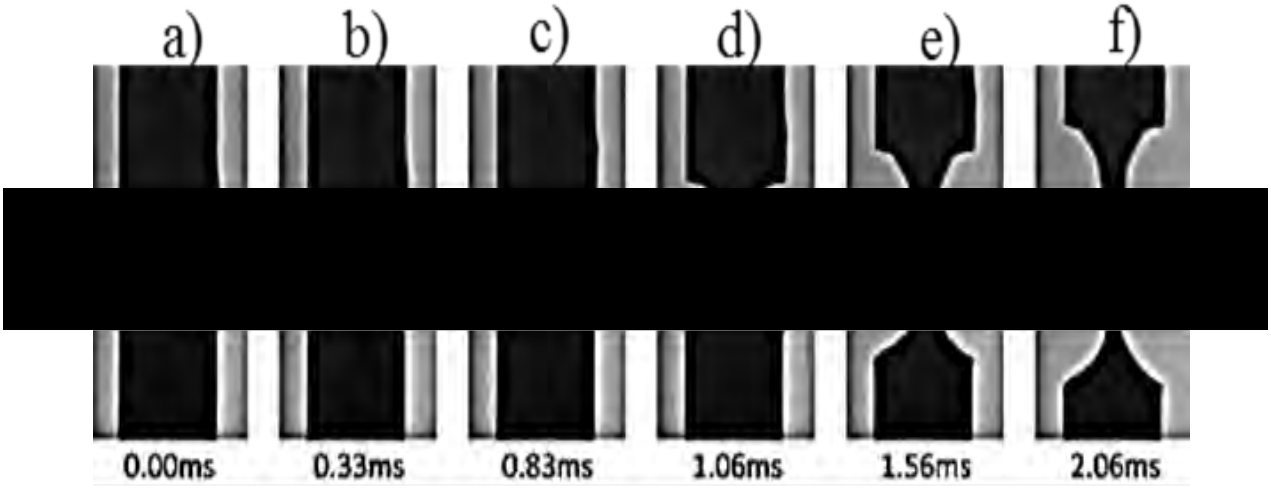

Figure 1.15: The filament breakup of yield stress material [Mackley et al., 2017]

Figure 1.15 shows the filament breakup of tomato ketchup. Similar to Newtonian filament breakup, at the initial deformation, the filament took form of wine glass thinning process (b). However, there was rapid thinning during stretching, then followed by necking (e), and eventually the "ductile fracture" occurred without end pinching (f). This filament breakup behaviour was different to Newtonian or viscoelastic polymer liquids. It was the filament breakup expected from a liquid with yield stress (tomato ketchup had an approximate yield stress of 20 Pa) [Mackley et al., 2017].

Comparing to the shear viscosity, the extensional viscosity greater magnitude than the shear viscosity because it requires more force to stretch the liquid [Sachdev, Muralidharan and Boukany, 2016].

The larger extensional viscosity indicates the longer filament; improving the pickout fraction. The pickout fraction of non-Newtonian liquid could increase by up to 71% comparing to the Newtonian liquid [Khandavalli and Rothstein, 2017].

The extensional viscosity of the ink could indicate the pickout fraction of the ink. However, the longer time for the ink filament to breakup could hinder the ink release. Besides the extensional viscosity, the filament breakup time of the ink is another indicator whether the pull-out ink would be split from the anilox

cells to the plate.

1.3 Aim and Objectives of the Research

Advances in laser engraving techniques has enabled the creation of anilox with cells of variable geometry and open continuous channel cell structures. Although there are many commercial claims for the improved ink release and volume of ink transferred, the manufacturers specifications are not directly comparable with traditional cell volumes or even with each other. The aim of the research was to study the effect of these latest anilox geometries on the ink release from the anilox cells to the plate. This required the accurate characterization and volumetric measurement of the cell patterns The interaction of the inks and print speed with the geometries was also studied. The ink was considered because it was directly involved in the ink release mechanism. Also, the inks required for functional printing such as for sensors and printed electronics, have more inherent viscoelastic structure which will impact on the ink release.

The project was in four phases:

1. Ink release onto a non-absorbent substrate (glass) with conventional anilox (Chapter 4)
2. Evaluation of the extended hexagonal and open channel anilox on a commercial printing press (Chapter 5)
3. Ink release from Closed and Open channel anilox rolls to a solid plate (Chapter 6)
4. Ink release to a half tones (Chapter 7)

Phase 1 was to evaluate ink release from conventional closed hexagonal cells with a UV flexo Black ink and the non-absorbent substrate on a sheet fed flexo press and compare with previous results as a precursor to trials on the commercial printing press. The effect of the anilox cell geometries on the ink release was investigated. "The ink release" refers to the ink release out of the anilox cells to the plate. Two anilox cell bands with the closed range of cell volume but different cell width and depth were evaluated. The features on the printing plate were the tonal patches of 1-100% dot area coverage, and the track width of 20-600um. The measured parameters were the optical density for the tonal patch prints, and the track ink volume and width for the track prints as these parameters could indicate the ink release of the anilox cells.

Phase 2 compared the ink release-using a tonal patch plate on a commercial flexographic central impression (CI) press from two anilox rolls with elongated

closed cells and wavy cells, for two inks with low and high viscosity, printed onto a PET substrate. The prints were only evaluated against anilox measurements and ink properties because of the commercial sensitivity of other press parameters. However, it was possible to make a comparison of print parameters including the physical dot area, the optical density of the tonal patch printed substrates, and the visual examination of the ink lay-down.

Phase 3 was an investigation using a laboratory flexographic printability tester. This replicated the ink transfer process and enabled a controlled study of ink viscosity and anilox geometry. The anilox rolls used with printability tester could be examined by a microscope to determine the ink volume before and after printing. A solid flexo plate was used to prevent the results being influenced by dot dipping and local distortion as commonly occurs with half tone printing. Three inks; UV Cyan, UV Conductive Carbon and UV Conductive Silver were printed onto a PET substrate at print speeds from 50m/min to 90m/min.

Three generic types of anilox engravings were compared:

- Closed anilox cells
- Open and wavy anilox cells
- Mechanically engraving quadratic channel anilox cells

Phase 4 builds on phase 3 but uses a half tone plate which would dip into the cells. This was to explore whether there was any benefits, particularly with the new open channel anilox for half tone printing. The same inks were used as in phase 3 with a selection of the aniloxes.

1.4 Thesis Layout

The literature on ink transfer reviewed in chapter 2 was used to inform the scope and methods of the research. Chapter 3 covers the methods and equipment used in the investigation. Chapter 4 presents the results from phase 1. an initial evaluation from conventional anilox cells onto a non-absorbent glass substrate to confirm some of the literature review. Chapter 5 presents phase 2, an industrial trial to examine the effect of anilox cell geometries on ink release. Chapter 6 and 7 are a study of ink release from hexagonal closed cell anilox geometry and open cell geometries with inks of different viscosity using a laboratory printability tester. Chapter 8 discusses the advances in understanding of ink release from anilox with the conclusion and future work.

Chapter 2

Literature Review of the Ink Transfer in Flexography

2.1 Introduction

Despite its growing market share, there is little peer reviewed literature on flexography. There has tended to be a focus on the ink transfer from the plate to the substrate, as this has been deemed critical to the final product, particularly for high value-added products based on functional materials. Therefore, there is not the depth of literature which one would encountered with processes such as ink jet and screen printing, where the development of both these printing processes is driven by industries desire to print functional materials as required for example by printed electronics and sensors.

The anilox has frequently been overlooked despite its role at the heart of the process. However, recently new engraving patterns have been promoted where it is claimed a more efficient transfer of materials occurred. There are studies published in the non-peer reviewed trade journals, but these tend to be limited in depth and to focus on commercial aspects of the products, particularly when the work has been undertaken by suppliers on commercial presses. There has not been the critical assessment that would be expected in a scientific journal.

The literature review in this chapter has been divided according to the process steps in the flexographic printing train together with a consideration of the ink. The review is divided into three parts:

- Anilox
- Ink rheology
- Ink transfer

2.2 Anilox Rolls

The review has been divided into three sections, the first is an amplification of details concerning anilox roll engraving, the second section summarises the work that has been conducted by industry and the third section reviews scientific literature in connection with the anilox cylinder and fluid transfer from engraved surfaces.

2.2.1 Anilox Engraving

There are few studies of the effect of the engraving on the ink release. Cherry (2007) studied the effect of the engraving techniques on the ink release in the flexographic printing process. He compared the ink flow of the YAG against the CO_2 engraving techniques using a banded anilox (**Table 2.1**).

Table 2.1: Anilox information of CO_2 and YAG engraving [Cherry, 2007]

Band	**CO_2 Anilox (500lpi)**		**YAG Anilox (500lpi)**	
No	Specified (cm^3/m^2)	Produced (cm^3/m^2)	Specified (cm^3/m^2)	Produced (cm^3/m^2)
1	1.7	1.62	1.7	1.63
2	3.1	3.09	3.1	3.04
3	4.2	4.21	4.2	4.18
4	5.6	5.38	5.6	5.49
5	6.8	5.96	6.8	6.59
6	8.2	4.02	8.2	8.31
7	1.7	1.66	1.7	1.61

Two banded anilox rolls with 7 bands of the hexagonal closed cell and the same screen count of 500LPI were used. The cell volume was increased by increasing the cell depth. One roll was CO_2 and the other YAG engraving. The YAG engraved anilox cells had a greater ink release. There were two possible explanations: anilox surface energy and the internal surface roughness. However, neither the surface energy nor the internal surface roughness of these anilox rolls could be measured [Cherry, 2007]. The CO_2 engraving technique generated more residual material on the surface and had narrower cells; these two factors increased the adhesion between the anilox surface and the ink, more ink was retained within the cells compare with the smoother surface and wider cells of the YAG engraving.

In this thesis, the effect of mechanically engraving and laser engraving techniques have also been compared including the impact of surface roughness (chapter 6) amongst other parameters not previously assessed due to the measurement limitations at the time of Cherry's work.

2.3 Ink

Characteristics of the ink are important attributes affecting the ink transfer. The ink rheology and filament breakup are the main characters of the ink.

2.3.1 Ink Rheology

Rheology means "the study of the deformation and flow of matter". [Barnes, Hutton, Walters, 1989]. Rheology plays an important role in printing applications. It can be used to evaluate the performance of the ink such as the flow and the ability to recover after prints [Franck, 2018]. There are industry measures, such as the flow cups, which give an indication of the resistance to flow but to understand the relationship with cell geometry, ink release and ink transfer there is a need to understand the shear and visco elastic properties. Measurement of dynamic shear viscosity and extensional tests will provide data that can be related to the ink transfer in printing.

2.3.1.1 Shear Viscosity

The ink shear viscosity is a main characteristic to determine whether the ink will flow during printing process. [Mai, Pekarovicova and Fleming, 2007]. Viscosity is the resistance of the liquid to flow. The shear viscosity of the Newtonian material is independent of the shear rate i.e. the change of the shear rate does not change (keep constant) the shear viscosity of Newtonian material. The viscosity of non-Newtonian material can significantly change with shear rate. When the shear viscosity decreases because of the shear rate increase, it is called "shear-thinning" behaviour of the material. When the shear viscosity increases because of the shear rate increase, it is called "shear-thickening" [Barnes, Hutton and Walters, 1989].

Mai et al (2007) investigated the shear viscosity of six water-based flexo inks to determine whether this rheological characteristic could be used to predict the ease of ink application during printing. The printing experiment was carried out using an industrial flexo press; a three-color ComCo Commander flexographic press.A banded anilox roll with 600, 700, and 800LPI was used. The press was set at 200ft/min, and the substrate was coated paper. The result showed that the ink should be shear-thinning, in which the shear viscosity decreased with the increase of shear rate, for the ease of application.

All six inks had higher shear viscosity at the low shear rate. When the shear rate increased, the shear viscosity decreased to less than 1Pa.s (**Figure 2.1**) indicating the inks were shear-thinning. The higher shear-thinning resulted in lower reflective optical density but greater tone gain indicated that the ink flowed less to the substrate, and the ink film was thinner with greater ink

spreading.

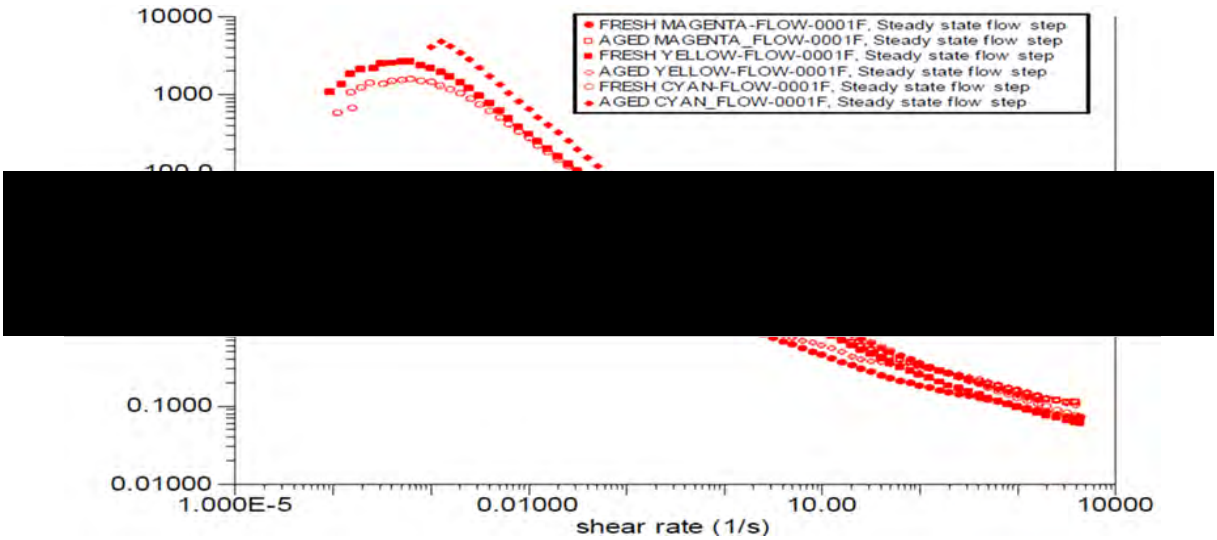

Figure 2.1: Viscosities as functions of shear rate for water-based flexo inks [Mai et al., 2007]

According to Kipphan (2001) shear-thinning ensures that the ink will flow out of the anilox cells during printing. To attain a good quality of print, the typical range of shear viscosity of flexographic printing is 0.05–0.5Pa.s. This range is to ensure no squeezing around the edges of the plate, sufficient supply of ink, good ink splitting, and filling of the anilox cells.

The shear viscosity relates to the ink tack, which indicates the stickiness of the ink. This attribute is more important in high viscosity ink such as paste inks than the low viscosity ink such as flexographic ink. Tack of high viscosity inks is higher than the tack of low viscosity inks. The appropriate ink tack aids in the ink transfer [Mao, 2017]. The increase of ink viscosity increases the ink transfer [Elsayad et al., 2002].

Additional to the investigation of the shear viscosity of six water-based flexo inks, Mai et al (2007) investigated the storage modulus of these inks corresponding to the applied stress at a constant frequency of 1Hz (An oscillatory stress sweep test). The elastic modulus of all inks were linear up to its critical stress (linear viscoelastic region, LVER, **Figure 2.2**), which was the point where the elastic modulus would suddenly decrease. It is the point, where the ink structure is disrupted. The higher critical stress indicated the stronger structure of the ink and would require greater energy to break up its elastic structure.

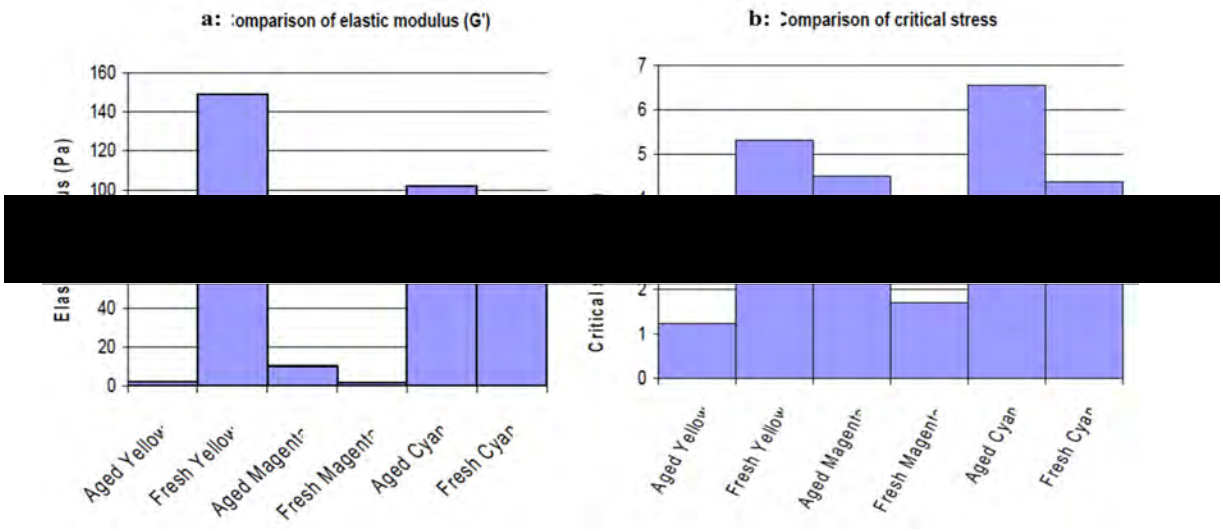

Figure 2.2: a:the comparison of elastic modulus, b:the comparison of critical stress [Mai et al., 2007]

The elastic modulus could be used to compare the release of the ink out of the anilox cells. The greater elastic modulus would elongate longer and increases the pull-out fraction.

2.3.1.2 Ink Filament Breakup Time

The studies of filament deformation of Newtonian and non-Newtonian fluids showed the difference in the characteristic shapes of the evolution of the midpoint diameter. Due to the difference in the evolution of the midpoint diameter between the Newtonian and non-Newtonian fluids; the filament breakup time of Newtonian fluid was very short but the filament breakup time of non-Newtonian was longer. Morgan et al (2017) showed that the filament breakup time of non-Newtonian fluid increased as its elasticity increased.

The evolution in the midpoint diameter of four fluids was measured over time using the Capillary Breakup Extensional Rheometer (**Figure 2.3**). One of the four fluids was Newtonian (N) and the rest were non-Newtionian (E1-E3). The elasticity of non-Newtonian fluids increased from the smallest of E1 to largest of E3. The Newtonian fluid had the very small (closed to zero) filament breakup time. As the elasticity increased, the filament breakup time increased [Morgan et al., 2017].

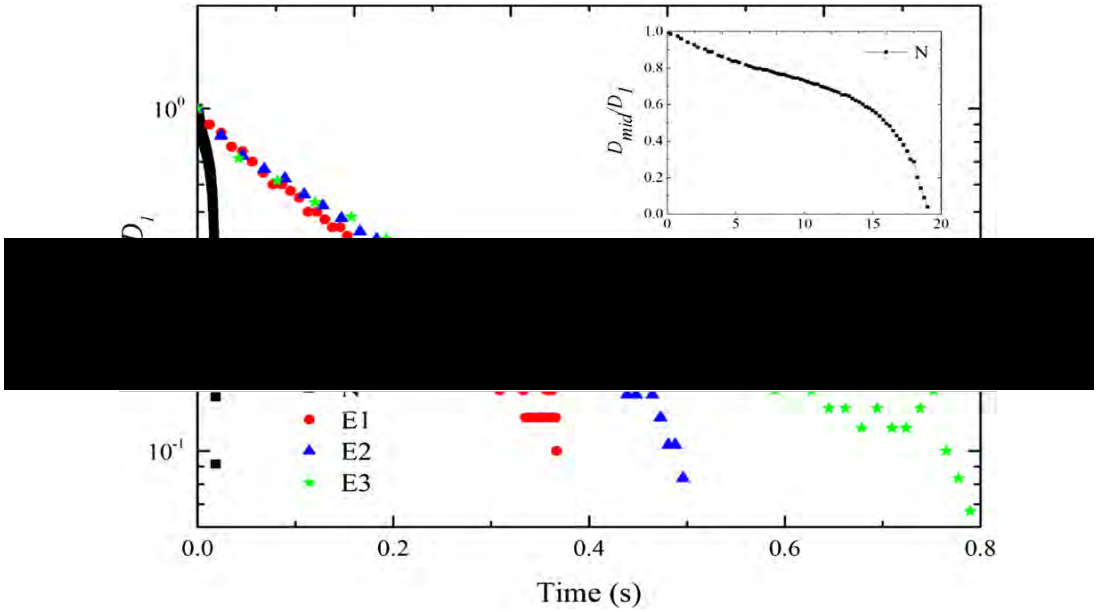

Figure 2.3: The evolution in the midpoint diameter of Newtonian and non - Newtonian fluids using the Capillary Breakup Extensional Rheometer. Inset: typical Newtonian breakup with a linear normalised diameter scale [Morgan et al., 2017]

The filament breakup time could be used to indicate the degree of ink splitting between the anilox cells and the plate. The smaller filament breakup time would indicate the ink could be split and released better than the ink which had the bigger filament breakup time. Because the filament breakup time of non-Newtonian fluid increased as its elasticity increased [Morgan et al., 2017], the viscoelastic characteristic of the ink will be examined to determine its elastic property.

2.4 Ink Transfer

Ink transfer determines the quality of the product. In graphic prints, the transferred volume of ink dictates the shades of the colour. In functional prints, the amount of ink affects functional parameters such as conductivity. The studies of ink transfer have been carried out through numerical simulation and printing experiments. The numerical simulation provide an insight into the liquid flow through the nip between the anilox and plate roll. The simulation could be run as many times as required and the controlled parameters such as viscosity, printing speed, or pressure varied, saving time and resources. However, the numerical simulation method require validation from the experiments to ensure the accuracy of the model.

The printing experiments to study the ink transfer in the flexographic printing process are limited with most analysis based on examining the printed

substrates optical density. Cherry (2007) quantified the ink release from the anilox cells by directly measuring the anilox cells. The ink used for the investigations was a low viscosity, Newtonian graphics ink. Besides the limitation of quantification of ink release from the anilox cells and small ink viscosity,the investigation was mostly done at the low printing speed, compared with the flexographic printing speed which could be 600 metres per minute.

The following sections explore the investigations of ink transfer through numerical simulation and experimental printing methods.

2.4.1 Studies of Ink Transfer by Numerical Simulation

Numerical study of ink transfer simulates the flow regions between two rotating cylinders. There are two main flow regions; liquid flow between the nip and free surface flow (liquid/air interfaces) before the liquid split as shown in **Figure 2.4**. Classical lubrication model was used to model the liquid flow in the coating process.

Figure 2.4: The modified schematic of the flow between rolls [Johnson, 2003]

The results were displayed as a relationship between capillary number and quantification of liquid; for example: flow rate, film thickness. The capillary number has often been chosen as it was a dimensionless number which relates the viscous and surface tension forces, and a number related to the operational parameter, coating or printing speed. The viscous and surface tension forces were the main forces acting during the flow between two rotating cylinders [Coyle et al., 1986]. When the capillary number was less than one, the surface tension dominated the flow. When the capillary numberwas greater than one, the viscous force dominated the flow [Lecuyer et al., 2009].

Most of the studies were carried out at a capillary number of 1 or less [**Ascanio et al.**, (2004)]. The capillary number is the ratio of liquid shear viscosity and its surface tension multiplied by the velocity of rotation cylinders, the capillary

number during the printing process is much higher than one. For example, if the printing speed was 50m/min, and UV Cyan ink was used, its shear viscosity approximately 1.0Pa.s at the printing speed, and surface tension of approximately 29x10^{-3} N/m. The capillary number during the print would be approximately 29. Even though the studies were carried out at a low value of capillary number, they provided insight into the flow between the nip. The lubrication model gave a good approximation for the high speed coating process in which the viscous force would dominate the flow and the surface tension was negligible [Coyle et al., 1986]. However, the lubrication model could not explain the filament breakup of the liquid, which happened in the free surface flow region.

The numerical simulation methods such as developed by **Zevallos** (2005) were able to capture the free surface flow of the filament breakup of the coating process using configuration of two solid surface rolls. Later, **Lecuyer** (2009) developed a model to accommodate a deformable roll, which was normally used in the printing process. The continuity and momentum equations of Navier-Stokes equations coupled with the constitutive equations, which corresponded to the types of liquid such as Newtonian or non-Newtonian, were applied. The example of constitutive equations were the power law, Carreau, or Ellis fluid models. Then, the numerical methods such as finite element were used to solve the equations.

There have been some studies of ink transfer of the gravure printing process, which accommodated the cavity in the numerical configuration. **Lee** (2010) developed a simple analytical model to simulate the flow of a Newtonian liquid between printing roll with a cavity and the substrate (**Figure 2.5**).

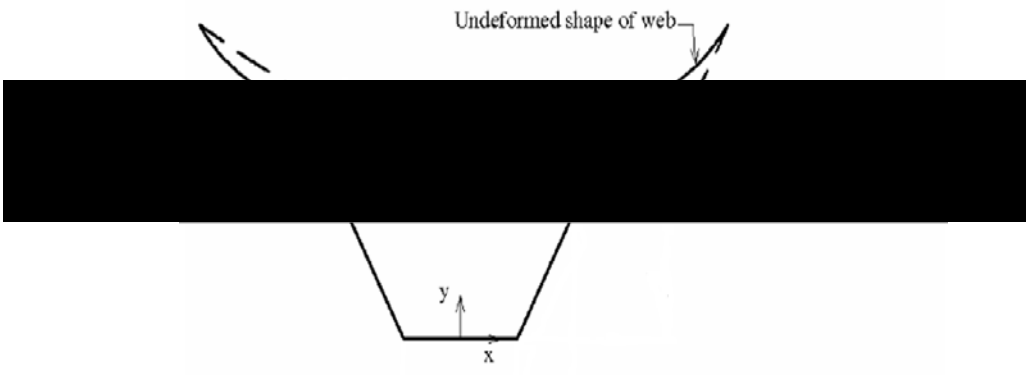

Figure 2.5: The configuration accommodated the cavity of flow simulation in the gravure printing process [Lee, 2010]

Wu (2019) developed a simulation model to study the flow of a shear-thinning liquid using the Carreau model as a constitutive equation. His simulation configuration combined the hyperbolic tangent function to define the cavity

geometry as shown in **Figure 2.6**. The results could be shown as a contour of the liquid over times.

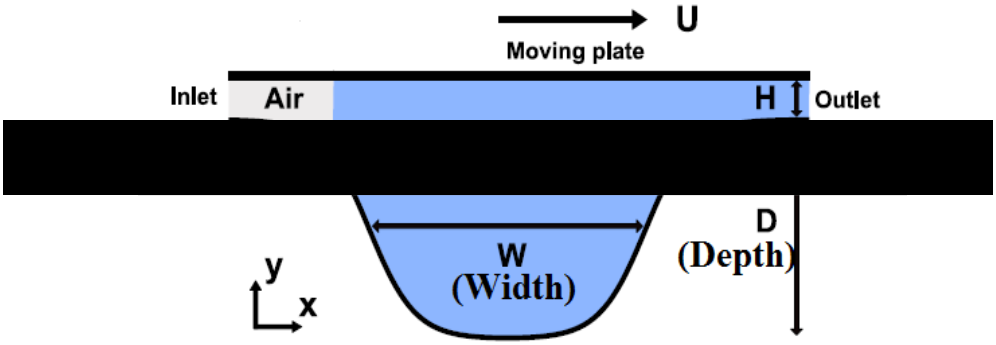

Figure 2.6: The configuration combined the hyperbolic tangent function to define the cavity geometry [Wu, 2019]

The use of numerical methods as a tool to predict the flow of the liquid in printing process has advanced in recent years due to the advance in computer technology. It became possible to simulate pick-out fraction of liquid out of the cavity to gain more understanding of the flow between the nip. However, the numerical methods could still only be qualitative, not quantitative. The method could provide the trend of pick-out fraction such as shown in **Figure 2.7** when the capillary number changed, but could not specify the amount. To quantify the amount of pick-out fraction still requires laboratory experiments. Additionally, the numerical method requires validation by experiment to confirm its accuracy.

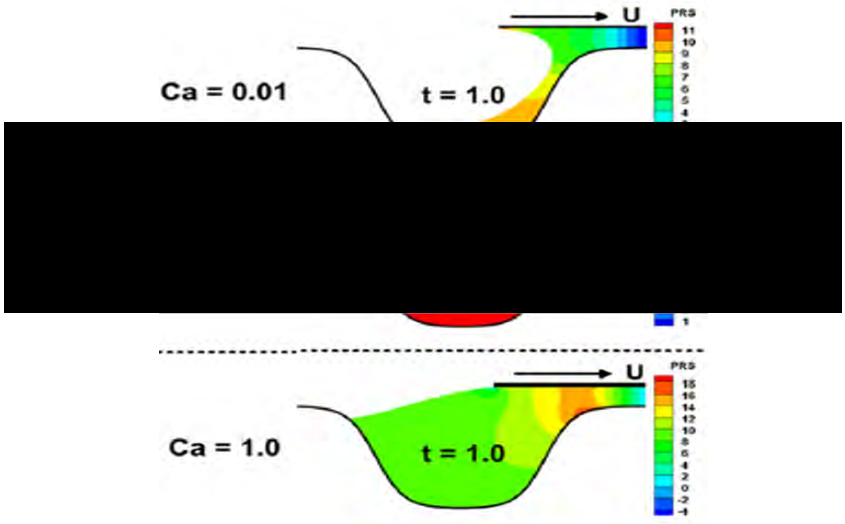

Figure 2.7: The liquid left in the cavity of different capillary numbers [Wu, 2019]

2.4.2 The Experimental Studies of Ink Transfer

Studies of ink transfer in flexographic printing have been carried out by examining the effect of the anilox geometries, ink characteristic, and the operational parameters such as the printing speed. Damroth's work in 1966 explored ink release in flexography.

Table 2.2: Anilox Information [Damroth et al, 1996]

The Anilox Information		
Anilox Volume (BCM)	**Anilox Screen Count (LPI)**	**Depth-to-Opening Ratio (%)**
6.0	250	25
7.0	250	30
8.0	250	35
2.6	400	18
4.1	400	25
5.5	400	35
6.9	400	45
1.5	700	18
2.3	700	27
3.1	700	37
4.2	700	47
Note: 1. Ink viscosity 590/982/2,148/2,951/479 cPs 2. The printing plate was Epic photopolymer with 0.067 inch thickness with the line ruling of 85/110/130 featured the tonal patch of 1-100% dot coverage 3. The substrate was polyester 4. The depth-to-opening ratio increased with the increase of cell volume 5. The anilox cell volume reduced whilst its screen count increased 6. The print speed was set between 100-300fpm 7. The result was measured using one densitometer		

Damroth et al (1996) studied the effect of anilox cell parameters; of cell volume, screen count (the width or opening effect), and the depth-to-opening ratio. The details of the anilox rolls are in **Table 2.2**. The results were obtained by examining the optical density of the prints. The width and depth of the anilox hexagonal closed cells were the controlled parameters. When the screen count was fixed, the cell volume increased by increasing the cell depth. When the screen count increased, the cell opening decreases, and the cell volume decreases. Hence, the cell depth was shallower in the higher screen count. His method was generally the standard practice used in ink transfer studies. The anilox cell geometries affected the optical density of the prints. The anilox cell volume had the greatest impact on the ink transfer. The smaller depth-to-opening ratio could release the ink better. The increase of press speed decreased the optical density especially at higher ink viscosity, implying there was less amount of the ink passed to the printed substrate. There was no

explanation given how the increase of printing speed reduced the amount of the ink transfer.

Table 2.3: Anilox information [Hamblyn, 2004]

	Band 1	**Band 2**	**Band 3**	**Band 4**	**Band 5**	**Band 6**
Screen ruling (lpcm)	99.30	119.30	197.50	240.20	296.20	394.90
Manufactures Cell Volumes (cm^3/m^2)	10.00	8.60	4.50	3.80	3.35	2.27
Average Measured Cell Volumes (cm^3/m^2)	10.28	8.56	4.92	4.31	4.15	2.68

Hamblyn (2004) studied the ink transfer between the printing plate and the non-porous substrate in the flexographic printing process. A six banded anilox roll was used (**Table 2.3**). The screen count of the anilox cells increased whilst the cell volume decreased. The volume of the printed dots was the parameters used to indicate the ink transfer performance. The quantification of the area and volume of the printed dots was done using the white light interferometer [Hamblyn, 2004].

His results agreed with the finding of Damroth et al. (1996) When the anilox cell volume increased, it increased the optical density. Additionally, the increase of the anilox cell volume enhanced the tone gain. The anilox cell geometries had the greatest effect on the volume of ink transfer to the substrate and the optical density. The anilox cell volume was the prominent parameter. Additionally, the anilox cell shape affected the ink transfer but no explanation was offered. Other than the anilox cell volume and screen ruling, the information of the anilox cell depth and width was not displayed [Hamblyn, 2004].

Cherry (2007) studied the ink transfer between the anilox cells and the printing plate. The studies were carried out using a narrow web press with the anilox as specified in **Table 2.4** and lab scale press with the anilox as specified in **Table 2.5**.

Table 2.4: Anilox information of CO_2 and YAG engraving [Cherry, 2007]

Band	**CO_2 Anilox (500lpi)**		**YAG Anilox (500lpi)**	
No	Specified (cm^3/m^2)	Produced (cm^3/m^2)	Specified (cm^3/m^2)	Produced (cm^3/m^2)
1	1.7	1.62	1.7	1.63
2	3.1	3.09	3.1	3.04
3	4.2	4.21	4.2	4.18
4	5.6	5.38	5.6	5.49
5	6.8	5.96	6.8	6.59
6	8.2	4.02	8.2	8.31
7	1.7	1.66	1.7	1.61

Table 2.5: Anilox information used with IGT F1 press [Cherry, 2007]

	Volume (μm^3)	**Depth-to-Opening**	**Open Area (mm^2)**	**Cell Depth (μm)**	**Screen Count (lpi)**
Anilox 1 (402409)	32,029.91	0.35	0.0030	16.34	350
Anilox 1 (402411)	58,812.81	0.36	0.0039	18.72	300

The anilox cells used with the narrow web press had a constant anilox screen count of 500lpi to maintain the same cell opening. Cell depth was used to vary the cell volume. It was impossible to directly measure the anilox rolls because of the sizes. Therefore, the investigation had to examine the printed substrate, and determine the printed dot volume. The direct correlation of the printed dot volume and the ink release from the anilox cells was established. The cell depth of the lab scale anilox rolls was kept approximately constant, but the cell opening was varied (**Figure 2.8**). The effect of the anilox cell geometries on the ink transfer between the anilox cells and the printing plate was investigated. The anilox cells were directly measured to determine the empty anilox cells, the amount of ink before and after prints. Therefore, the ink transfer volume was determined [Cherry, 2007]. Furthermore, for the lab scale investigation, even though the anilox cell depth was kept approximately constant and different in the cell width, the anilox used with IGT F1 press had a difference in anilox cell volume of approximately 46%, the difference in open area was approximately 23%, and the difference in cell depth was 13%.

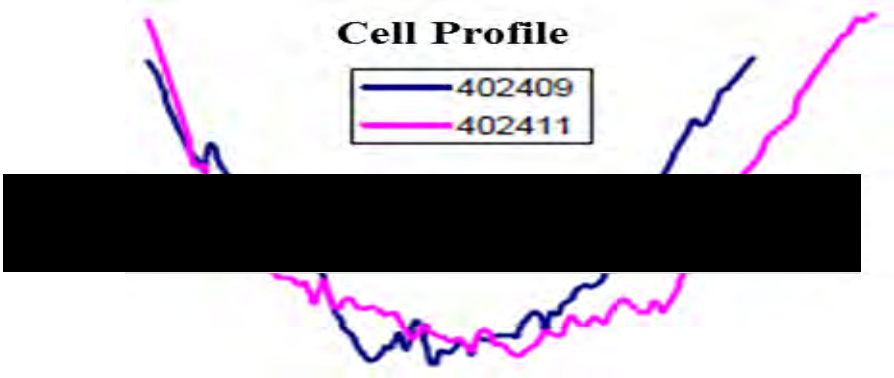

Figure 2.8: Anilox cell profile [Cherry, 2007]

Cherry (2007) results on the narrow web press showed the same trend as of Damroth et al, (1996) and Hamblyn, (2004). The optical density of the print decreased when the depth increased. The anilox cells, which had the greater volume and deeper cells, had the lower ink release than the ones with the lower volume but shallower. When the anilox cells were deeper, the anilox wall was steeper. Cherry (2007) suggested this increased the drag from the wall surface to the ink. Additionally, the increase of the depth increased the contained ink volume. Cherry (2007) suggested this increased viscous-cohesive force of the bulk ink in the anilox cells. The combination of greater adhesive force of the liquid ink to the anilox cell wall, and the cohesive force of the bulk ink in the deeper cell made it more difficult releasing the ink comparing to the shallower cell [Cherry, 2007].

The anilox cells with the constant depth but wider opening, transferred more ink because the plate could deform into the anilox cells as previously found by Bould which established that the plate could be deformed by barrelling and expansion mechanisms during the engagement. The plate dot could expand in a vertical and lateral direction (**Figure 2.9**). During printing, the withdrawal of the ink happened at the top half of the anilox cells, and the large amount of ink remained in the anilox cells. The ink release between the anilox cells and the solid plate was approximately 40%. The optical density on the printed substrate increased with the increasing of the ink release of the anilox cells. The greater the anilox cell volume, the higher the optical density. The examination of the tone gain gave the similar results. The increase of the anilox cell volume increased the ink spreading [Cherry, 2007].

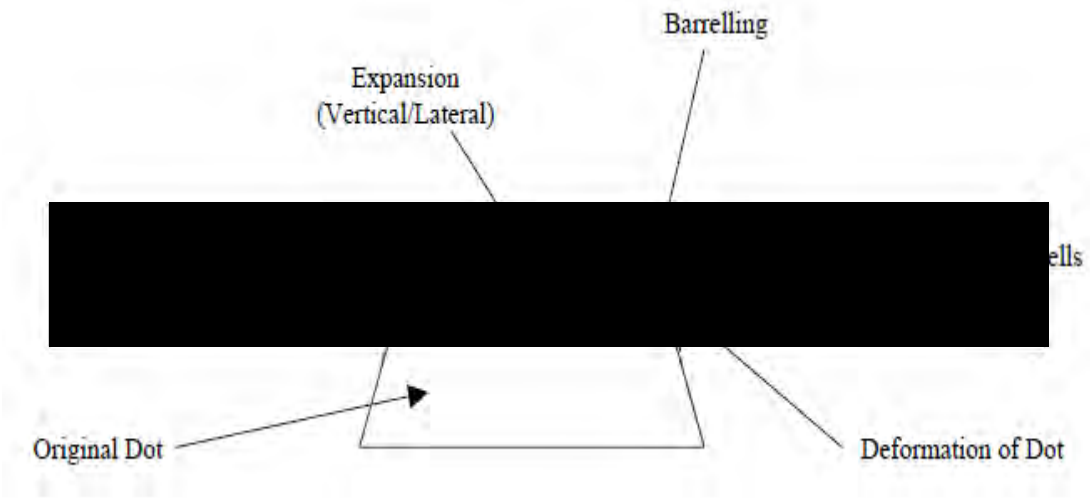

Figure 2.9: Dot deformation into anilox cell [Cherry, 2007]

Beynon (2007) studied the ink transfer from the printing plate to the substrate with a banded anilox roll as detail in **Table 2.6**. The anilox cell width was kept approximately constant with increasing the cell depth to increase the cell volume. The optical density, the optical and physical coverages (to determine dot gain) of the printed substrates were measured to examine the ink transfer performance. The effect of anilox cell volume was examined. Whilst Cherry (2007) used one ink viscosity, Beynon (2007) explored the effect of different ink viscosities on the ink transfer from the anilox to the plate by changing the ratio of conventional flexo ink and a reducer [Beynon, 2007].

Table 2.6: Anilox Information [Beynon, 2007]

Band	**Volume** (cm^3/m^2)	**Width** (μm)	**Depth** (μm)	**Depth-to-Opening** (%)
1	1.63	50.59	4.14	8
2	3.04	49.37	6.79	14
3	4.18	49.21	10.09	21
4	5.49	48.42	14.99	31
5	6.59	47.17	19.65	42
6	8.31	52.50	28.33	67
7	1.63	50.32	3.93	8

Similarly to the previous studies, increasing the anilox cell volume generally increased the optical density, and the dot gain especially in the mid-tone area. The anilox cell shape also affected the ink supply to the plate. The deeper anilox cells hindered the ink release even though the deeper anilox cells had greater cell volume. Ink viscosity had an impact on the optical density; decreased ink viscosity reduced the optical density. The degree of decrease

increased with the increase of dot coverage; there was a small decrease over the range of 1-80% dot coverage, but over 80% dot coverage the degree of decrease was greater and the largest drop was at 100% dot coverage. The decrease in ink viscosity led to a decreased amount of ink transferred to the plate [Beynon, 2007]. However, there was no explanation of how the lower viscosity would change the ink release from the anilox cells as all the trials were done with the narrow web press, which made it impossible to measure the anilox cells as Cherry (2007) had been able to with IGT F1 press.

The effect of the print speed has been investigated by examining either the printed substrate through the measurement of the optical density, or ink filament profile through the numerical modelling and experiment. The investigations showed the similar trend of the decrease of the ink transfer when the speed increased.

Damroth et al (1996) found that the increase of the press speed decreased the optical density especially in the higher ink viscosity. However when the anilox screen count increased from 400 to 700LPI, the increase of the press speed had no significant effect on the optical density [Damroth, 1996]. Similarily, Elsayad et al (2002) found that increasing the print speed decreased the ink transfer but offered no explanation [Elsayad et al., 2002].

Hamblyn (2004) used a Timsons T-Flex narrow web flexo press. The engagement of the anilox and printing plate was kept constant. The ink transfer performance was determined by measuring the printed substrates using the spectrophotometer for the optical density, and the white light interferometer for the physical changes [Hamblyn, 2004].

When the press speed increased, the optical density of the prints decreased. When the anilox cell volume increased, it increased the optical density. Additionally, the increase of the anilox cell volume enhanced the tone gain. However, the increase of the press speed did not have significant effect on the tone gain [Hamblyn, 2004].

Cherry (2007) found that when the print speed increased, the optical density of the prints reduced. This indicated the reduction in the ink transfer from the anilox cells [Cherry, 2007].

Deganello (2007) studied the ink release in the rotogravure printing process using the Artificial Neural Network approach (ANN) and the Computational Fluid Dynamic (CFD) model with experimental and literature data. The method took into account of the dynamic contact angle on the ink release

mechanism, which was an improvement on the previous modelling studies which used a static contact angle. The model showed the extensional flow during the ink release as the fluid was pulled from the gravure cells to the substrate. The dynamic contact angle increased when the speed of wetting increased. The increase of the contact angle indicated the reduction in wettability of the ink. The ink was pulled less when the print speed increased. The effect of the press speed was investigated through the filament breakup. With a press speed of approximately 500m/min, the filament breakup happened instantly within $0.62\text{x}10^{-3}$ second. However, when the press speed reduced to approximately 10m/min, the filament breakup took longer time to break up at $1.12\text{x}10^{-2}$ second [Deganello, 2007].

Khandavalli and Rothstein (2017) had similar trend to the previous studies. When the speed increases, it increased the extension rates. This causes the severe thinning extensional viscosity reducing the pulling and hence the inks transfer [Khandavalli and Rothstein, 2017].

Addition to the printing experiments, some studies of filament breakup were carried out. The studies offered more insight on how the ink filament would possibly breakup out of the anilox cells during the printing process.

De Grice et. al. (1992) showed that when the feed of the amount of the fluid increased, the rupture length of the filament increased. The increase of the volume allowed the filament to elongate. However, when the speed increased, the rupture length decreased because of the increase of the tensile force applied to the filament.

Yao and McKinley (1998) used numerical simulation to study the extensional deformation of non-Newtonian fluid bridge in a filament stretching instrument. There was no strain hardening in the Newtonian fluid. Its necking was always largest at the mid-plane between two end-plates, and its filament would break in the middle. The non-Newtonian fluid had strain hardening which became important when the strain rate increased because of the elongation of the polymer chains. The strain hardening caused the extensional strain rate in the central part of the liquid bridge decreased and made it difficult for the filament to stretch. The unstretched fluid at the foot area adjacent to the two endplates was easier to pull out. The strain hardening prevented the filament breakup in the middle, and instead pulled the fluid from the foot area of the two endplates and created the uniform cylindrical viscoelastic filament. The polymeric stress of the viscoelastic filaments grew when the strain increased and provided extra resistance to the extensional deformation.

Ercan (2001) showed that at high rates of film separation, the shorter ink

filament was generated. When the speed of the ink splitting increased, the ink filament ruptured and recoiled back to its ink surface. Generally, when the extensional strain increased, the ink extensional resistance increased; therefore, the ink holdout of the extensional behaviour increased at the higher printing speeds. The high printing speed led to high extensional rate. There was a high extensional resistance for ink as it contained long chain polymer resins, and had high relaxation time.

SMOLKA et al. (2004) found that the non-Newtonian fluid had larger in length and time scales comparing to the Newtonian fluid. The results of the pinch-off filament breakup was 1.4cm for Newtonian comparing to 1m for non-Newtonian fluid. When the fluid elasticity increased, the filament thinning decreased and filament length increased; therefore the filament breakup time increased. The viscoelasticity could enhance the stability of the fluid filament to capillary breakup because the elasticity stabilized the filament against surface tension effect, resulted in delay in filament breakup.

Castrejón-Pita, Castrejón-Pita, and Hutchings (2012) studied the breakup of the liquid filaments. The Newtonian liquid with low viscosity, the surface pinch-off happened rapidly and the filament had no time to grow. However, when the viscosity increased, the filament stretched for much longer and the breakup time increased. The results showed the increase of the pinch-off times for the higher viscosity of Newtonian liquid.

Khandavalli and Rothstein (2017) studied the ink transfer of the non-Newtonian fluids in the gravure printing process. A liquid bridge was formed and stretched between the gravure cells and web. The ink transfer happened during this process to move the ink from the gravure cells to the substrate. The combination of the shear, extension and rotation occurred due to the motion of gravure and substrate rolls. The effect of the shear and extensional deformations were investigated. The fluid pick out from the gravure cells was correlated to the magnitude of the extensional and shear deformation rate. The profile of the fluid filament was captured using a high-speed camera. The constant shear viscosity viscoelastic and shear-thickening inelastic nanoparticle dispersion fluids were used. A range of the extensional and shear deformation rates were applied. A filament stretching extensional rheometer was used to create a uni-axial extensional motion on the fluids (**Figure 2.10**). The bottom plate was attached to a rotating motor to create the shear deformation. The top plate was the gravure cavity. The cavity has a side wall angle α=75^0 from horizontal, R=2.5mm, h=1mm, and with L_i/R ratio of 0.3.

Pure extension increased the pickout fraction because of the extensional thickening of the fluid, and the highly elongated filament which was pulled from the gravure cells. Pure shear-induced pickout process was similar to that of the

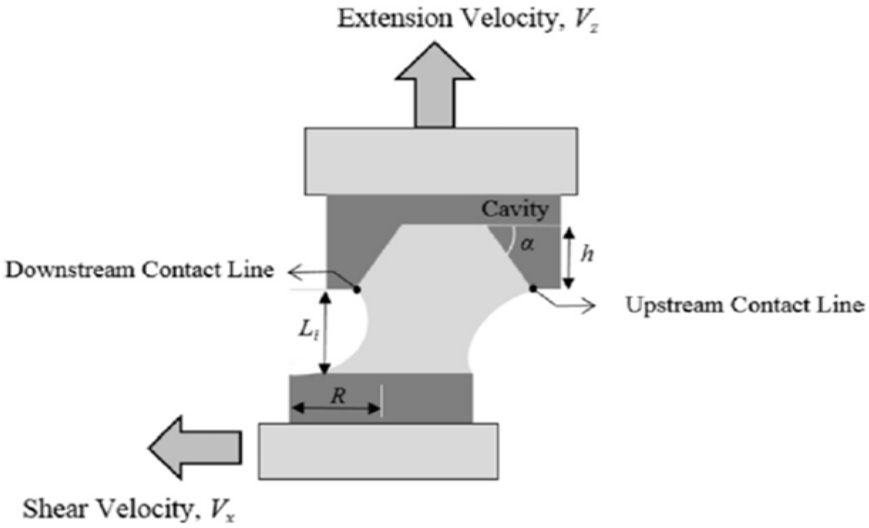

Figure 2.10: Schematic diagram of experimental setup

pure extensional pickout process (extraction from the cavity). The increase of the pickout fraction happened at a late stage where the pure shear transformed to elongation deformation and split. The long uniform and long-lived filament enhanced the pickout fraction. However, the increasing and decayed rates were less than those of the pure extensional pickout process. The shear-induced pickout fraction was significantly lower than the extensional pickout fraction for the same speed. The shearing motion pulled the fluid from the gravure cells, and then forced the fluid to the land bordering of the gravure cavity, which increased the fluid-solid contact. The increase of the fluid-solid contact increased the adhesion force, and hindered the pickout process. The results for the combination of the shear and extensional deformation on the pickout process showed that by imposing extensional velocity over the shear velocity, where the fluid was thickening, increased the pickout fraction by 10%. Superimposing extensional flow over shear prevented the adhesion of fluid-solid contact. When the shear velocity was large and the fluid was thinning; increasing extensional velocity over shear velocity did not significantly show the improvement of the pickout fraction and could reduce the pickout fraction [Khandavalli and Rothstein, 2017].

The right combination of the anilox cell geometries, the ink characteristics and the operational setup is required to deliver the desirable print quality. The ink transfer in the printing process can be improved by choosing the anilox cell geometry, which makes the ink easily being released. The inks, which enhance the elongation of the filament and the pull-out fraction but easily breaking up, should be used. The print speed, which does not increase the extensional strain to the point that it hinders the elongation of the ink filament, should be set.

2.5 Summary

There has been little direct measurement of the ink release from the anilox cells during printing. Much of this work was done by Cherry and Bould at a time when the industry was moving from mechanically engraved to laser engraving, where the ambition was to replicate the mechanical engraving with greater control and efficiency. There have been no systematic studies of ink release from the new geometries particularly extended hexagonal and open channel anilox cells. There have been a limited number of previous studies of ink transfer from the anilox.

Most experimental studies rely on examining optical density of the prints. The printing experiments have provided trends for the ink transfer when the anilox cell width or depth changed; the small depth-to-width ratio increased the ink transfer. However, these have all been on conventional closed cells. There has not been any scientific study of the ink transfer from open channel anilox or even from extended hexagonal cells (another of the cell shapes enabled by the advances in laser engraving technology).

The previous work has used low viscosity graphic inks. Not only are graphic inks, such as UV, becoming both more viscose and also have elastic properties the more structured, heavily pigment laden functional inks for applications such as printed electronics and sensors possess considerable viscoelasticity. Few studies have included the viscosity of the ink, yet alone the viscoelastic properties or extensional properties, which have been shown to be important from the numerical modelling. The numerical simulation methods provide the trends and display results of the ink left in the cavity. However, the numerical methods could still offer only qualitative, not quantitative information.

Studies of the filament extension and breakup using Newtonian and non-Newtonian fluids have shown that this will probably affect the pickout of ink from the anilox cells. There has only been limited studies of the ink release from conventional closed cell anilox and no studies of the ink release with the extended hexagonal or open channels. All the research has used conventional low viscosity graphic inks for which it has been assumed they have no viscoelastic properties. This project builds on the previous work, improving the analysis technique to include all asepcts of cell geometry. A comprehensive study of anilox closed cells has been undertaken to establish the relationship between cell geometry and ink release. Some of the newly developed engraved cell geometries, the extended hexagonal and open channel, are then compared in terms of ink release.

This research also includes the effect of viscoelasticity on ink release. A conventional graphics ink, assumed to be low viscosity and Newtonian, is used

to relate this study to previous investigations. These will be compared to functional inks, which have higher viscosity and pigment loading as well as being non-Newtonian. The ink shear viscosity will be determined to better understand the ink flow and behaviour during printing process. The viscoelasticity can indicate the filament breakup time. Additionally, when coupled with the extensional viscosity can be used to predict if the ink filament will have a prolong and pull-out more, and whether it will be easily released from the anilox cells. While these fundamental studies will be carried out with a benchtop proofing system, parallel experiments on full scale printing presses to provide background to these results.

Chapter 3

Methodology

3.1 Introduction

The methods used for the investigations are described. The preliminary experiments were carried out in chapter 4 to gain fundamental understanding of the ink release using the flexographic printing process. The cooper sheet-fed flexographic press was used with two bands of the anilox closed cells. The UV process Black ink was used with the glass substrate. A printing plate with the tonal patch of dot coverage 1-100% and tracks was used.

Chapter 5 investigated the effect of the elongated anilox closed cells and wavy channel anilox cells. The experiments were carried out using the industrial flexographic press; KBA flexotecnia XG press. Commercial solvent-based inks; the high definition Black and Yellow, were used with the flexible substrate (PET). The printing plate with the tonal patch of dot coverage 1-100% was used.

Chapter 6, a flexographic proofing press was used with a range of anilox including hexagonal anilox closed cells, extended hexagonal, wavy channels and mechanically engraved quadratic open cells. Three UV inks: Cyan, Carbon, and Silver inks were used with a flexible substrate (PET). The experiments in this chapter were carried out to establish the understand of the ink release by quantification of the ink release volume by directly measuring the amount of the ink released out of the anilox cells to a solid plate. . Chapter 7 was to study the effect of the ink release to half tones using anilox rolls selected on the basis of the results in chapter 6.

The methods and characterisation of the anilox, plate, inks, and the printed substrates are described in the following sections.

3.2 Anilox Measurement

Anilox bands were measured using two instruments; Wyko white light interferometry and Alicona InfiniteFocus microscope. The Wyko white light interferometry was used to measure the anilox bands used in chapter 4 and 5. The anilox cells used in chapter 4 were of closed cells; however, one of the anilox cells used in chapter 5 was wavy channels. Therefore, the method to determine the anilox cell volume was different from the anilox closed cells. Two methods are described for volume determination; closed and open cells, but the method to determine the width and depth are the same.

The Alicona InfiniteFocus microscope was used to measure the anilox bands used in chapter 6 and 7. The anilox cells were closed cells, elongated open cells and wavy channels. The method to determine the anilox cell volume was different because of the difference in shapes of anilox closed and open cells. Two methods are described for volume determination, but the method to determine the width and depth were the same.

An anilox roll with the screen count of 203LPI and cell volume of 14cc/m^2 was measured using a white light interferometry (Wyko) and Alicona InfinitFocus microscope with 20x optical magnification. The data was extracted to get the anilox cell profile, which informed the cell width and depth. Additionally, the anilox cell profile was used to check the consistency of the data and compare the consistency and accuracy of the instruments.

The data restore function in Wyko software was used to interpolate the missing data, where the instrument could not measure during scanning process (**Figure 3.1**). When the data restore function was applied, there was more data points, however the anilox cell shape was altered to be wider along the length of the cell wall and deeper. The alteration of the shape did not change the width of the anilox cell, but the cell depth and volume. The cell depth and volume were exaggerated. However, the same procedure of applying the datarestore function was used throughout the investigations; so, the data was consistent.

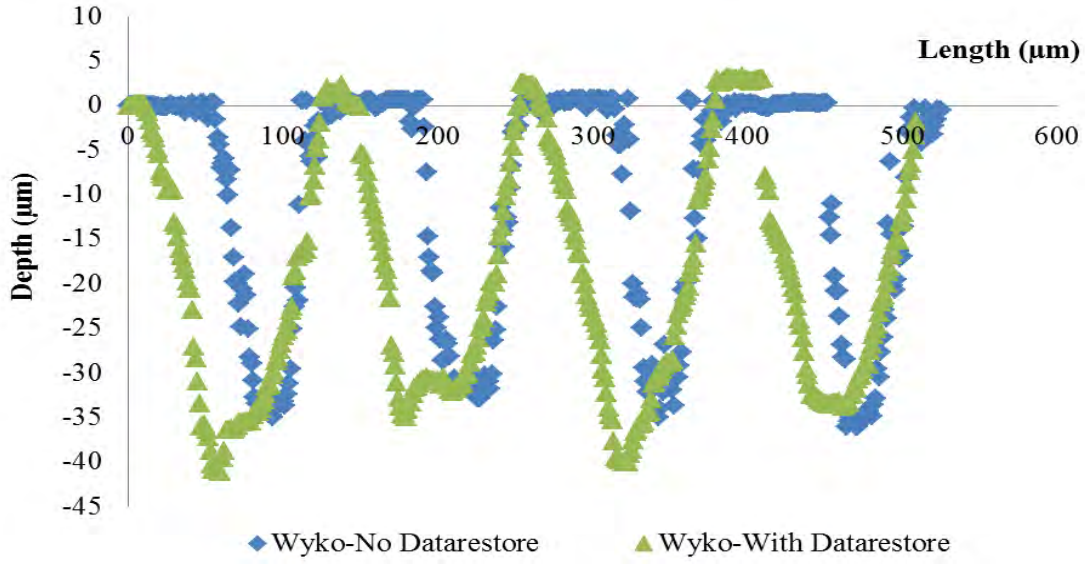

Figure 3.1: Comparison of anilox cell profile using Wyko with and without datarestore function

To compare the consistency and accuracy of the instruments, the data of cell profile extracted from Wyko white light interfermetry without using datarestore function was compared to the measurement using Alicona InfiniteFoucus microscope without datarestore function (**Figure 3.2**). The Alicona InfiniteFocus microscope could measure and get more consistent data than Wyko white light interferometer.

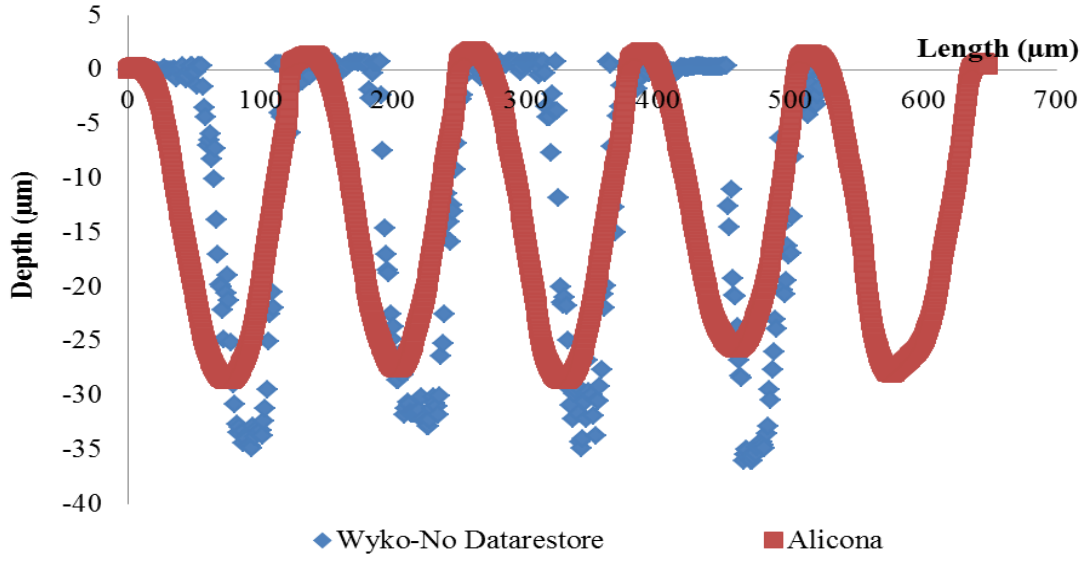

Figure 3.2: Comparison of anilox cell profile using Wyko and Alicona microscope without datarestore function

Alicona InfiniteFocus microscope could extract more data and was more consistent than the Wyko white light interferometry, the Alicona InfiniteFocus

microscope was chosen for all the investigations using the laboratory scale press (**Figure 3.3**). The Alicona had not been available for the preliminary investigations in chapter 4. The Rollscope, a portable version of the WYKO Inteferometer was used on site with the commercial press in chapter 5.

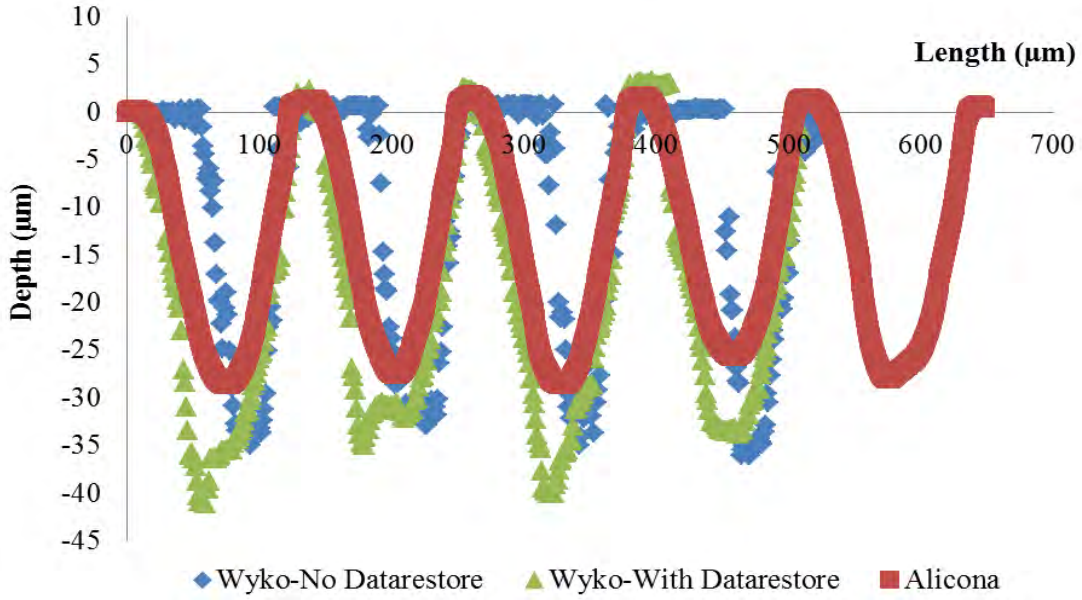

Figure 3.3: Anilox measurement

3.2.1 Wyko White Light Interferometry

Anilox bands were measured using the Wyko white light interferometry (**Figure 3.4**), which is a non-contact optical profiler using white light in scanning the samples. The Wyko software was used to extract the anilox cell width and depth. The anilox cell width was used to determine the anilox screen count; the number of anilox cells per inch (LPI). The anilox cell volume was calculated using the WCPC in-house software [Deganello, 2007].

Figure 3.4: Wyko NT2000 white light interferometry [Soruce: wcpcswansea.com]

3.2.1.1 Anilox Cell Width and Depth Measurement

The cell profiles were generated by Wyko software (**Figure 3.5b**). There were missing data (black area), and the corresponding cell profile. The white light interferometry could not capture data around the steep area such as the cell wall. The data restore function was used to interpolate and build the cell profile.

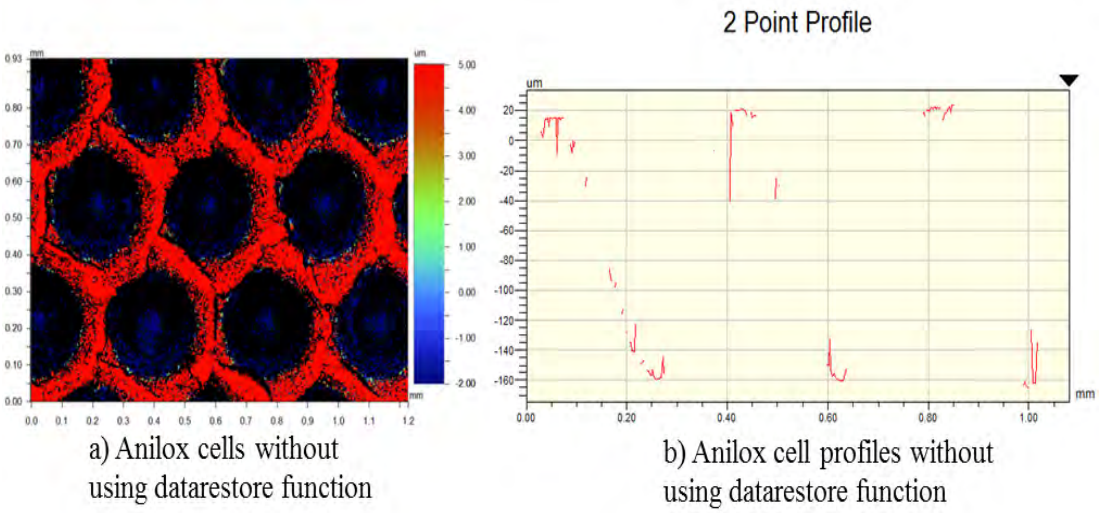

Figure 3.5: The image of the anilox cells (a) and profiles (b) captured by Wyko white light interferometry without using the datarestore function

The full image of the anilox cells enabled the anilox cell width and depth to be determined (**Figure 3.6**).

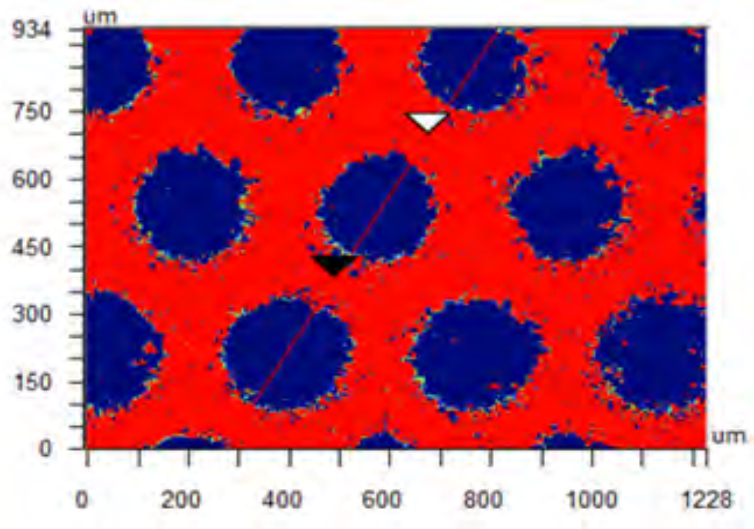

Figure 3.6: The image of the anilox cells after applying the datarestore function on Wyko software

The cell width and depth were measured in micrometre (**Figure 3.7**). The cell width is the measurement of the distance between the left and right cell wall (a). The cell width is used to determine the anilox screen count; the number of the anilox screen count per inch (LPI) is equal to 25,400 divided by the anilox cell width. The cell depth is the measurement of the distance from the highest point on the cell wall to the lowest point at the bottom of the anilox cell (b).

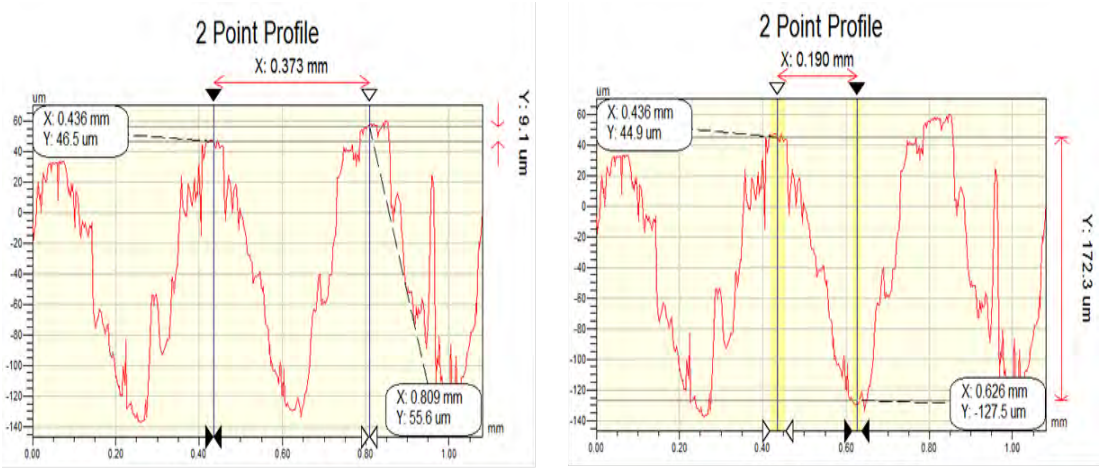

Figure 3.7: The cell profiles of anilox cells to extract the anilox cell width and depth using Wyko software

3.2.1.2 Anilox Cell Volume Measurement

Anilox Closed Cells Volume Measurement

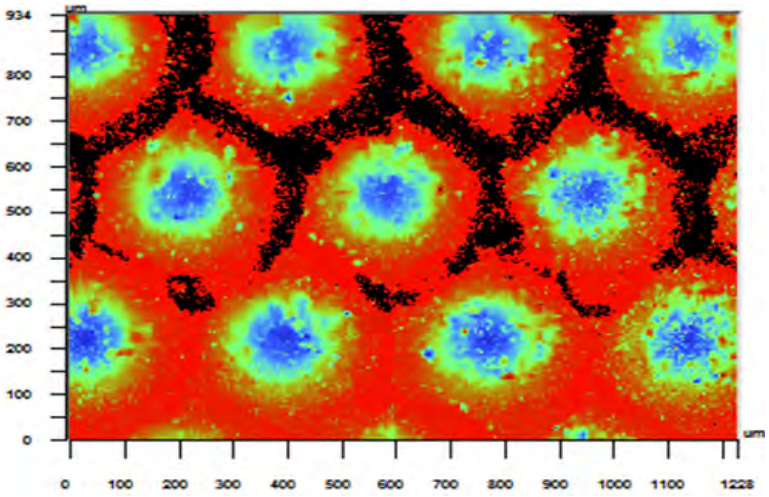

Figure 3.8: The image of the anilox cells to extract the volume using Wyko software showing incomplete and not-align with reference plane

The generated by the Wyko data was incomplete and not align with reference plane (**Figure 3.8**). Wyko software greatly depends on the operator to align the reference point; this can cause inconsistency in the data. The WCPC in-house software [Degenello, 2007] was used because it aligned automatically and the anilox cell profile could be generated to check the alignment; the data generated by WCPC in-house software was more consistent and accurate. The anilox cell was aligned and the volume was extracted (**Figure 3.9**).

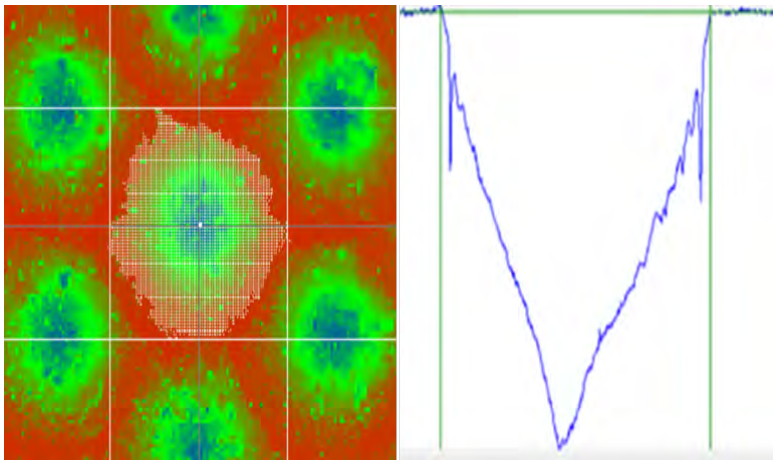

Figure 3.9: The image of the anilox cell and its cell profile to extract the volume using WCPC software

A volume of each pixel, which is a rectangular cuboid, is calculated by

multiplying surface area by the depth of each pixel (**Figure 3.10**). All of the cuboids within selected area are then added together to get the volume of the anilox cell. To establish the consistency and accuracy of the data, the extracted volume is compared to the manufacturing data. Additionally, WCPC software provides the anilox cell depth and width. The anilox cell volume is then given in the unit of cm^3/m^2.

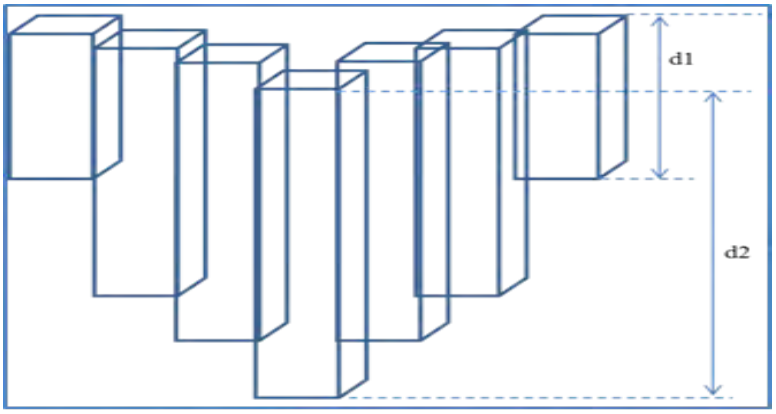

Figure 3.10: The image of grid (pixel) blocks generated by WCPC software to extract the volume of anilox cells

Table 3.1 shows the example of the anilox cell volume, width, and depth data.

Table 3.1: The example of the anilox cell volume, width, and depth data

Measurement	**Volume/Area (cc/m^2)**	**Width (μm**	**Depth (μm)**
1	40.21	196	149
2	43.03	202	182
3	45.18	210	207
4	47.16	209	190
5	43.80	201	180
6	55.68	201	177
7	50.06	201	173
8	51.59	199	191
9	52.93	211	204
10	46.36	211	167
Average	47.60	204	182
Standard Deviation	4.87	6	17
Standard Deviation (%)	10%	3%	9%

Table 3.2 shows the summary of the measurement of two anilox bands used for

the printing experiments.

Table 3.2: The summary of anilox measurement

Screen Count (LPI)	**Cell Volume (cc/m^2)**	**Width (μm)**	**Depth (μm)**	**Surface Roughness (μm)**	**Shapes**
68	49.22	361	187	19	Closed Cell
120	47.60	204	182	30	Closed Cell

Table 3.3 shows the manufacturing specification of the two anilox bands (**Table 3.2**) in which the cell volume and screen count were given but no details of cell width and depth. The measurement screen count was similar to those given by manufacturer but there was a significant difference in cell volume; the variation was in the cell depth measurement. There was no detail of how the manufacturer measured the anilox cells; therefore, no further comment could be made. The measured data was used for the investigation.

Table 3.3: The manufacturer's specification of anilox cells

Screen Count (LPI)	**Cell Volume (cc/m^2)**
70	43.14
120	36.34

Anilox Open Cells Volume Measurement

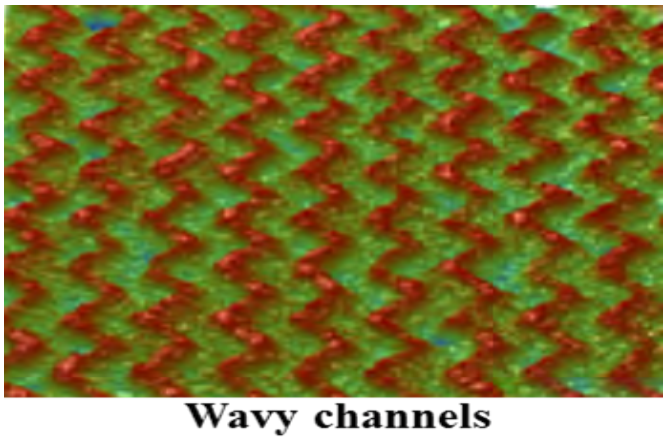

Figure 3.11: The image of anilox wavy channel cells

The anilox wavy cell shape was different from the anilox closed cell, which had

cell walls to set clear boundary against its neighbouring cells (**Figure 3.11**). To determine the volume of the anilox open cells requires the boundary to be defined. To keep the consistency of data of the measurement, the area was defined by covering the area from wall to wall in the rectangle as shown in **Figure 3.12**. The same protocol was followed through out to keep the consistency of the extracted data. The data was extracted using WCPC software.

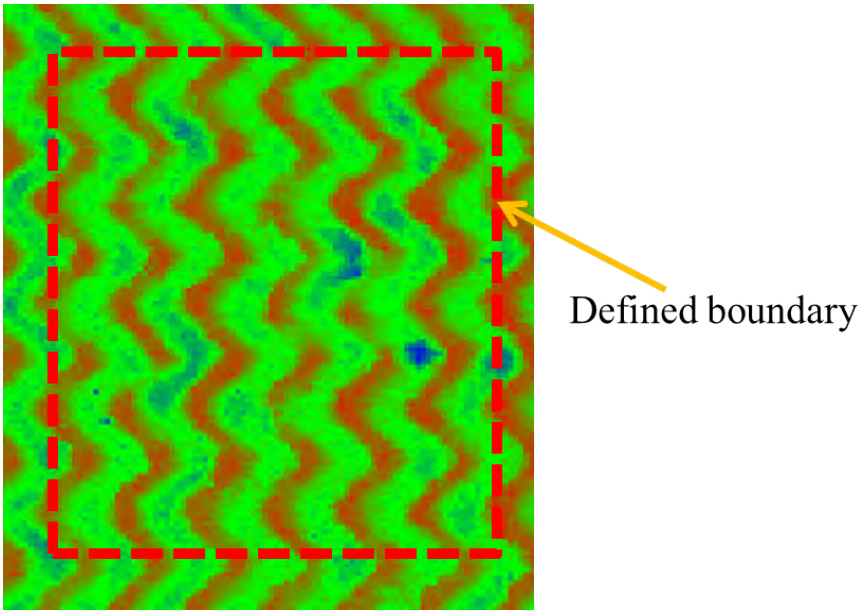

Figure 3.12: Defined boundary to determine volume of anilox wavy cells

The anilox roll had 2 anilox bands engraving; each band covered half the width of the anilox roll (**Table 3.4**). Because the length of anilox wavy channel cell band was half comparing to the full length of the anilox elongated hexagonal closed cells, the measurement was done 3 times along its length, and repeated along the four sides. Therefore, the measurement was done 12 times for the wavy channel cells.

Table 3.4: The anilox wavy channel cell measurement

Measurement	**Surface Roughness (Ra, nm)**	**Width (μm)**	**Depth (μm)**	**LPI**	**Volume (cc/m^2)**
1	1.52	20	5	1,090	2.20
2	1.67	22	6	1,031	2.35
3	1.67	22	5	1,004	2.24
4	1.50	24	5	1,139	2.00
5	1.54	21	5	1,045	2.51
6	1.49	23	5	1,139	2.10
7	1.53	19	5	1,045	2.07
8	1.73	20	5	1,187	2.59
9	1.72	19	5	1,045	2.46
10	1.58	19	5	1,045	2.23
11	1.69	19	6	1,045	2.37
12	1.68	22	5	1,139	2.57
Average	1.61	21	5	1,074	2.31
Standard Deviation	0.09	2	0	64	0.20
Standard Deviation (%)	6	8	6	6	9

3.2.2 Alicona InfiniteFocus Microscope

The anilox bands were measured using Alicona InfiniteFocus microscope. **Figure 3.13** shows the example of the images of the anilox cells with the cell volume of 6.45cc/m^2 and 2.76cc/m^2 (a), and their cell profiles (b). The anilox cell width, depth, and cell volume were using Alicona software.

a: The image of anilox cells captured by Alicona infiniteFocus microscope

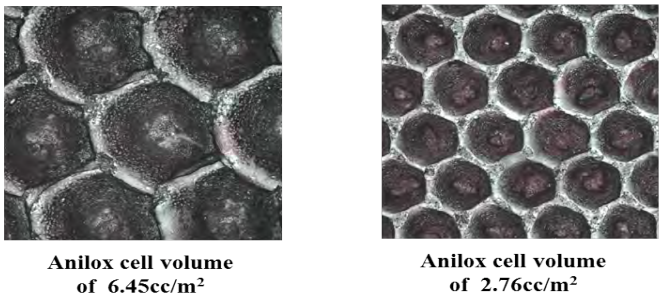

b: The anilox cell profiles of 6.45 and 2.76cc/m²

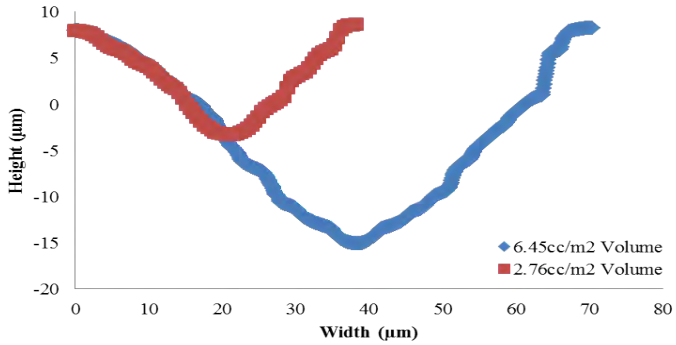

Figure 3.13: a: The image of anilox cells captured by Alicona InfiniteFocus microscope, b: Their cell profiles of 6.45cc/m^2 and 2.76cc/m^2

3.2.2.1 Anilox Cell Width and Depth Measurement

20 measurement points around the anilox roll were used to determine the anilox cell width, depth, and volume data (**Figure 3.14**).

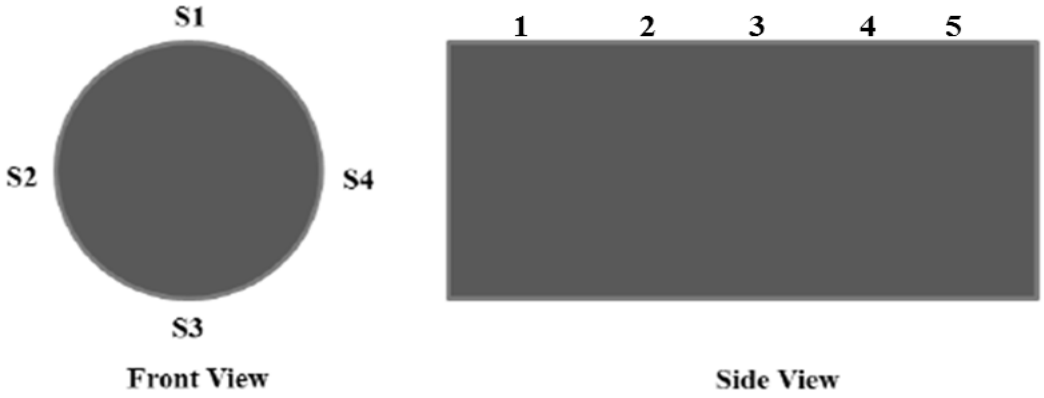

Figure 3.14: The points of the measurement around the anilox roll

The same method was applied as used with Wyko white light interferometry (**Figure 3.15**). The cell width is the measurement of the distance between the left and right cell wall (b). The cell width is used to determine the anilox screen

count. The cell depth is the measurement of the distance from the highest point on the cell wall to the lowest point at the bottom of the anilox cell (c). The example of the anilox cell width and depth data is shown in **Table 3.5**.

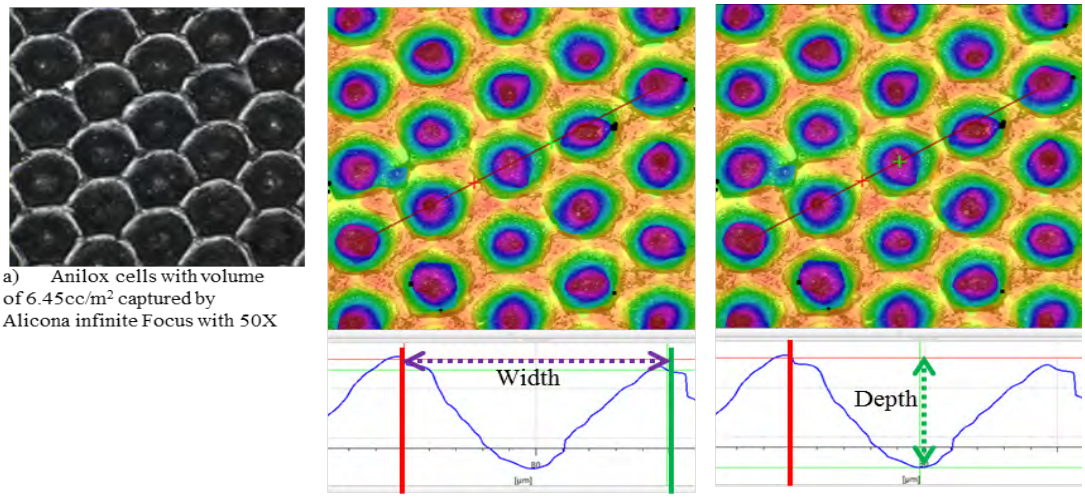

a) Anilox cells with volume of 6.45cc/m² captured by Alicona infinite Focus with 50X

b) Cell width measurement

c) Cell depth measurement

Figure 3.15: The image (a) and cell profiles of the anilox cells for the extraction of the width (b) and depth (c) of the anilox cells

Table 3.5: The example of the anilox cell width and depth data

Measurement	**Width (μm)**	**Depth (μm)**	**Measurement**	**Width (μm)**	**Depth (μm)**
1	73	18	11	73	16
2	72	16	12	72	16
3	73	15	13	73	16
4	73	15	14	72	15
5	73	15	15	73	15
6	73	16	16	72	15
7	73	16	17	72	14
8	73	15	18	73	15
9	73	16	19	72	15
10	74	16	20	73	15
Average				73	16
Standard Deviation				1	1
Standard Deviation (%)				1%	8%

3.2.2.2 Anilox Cell Volume Measurement

Anilox Closed Cells Volume Measurement

The Alicona software could determine the volume within the selected boundary (**Figure 3.16**). Due to the time consuming of selecting large area, one anilox cell was selected for each measurement. The defined boundary was generated between the cell wall of the anilox cells. The Alicona software provided the data of the volume above and below the red reference plane and the projected area. The anilox cell volume was determined by dividing the total volume (volume above and below the red reference plane) by the projected area. Before the printing experiments, the anilox roll was measured to check the consistency of the measurement.

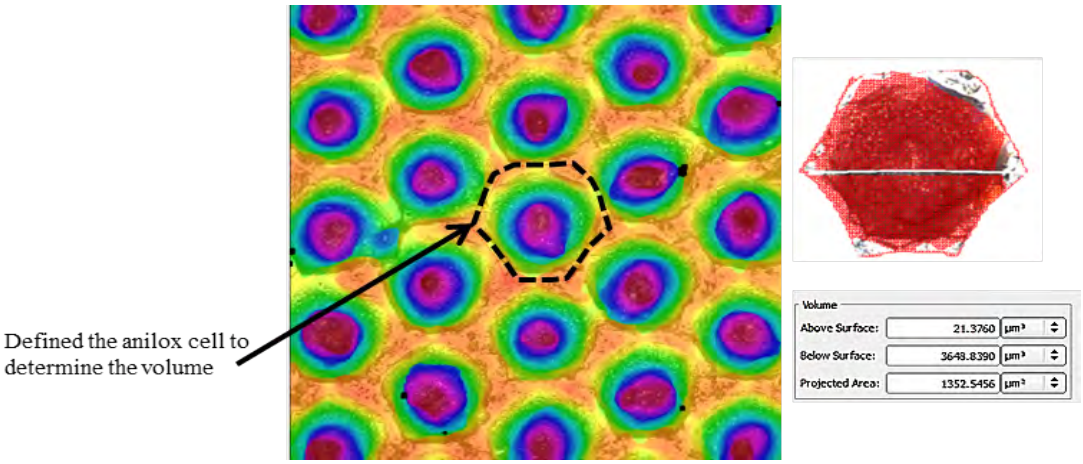

Figure 3.16: The extraction of the anilox cell volume

Table 3.6 shows the example of the anilox cell volume data.

Table 3.6: The example of the anilox cell volume data

Measurement	**Above Surface Volume (μm^3)**	**Below Surface Volume (μm^3)**	**Total Volume (μm^3)**	**Projected Area (μm^2)**	**Volume/Area (cc/m^2)**
1	5.9024	30,198	30,204	4,582	6.59
2	2.7552	32,043	32,046	4,715	6.80
3	2.4949	30,687	30,690	4,465	6.87
4	3.0424	31,219	31,222	4,588	6.81
5	4.5586	31,243	31,247	4,736	6.60
6	7.3553	29,947	29,954	4,579	6.54
7	5.9041	28,724	28,730	4,602	6.24
8	7.9091	28,683	28,691	4,552	6.30
9	7.6819	29,892	29,900	4,775	6.26
10	7.5722	29,274	29,281	4,616	6.34
11	7.0733	29,232	29,239	4,692	6.23
12	3.9901	30,046	30,050	4,515	6.66
13	7.8386	28,726	28,734	4,703	6.11
14	5.0569	30,285	30,290	4,712	6.43
15	4.536	30,354	30,359	4,733	6.41
16	4.7872	32,934	32,939	4,727	6.97
17	2.6347	30,714	30,717	4,384	7.01
18	4.0012	30,865	30,869	4,618	6.68
19	3.314	29,878	29,881	4,648	6.43
20	2.8053	30,516	30,518	4,655	6.56
Average			30,278	4,630	6.54
Standard Deviation			1,092	100	0.26
Standard Deviation (%)			4%	2%	4%

The cell depth and width of the anilox cell volume of 6.45cc/m^2 were approximately 2.3 and 1.9 times respectively larger to those of anilox cell volume of 2.76cc/m^2 (**Table 3.7**). Its depth-to-width ratio was approximately 22% whilst the anilox volume with 2.76cc/m^2 had the ratio of approximately 18%. The specification given by the anilox manufacturer is shown in **Table 3.8**,

Table 3.7: The summary results of the anilox measurement

Screen Count (LPI)	**Cell Volume (cc/m^2)**	**Depth (μm)**	**Width (μm)**	**Depth-to-Width Ratio (%)**	**Cell Shape**
348	6.45	16	73	22	Closed Cell
668	2.76	7	38	18	Closed Cell

Table 3.8: The manufacturing specification of anilox

Screen Count (LPI)	**Cell Volume (cc/m^2)**	**Cell Shape**
356	8.00	Closed Cell
635	3.50	Closed Cell

The details of the cell width and depth, and how they were measured was not given. The comparing of measurement and manufacturing data, the difference in the screen count per inch were approximately 2 to 5%. The differences in the screen count were not significant. The difference in the cell depth caused the difference (because the anilox cell volume was made up of the cell width and depth), and made the cell volume between the measurement and manufacturing data to be different of approximately 20%.

Anilox Open Cells Volume Measurement

Anilox elongated hexagonal open cells, wavy channels, and quadratic open cells (**Figure 3.17**).

Figure 3.17: Anilox elongated hexagonal open cells (a), wavy channels (b), and quadratic open cells (c)

The Elongated Anilox Open Cell Measurement

The depth of the elongated hexagonal cells was measured between the highest points of the walls of the cell and the deepest point of the cell (**Figure 3.18**). Because of the shape of the elongated anilox cell, the length of the anilox cell was measured between two walls along the horizontal position. The anilox cell width was measured between two walls along vertical position.

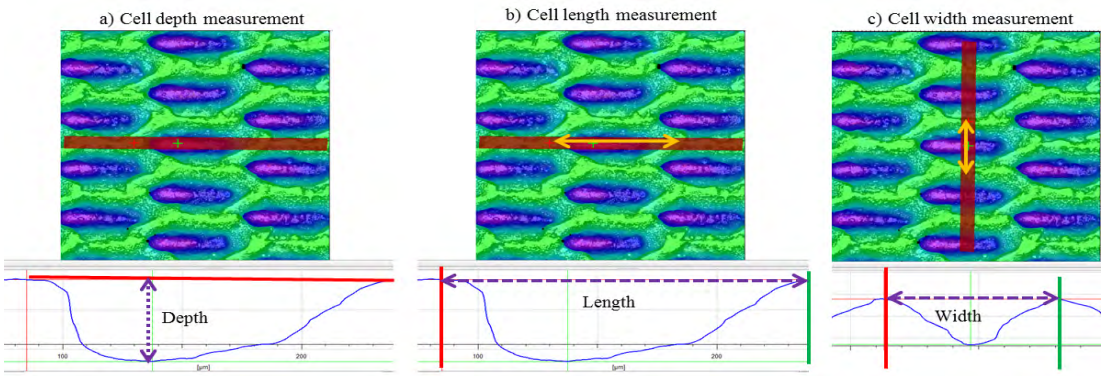

Figure 3.18: The measurement of the depth (a), length (b), and width (c) of the elongated hexagonal open cells

The cell shape of the elongated hexagonal open cells is different from the anilox closed cells. Its walls are removed to open up as a canal to let the ink stream flow; there is no specified boundary between cells. Therefore, the area to determine the volume has to be defined. Similarly to the method used with Wyko white light interferometry, the area was defined to extract the cell volume (**Figure 3.19**). The cell volume was then determined by dividing the volume by the projected area.

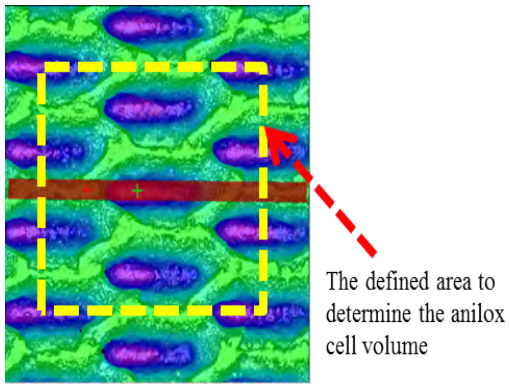

Figure 3.19: The measurement of the volume of the elongated hexagonal open cells

The Wavy Channel Anilox Cell Measurement

Similarly to the method used to determine the cell width and depth of the anilox elongated open cells, the depth was measured between the highest points of the walls of the cell and the deepest point of the cell (**Figure 3.20**). The anilox cell width was measured between two walls along vertical position.

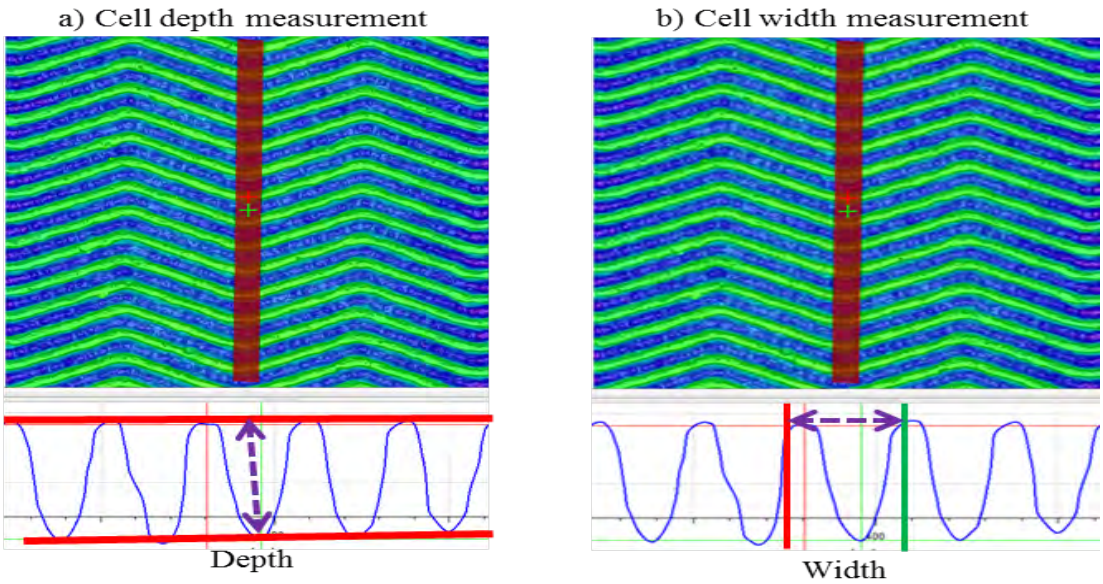

Figure 3.20: The measurement of the depth (a) and width (b) of the anilox wavy channel cells

Similarly to the method used to determine the cell volume of the anilox elongated open cells, the area was defined to extract the cell volume (**Figure 3.21**). The cell volume was then determined by dividing the volume by the projected area.

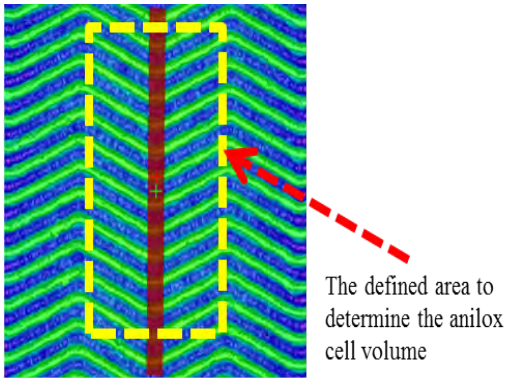

Figure 3.21: The measurement of the volume of the wavy channel anilox cells

The Quadratic Anilox Open Cell Measurement

Similarly to the method used to determine the cell width and depth of the anilox elongated open cells, the depth was measured between the highest points of the walls of the cell and the deepest point of the cell (**Figure 3.22**). The anilox cell width was measured between two walls.

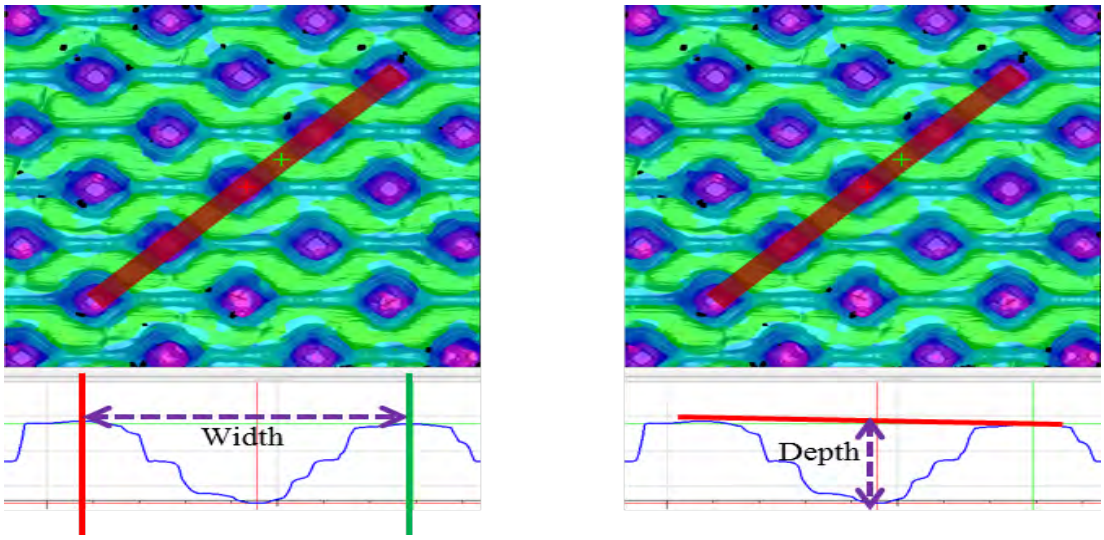

Figure 3.22: The measurement of the width and depth of the quadratic anilox open cells

Similarly to the method used to determine the cell volume of the anilox elongated open cells, the area was defined to extract the cell volume (**Figure 3.23**). The cell volume was then determined by dividing the volume by the projected area.

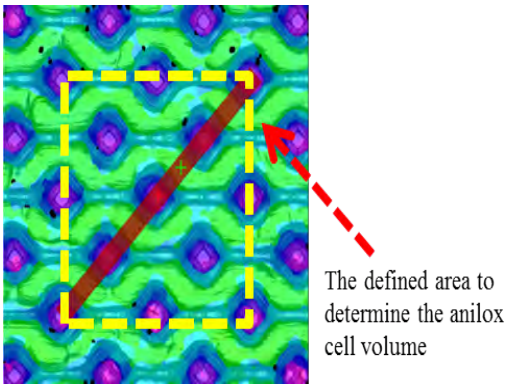

Figure 3.23: The measurement of the volume of the quadratic anilox open cells

3.3 Printing Plate Measurement

Printing plates with and without features were used. The plate with features had a combination of tonal patches and tracks. The tonal patches are used for the graphic print, and the tracks used for functional print. The tonal patch was composed of dot coverages of 1-100%. The dot size was measured to determine coverage. The track width was measured to determine the actual size. These were done to establish the original sizes as during the printing process, the dot and track sizes expanded due to the engagement with the anilox and the impression rolls; this and the ink spreading caused the printed dot and track to be larger than the original sizes. Knowing the original sizes helped in the interpretation of the ink spreading from the ink flow. The measurement was done using Wyko software for investigation done in chapter 4. Alicona InfiniteFocus microscope was used for the investigation done in chapter 7. The plate without features was a plain (solid) plate. The features of the printing plate were used for the printing process (**Figure 3.24**).

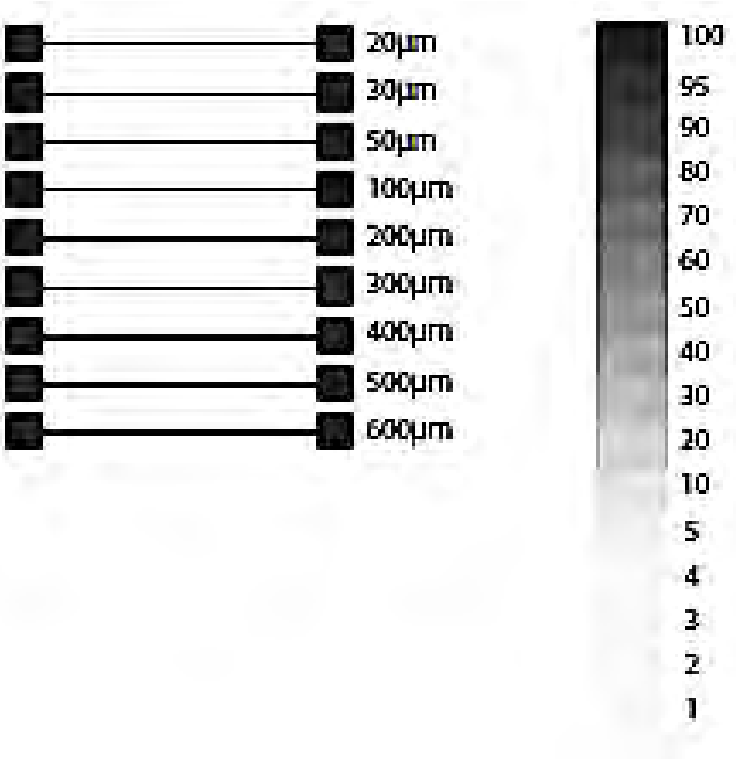

Figure 3.24: The features of the plate

3.3.1 Dot Area and Coverage Measurement

There are many dots on the plate (**Figure 3.25**). The size of the whole dot cell area is used to determine the numbers of dots per inch (LPI). The size of the top dot is determined to get the dot coverage area.

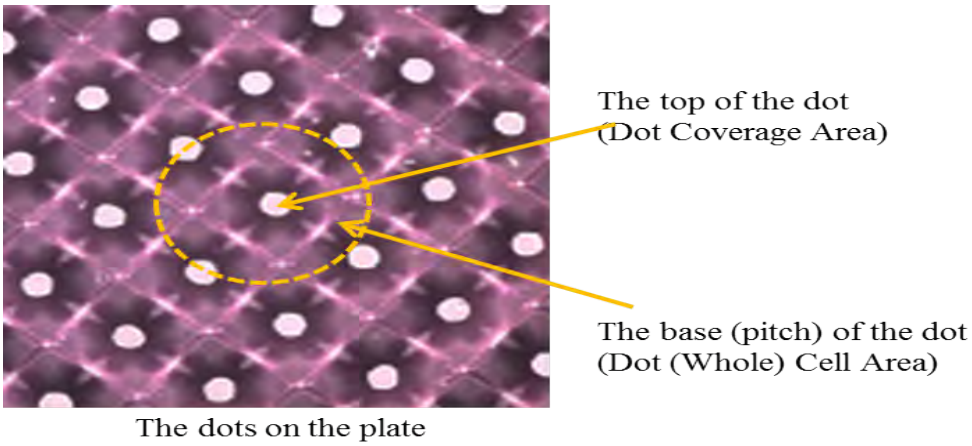

Figure 3.25: The example of the dot on the printing plate

3.3.1.1 Measurement by Wyko White Light Interferometry

The measurement of the printing plate was done using the Wyko white light interferometry with the optical magnification of 20x. The example of the determination of the dot cell area by measuring the width or length of the pitch (**Figure 3.26**). The dot cell area is then equal to the width^2. The dot coverage area is equal to the dot area divided by the dot cell area.

a: The image of the 50% dot coverage

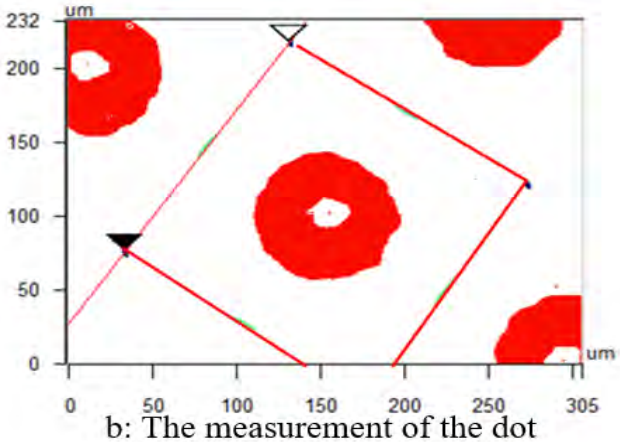

b: The measurement of the dot cell area using Wyko software

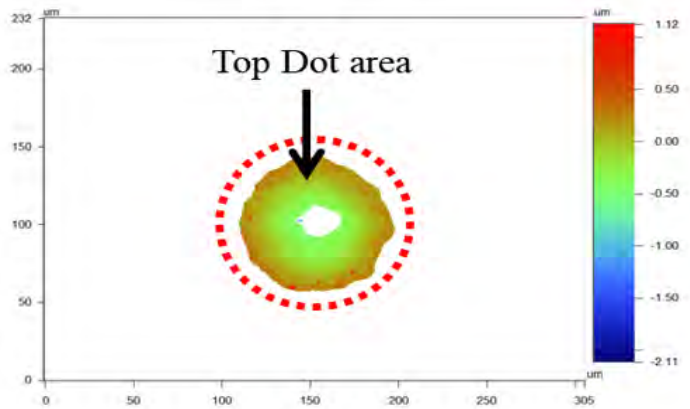

c: The measurement of the dot area coverage using Wyko software

Figure 3.26: The measurement of the dot cell area using Wyko software

Table 3.9 shows the dot measurement of 50% dot coverage.

Table 3.9: The measurement of dot coverage of 50%

Measurement	**Top Dot Area** ((μ**m**^{2}))	**Dot Cell Area** ((μ**m**^{2}))	**Dot Coverage** (%)
1	13126	31577	
2	12837	30415	
3	13031	30485	
4	13094	30345	
5	13115	31612	
6	12794	29206	
7	12601	29343	
8	12807	29825	
9	12663	31897	
10	12652	30555	
11	13124	31933	
12	13063	30206	
13	12971	29859	
14	12826	29790	
15	13009	29138	
Average	12915	30413	42
Standard Deviation	185	950	
Standard Deviation (%)	1	3	

3.3.1.2 Measurement by Alicona InfiniteFocus Microscope

The pitch area was used to determine the plate line ruling i.e. numbers of dots in a square metre (**Figure 3.27**).

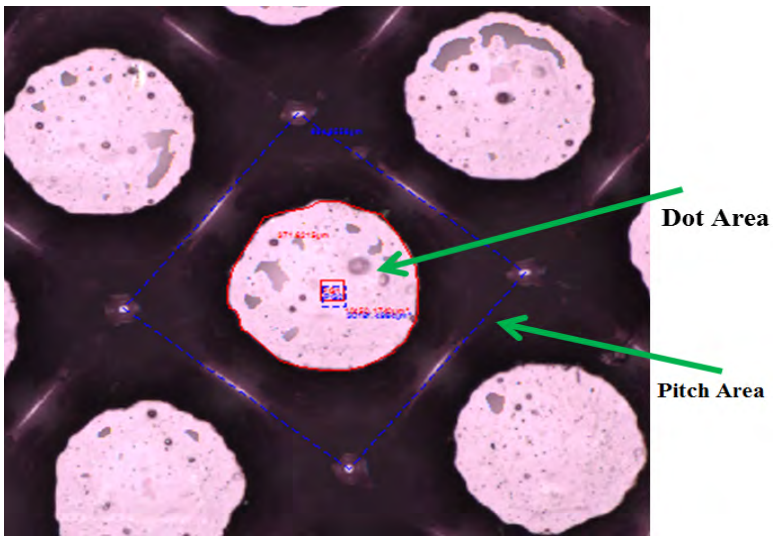

Figure 3.27: Dot and pitch areas

The dot coverage of 100% or solid plate was measured for surface roughness because the dot merged to the point that was impossible to identfy as dot (**Table 3.10**).

Table 3.10: Dot area coverage data

Nominal Dot Area (%)	**Measurement**	**Dot Area (μm^2)**	**Pitch Area (μm^2)**	**Dot Area Coverage (%)**
1	1	310	29,917	1
	2	302	28,587	1
	3	310	28,564	1
	4	298	29,050	1
	5	340	30,274	1
Average		312	29,278	1
Standard Deviation		16	781	0
Standard Deviation (%)		5	3	4
10	1	2105	30,233	7
	2	2115	29,962	7
	3	2074	29,692	7
	4	2035	29,715	7
	5	1903	29,300	7
Average		2046	29,780	7
Standard Deviation		86	347	0
Standard Deviation (%)		4	1	3
30	1	5976	29,277	20
	2	5859	29,504	20
	3	5944	29,371	20
	4	5873	29,571	20
	5	5881	28,946	20
Average		5907	29,334	20
Standard Deviation		51	245	0
Standard Deviation (%)		1	1	1
50	1	10,702	29,610	36
	2	10,984	30,033	37
	3	10,836	30,245	36
	4	10,726	29,585	36
	5	10,890	29,322	37
Average		10,828	29,759	36
Standard Deviation		117	372	0
Standard Deviation (%)		1	1	1

The standard deviation of the solid plate was higher than the threshold of 10%, however the surface roughness was less than 50nm (**Table 3.11**). Therefore, the surface roughness was ignored. When the size of the dot was small; the measurement numbers repeated five times, which was not significant in term of statistics. However, it confirmed was the consistency of the data, as the standard deviation was small.

Table 3.11: Surface roughness of dot area coverage of 100% /solid plate

Nominal Dot Area (%)	**Measurement**	**Surface Roughness (nm)**
100/Solid	1	36
	2	28
	3	22
	4	27
	5	33
Average		29
Standard Deviation		5
Standard Deviation (%)		19

3.3.2 Track Width Measurement

The track on the plate was measured using Wyko software (**Figure 3.28**). The profile was generate by selecting the whole area of the track and the average of the width is obtained. The example of the track measurement of track width of 100μm is shown in (**Table 3.12**).

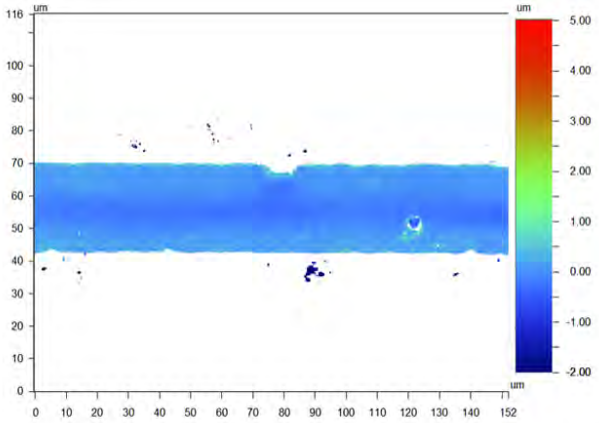

a: The image of the track on the plate using Wyko software to measure the track width

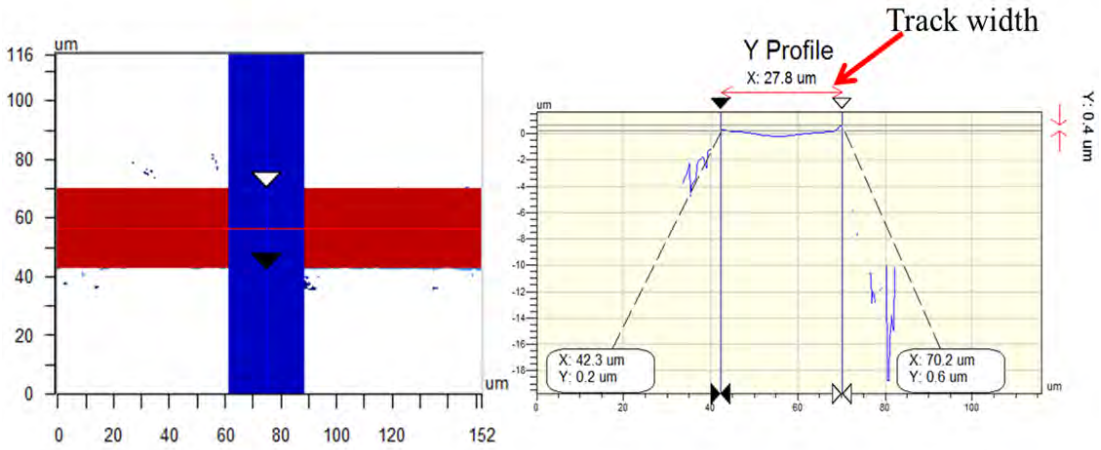

b: The track on the plate and its prole to measure the track width using Wyko software

Figure 3.28: The image of the track on the plate using Wyko software to measure the track width

Table 3.12: The measurement of track width of 100μm

Measurement	**Track Width (μm)**
1	115
2	115
3	117
4	114
5	114
6	120
7	122
8	119
9	117
10	118
11	112
12	111
13	112
14	112
15	113
Average	116
Standard Deviation	3
Standard Deviation (%)	3

3.4 Ink Characterisation

Density, surface tension, shear and extensional viscosity, viscoelastic, and filament breakup were measured to characterise the ink.

3.4.1 Density

The ink density was used to determine the surface tension. The Jaytec density bottle with the volume of 25ml used to determine the ink density (**Figure 3.29**). The dry and empty Jaytec density bottle was weighed. Then, it was filled with ink and full bottle was weighed; the ink weight was determined. The density was then calculated by dividing the weight of ink by the Jaytec bottle volume of 25ml.

Figure 3.29: The Jaytec density bottle used to determine the ink density

3.4.2 Surface Tension

Surface tension was measured to be used as a parameter to examine the wettability of the ink and used in the calculation of the extensional viscosity. The surface tension was measured using the Fibro DAT 1100 dynamic contact angle measurement system, which followed the principle of the pendant drop measurement. The pendant drop follows two principal assumptions; the drop is symmetric about the central vertical axis, and the drop is not in motion and surface or interfacial tension and gravity are the only two forces shaping the drop. The drop volume and surface area are calculated, and then the surface tension can be quantified [Woodward, 2018].

Figure 3.30: The Fibro DAT 1100 Dynamic Contact Angle Measurement System is used to determine the surface tension

The Fibro DAT 1100 Dynamic Contact Angle Measurement System used to determine the surface tension (**Figure 3.30**). The calibration with a liquid of known surface tension was performed to ensure the accuracy of the measurement. The known surface tension of the deionize water of approximately 73.1 dyn/cm was measured, prior to the ink surface tension being measured.

The surface tension measurement was carried out under the setup shown in

Table 3.13.

Table 3.13: The setup of the surface tension measurement

Description	**Units**	**Values**
Number of measurement	-	8
Drop size	μl	15
Density (DI water)	g/ml	1.00
Temperature	oC	20.0

The example of the surface tension measurement is shown in **Table 3.14**.

Table 3.14: The example of the measurement of surface tension

Measurement	Surface Tension (x10^{-3} N/m)
1	28.254
2	28.058
3	28.642
4	29.429
5	30.084
6	30.676
7	30.795
8	30.656
9	26.632
10	29.196
11	30.021
12	30.805
Average	29.437
Standard Deviation	1.27
Standard Deviation (%)	4

3.4.3 Shear Viscosity

The shear viscosity measurement was carried out to gain understanding of the ink flow during the printing process. The Bohlin Gemini HR nano rheometer was used (**Figure 3.31**). The measurement was repeated 3 times for each ink under the conditions described in **Table 3.15**.

Figure 3.31: The Bohlin Gemini HR nano rheometer used to determine the shear viscosity

Table 3.15: The shear viscosity measurement setup

Description	**Units**	**Values**
Plate	-	CP 4^0/40mm
Pre Shear conditions		
Apply pre-shear		
Each test run		
Controlled rate		
Shear rate	1/s	0.005
Apply time	s	10
Equilibrium time	s	10
Viscometry Parameters		
Minimum shear rate	1/s	1
Maximum shear rate	1/s	1,000
Samples		61
Temperature	^{0}	20

Table 3.16 shows the example of the shear viscosity measurement. The shear viscosity of each measurement was determined using the shear rate from 1 to $1{,}000^{-s}$ and the numbers of data was 31 for each measurement by measuring 3 times gave the data of over 90, which could significantly give the information whether the data was consistent.

Table 3.16: The shear viscosity data of the UV Black ink

Shear Rate (1/s)	**Viscosity 1 (Pa.s)**	**Viscosity 2 (Pa.s)**	**Viscosity 3 (Pa.s)**	**Average**	**Standard Deviation (%)**
1.00	1.20	1.04	1.03	1.09	9
1.16	1.17	1.02	1.01	1.06	8
1.35	1.13	1.00	0.99	1.04	8
1.58	1.10	0.98	0.96	1.01	7
1.84	1.07	0.95	0.93	0.98	7
2.14	1.03	0.92	0.91	0.95	7
2.50	1.00	0.90	0.89	0.93	7
2.92	0.97	0.87	0.86	0.90	6
3.40	0.94	0.85	0.84	0.87	6
3.96	0.91	0.82	0.81	0.85	6
4.62	0.88	0.80	0.79	0.82	6
5.39	0.85	0.77	0.77	0.80	6
9.96	0.75	0.69	0.68	0.70	5
25.01	0.63	0.58	0.57	0.59	5
29.16	0.61	0.56	0.56	0.58	5
33.99	0.59	0.55	0.54	0.56	5
39.63	0.58	0.54	0.53	0.55	5
46.21	0.56	0.52	0.51	0.53	5
53.88	0.55	0.51	0.50	0.52	5
62.81	0.53	0.49	0.49	0.50	5
73.23	0.51	0.48	0.47	0.49	4
85.38	0.50	0.47	0.46	0.48	4
99.55	0.48	0.45	0.45	0.46	4
214.48	0.40	0.38	0.38	0.39	3
339.92	0.35	0.34	0.34	0.34	3
396.32	0.34	0.33	0.32	0.33	3
538.75	0.31	0.30	0.30	0.30	2
628.11	0.30	0.29	0.29	0.29	2
732.34	0.29	0.28	0.27	0.28	2
853.85	0.28	0.27	0.27	0.27	2
995.54	0.26	0.26	0.26	0.26	2

3.4.4 Extensional Viscosity and Filament Breakup Profiles

The extensional viscosity measurement was carried out to gain understanding of the ink flow and its filament breakup during the printing process. The in-house extensional rheometer, was used to perform a CABER test.

The in-house extensional rheometer was used to determine the extensional viscosity (**Figure 3.32**). The measurement was repeated 3 times for each ink under, with the setup described below;

Figure 3.32: The in-house extensional rheometer used to determine the extensional viscosity

The plates with the diameter of 3mm were selected. The frame rate was set at 2,000 frames per second. The gap between 2 plates was set to approximately 0.4 aspect for the plate of diameter 3mm. This could be done by measuring the plate diameter on the computer monitor, which was approximately 8cm. Next, the gap between 2 plates was adjusted to approximately less than 4cm (on the computer monitor). The speed of the top plate was set with a velocity of 1,700 microns per second. The filament breakup of the ink was recorded using the high-speed camera. The CaBER software was used to extract the diameter profile of the ink. A graph of "time (s)" vs "deformation rate of ink diameter, D/D_0" was plotted. The slope or gradient of the data closed to the filament breakup was determined. The extensional viscosity was calculated using the formula of [Morgan et al., 2017]. The example images of the ink filament breakup were captured using the high speed camera (**Figure 3.33**).

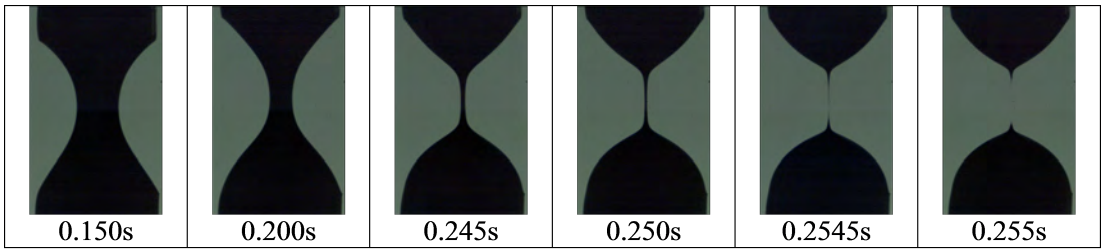

Figure 3.33: The images of UV Black ink filament breakup

The consistency of the measurement showed when all the measurements gave similar trend of behaviour. Then, the gradient of the plotted was examined. The gradient was used to determine the extensional viscosity as the formula below;

Apparent Extension Viscosity= [(2X-1)(Surface Tension)/-(Rate of change of mid-filament diameter)].

Where X is a dimensionless variable dependent on the tensile force and radius of the filament; it is equal to 0.7127 for Newtonian and 1 for non-Newtonian. (2X-1) is the correction factor. Therefore, the factor of 0.4254 (=2(0.7127)-1) was to multiply for the Newtonian ink, and 1 for the non-Newtonian ink [Morgan et al., 2017]. The accuracy of the apparent extensional viscosity was then compared to the theoretical value followed Trouton ratio in which the extensional viscosity was approximately 3 times of the shear viscosity. The rate of radius change of UV Cyan ink is shown in **Figure 3.34**.

As the shear rate increased and up to 1,000 (1/s), the shear viscosity of UV Cyan was constant in which the ink displayed the Newtonian attribute. Therefore, the Trouton ratio could be applied to check for the accuracy, and the value should be approximately three times of shear viscosity. The slope of graph was the rate of change of the mid-filament diameter, which was used to determine the apparent extensional viscosity.

The example of the calculation to get the apparent extensional viscosity, and then compare to the theoretical extensional viscosity (**Table 3.17**). The linear trend equation retrieved from the graph of rate of radius change, and its slope of -1.43 was used in the calculation with the initial filament diameter (D_0) of 0.003m, the surface tension of the ink of 29.437x10^{-3} N/m, the shear Viscosity at 1000 (1/s) of 1.05, and correction factor of 0.4254 for Newtonian material. The calculation of apparent extensional viscosity showed a good proxy to the theoretical extensional viscosity. This confirmed that the data could be used for further analysis.

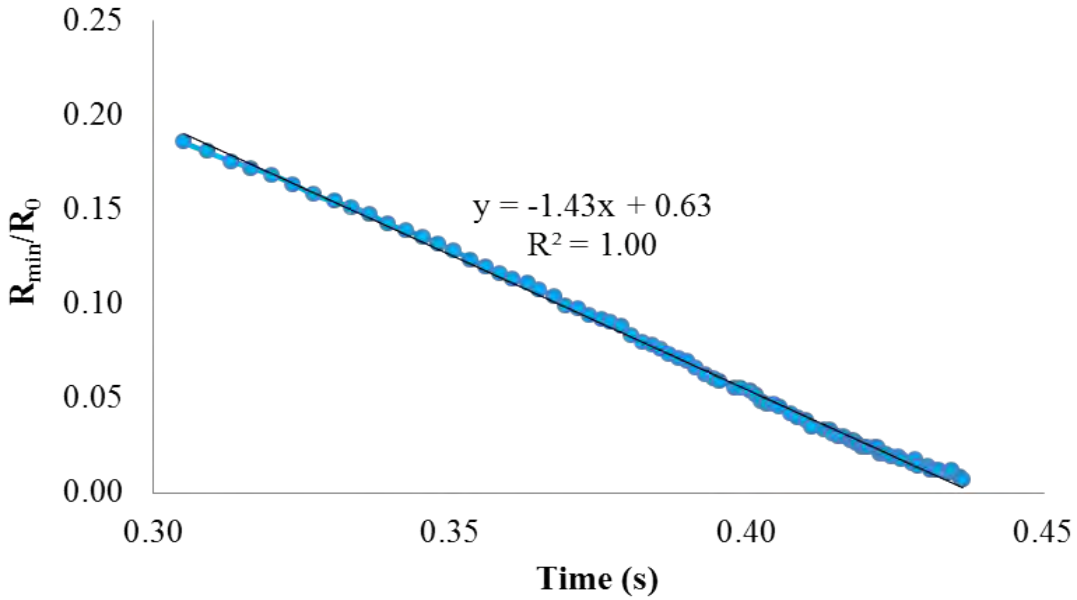

Figure 3.34: Rate of radius change of UV Cyan ink

Table 3.17: The comparison of apparent extensional viscosity to the theoretical value of UV Cyan ink

Linear Trend Equation	**Extensional Viscosity ($k/s^2.m$)**	**Apparent Extensional Viscosity ($k/s^2.m$)**	**Theoritical Extensional Viscosity–Trouton ($k/s^2.m$)**
y1=-1.43x+0.63	6.86	2.92	3.15
y2=-1.43x+0.63	6.86	2.92	3.15
y3=-1.43x+0.63	6.86	2.92	3.15

3.4.5 Viscoelastic Test

The oscillation test (stress-sweep test; measurement by increasing the shear stress) was carried out to examine the viscoelastic behaviour of the inks. The test could also be use to determine the linear viscoelastic region (LVR) of the materials in which the elastic and viscous modulus were constant or independent of shear stress, and where there was no structure break down of the material. LVR region indicates the maximum shear stress that the materials can withstand before the structure break down. The test was used to determine the crossing over point where elastic and viscous modulus were equal, and where if the shear stress increased, the material would change behaviour from solid-like to liquid-like or vice versa [Mallik, 2009]. Solid-like behaviour of the ink happens when its elastic modulus was greater than its' viscous modulus. During printing process, if the ink behaviour is solid-like, the ink will resist the stretching (deformation) and the ink will tend to recoil back to the anilox cells.

If the ink behaviour is liquid-like, the ink will stretch and flow out of the anilox cells.

The elastic modulus indicates the filament stretching behaviour of the ink. The greater elastic modulus will elongate longer and increases the pull-out fraction. The ink, which had greater elastic modulus and was under the region of liquid-like, would be pulled out and flow more out of the anilox cells.

The small amplitude oscillatory shear (SAOS) test is used to measure viscoelastic properties of the ink. The sample is oscillated between two plates (**Figure 3.35**). The amplitude of oscillation is equal to the maximum applied stress or strain.

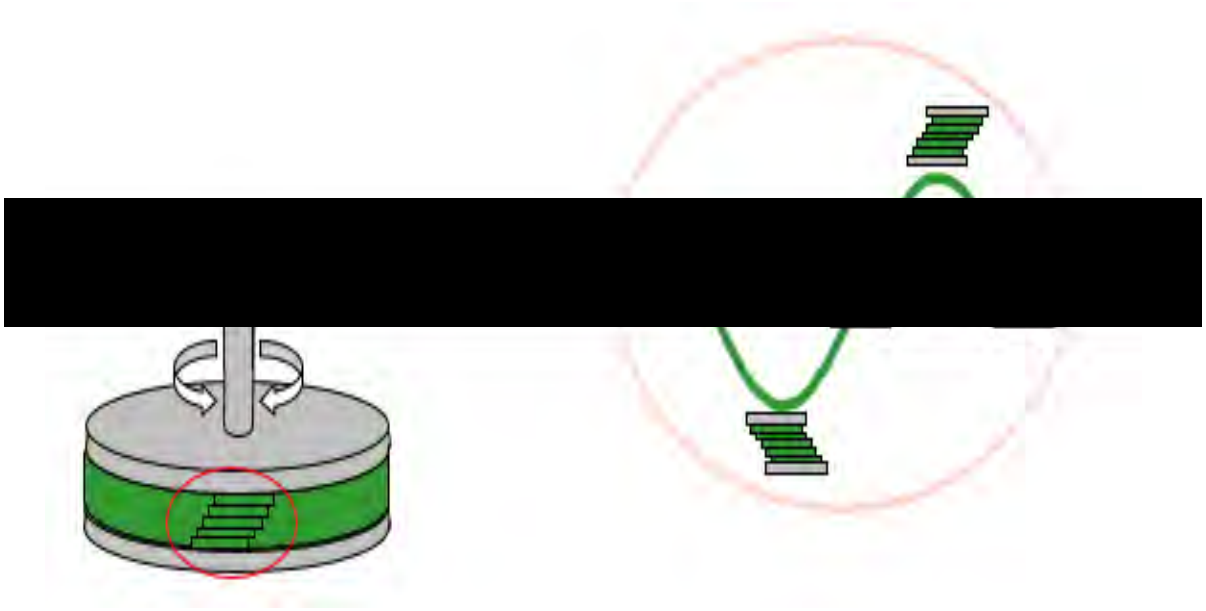

Figure 3.35: A sample loaded between parallel plates with an oscillatory (sinusoidal) shear profile applied [Malvernpanalytical.com, 2019]

For a purely elastic material, the maximum stress occurs at the maximum strain where the deformation is the greatest. Both stress and strain are in-phase at this point (**Figure 3.36a**). For a purely viscous material, the maximum stress occurs at the maximum strain rate, the flow rate is the greatest, and the stress and strain are out-of-phase by 90^o (**Figure 3.36c**). For a viscoelastic material, the phase difference between stress and strain is between 0^o and 90^o (**Figure 3.36b**). The phase difference indicates whether the ink will behave as solid-like or liquid-like. If the phase is between 0^o and 45^o, the ink will be dominant by solid-like behaviour; the shear stress has to be greater than its yield stress or the point where the shear stress causes the phase to be greater than 45^o for the ink to start flowing. If the phase is between 45^o and 90^o, the ink will be dominant by liquid-like behaviour; the ink will flow with a small

initial shear stress. The phase of 45^o is the threshold between the solid-like and liquid-like.

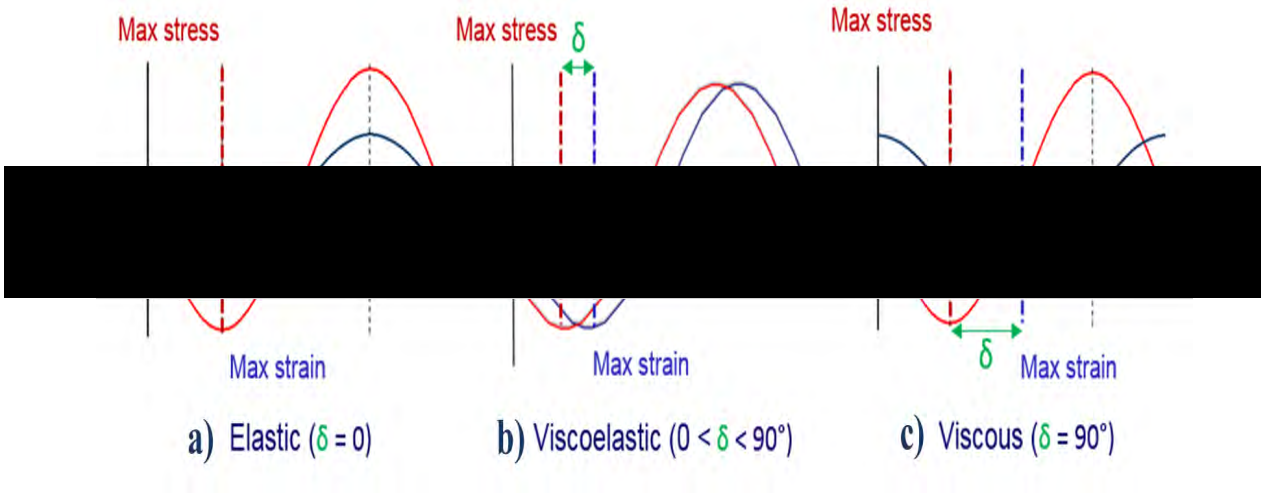

Figure 3.36: Stress and strain wave relationships for a purely elastic (ideal solid), purely viscous (ideal liquid) and a viscoelastic material [Malvernpanalytical.com, 2019]

The ratio of the applied stress to the measured strain gives the complex modulus (G*), which is a quantitative measure of material stiffness or resistance to deformation. The elastic modulus (G') and viscous modulus (G") can be determined from the complex modulus and phase angle.

G'=G*cos(phase angle) and **G"=G*sin(phase angle)**

The linear viscoelastic region (LVER) of the ink can be determined by displaying the independent of elastic and viscous modulus over the range of the shear stress (**Figure 3.37**). The shear stress is insufficient to breakdown the structure of the ink in the linear viscoelastic region. Beyond this point, the structure of ink is broken down, and cause the properties of the ink to change. For example, the solid-like behaviour changes to liquid-like behaviour as the shear stress increases.

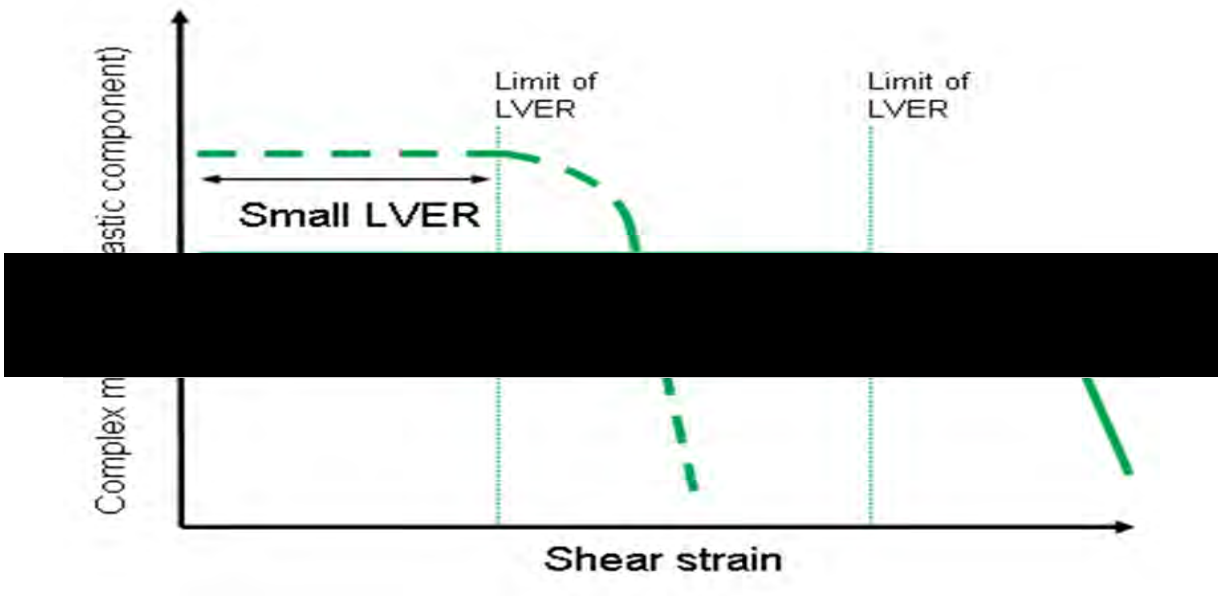

Figure 3.37: The LVER for different materials as a function of applied strain [Malvernpanalytical.com, 2019]

The ink elastic modulus was measured using the Bohlin Gemini HR nano rheometer. The small amplitude oscillatory shear (SAOS) mode (stress-sweep test; measurement by increasing the shear stress) was used. The measurement setup is shown in **Table 3.18**.

Table 3.18: The elastic modulus measurement setup

Description	**Units**	**Values**
Amplitude Sweep		
Frequency	Hz	1
Control Stress		
Minimum Stress	Pa	0.1
Maximum Stress	Pa	10.0
Temperature	^{o}C	20

Figure 3.38 shows the example of the elastic (G') modulus of HD Black and Yellow inks.

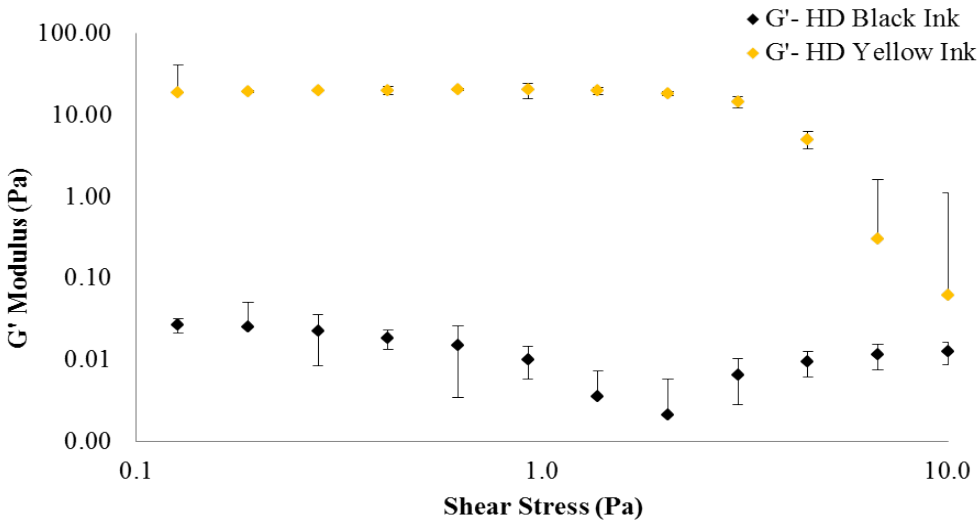

Figure 3.38: The comparison of elastic (G') modulus of the HD Black and Yellow inks

3.5 Printed Substrate Measurement

Three parameters; the optical density, the track width and its ink volume were measured for the glass substrate. The optical density and the ink volume of tracks were measured for the comparison of the ink release from the anilox cells. The track width was measured to examine the ink spreading effect. The optical density of the printed tonal patches on the glass substrate was measured using the spectrophotometer with the white background. The ink volume and width of the printed track were extracted using the WCPC software.

The printed substrate in the commercial press trial (chapter 5) was reverse printed and then coated with white ink; hence it could not be examined using Wyko white light interferometry. The samples had to be examined using the Leica Wild M3Z Stereo microscope. Image J software was used to extract the data; printed dot area.

3.5.1 Optical Measurement

Spectrophotometer (**Figure 3.39**) was operated under the conditions in **Table 3.19**. Because the size of the printed area of each area coverage was small, each area coverage was only measured 3 times for each sample. There were 9 measurements done for each area coverage. The average and standard deviation for each area coverage were calculated. The result was reported using the average data.

Figure 3.39: The spectrophotometer used to measure the optical density

Table 3.19: The spectrophotometer measurement setup

Description	**Values**
Illumination	50
Observe angle	2
Density standard	ANSI T
White base	Abs
Filter	No
Measuring mode	Reflectance

Table 3.20 shows the example of the optical density measurement of the 50% nominal dot area coverage.

Table 3.20: The example of the optical density measurement of the 50% nominal dot area coverage

Measurement	**Optical Density**
1	2.21
2	2.21
3	2.20
4	2.21
5	2.21
6	2.21
7	2.21
8	2.21
9	2.21
Average	2.21
Standard Deviation	0.00
Standard Deviation (%)	0.15

3.5.2 Ink Volume of Printed Track

The data of the ink volume of the tracks was extracted using the WCPC software (**Figure 3.40**) as described in 3.2.1.2. The examples of the data of the ink volume of track of the nominal track width of 600μm (**Table 3.21**).

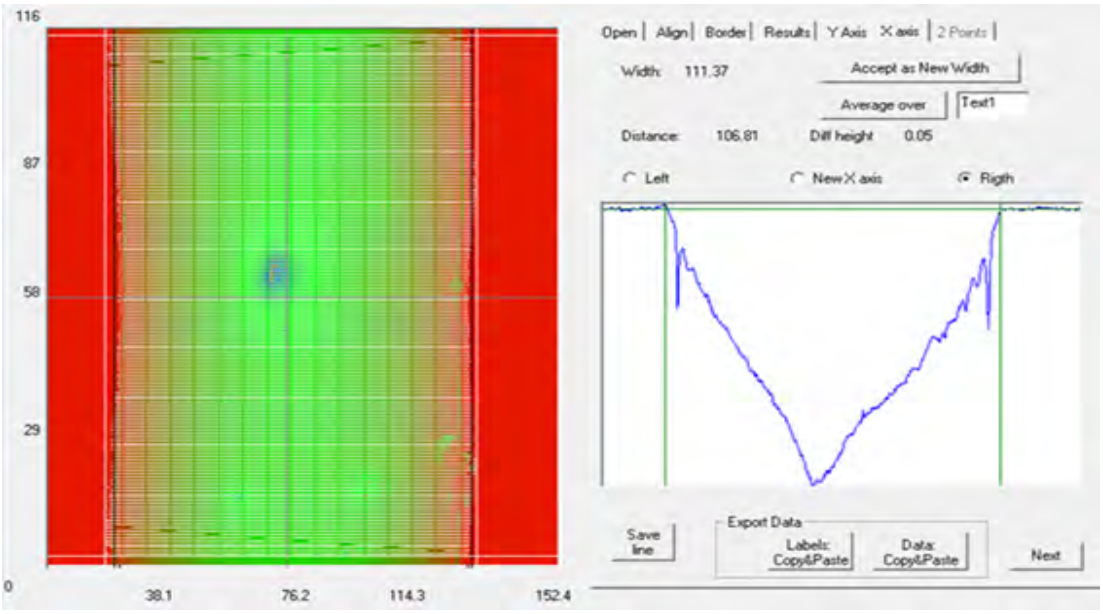

Figure 3.40: Track ink volume determination using WCPC software

Table 3.21: The example of the data of the ink volume of track and width

Measurement	**Ink Volume of Track (μm^3)**	**Projected Area (μm^2)**	**Width (μm)**	**Ink Transfer (cc/m^2)**
1	7,727,062	875,054	977	8.83
2	6,569,301	862,546	972	7.62
3	7,183,982	867,474	979	8.28
4	6,351,011	789,681	888	8.04
5	6,981,055	809,613	900	8.62
6	7,344,588	817,356	908	8.99
7	6,271,862	803,546	905	7.81
8	7,332,565	820,565	922	8.94
9	8,395,112	824,714	930	10.18
Average	7,128,504	830,061	931	8.59
Standard Deviation	682,528	30,642	35	1.00
Standard Deviation (%)	10	4	4	9

3.5.3 Printed Dot Area Measurement Using Leica Microscope

A stereo microscope, Leica Wild M3Z Stereo Microscope (**Figure 3.41**), was used to examine the printed dots. Optical magnification of 40X (maximum available) was used to capture the images of the printed dots on the substrate. The printed dot area data was extracted using the image J software. Before the determination of the printed dot, the area calibration of a known area specimen was done to ensure the consistency and accuracy of the data.

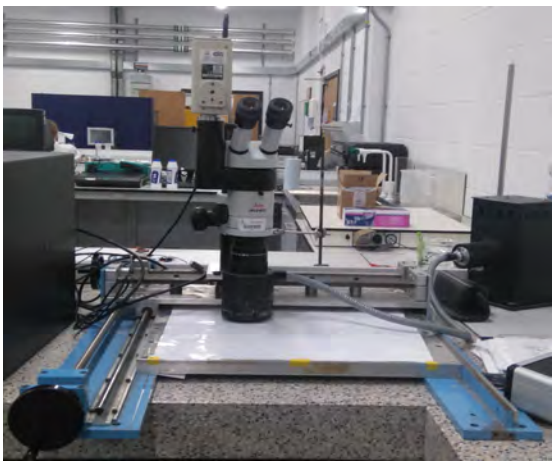

Figure 3.41: Leica Wild M3Z Stereo Microscope used to examine the printed substrate

3.5.3.1 Measurement of the Printed Dot Area and Dot Coverage

The software gave the total area of all the captured whole square area, and the percentage of dot coverage (**Figure 3.42**). The dot coverage of nominal dot coverage of 5% was given as the example of measurement (**Table 3.22**).

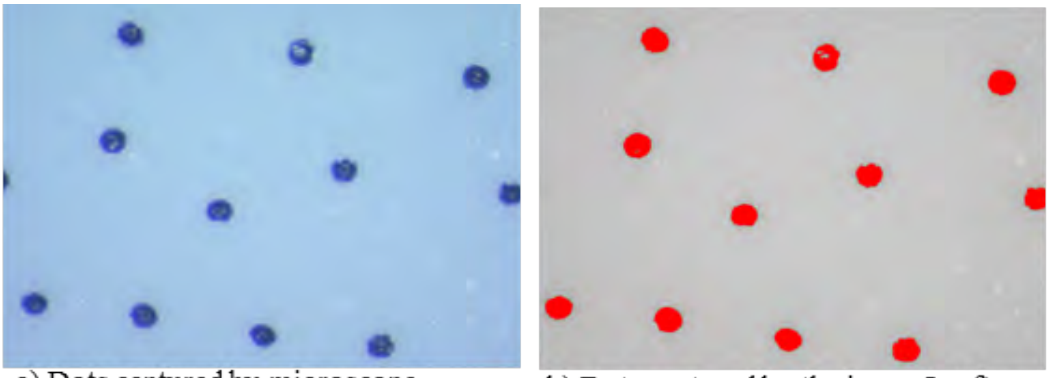

a) Dots captured by microscope

b) Dots captured by the imageJ software to extract the area of all the dots

Figure 3.42: Printed dots (a) captured by the Leica Wild M3Z Stereo Microscope, and the printed dots captured by the imageJ software to extract the printed dot area (b)

Table 3.22: Example of the dot coverage of 5% nominal dot coverage

Measurement	**Whole Square Area (μm^2)**	**Dot Coverage (%)**
1	108672	5
2	102527	5
3	114008	5
4	100758	5
5	111546	5
6	100273	5
7	110222	5
8	128062	6
Average	109509	5
Standard Deviation	9106	0
Standard Deviation (%)	8	8

3.6 Determination of Number of Revolution To Fill the Anilox Cells

The engagement between the doctor blade and the anilox roll on the RK flexiproof 100 press (**Figure 3.43**) create the ink chamber to supply ink to the anilox cells. The contact between the doctor blade and anilox roll was adjusted until the ink coated evenly and over the anilox roll. The blade was not forced to avoid the damage on the anilox surface.

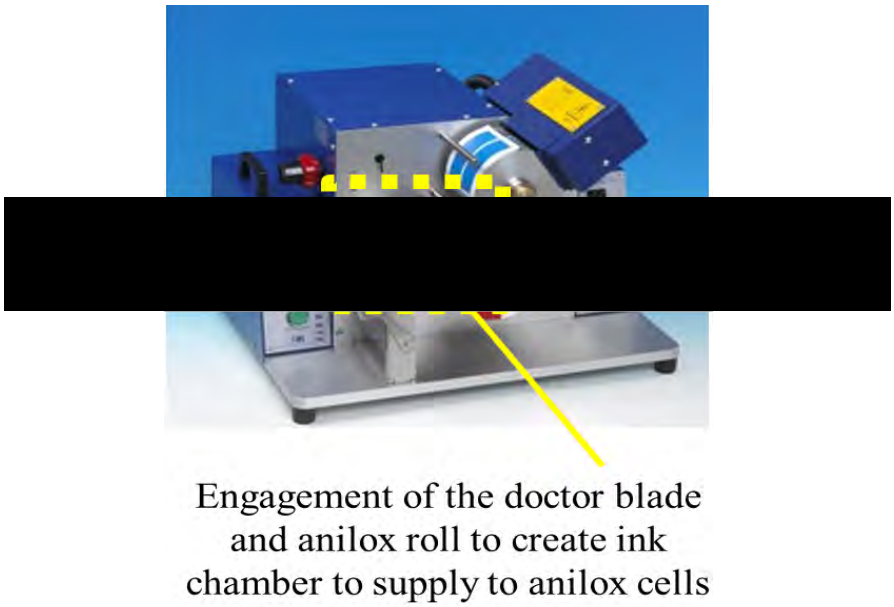

Figure 3.43: The reel-to-reel (RK flexiproof 100) press [rkprint.com]

The following procedure was used to determine the number of revolutions required to fill the anilox cells. After one revolution, the inked anilox roll was measured using Alicona InfiniteFocus microscope (**Figure 3.44**) and the inked volume was calculated. The number of revolutions were increased to two and three. After the third revolutions, the inked volume started to plateau. Therefore, the last step was to increase the revolutions to five.

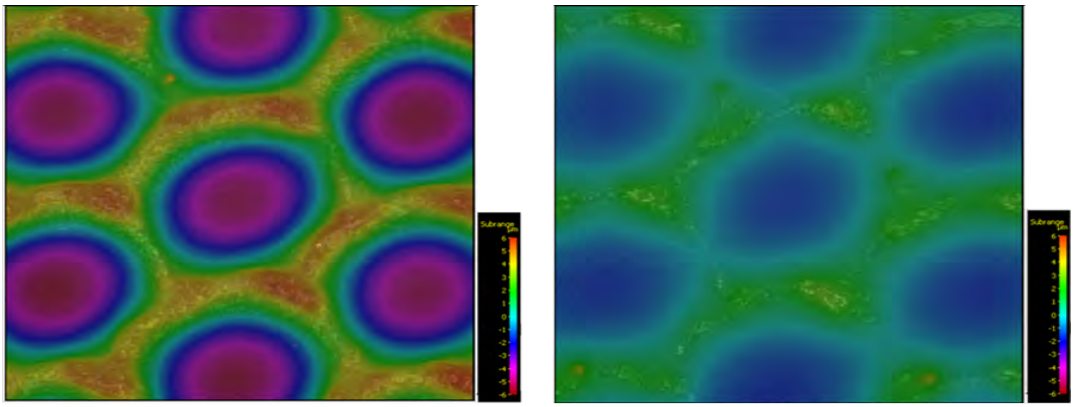

a) The image of the anilox empty dry cell

b) The image of the anilox inked cell

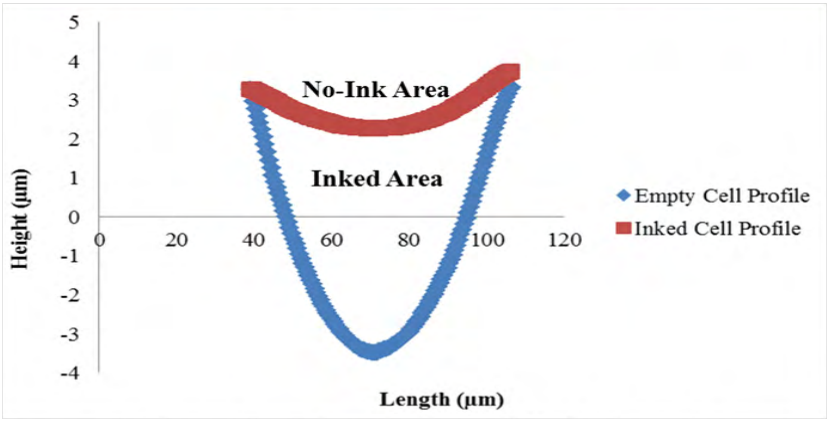

c:The profiles of empty dry and inked anilox cells

Figure 3.44: The image of the anilox empty dry (a), inked cells (b), and their cell profiles (c)

There was no significant increase of the inked volume after the third revolution (**Figure 3.45**). To optimize the inked volume, five revolutions were used to fill the anilox cells.

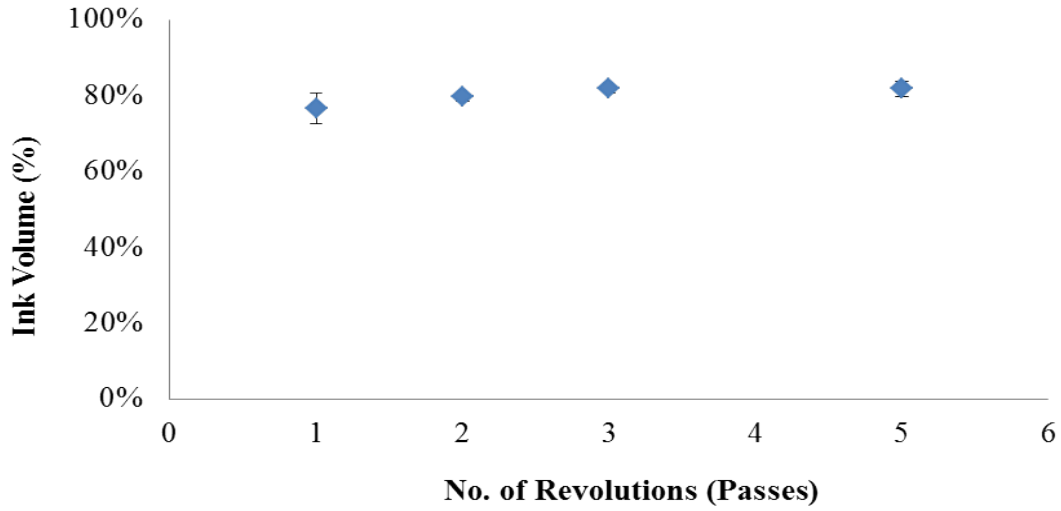

Figure 3.45: Numbers of revolution against the inked volume in anilox cells

To establish the number of revolution to ink the anilox open cells, further investigation of the inked volume was carried out using the elongated hexagonal open cell with the cell volume of 8.62cc/m^2. The UV carbon ink was used. The numbers of the revolutions used for inking were 5, 6, and 7. The profiles of empty and inked anilox cells with revolutions of 5, 6, and 7 were compared (**Figure 3.46**). The cell profiles showed no significant difference of the ink volume of those revolutions.

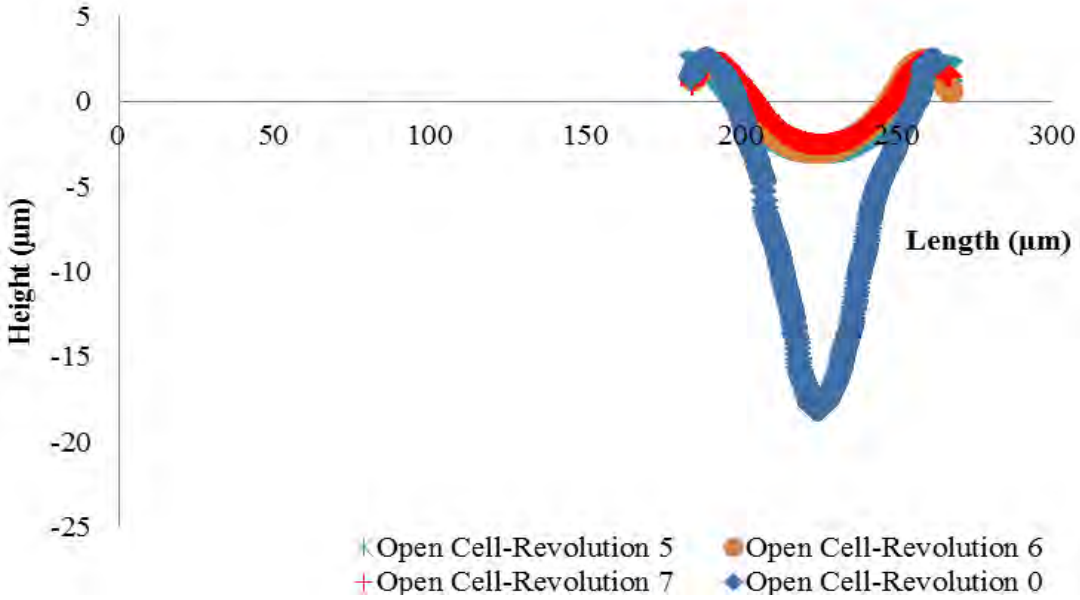

Figure 3.46: The comparison of cell profiles of the empty and inked anilox cells

The increase number of the revolutions to 7 from 5 did not give significant increase (**Figure 3.47**). For consistency, the revolutions were kept at 5 for all

experiments.

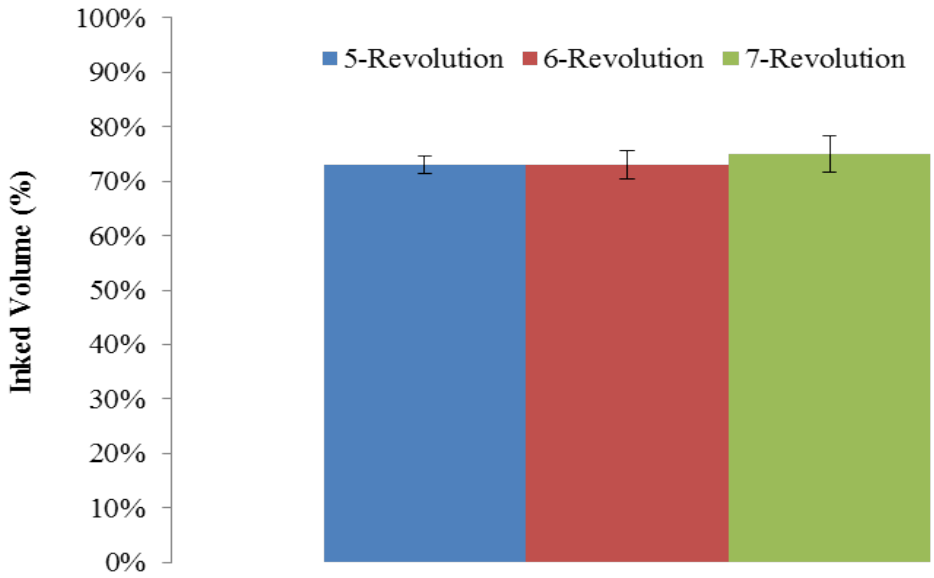

Figure 3.47: The comparison of the inked volume using revolutions of 5, 6, and 7

3.7 Closure

The methods described in this chapter were applied throughout the investigation to characterise the laboratory scale anilox roll, dot plate, and inks which will be used for the investigation of ink release from the anilox cells. In the next chapter, the ink transfer to glass, a non-absorbent substrate, is investigated.

Chapter 4

Flexographic Printing Process on Glass Substrate

4.1 Introduction

Flexo printing was carried onto glass to evaluate ink release from conventional closed pyramid cells onto a non-absorbent substrate to gain initial understanding the effect of the anilox cell geometries on print quality. These were compared with previous results as a precursor to the trials on the commercial printing press (chapter 5). Two anilox cell bands with similar cell volume but different cell width and depth were evaluated with a UV flexo Black ink on a sheet fed flexo press. The investigation started by characterizing the anilox cells, the printing plate, and the ink. The features on the printing plate were tonal patches of 1-100% dot area coverage, and tracks of width of 20-600μm. The measured print parameters were the optical density for the tonal patch, and the track ink volume and width as these parameters would indicate the ink release of the anilox cells.

A cooper sheet-fed flexographic press was used for the investigation (**Figure 4.1**). The press was developed for printing packaging. It features automatic sheet detection, running register adjustment and automatic print cylinder throw-off. It can be used with a wide range of flat packaging substrates such as collapsed corrugated cases, solid board, plywood (**Table 4.1**) [Cooper Printing Machinery LTD, 2020].

Table 4.1: Printing capacity of cooper sheet-fed flexographic press [Cooper Printing Machinery LTD, 2020]

Max sheet width (mm)	**Max sheet length (mm)**	**Max print width (mm)**	**Max print length (mm)**	**Maximum machine speed (sheets/hour)**
950	1450	800	710	5000

Figure 4.1: Cooper sheet-fed flexographic press [Cooper Printing Machinery LTD, 2020]

4.2 Experimental Method

To operate the press, the ink chamber was filled to supply the ink to the anilox cells. The engagement was adjusted by setting the gap between the anilox roll and the printing plate roll untill it reached the "kiss contact" position, where the ink coated over the plate while causing minimum deformation to the plate. The gap distance could not be specified as the cooper flexo sheet press had no function to set the distance between the rolls. The engagement between the printing plate roll and the glass substrate was set. Similarly to adjustment of the engagement between the anilox roll and the printing plate roll, the gap between the printing plate roll and the glass substrate was adjusted until the image on the printing plate was printed evenly without breaking the glass substrate. The printing speed was set at approximately 20% of the maximum speed of approximately 120m/min [Cooper, 2019]. A sheet of glass substrate was aligned to the reference point. When the press is operated; the glass substrate engages with the printing plate, which pulls the glass substrate through and the image on the printing plate is printed on the glass substrate. Three sheets of glass substrates were printed. Each print was dried immediately after print using the UV dryer.

Table 4.2: The summary of anilox measurement

Screen Count (LPI)	Cell Volume (cc/m^2)	Width (μm)	Depth (μm)	Depth-to-Width Ratio	Surface Roughness (μm)	Shapes
68	49.22	361	187	0.52	19	Closed Cell
120	47.60	204	182	0.89	30	Closed Cell

The engraving bands on the anilox were approximately the same volume even though the cell count of one was approximately twice the other and the cell depths were similar (**Table 4.2**). The anilox roll with 120LPI had the width of approximately 42% smaller than the anilox roll with 68LPI. Even though the anilox cells of anilox roll with 120LPI was smaller, it had approximately the same cell volume by virtue of having more cells per square metre with similar cell depth. The anilox cell with the wider cell (68LPI) expected to release the more ink than the narrower cell because it had greater opening for the ink to easily flow out (**Figure 4.2**). The cell walls of the 68LPI are both shallower angle and smoother which would further improve ink flow.

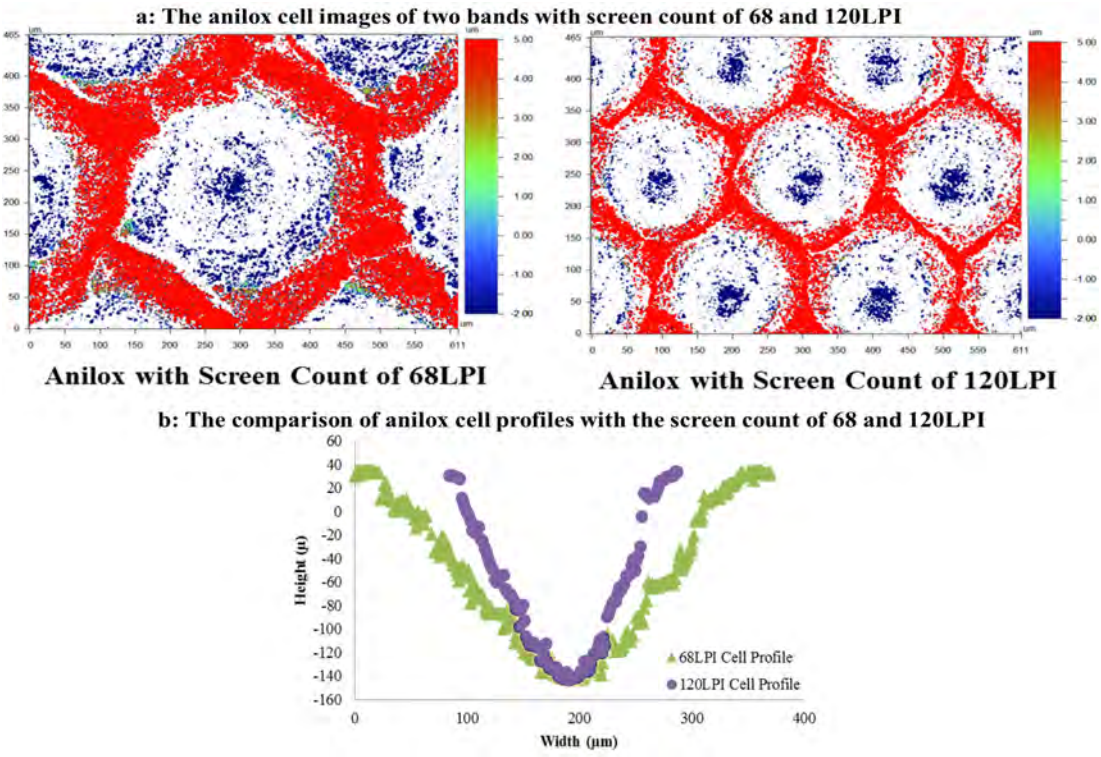

Figure 4.2: a: The anilox cell images of two bands with screen count of 68 and 120LPI, b: The comparison of anilox cell profiles with the screen count of 68 and 120LPI

The dot area coverage and track width on the printing plate were determined using white light interferometry with the optical magnification of 20x (**Figure 4.3**). During the printing process, the dot and track sizes became larger than the original size on the plate due to the engagement with the anilox and the impression rolls; and ink spreading.

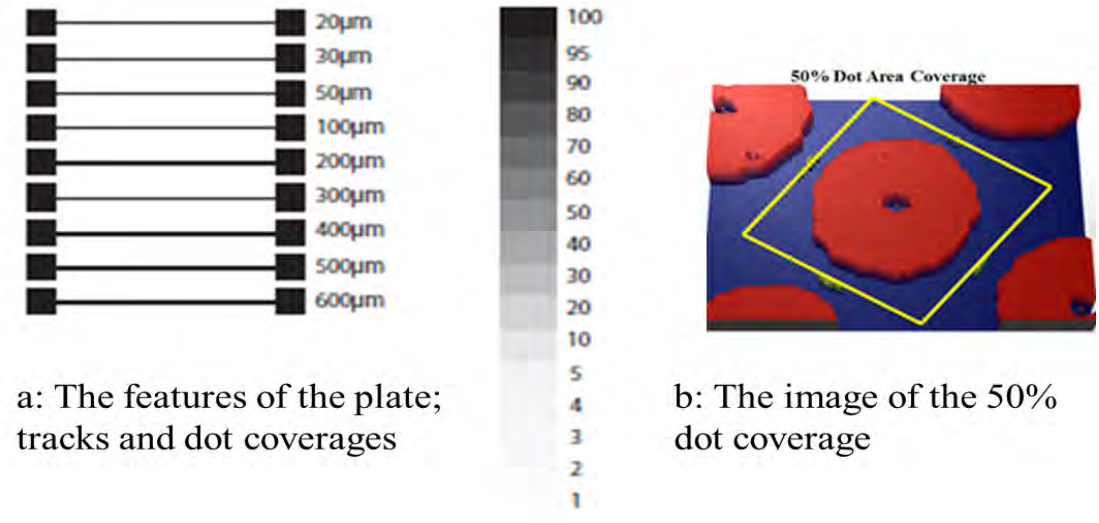

Figure 4.3: a: Plate features and b: Example of the image of the 50% dot coverage

The actual dot coverages below 20% are larger than the nominal coverage (**Figure 4.4**). The size of dots reaches the minimum dot size. Whilst above 50% the actual coverage is lower than the nominal, to compensate for the expansion during the contact with the substrate. At 5%, the actual dot coverage was double the nominal due to the limitation of production. The percentage difference dropped rapidly to be negative at above 20% to compensate for the expansion of dot during the printing process.

a: Dot coverages of tonal patch compared to nominal dot coverage

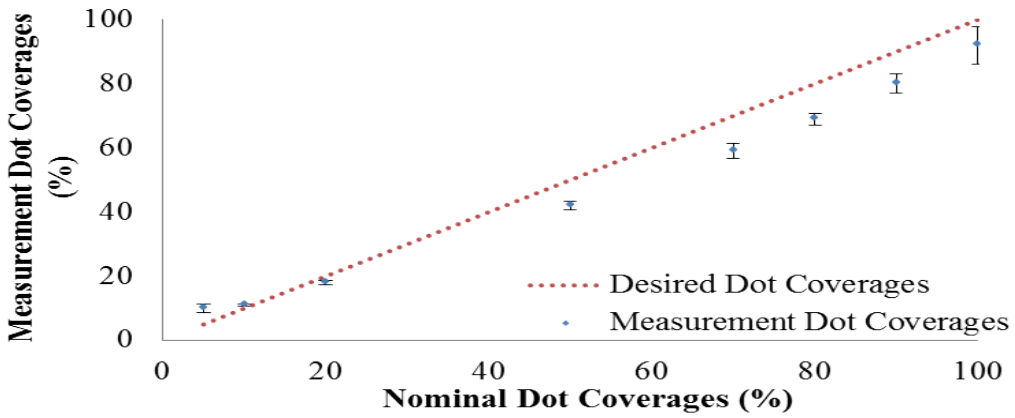

b: Percentage of the difference between the nominal and measured values

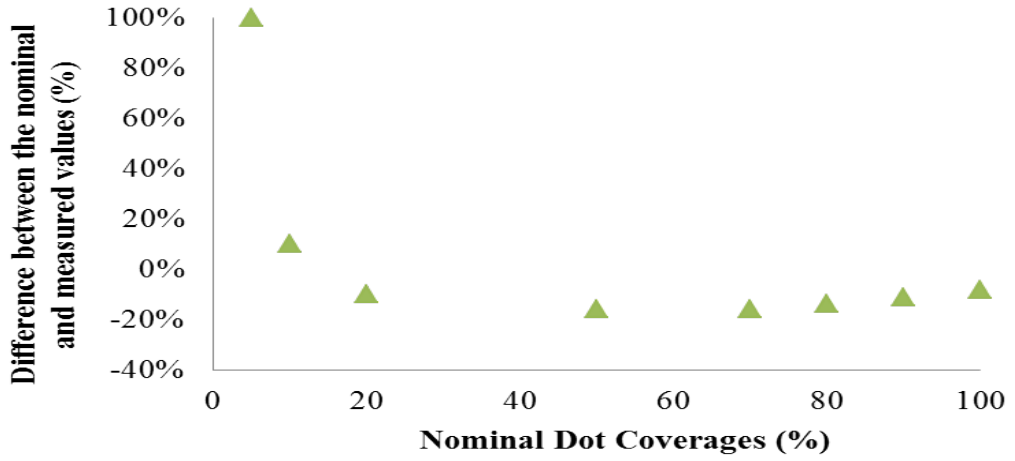

Figure 4.4: The graph of measurement dot coverages of tonal patch against nominal dot coverages

The actual track widths were slightly wider than the nominal widths (**Figure 4.5**). When the printed track widths were measured any significantly difference would indicate ink spreading because the actual size of the track width was approximately the same as the nominal values.

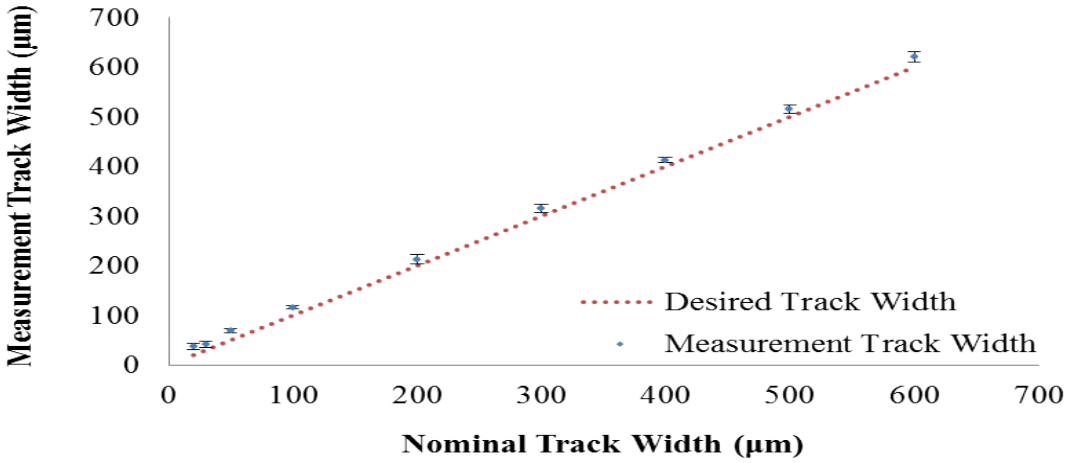

Figure 4.5: The graph of measurement track widths against nominal track widths

The ink had a shear viscosity at $1s^{-1}$ of approximately 1Pa.s and was shear-thinning (**Figure 4.6**). While this was a typical initial value of shear viscosity for an ink used flexographic printing, these are normally assumed to be approximately Newtonian i.e. the viscosity is constant with shear. However, flexographic inks are traditionally solvent based, whereas this was a black UV cured ink.

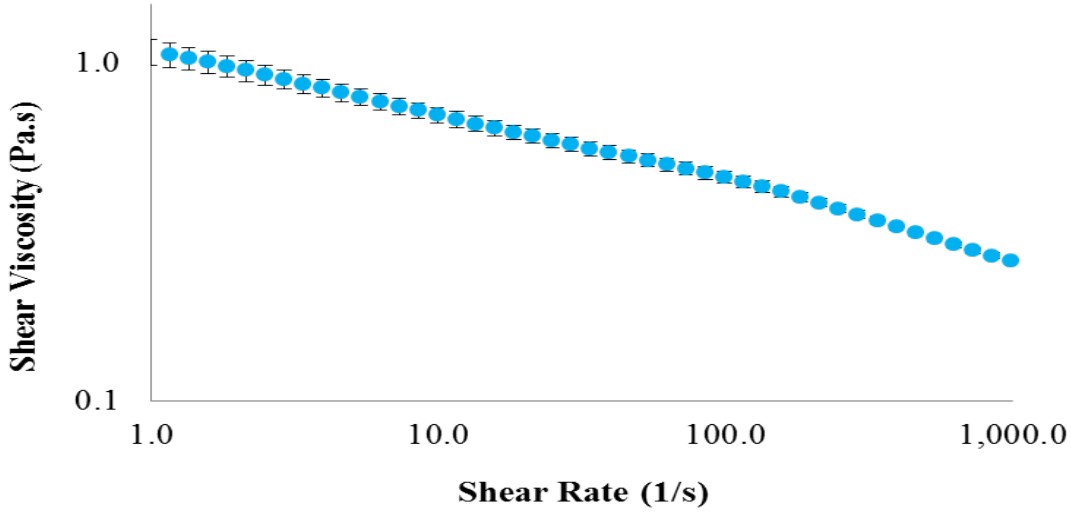

Figure 4.6: Effect of shear rate on viscosity

The images of the ink filament breakup (**Figure 4.7**) were captured using the high-speed camera.

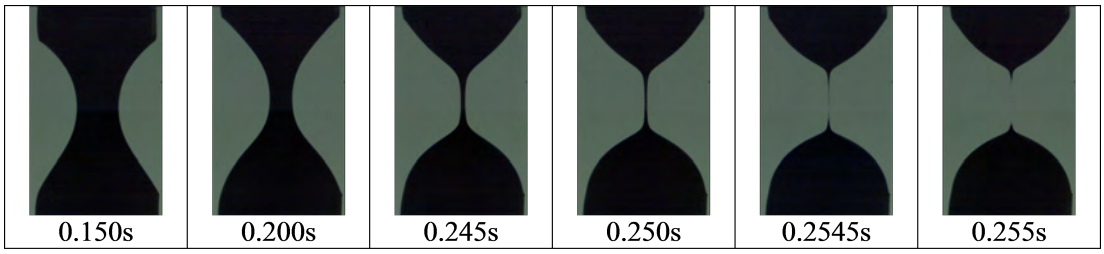

Figure 4.7: The images of UV Black ink filament breakup

The extensional viscosity was derived from the radius deformation (**Figure 4.8**) and was approximately 3 times its shear viscosity as its characteristic was closed to a Newtonian liquid (**Table 4.3**). The shape of the breaking filament was similar to a Newtonian liquid; indicated the ink was very thin corresponding to its low shear viscosity. Its filament breakup times was very short, so the ink filament would instantly break. There would also be limited pull-out of ink from the anilox cell. The ink release to the plate would depend on the ink flow. Its surface tension was also low so it would spread and adhere to the substrate.

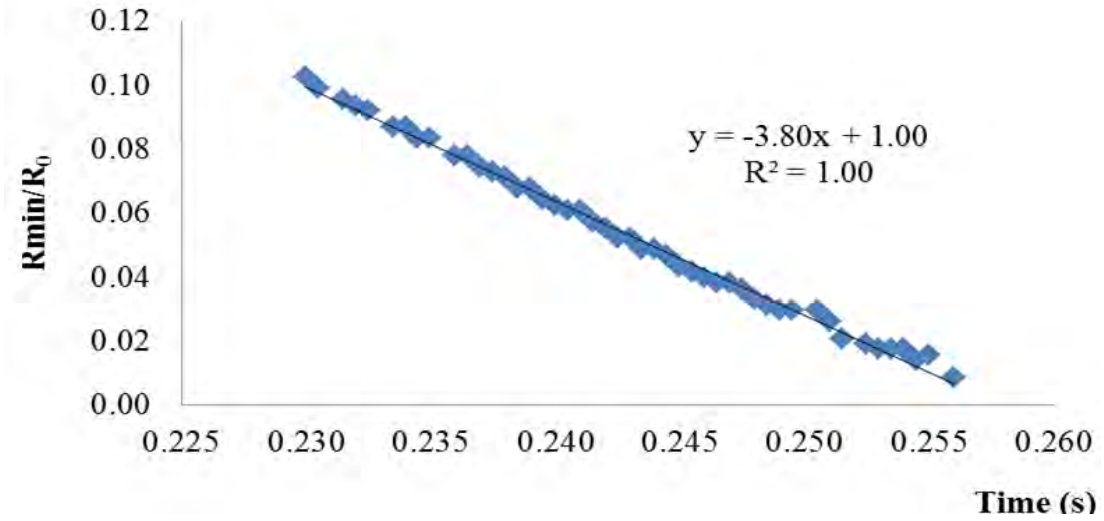

Figure 4.8: The radius deformation rate of the UV Black ink

Table 4.3: The ink properties of the UV Black ink

Ink	**Filament Breakup Time (s)**	**Extensional Viscosity (Pa.s)**	**Surface Tension (x10^{-3} N/m)**	**Density (x10^{-3} kg/m^3)**
UV Black	0.255	2.96	33.74	1.17

4.3 Results of the Experiments

4.3.1 Optical Density of the Tonal Patches

Discrete dots were not being printed even at the lowest coverages with the coarse (68LPI) anilox whereas the higher line ruling (120LPI) gave some indication of tonal range (**Figure 4.9**). This was confirmed by the measurement of optical density (**Figure 4.10**). The optical density remains almost constant to approximately 5% with the 68LPI anilox. The ink transferred is the equivalent to a solid above 5%, whereas with the 120LPI anilox the density equivalent to 100% coverage is not reached until the 60% tone value. There is also indication of discrete dots being reproduced at the lower tone values.

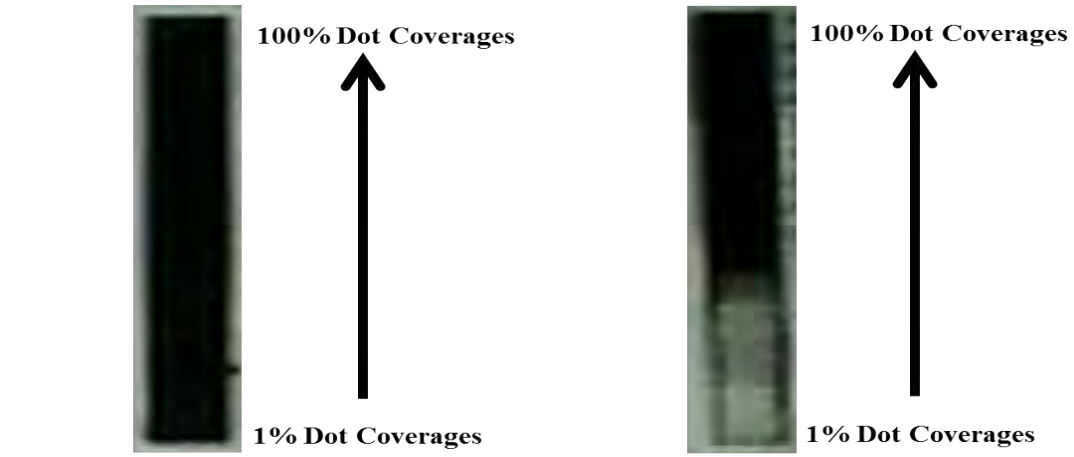

a) Tonal patch print using anilox roll of 49.22cc/m² with 68LPI

b) Tonal patch print using anilox roll of 47.60cc/m² with 120LPI

Figure 4.9: Tonal patch on glass substrate using anilox cell volume of a) 49.22cc/m^2 with 68LPI and b) 47.60cc/m^2 with 120LPI

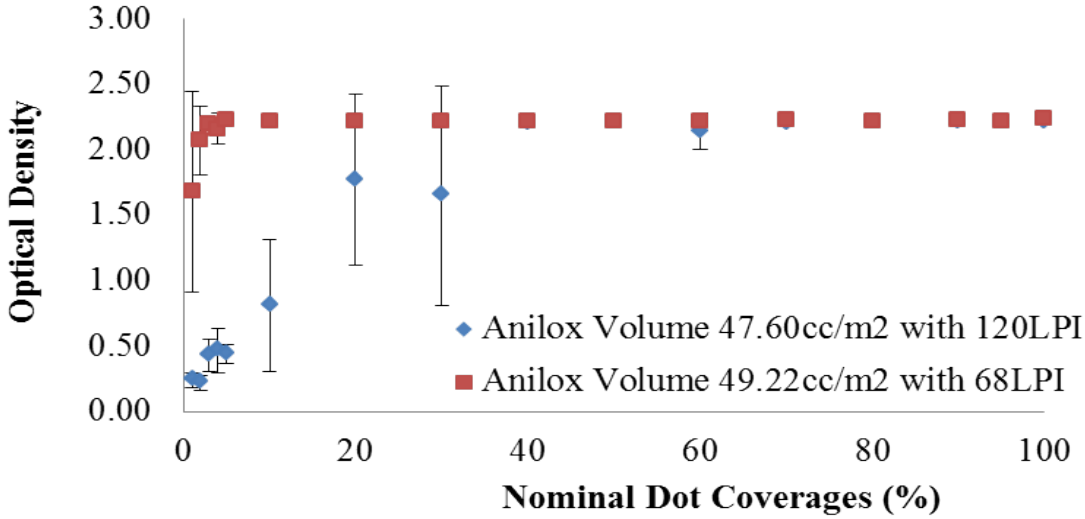

Figure 4.10: The graph of optical density against nominal dot coverages

An almost transparent patch can be seen at the bottom of the tonal patch print using anilox cell volume of 47.60cc/m^2 (120LPI). Whilst, the tonal patch print using anilox cell volume of 49.22cc/m2 (68 LPI) was completely covered with the ink throughout.

The profile for dot coverage 5% was captured by Wyko white light interferometry with the magnification of 10X in the WCPC laboratory (**Figure 4.11**). The 120LPI anilox produced discrete dots, some with a high point in the centre which is as one would expect for a half tone image. The dots have merged into one with the 68LPI anilox, with slight patterning. The high deviation of the optical density of the nominal dot coverage below 40% was due to the unsmooth coating of the print. The two anilox bands had similar high volume and almost identical cell depths. In order to achieve the same volume with one cell count per unit area almost double the other, the width of the 68LPI anilox cells had to be almost double and as a consequence the depth-to-width ratio was almost double.

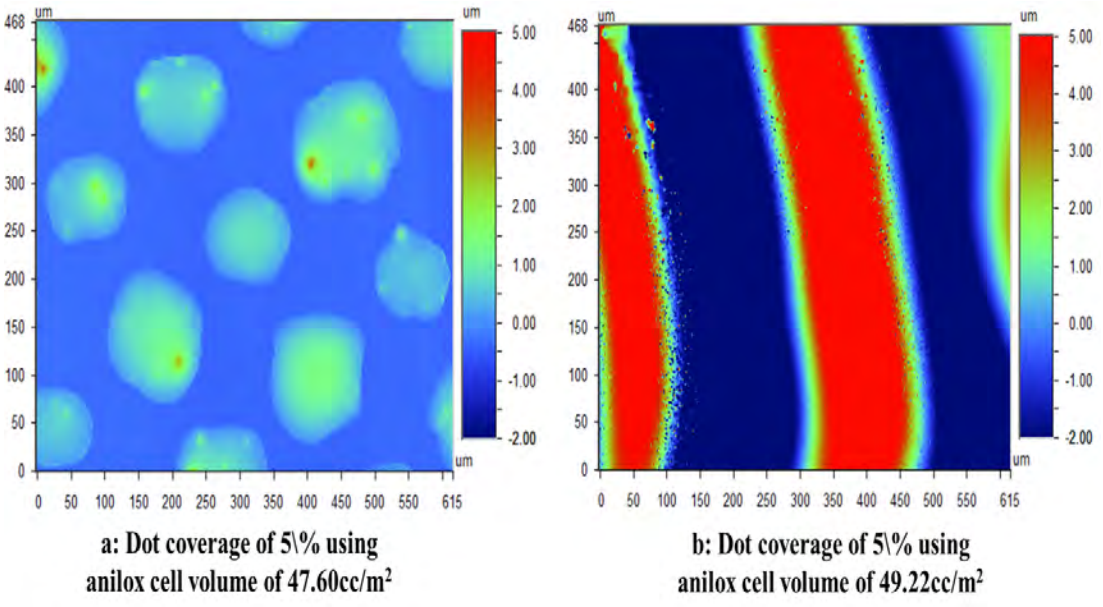

Figure 4.11: Dot coverage of 5% using anilox cell voloume of 47.60 (a) and 49.22cc/m^2 (b)

The larger cell width of the anilox cell volume of the 68LPI anilox would release more ink to the plate [Powell, 2000]. Its wider anilox cells allowed the plate dot to deform into the anilox cells and extract more ink [Bould, 2004; Cherry, 2007]. Its larger depth-to-width ratio made its cells proportionally shallower compared to its width, which encouraged more ink to be released out of the anilox cells [Kapur, 2003]. The combination of high ink volume supply and better ink release to the printing plate made the ink of anilox cell volume of 49.22cc/m^2 (68LPI) anilox flood the highlight dots causing print as a track (**Figure 4.11b**), and resulted in completely covered tonal patch print for nominal dot coverages below 40%. The narrower cell width of 47.60cc/m^2 ((120LPI) released less ink to the plate, and the printed dots maintained their shape creating a gradient in the tonal patch print.

The increased availability of plate area as dot coverage increased, allowed more ink to flow from the plate to the substrate, and the print above the nominal dot coverage of 40% became flooded with the ink for both anilox bands. This resulted in having similar optical density for both anilox cell volumes in the higher coverage mid and shadow tonal region. The printed tracks enabled the effect of these two anilox bands on a print pattern as would be used in the functional print.

The printed tracks were used to compare the ink release of these two anilox bands. The printed track was measured by Wyko software and then the WCPC software was used to extract the ink volume. The ink volume of the track was normalized by the ink volume per projected area (width and length) of the printed track.

The ink volume of the track was plotted against its nominal track width (**Figure 4.12**).There is a linear relationship between the nominal track width and ink volume i.e. the ink volume increased as the track was getting wider. A similar trend to the optical density of the tonal patch print is seen. The ink volume of the tracks printed with greater individual cell volume of the 68LPI had greater ink released. The ink volume of tracks was less fluctuate the optical density of the tonal patch print. The track on the plate had the same feature as of 100% solid coverage on the plate which showed much less fluctuation of its optical density comparing to the dot coverage below 40%.

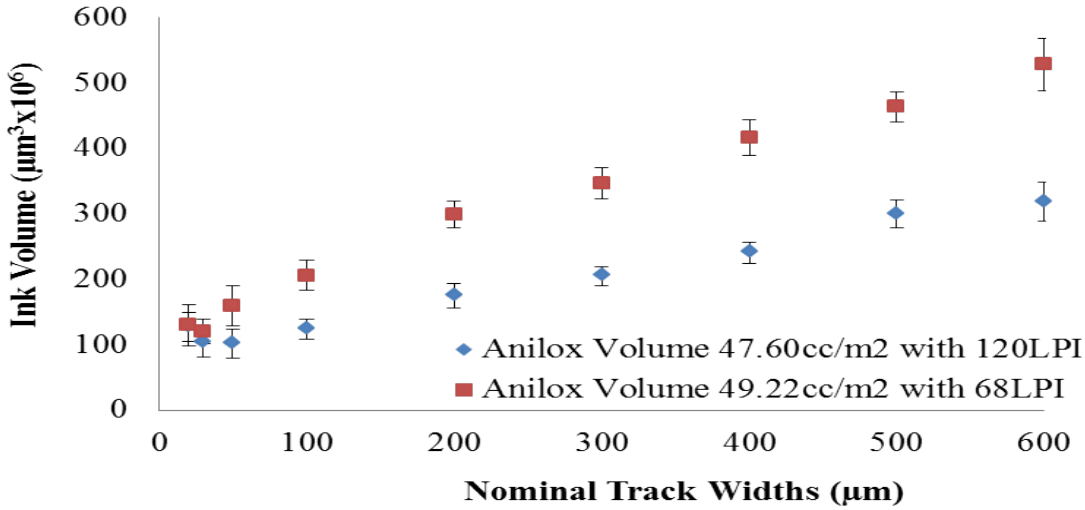

Figure 4.12: The graph of ink volume of tracks using anilox cell volume of 47.60 and 49.22cc/m^2

The ink volume of the printed track was converted to the ink volume per square meter and compared to the anilox cell volume of each band (**Figure 4.13**). The smaller track widths had significant deviation because of their greater deformation during engagement with the substrate. The deviation was smaller when the track width was wider, as the track was more self supporting mitigate the deformation effect.

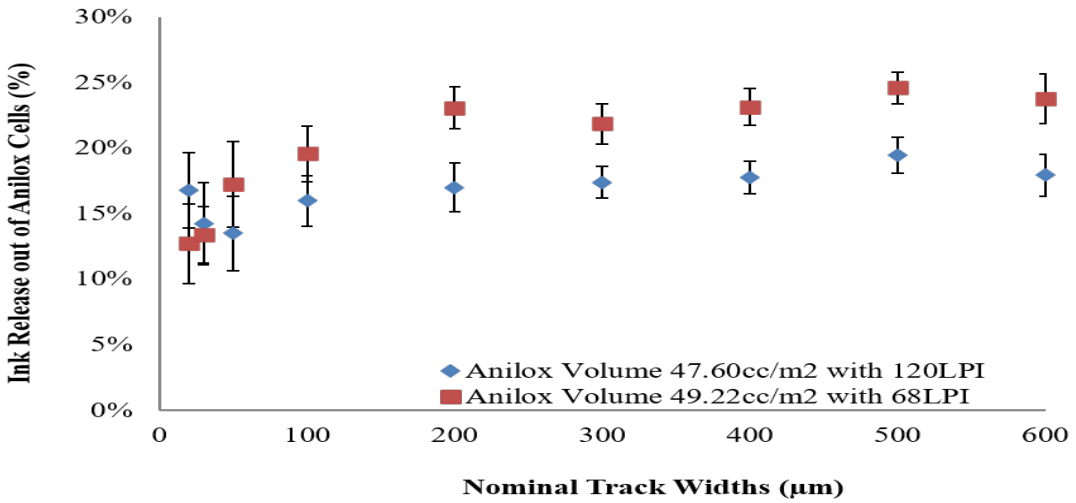

Figure 4.13: The ink release in the portion (%) of the anilox cell voloume of 47.60 and 49.22cc/m^2

The 68LPI anilox with cell volume of 49.22cc/m^2 released approximately 20% out of its cells comparing to approximately 17% for the 120LPI anilox with cell volume of 47.60cc/m^2. The anilox cell volume of 49.22cc/m^2 released greater ink due to its wider cells. Another parameter examined was the ratio of anilox cell depth to cell width (depth-to-width ratio). The anilox cell volume of 49.22cc/m^2 had the ratio of depth-to-width of approximately 0.52, whilst the anilox cell volume of 47.60cc/m^2 had the ratio of depth-to-width of approximately 0.89. The studies of Damroth et al (1996) showed that the smaller depth-to-opening ratio would better release ink. The attributes of having wider cells and smaller depth-to-width ratio made the anilox cell volume of 49.22cc/m^2 released ink better.

4.3.2 Track Widths

The printed track widths for both anilox cell volumes were greater than the nominal widths (**Figure 4.14**). This can be attributed to the low viscosity of the ink and the expansion of the printing plate when they engaged with the glass substrate during the printing process [Bould, 2004].

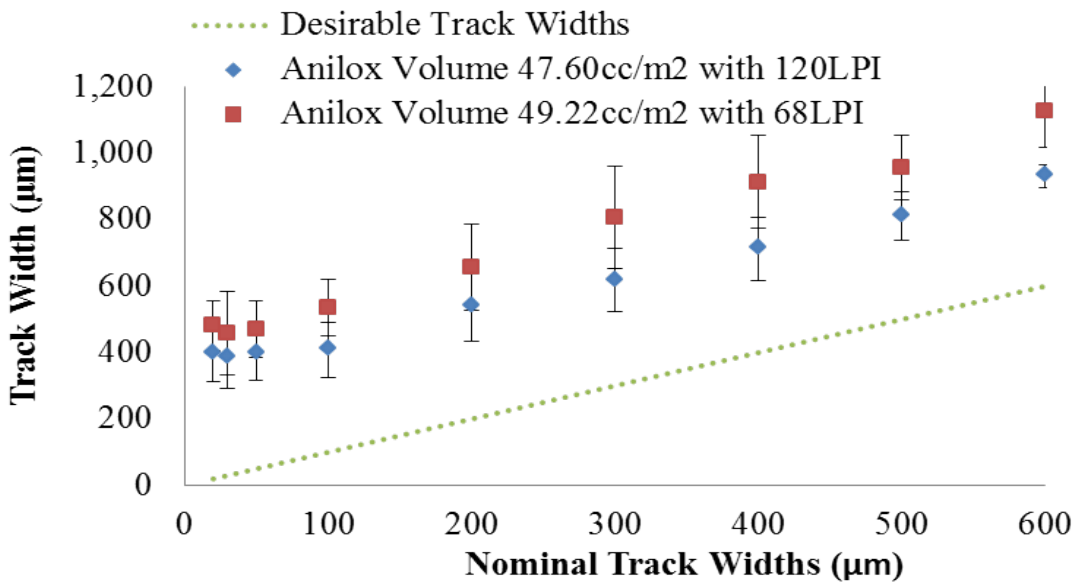

Figure 4.14: Track widths using anilox cell volume of 47.60 (120LPI) and 49.22cc/m^2 (68LPI)

The printed track width was larger than its actual size of approximately 19 and 23 times for the anilox cell volume of 47.60 (120LPI) and 49.22cc/m^2 (68LPI) respectively for the nominal width of 20μm (**Figure 4.15**). When the nominal track width increased, the difference exponentially decreased to approximately 2 times for the nominal width of 600μm. The ink spreading due to the low viscosity of the ink was the dominant cause.

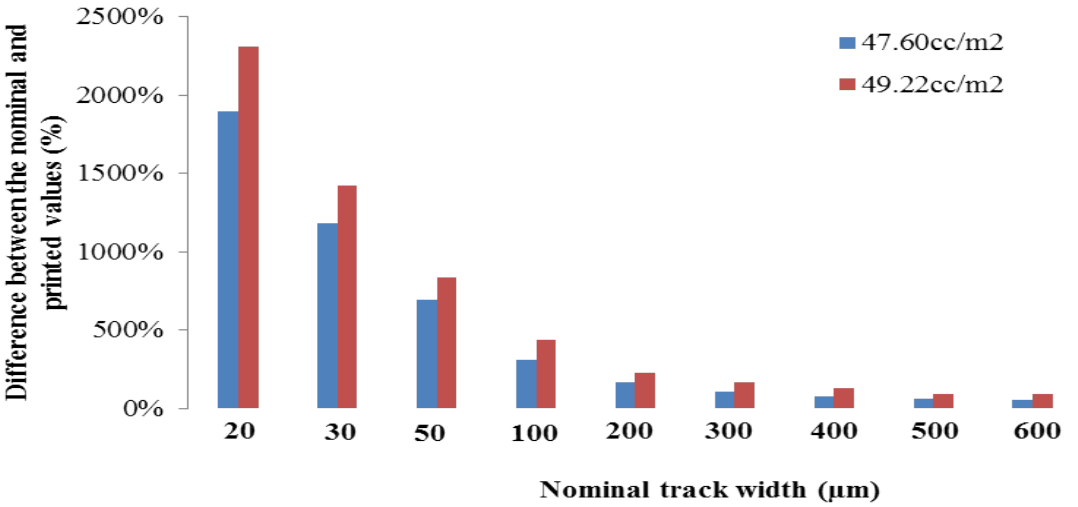

Figure 4.15: The difference between the nominal and printed track widths of anilox cell volume of 47.60 and 49.22cc/m^2

The printed track widths of anilox cell volume of 49.22cc/m^2 (68LPI) had the wider tracks comparing to the printed track widths using the anilox cell volume

of 47.60cc/m^2 (120LPI). The anilox cell of 68LPI released more ink. The greater ink release increased the ink spreading [Beynon, 2007]. The deviation of the track widths could be observed (**Figure 4.14**). This resulted in rough edges along the length of the track (**Figure 4.16**).

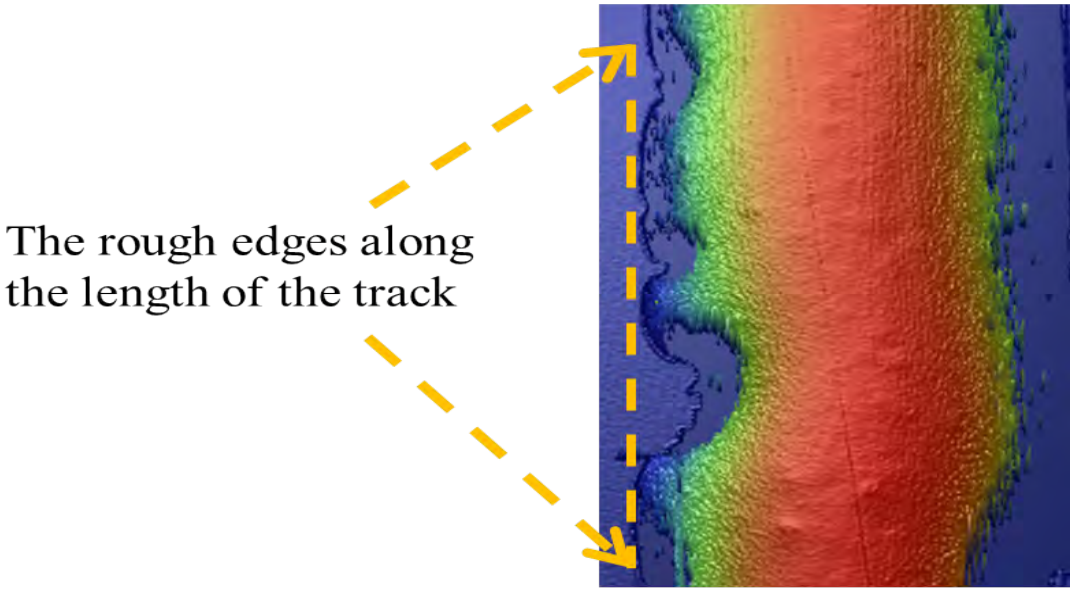

Figure 4.16: The image of 30μm nominal track width printed using the anilox cell volume of 49.22cc/m^2 (68LPI)

4.4 Closure

The ink release was examined using the tonal patch and track images. The high anilox cell volume to print the tonal patch caused the dots to be flooded with ink preventing the quantification of the ink release. Even though the trend of the ink release could be observed and compared in the small dot coverage, the ink release could not be compared in the large dot coverage because of the ink flooding. The printed tracks enabled the ink release volume to be quantified and the different anilox geometries compared.

The results gave similar trend to that which has been reported for flexography with the flexible substrates. The anilox with wider cells and smaller depth-to-width ratio released more ink. Even though, there was the fluctuation of the optical density below the dot coverage of 40%, the results of the track prints affirmed by giving the consistency of greater ink release using the anilox cell with wider cells and smaller depth-to-width ratio.

The low ink viscosity, which normally used with the flexible substrate in flexographic printing process, made the track width much greater than the nominal specification for functional applications. Additionally, the rough edges

along the length of the tracks caused significant deviation. However, the previous studies of printing flexible substrates can be a foundation to enhance the role of flexography in printing rigid substrates for the functional prints. The effect of high ink viscosity such as the conductive inks of Carbon and Silver inks, and more variety of anilox cell geometries are explored in chapters 6 and 7.

Chapter 5

An Industrial Trial of Anilox Cell Geometry Effects

5.1 Introduction

Elongated hexagonal closed cells and wavy channels anilox rolls designs (**Figure 5.1**) are increasingly being used in the packaging industry to improve the print quality. The ink release of the wavy channel anilox cells and the anilox elongated hexagonal closed cells were compared on a commercial packaging printing press. The effects of the ink types and plate line ruling on ink release was also investigated. The experiment was performed on a central impression (CI) press (**Figure 5.2**). It uses a single impression cylinder to engage with a series of plate cylinders (each plate cylinder receives the ink from its anilox cylinder) to lay down successive colours. The press is a fully automated for processing film, paper and cardboard at production speeds of up to 600m/min. It can be configured for up to 12 printing units with the maximum print width of 1.6m [Koenig & Bauer, 2020].

The ink release was evaluated using optical density and the physical dot area on the printed substrates. The methodology of the investigation is described in the following section. The results of the investigation were used as the guidance for further detailed laboratory investigation explored in chapters 6 and 7.

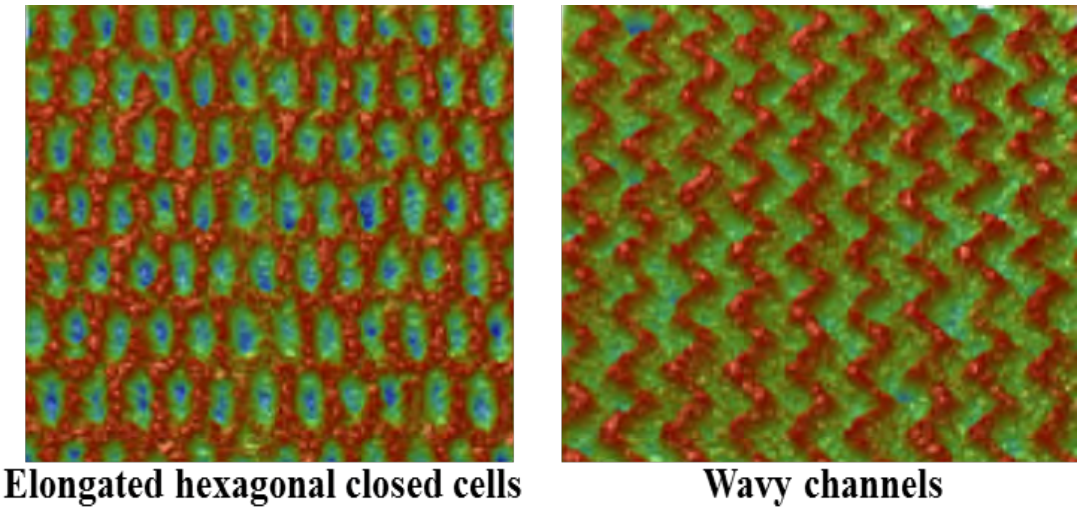

Figure 5.1: Anilox elongated hexagonal closed cells and the wavy channels

Figure 5.2: KBA flexotecnia XG press

5.2 Experimental Method

The ink release from two shape cell shapes was compared using a two banded anilox. The cell shapes, volume, and screen count were considered to be similar by the suppliers (**Table 5.1**).

Table 5.1: Anilox cells specification

Screen Count (LPI)	Cell Volume (cc/m^2)	Width (μm)	Depth (μm)	Surface Roughness (nm)	Shapes
1,012	2.82	32	8	1.87	Elongate anilox closed cell
1,074	2.31	21	5	1.61	Wavy channel

The printing plates had line ruling of 137LPI and 122LPI tonal patches with dot area coverage of 0.5-100%. Two commercial high definition (the pigment loading was greater than the standard ink to increase the vibrancy of colour), Black and Yellow, were used. The printing procedure followed the standard operating procedures of the packaging manufacturer.

Ink Shear Viscosity

The high definition Black ink was a low viscosity Newtonian fluid (**Figure 5.3**). The viscosity was typical of a flexographic ink, if towards the low end of viscosity. The high definition Yellow was shear-thinning reaching the same viscosity as the black at approximately $500s^{-1}$. The high definition Black ink would easily flow to the printing plate at any printing speed; however, it would require to greater printing speed for the high definition Yellow ink to flow compare to the high definition Black. Because the printing process was carried out at the high speed, the high definition Yellow ink should flow to the plate during the printing process.

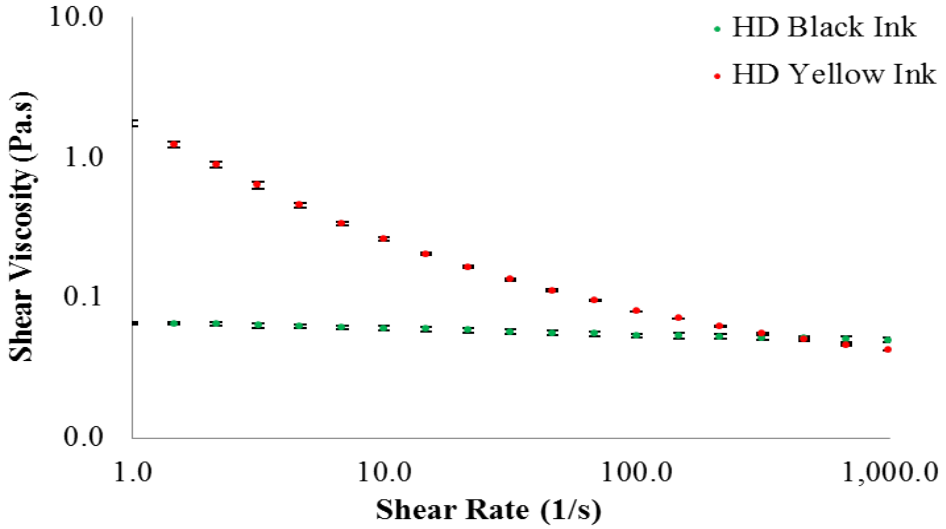

Figure 5.3: The shear viscosity of the high definition Black and Yellow inks

Ink Extensional Viscosity

The radius deformation correspond to filament stretching and breakup (**Figure 5.4**). The trend lines were plotted to get the slope to calculate for the extensional viscosity.

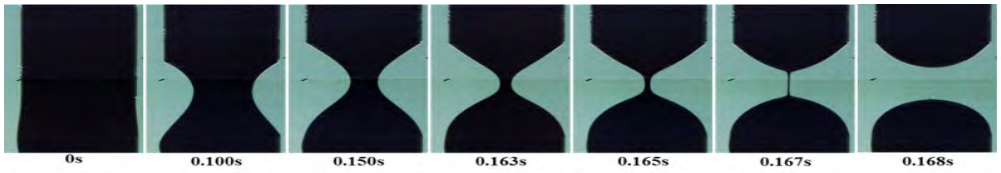

a: Filament stretching and breakup of HD Black ink

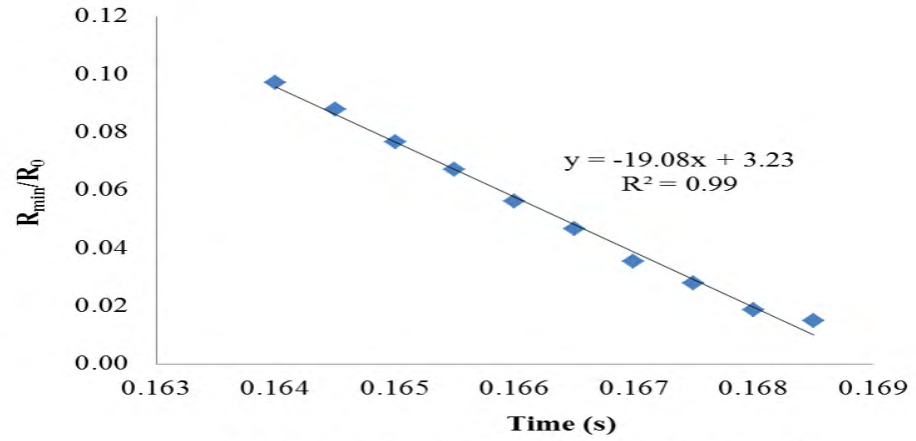

b: Radius deformation rate of the HD Black ink

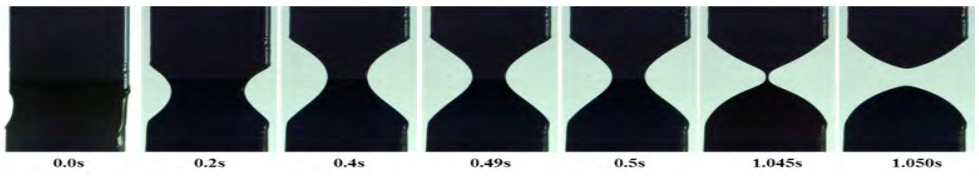

c: Filament stretching and breakup of HD Yellow ink

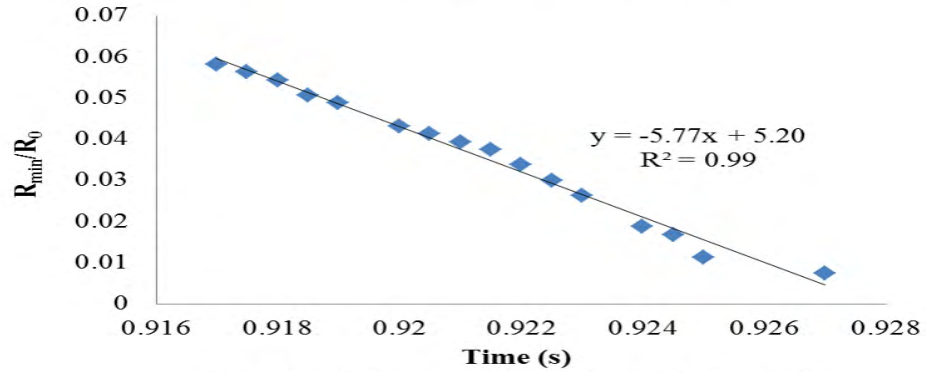

d: Radius deformation rate of the HD Yellow ink

Figure 5.4: Radius deformation correspond to filament stretching and breakup

The extensional viscosity of the inks were obtained using a CaBER test (**Table 5.2**). The high definition Black and Yellow inks had similar values of the surface tension and density. The high definition Black ink had approximately five times filament breakup time and eight times lower extensional viscosity than the Yellow ink. The HD Yellow ink would have greater elongation of ink filament, whilst the HD Black ink would have a shorter ink filament and breakup faster during the printing process. The HD Yellow ink would tend to be pull out more during the printing process.

Table 5.2: The ink properties

Ink Properties				
Ink	**Filament Breakup Time (s)**	**Extensional Viscosity (Pa. s)**	**Surface Tension (x10^{-3} N/m)**	**Density (x10^{-3} kg/m^3)**
HD Black	0.169	0.18	24.19	0.96
HD Yellow	0.928	1.48	25.65	0.89

Ink Viscoelastic Behaviour

According to the previous studies of Turkoz, Deike and Arnold (2017), the stretching of the viscoelastic ink depends on its elasticity. Small amplitude oscillatory shear (SAOS) was used to access the viscoelastic behaviour.

The oscillation test (stress-sweep test; measurement by increasing the shear stress) was carried out to examine the viscoelastic behaviour of the inks. The test could also use to determine the linear visco-elastic region (LVR) of the materials in which the elastic and viscous modulus were constant or independent of shear stress, with no breakdown of material structure in this region. The test was used to determine the cross over point where elastic and viscous modulus were equal, and if the shear stress increased, the material would change behaviour from solid-like to liquid-like or vice versa [Mallik, 2009]. Solid-like behaviour of the ink happens when its elastic modulus is greater than it's viscous modulus. If the ink behaved as a solid, the ink would resist the stretching (deformation) and it would cause the ink to recoil back to the anilox cells. If the ink behaved as liquid-like, the ink would be stretched and flow out of the anilox cells.

Additionally, the elastic modulus could indicate the filament stretching behaviour of the ink. More of the ink, which had greater elastic modulus and was liquid, would be pulled out of the anilox cells.

Extreme caution must be taken in interpreting the data outside the LVR (non-linear region) where the elastic and viscous moduli are dependent on shear stress. The resulting strain does not proportionally response to the applied stress. Large Amplitude Oscillatory Shear (LAOS) has to be used to study the non-linear response of the materials [Lamer, 2018].

The viscous modulus of HD Black ink was dominant compared to its elastic modulus (**Figure 5.5**), indicating liquid-like behaviour. Its viscous modulus was almost constant. It's elastic modulus was small and fluctuated as the shear stress increased. It's elastic modulus steadily decreased until the shear stress reached approximately 3.0 Pa, when the elastic modulus started increasing. There were two possible causes for the elastic modulus to be disrupted: the breaking of structure of ink, or wall-slip effect. However, as the elastic modulus increased after dropping, it was more likely that wall-slip was the cause. There were two possible scenarios; a discontinuity at the wall of the plate, or a thin layer of the ink forming as the ink particles were re-arranged during the shear so the ink formed two layers; one was thinner and attached to the upper wall of the plate, and the other was thicker. The thinner layer was treated as a slipping layer and caused the elastic modulus to drop [Chang, 2003]. The elastic modulus was more likely to have dropped due to the slipping layer because when the shear stress increased, the elastic modulus value recovered as the particles adjusted and re-arranged due to the increase of shear stress. The elastic modulus showed significant discontinuity compared to the viscous modulus because the elastic modulus had a very small value so even slightly decrease would have a severe impact to its value.

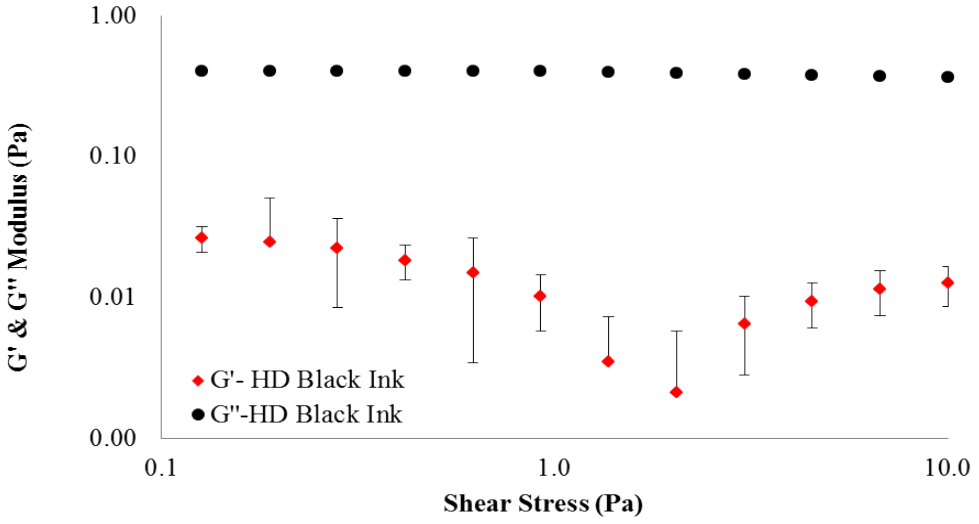

Figure 5.5: Shear stress against elastic (G') and viscous (G") modulus of the HD Black ink

The elastic and viscous modulus of HD Yellow ink were much greater than those of HD Black ink (**Figure 5.6**). The elastic modulus of HD Yellow ink was

greater than its viscous modulus in the linear visco-elastic region of shear stress below 6.0Pa. Its elastic modulus started decreasing at approximately 6.0Pa, and approximately equal to its viscous modulus at 7.0Pa. The profiles of elastic and viscous modulus of HD Yellow ink were consistent. The decrease of the elastic modulus indicates its structure broke down as the shear stress increased, causing its elastic modulus to decrease below its viscous modulus and caused the significant fluctuation as the shear stress increased. Its critical shear stress was approximately 7.0Pa, shear stress above this value would cause HD Yellow ink to be liquid-like.

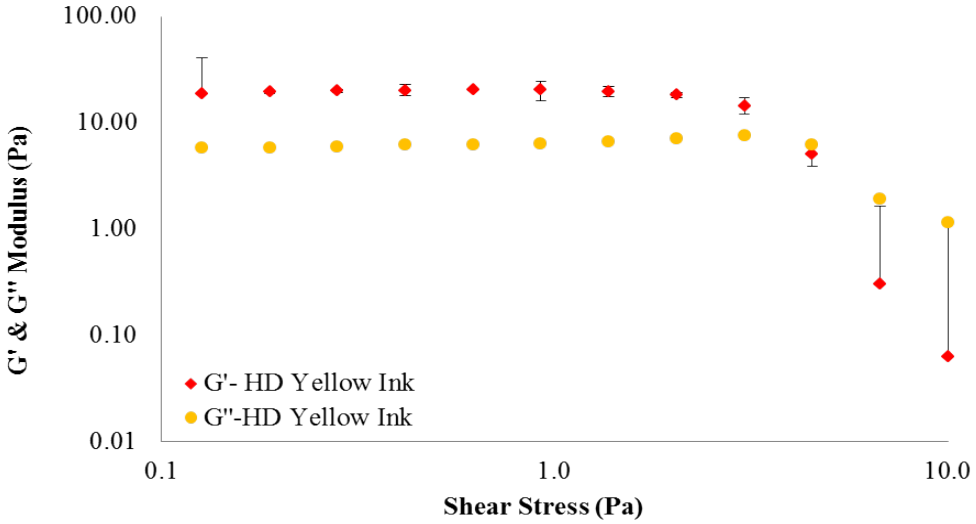

Figure 5.6: Shear stress against elastic (G') and viscous (G") modulus of the HD Yellow ink

Based on their viscoelastic behaviour, HD Black ink was liquid-like at initial low shear stress and continued as shear stress increased. HD Yellow ink was solid-like at initial shear stress and would require the shear stress to be beyond 7.0Pa to make it liquid-like. Therefore, HD Black ink was more likely to flow better.

Initially, the elastic modulus of HD Yellow ink was much greater than that of HD Black ink (**Figure 5.7**) . However, when the shear stress passed its critical point where its' structure broke down, the elastic modulus of HD Yellow ink dropped rapidly and became closed to the elastic modulus of HD Black ink. The elastic modulus of HD Yellow ink was greater than the HD Black ink, indicating it could stretch longer and more could be pulled out from the anilox cells.

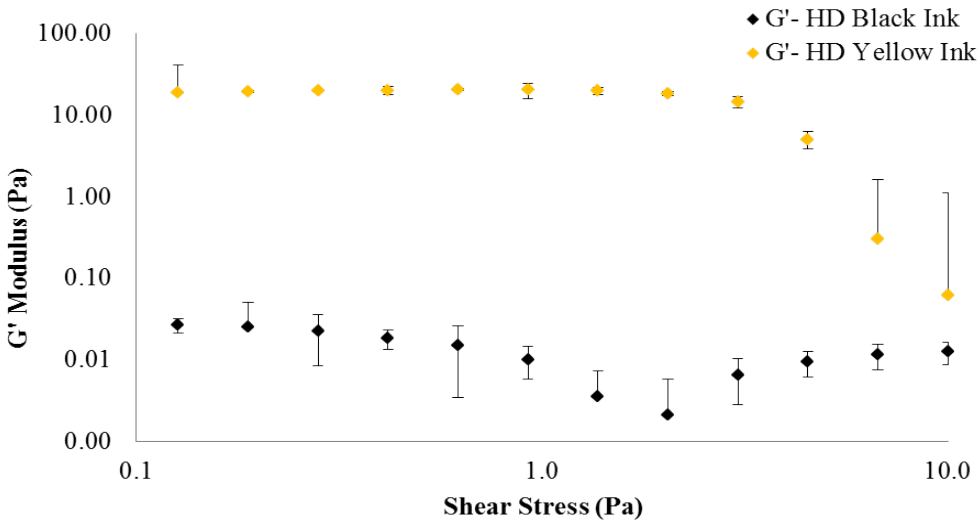

Figure 5.7: Comparison of elastic (G') modulus of the HD Black and Yellow inks

The HD Black ink had smaller viscosity, filament breakup time, and elastic modulus. It was liquid-like at all shear stress. HD Yellow ink had greater viscosity, filament breakup time, and elastic modulus. It was solid-like in the low region of shear stress below 6.0Pa and was liquid-like beyond this point. The HD Yellow ink would have greater elongation of ink filament and pull-out fraction compared to the HD Black ink; however, the filament breakup time would affect ink release and have to be determined by experiment comparing the optical and printed dot area.

5.3 Results of the Experiments

5.3.1 Effect of the Anilox Cell Geometries

The Image Examination

The prints were examined using the Leica Wild M3Z Stereo Microscope with 40x magnification. For the HD Black ink, over 0.5-5% nominal coverage; the dots were inconsistent in size with more missing dots when the elongated closed cells were used (**Figure 5.8**). The dot merging started at the 40% coverage with the anilox wavy channels whilst the dot merge started at the dot coverage of 50% for the anilox elongated closed cells. The merge of the printed dots at the lower dot coverage indicated that there was more ink released on the substrate, which caused greater ink-spreading. The dots printed by the anilox wavy channels showed a stronger colour density than the dots printed by the anilox elongated closed cells.

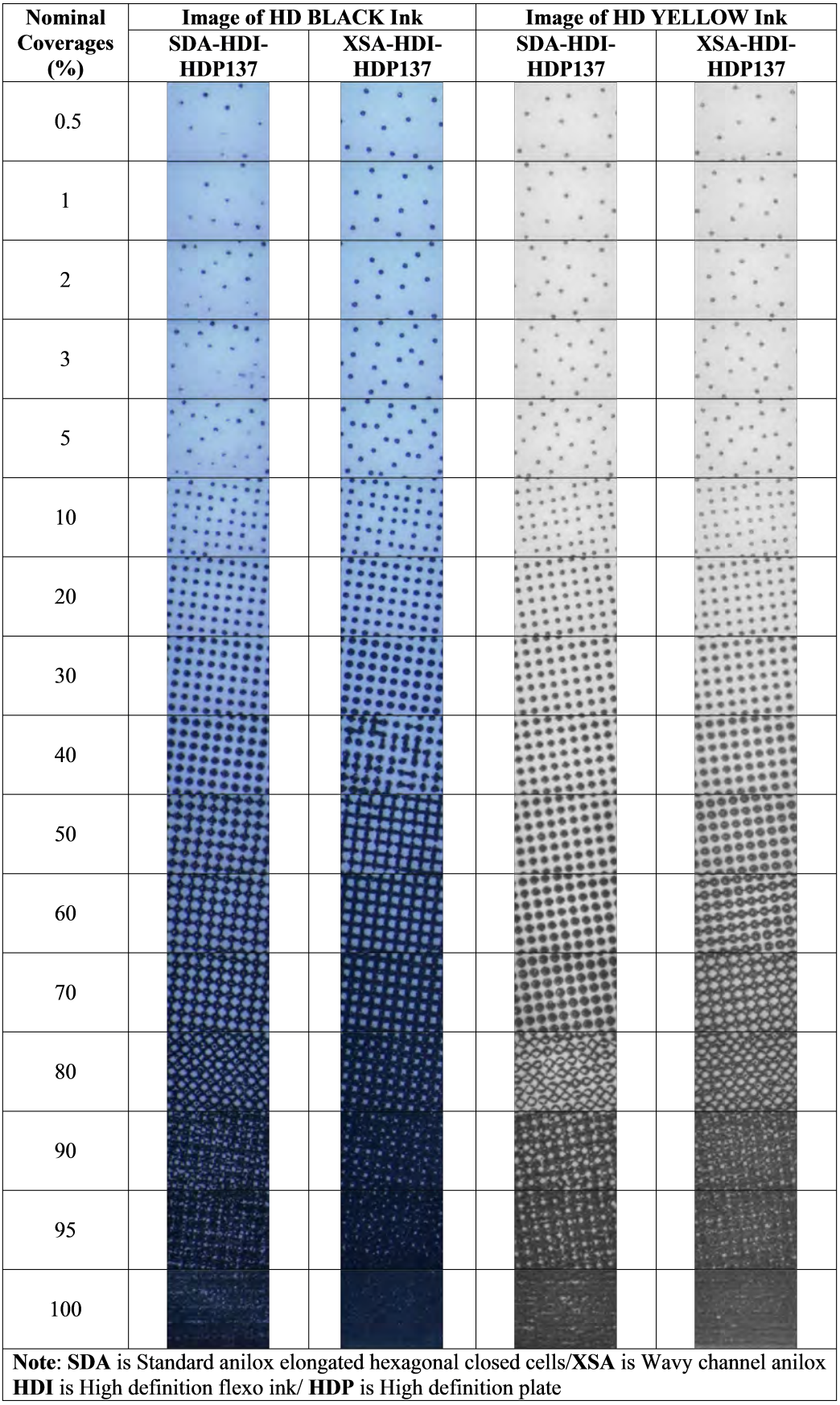

Figure 5.8: Tonal test strips at 137 LPI with the elongated hexagonal closed cells and wavy channels

Similar trend was observed with HD Yellow ink; however, the difference was smaller. There was no significant difference between the anilox elongated closed cells and wavy channels below 40% dot coverage. However, when the dot coverage increased, the print using the anilox wavy channels gave stronger colour and merged at lower coverage of 60% compared to the anilox elongated closed cells which merged at 80%.

5.3.1.1 Optical Density and Printed Dot Area using HD Black Ink

The optical density with HD Black Ink corresponds to the trend seen in the visual examination. Anilox wavy channels gave a greater optical density compared to the anilox elongated closed cells (**Figure 5.9a**), indicating the anilox wavy channels were releasing more ink to the plate.

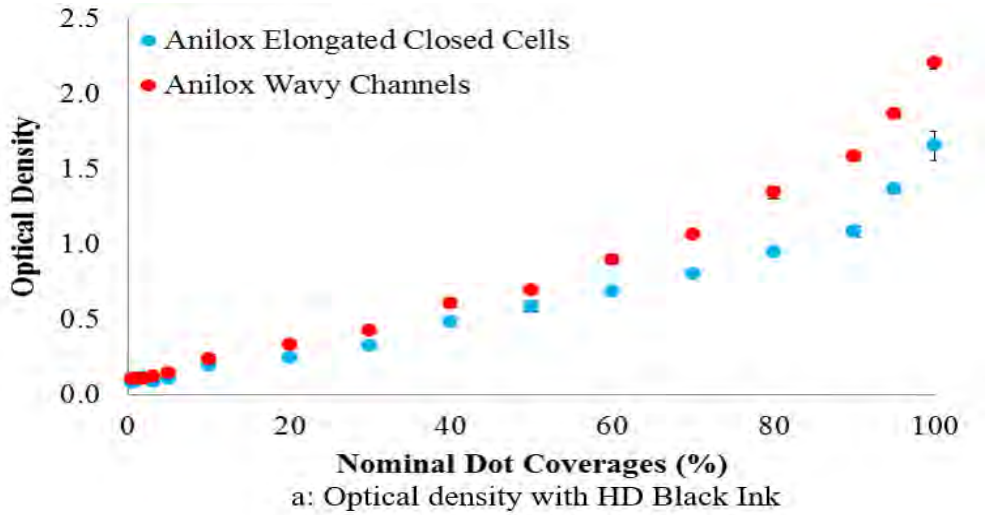

a: Optical density with HD Black Ink

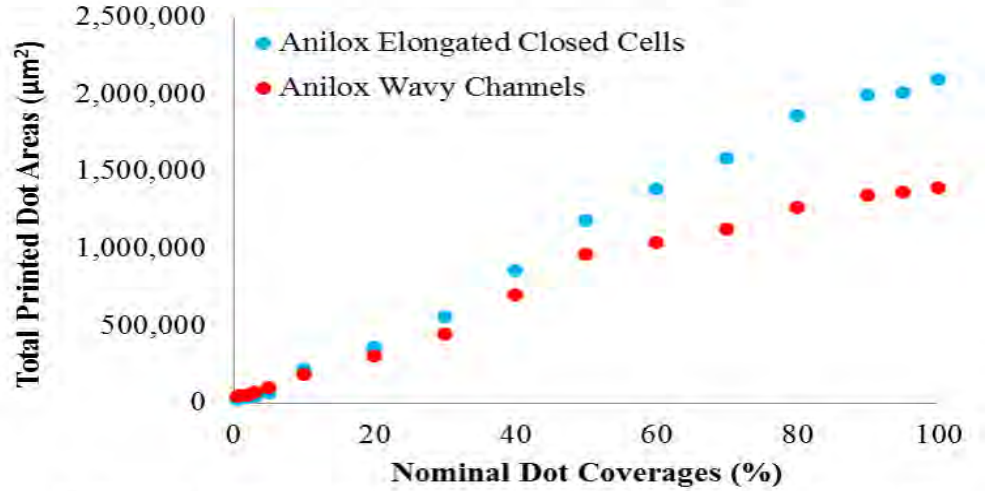

b: Printed dot area using the anilox elongated hexagonal closed cells and wavy channels with HD Black Ink

Figure 5.9: Optical density and printed dot area of HD Black Ink

The printed dot area using the anilox wavy channels was expected to be larger because the greater ink release to the substrate would encourage the ink-spreading (**Figure 5.9b**). The printed dot area using the anilox elongated closed cells was slightly smaller as expect below 10% which corresponded to the visual examination where there were some missing dots and inconsistency of print. However, above 10% dot coverage, the printed dot sizes using the anilox wavy channels were smaller than those using the anilox elongated closed cells. Therefore, as all the prints were done under the same conditions the anilox shape affected the printed dot area.

When the plate dots aligned with the elongated closed cells, some plate dots laid on the cell walls (**Figure 5.10**), reducing the contact area of the plate dots available to receive ink. This caused inconsistency in printing the dots; inconsistency in sizes, or not printed at all (missing printed dots). The anilox wavy channel had less obstruction for the plate dots to contact with the ink; more ink be released to the plate dot. This made its prints more consistent.

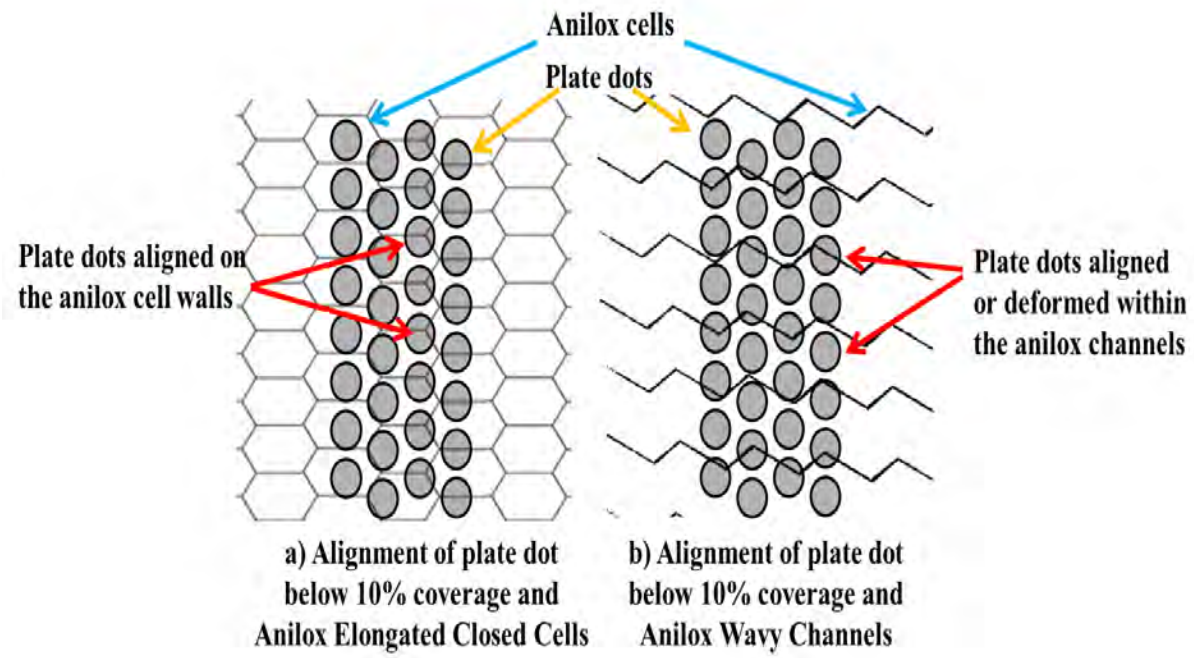

Figure 5.10: Schematic diagram of alignment of plate dots below 10% dot coverage with the anilox elongated closed cells and wavy channels

When the dot coverage increased, the size of the dot on the plate was larger than the anilox cells; this increased the contact area between the plate dot and the anilox cells (**Figure 5.11**). When the anilox elongated closed cells contacted the plate dots, the walls of many cells acted to block the free flow of the ink. The small gap between the edge of the plate dots and the anilox elongated closed cells would allow the ink to flow through; however, it caused

excess ink around the edge and shoulder of the plate dot. When the plate dot engaged with the substrate, the excess ink around the edge and shoulder of the plate dot would be released to the substrate and exaggerate the printed dot size due to the physical expansion of plate dot. By contrast, the wavy channels allowed the ink to freely flow along its tracks, this reduced the excess ink around the edge of the plate dot. Additionally, it offered more contact area to the plate dot because of less cell walls; the plate dot received more ink comparing to using the anilox elongated closed cells. This made its ink lay-down of printed dot better than the ink lay-down of the printed dot using the anilox elongated closed cells.

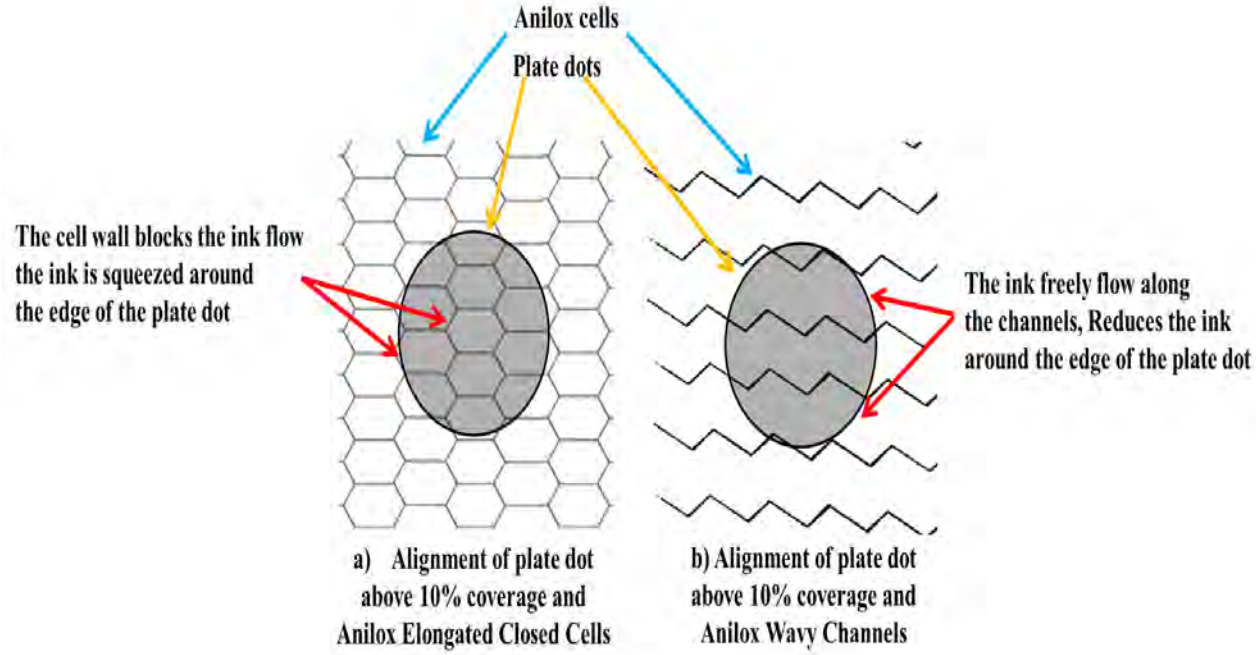

Figure 5.11: Schematic diagram of alignment of plate dots above 10% dot coverage with the anilox elongated hexagonal closed cells and wavy channels

The ink lay-down of printed dot with HD Black ink using the anilox wavy channel was better in quality; more consistency in size, and no ring of excess ink around the edge (**Figure 5.12**).

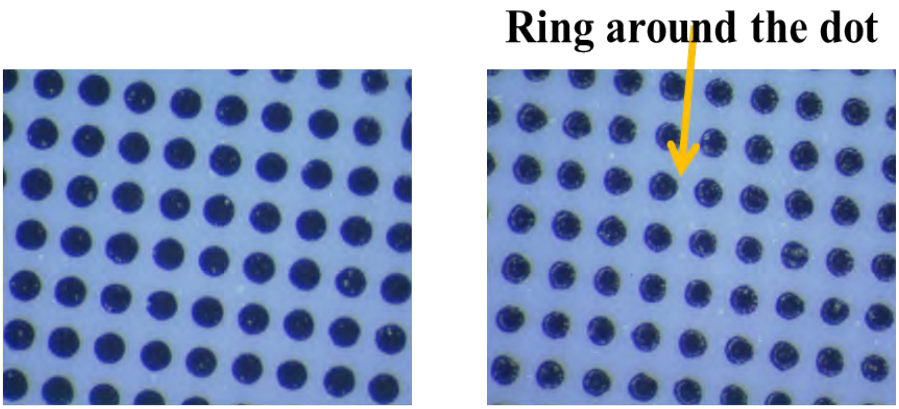

a) Print of 30% dot coverage using anilox wavy channels

b) Print of 30% dot coverage using anilox elongated closed cells

Figure 5.12: Ink lay-down of printed dots using the anilox elongated hexagonal closed cells and wavy channels with HD Black Ink

5.3.1.2 Optical Density and Printed Dot Area using HD Yellow Ink

The increased viscosity, surface tension, and filament breakup time of HD Yellow ink reduced the effect of the anilox cell geometries (**Figure 5.13a**). There was slightly greater ink release out of the anilox wavy channels. The increase of viscosity, surface tension, and filament breakup time greatly affected the ink release out of the anilox cells. The optical density of the printed dots printed with HD Yellow ink reduced below 1.5 whilst the optical density of the printed dots printed with HD Black ink was well above 1.5 for both anilox elongated closed cells and wavy channels. The optical density of the anilox elongated closed cells and wavy channels was essentially the same, therefore, their printed dot area would expect to show similar trends.

A similar trend was observed for the printed dot area with HD Yellow Ink as was seen with HD Black ink when comparing the elongated closed cells against wavy channels, (**Figure 5.13b**). The printed dot area using the elongated closed cells was significantly greater than for the wavy channels. The elongated closed cells exaggerated the printed dot size as described earlier.

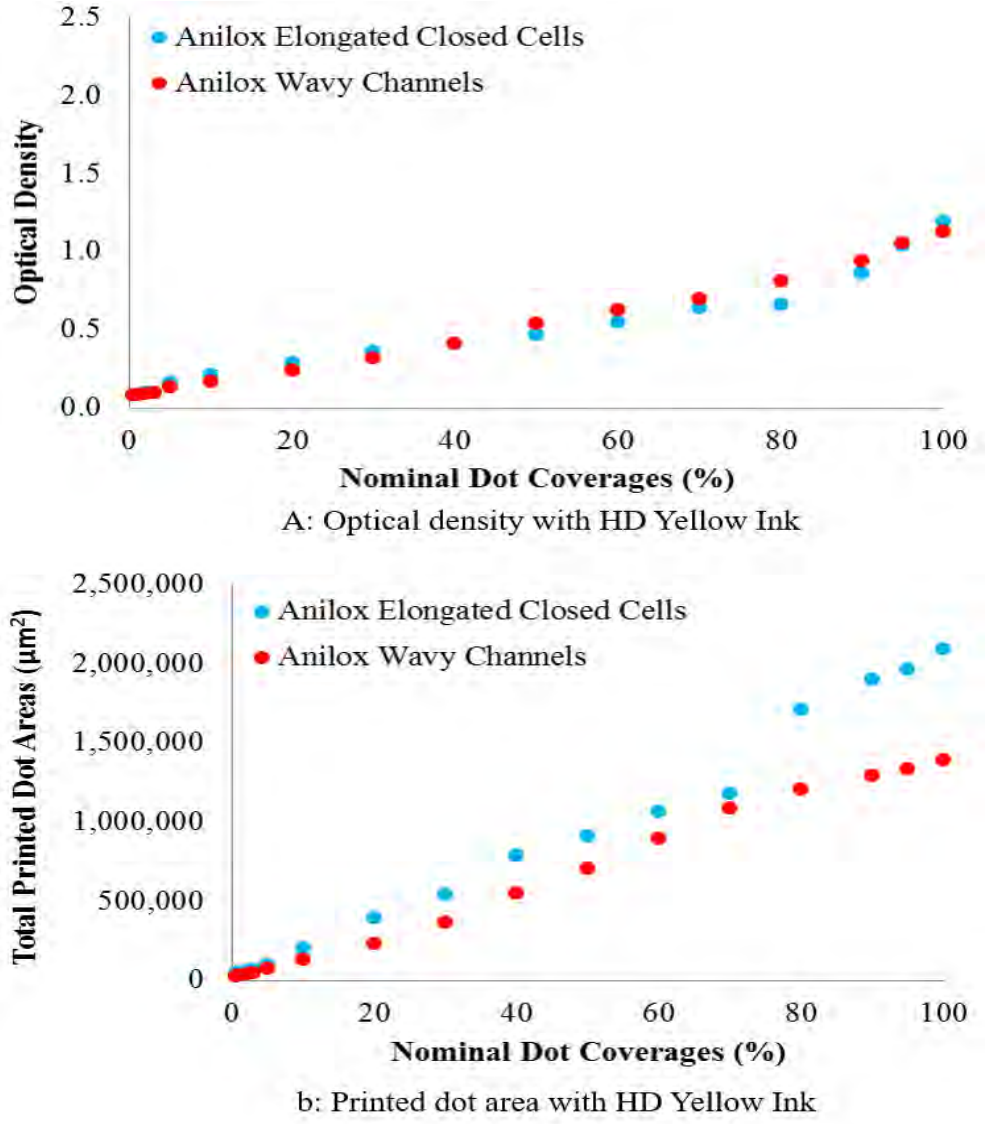

Figure 5.13: Optical density and printed dot area of HD Yellow Ink

There were similar results for ink lay-down of printed dots using the anilox elongated hexagonal closed cells and wavy channels with HD Yellow Ink (**Figure 5.14**). The printed dot using the wavy channels gave better quality without the exaggeration of excess ring.

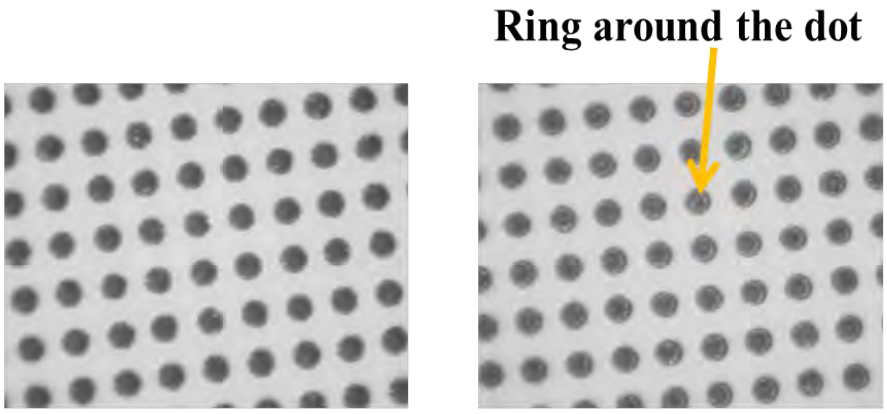

a) Print of 30% dot coverage using anilox wavy channels

b) Print of 30% dot coverage using anilox elongated closed cells

Figure 5.14: Ink lay-down of printed dots with HD Yellow Ink

5.3.2 Effect of Ink Characteristics

The HD Black ink had lower viscosity, surface tension, elastic modulus, and filament breakup time than the HD Yellow ink. The lower viscosity should make the ink flow more freely. However, the lower elastic modulus would cause less ink to be pulled out of the anilox cells. The shorter filament breakup time would make the filament split more easily. The lower surface tension would make the ink spread on the substrate; which would increase the printed dot area. The HD Yellow ink gave smaller optical density comparing to the HD Black ink. However, the difference of the ink attributes did not make a significant difference to the printed dot area, which was more influenced by the anilox cell geometries.

5.3.2.1 Optical Density and Printed Dot Area using the Anilox Elongated Closed Cells

The optical density and printed dot area were examined to see how these ink attributes affected the prints. There was no significant difference in optical density in the dot coverage below 30% using the anilox elongated hexagonal closed cells (**Figure 5.15a**). However, when the dot coverage increased, the optical density of the prints using the HD Black ink was significantly greater than the optical density of the prints using the HD Yellow ink, confirming the findings in the previous section.

The printed dot area of the prints using the HD Black ink with the elongated hexagonal closed cells gave greater printed dot area in the region above dot coverage of 30% because the HD Black ink gave greater optical density (**Figure 5.15b**).

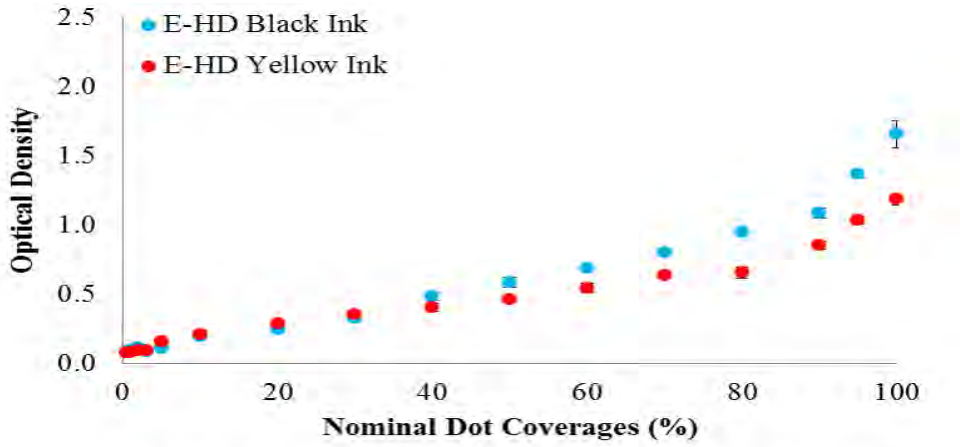

a: Optical density of printed dots using the anilox elongated hexagonal closed cells with HD Black and Yellow inks

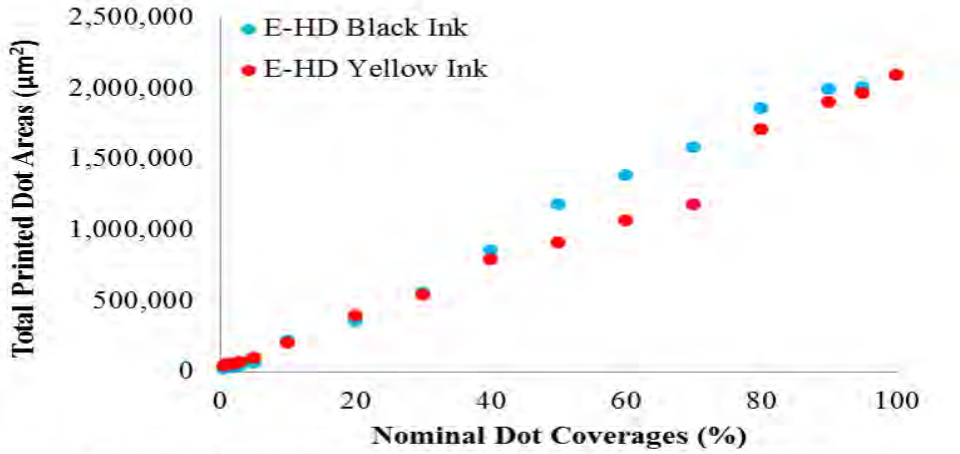

b: Printed dot area of printed dots using the anilox elongated hexagonal closed cells with HD Black and Yellow inks

Figure 5.15: Optical density and Printed dot area of printed dots using the anilox elongated hexagonal closed cells with HD Black and Yellow inks

5.3.2.2 Optical Density and Printed Dot Area using Wavy Channels

The same trend was seen with the anilox wavy channels (**Figure 5.16a**). The optical density of the prints using the HD Black ink gave greater optical density.

The printed dot area with the wavy channels also gave a similar trend (**Figure 5.16b**). The printed dot area of prints using the HD Black ink gave greater printed dot area as its optical density was greater than using the HD Yellow ink.

The HD Black ink with lower viscosity, surface tension, and filament breakup time had greater release from the anilox cells. Its smaller elastic modulus, which

should have made it pulled out less, appeared not to be a significant hindrance. However, these two inks had a small range of elastic modulus. In the following chapters, 6 and 7, will examine the inks; The Carbon and Silver paste inks have a much greater elastic modulus compared to these two inks.

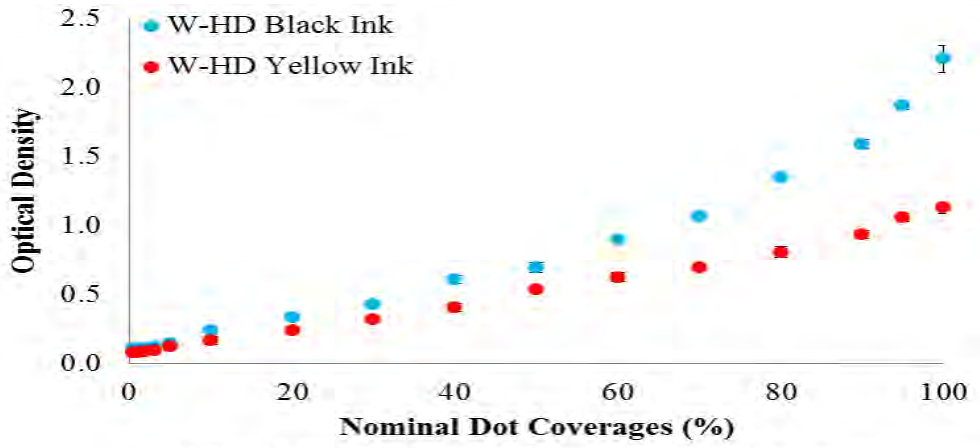

a: Optical density of printed dots using the anilox wavy channels with HD Black and Yellow inks

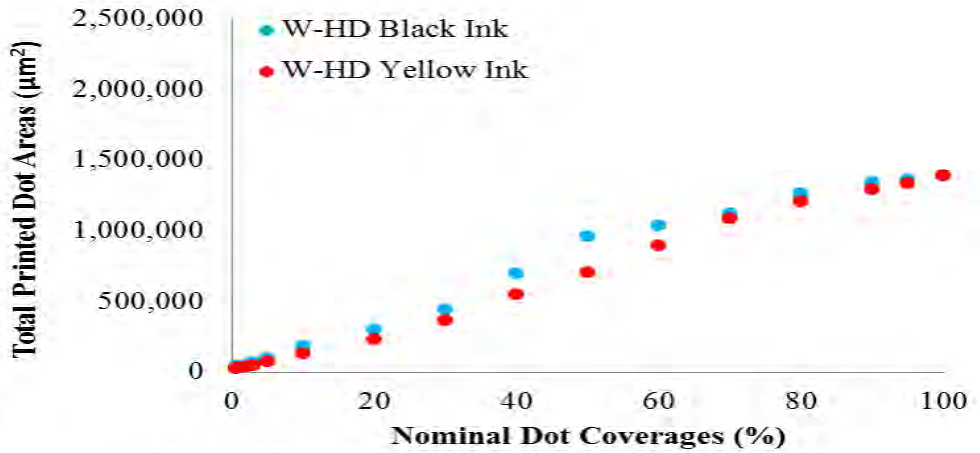

b:Printed dot area of printed dots using the anilox wavy channels with HD Black and Yellow inks

Figure 5.16: Optical density and Printed dot area of printed dots using the anilox wavy channels with HD Black and Yellow inks

5.4 Closure

The effect of anilox cell geometries: The anilox wavy channels released more ink than the elongated closed cells and gave greater optical density. The anilox elongated closed cells enlarged the printed dot cells because its cell walls blocked the flow of the ink. The ink could only flow through the small gap between the edge of the plate dot and anilox cells during engagement in printing process. This ink excess would be on the edge and shoulder of the plate dot.

When the plate dot engaged with the substrate, this excess ink around the edge and shoulder would show as the ring around the printed dot; enlarging the size of the printed dot. In contrast, the anilox wavy channels allowed the ink to freely flow along its track during the printing process. This reduced the excess ink around the edge of the plate dot. Additionally, the wavy channels allowed the ink to have more time attached to the plate dot as the ink filament was dragged along the channel without the wall to cut off and splash the ink; plate dot could receive more ink resulting in a greater consistency of ink lay-down of the printed dot. The cell walls of the anilox elongated closed cells reduced the contact area with the plate dot; plate dot received less ink which caused inconsistency in ink lay-down, with some plate dots not receive any ink resulting in missing dot on substrate.

The effect of ink characteristics: Viscosity, surface tension, filament breakup time, and elastic modulus affected the ink release from the anilox cells. The ink with smaller viscosity, surface tension, and filament breakup time better released out of the anilox cells. The greater elastic modulus indicated a longer ink filament and greater pull-out; however, these two factors did not have much effect. Because the elastic modulus of these two inks were small. The flow behaviour of the material had greater impact; the Newtonian ink flowing better than the non-Newtonian ink.

The combination of the anilox wavy channel coupled with the ink, which had small viscosity, surface tension, and filament breakup time, offered greater ink release during the printing process. The increase of ink release would increase the optical density, which increased the vibrancy of the colour. Additionally, the reduction in ink spreading would afford finer print quality.

This chapter has highlighted the different ink release and volume issues related to the open channel anilox. Although the supplier provided what they believed to be two similar engravings, the ink release was dependent on the tone values. This highlights the issues which the industry is facing in accepting these new geometries. There is also a need to relate the performance to conventionally engraved cylinders for which there is plenty of industry experience. The results both in this and the previous chapter highlight the impact of ink viscosity as inks become more heavily loaded with complex long chain polymers leading to non-Newtonian viscoelastic and extensional behviour, even in inks with low shear viscosity. Therefore, the following two chapters examines ink release using a laboratory scale flexo press with different anilox geometries for a range of capacities with three different inks: UV Cyan, conductive Carbon, and conductive Silver. The three inks represent a conventional graphics and two functional conductive inks. These had a greater range of viscosity, elastic modulus, and filament breakup time than those used so far, so as to enable the critical ink characteristic for ink release from anilox cells to be identify.

In chapter 6, a plain solid plate (100% coverage) was used which would bridge across the cells and the wavy channel to allow the impact of cell geometry on ink release to be investigated without the influence of flow around the edge of the feature. In chapter 7 a half tone plate is used to allow the interaction of the tonal patches with the anilox patterns to be examined independently.

Chapter 6

Ink Transfer from Anilox Cells

6.1 Introduction

The anilox cell geometries and the ink characteristics influence ink release from anilox cells. The amount of ink released is determined by cell volume, width, depth, depth-to-width ratio and shape. The anilox cell volume determines the capacity, i.e. the amount of ink available for ink transfer to the plate. However, the proportion of ink released depends on geometry. The ink release from a range of the anilox cell sizes and shapes using inks with different viscosities was investigated using a benchtop printability tester. A flexo plate with 100% coverage (i.e. a solid) was used as this would allow the effect of cell shape on ink release to be determined without the influence of half tone dot dipping, i.e. where the half tone dot does not cover the whole of the anilox cell and receives additional ink along the sides of the half tone or by the flow of ink through the channel. The interaction of the half tones with the anilox cell geometry is investigated in chapter 7.

A laboratory scale flexographic printing press, RK Flexiproof 100 was used (**Figure 6.1**). It is a scaled down version of a full sized flexo press. It can operate up to 99m/min print speed [rkprint.com]. The effect of print speed was also examined as this is relevant when scaling the work to industrial press.

As well as hexagonal closed cells, which are normally used in the flexographic printing process, elongated hexagonal open cells, wavy channels, and open quadratic cells were included in the investigation. These new shapes and configurations are being promoted by suppliers to improve the ink transfer. However, there is little scientific evaluation of these claims. Elongated hexagonal open cells and wavy channels were chosen because of the shape evolvement in which the height of cell wall between the neighbouring cells is reduced to connect (open cells) and then the cell wall was completely removed (wavy channels). When the wall is opened, it will allow the ink to flow out. This trend was found using optical density on prints produced by a commercial press in chapter 5, the anilox wavy channels appearing to release the ink out of its cells better than the anilox elongated closed cells. The anilox wavy channels

may allow the ink to freely flow along its track during the printing process and this might improve ink transfer. The reduced cell walls increased the contact area with the plate dot; plate dot could receive more with greater consistency in ink lay-down of the printed dot. The anilox open quadratic cells was developed using the mechanically engraving technique to improve the release of ink; The difference of engraving technique is also considered as to whether it alters the ink release. Kapur (2003) investigated and compared the ink release performance of the mechanically engraving against the laser engraving in the gravure printing process. His studies used low viscosity Newtonian inks with anilox closed cells.

As well as considering the impact of cell volume and geometry, the ink release using the high viscosity inks is compared with a conventional low viscosity graphics ink. As inks become more sophisticated using alternative carrier fluids such as for UV and with higher pigment loading for applications such as printed electronics and sensors, there is an increase in the viscoelasticity and extensional properties of the inks. Shear thinning and extensional viscosity was observed in the high definition inks used in the commercial press trials (chapter 5).

The experimental procedure is described in the next section, followed by the full physical characterisation of the inks. A comprehensive study of ink release for all three inks from 15 bespoke anilox produced specifically for this trial is then presented.

Figure 6.1: The reel-to-reel (RK flexiproof 100) press [rkprint.com]

6.2 Experimental Method

A standard solid plate with the thickness of 1.7mm supplied by RK PrintCoat was used for the investigation. Three commercial UV inks; Cyan, Carbon, and Silver were used. The substrate was a flexible thin film PET (Polyethylene terephthalate).

The engagement of the anilox, plate, and substrate rolls had to be set on the RK flexiproof 100 press. The engagement between the anilox roll and the printing plate roll was adjusted until the gap reached the "kiss contact" position, where the ink coated evenly over the plate with a small deformation but no damage to the plate. This kiss-contact gap was 240μm (64 steps engagement; 1 step is 4μm). Similarly, the engagement between the printing plate roll and the substrate roll was set, the gap adjusted until sharp and consistent images on the printing plate were printed on the substrate (**Figure 6.2**). The gap was 280μm (70 steps engagement). The printing speed was set at 50m/min. The prints were done 3 times for each investigation. The anilox cells were measured every print to determine; empty anilox cells volume, volume of filled ink before print, and volume of ink left after print. The measurement of anilox cells was done using the Alicona Infinite Focus microscope. The ink release volume was then quantified. The printing speed was increased to 90m/min to investigate the effect of the print speed.

Figure 6.2: Image to check the engagement gap

6.2.1 Physical Characterisation of the inks

The ink shear viscosity, filament breakup profiles, and elastic modulus measurement were carried out. The extensional viscosity of the UV Carbon and Silver inks could not be calculated, as their surface tension, which was required in determination of the extensional viscosity, could not be measured because of their thick paste consistency. However, the filament breakup profiles enabled the comparison of the ink release.

The manufacturing specification of the commercial inks used for the investigations is shown in **Table 6.1**.

Table 6.1: The commercial information of inks used in the printing process

Inks	**Main Contents (%)**	**Shear Viscosity at 50s^{-}1, 25^{o}C (Pa.s)**	**Suppliers**
UV Cyan	no information	no information	Solaflex Nova SL DK03 process (SNS25) SunChemical
UV Carbon	no information	1.0-3.0	Gwent Electronic Materials
UV Silver	Silver (Ag) min.72	3.0-6.0	Gwent Electronic Materials

Ink Shear Viscosity

The shear viscosity of UV Cyan ink was low compared to the other two inks (**Figure 6.3**). It was approximately 1Pa.s at shear rate of 1s^{-1} comparing to approximately 100 and 90Pa.s for UV Carbon and Silver inks respectively. When the shear rate increased, the shear viscosity of UV Carbon and Silver inks decreased, whilst the shear viscosity of UV Cyan ink was approximately constant. The UV Carbon and UV Silver inks were shear-thinning. UV Cyan ink should flow more readily than UV Carbon and Silver inks because it had much lower viscosity than those two inks before shear.

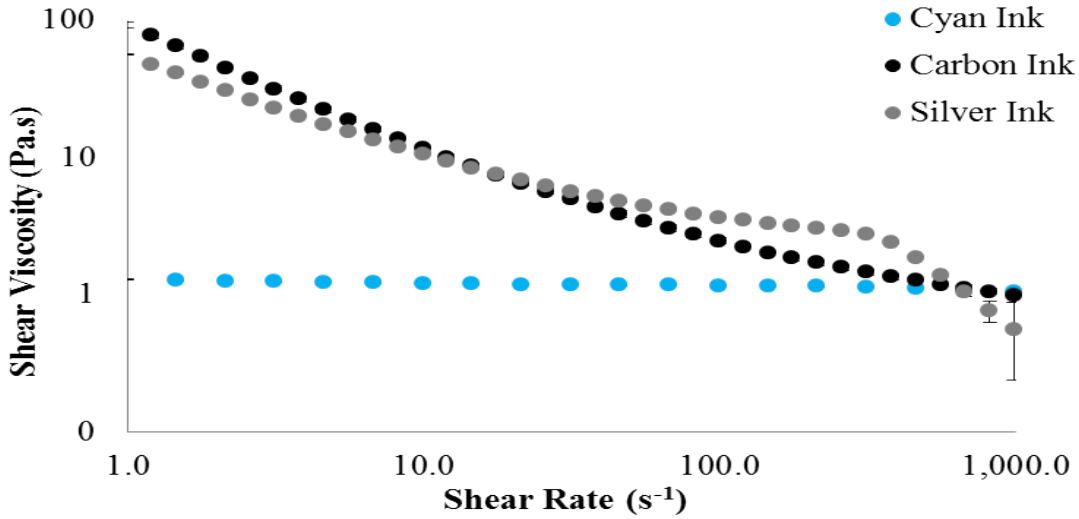

Figure 6.3: The shear viscosity of UV Cyan, UV Carbon, and UV Silver inks

When the shear rate was less than 50s^{-1}, the UV Silver ink should flow better than the UV Carbon ink because of lower shear viscosity. When the shear rate increased to approximately 50s^{-1}, the shear viscosity of UV Carbon and Silver inks approximately equal at 9s^{-1} This was slightly greater than the shear

viscosity given by the manufacturer; however, the manufacturer data was done at 25^{o}C. The shear viscosity test of UV Carbon and Silver was carried out at 20^{o}C, therefore their shear viscosity was consistent with the information given by manufacturer. When the shear rate was above 50s^{-1}, the shear viscosity of UV Carbon was smaller than that of UV Silver ink; therefore, UV Carbon ink should flow better than UV Silver ink in this region.

However, when the shear rate increased to approximately 600s^{-1}, the shear viscosity of UV Silver dropped rapidly, and became smaller than the shear viscosity of UV Cyan and Carbon inks. The sharp decrease of the shear viscosity of UV Silver ink could be due to its structure breaking down, and the wall-slip effect. When the shear rate reached approximately 50s^{-1}, the shear viscosity of UV Carbon ink was smaller than that of the UV Silver ink because of the structure breakdown. The wall-slip effect could be the cause of the sharp decrease of the shear viscosity of the UV Silver ink at the shear rate beyond approximately 800Pa.s. The content of Silver was very high in UV Silver ink (by its portion in the ink compared to other commercial silver ink, which typically had approximately 65% of silver component) [Dycotecmaterials.com., 2020]. A thin low viscosity layer of ink could have formed between the solid plate and thicker layer of ink. This thinner layer of ink gave a lower viscosity which did not represent the bulk of the ink. The large fluctuation of data observed during the last stage of measurement; showed the instability as the of material structure arranged under shear. Even though there was the error due to the wall-slip effect, the shear viscosity data was consistent prior to this point. The trend of shear viscosity data could be used for the interpretation of the results.

Ink Filament Breakup Profiles

The more liquid-like UV Cyan ink had a curved shape during the CaBER test, which is typical of the material with a very low viscosity and behaviour approximating to a Newtonian fluid (**Figure 6.4**). This contrasts with the filament profiles of the UV Carbon and Silver inks which are typical of a yield-stress material. UV Carbon ink filament was elongated much further and had a pointed cone comparing to the UV Cyan ink. UV Silver ink filament had the shape of pointed cone and the longest elongation.

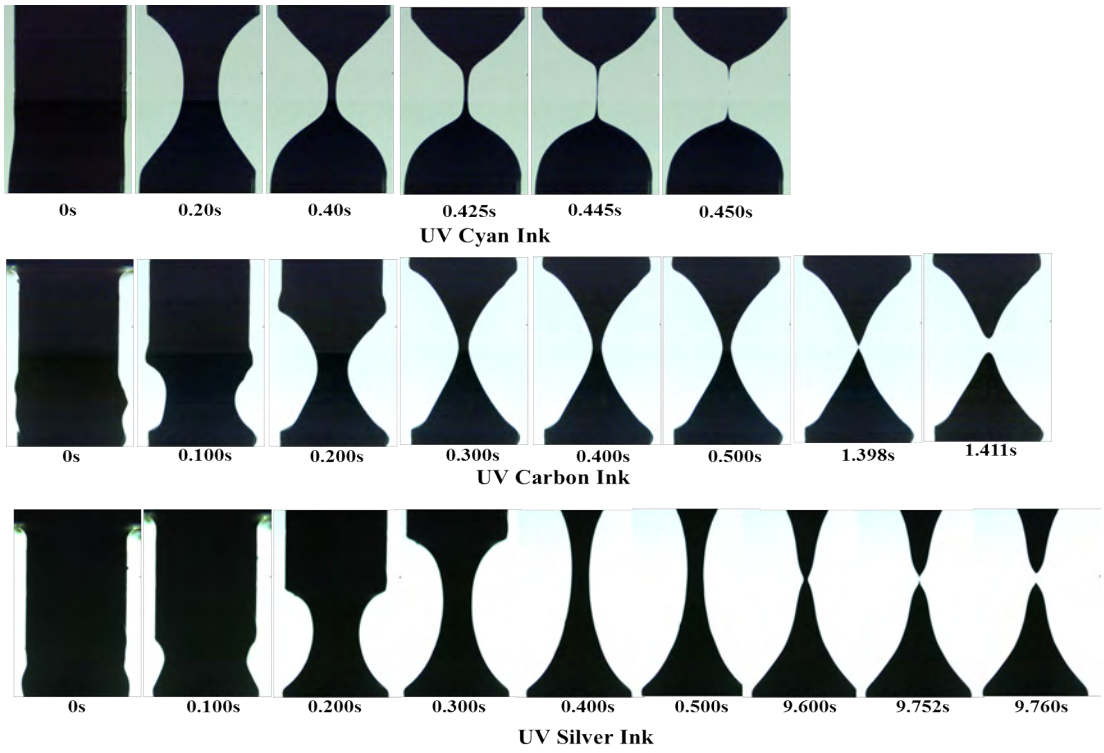

Figure 6.4: Filament stretching and breakup of UV Cyan, Carbon, and Silver inks

In the corresponding filament breakup profiles (**Figure 6.5**), the filament of UV Cyan ink broke instantly. The filament of UV Carbon ink took slightly over 1 second to break. It took approximately 10 seconds for the filament of UV Silver ink to break. The UV Cyan and Carbon inks were more likely to split between the plate and the anilox cell away whilst UV Silver ink would extend further. This could either draw more ink from the anilox cell or less be released to the plate as it remains attached to the anilox.

The elongation of ink filament would indicate the pull-out factor of the ink; the longer the elongation, the more ink would be pulled out. The UV Silver ink should be pulled out the most, then UV Carbon ink, and the least would be UV Cyan ink. Elastic modulus was the attribute used to examine the pull-out effect of the ink. Ink elastic modulus profile under shear stress could indicate the degree of ink being pulled out of the anilox cells during the printing process. The oscillation test using the small amplitude oscillatory shear (SAOS) mode was carried out to examine the viscoelastic behaviour of the inks.

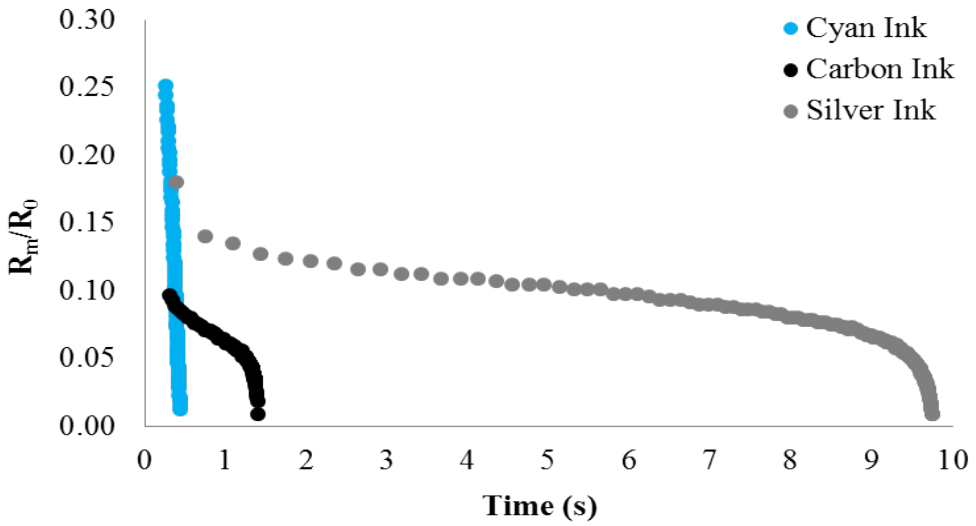

Figure 6.5: The filament breakup profiles of UV Cyan, Carbon, and Silver inks

Ink Viscoelastic Characteristics

The viscous modulus (G") of UV Cyan ink was approximately constant at 10Pa. Whilst its elastic modulus (G') was much smaller and lower than 1Pa, and started decreasing when the shear stress was approximately 8.0Pa indicating the structure breakdown (**Figure 6.6**). Its viscous modulus was greater than its elastic modulus (G') indicating it to be liquid-like.

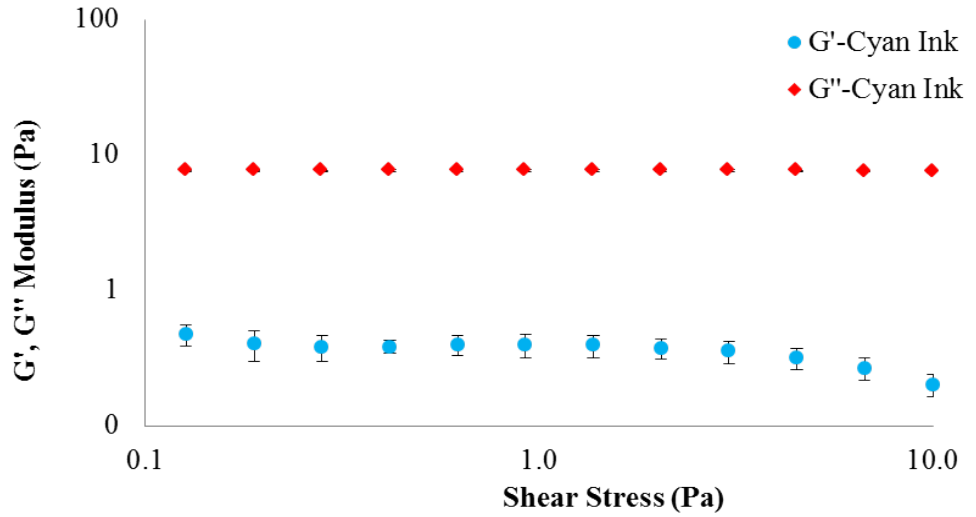

Figure 6.6: Viscoelastic characteristic of UV Cyan ink

Initially in the region of shear stress below 5.0Pa, there was a significant fluctuation of the measurement for both viscous (G") and elastic (G') modulus of UV Carbon ink (**Figure 6.7**). The trend of constant elastic modulus could be observed in this region of shear stress: indicating its linear viscoelastic region (LVR). In this region, the viscous and elastic modulus were approximately

3,000Pa.

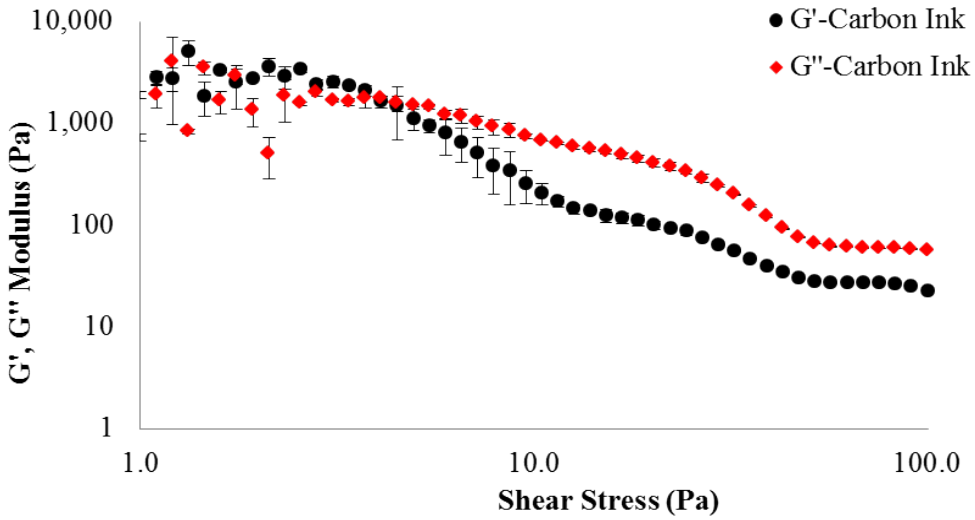

Figure 6.7: Viscoelastic characteristic of UV Carbon ink

When the shear stress increased beyond 7.0Pa, its elastic modulus was smaller than its viscous modulus indicating it was liquid-like. There was significant fluctuation of data when the elastic modulus started decreasing, the fluctuation occurred due to the structure breakdown and rearrangement of the particles of the ink. The data became stable at shear stress of approximately 10.0Pa. The viscous and elastic modulus appeared to be constant at approximately 100 and 60Pa respectively when the shear stress increased to approximately 80.0Pa. Its phase angle data was examined because it could indicate whether the ink was solid-like (phase angle smaller than 45^o) or liquid-like (phase angle greater than 45^o).

The phase angle in the low region of shear stress was fluctuating (**Figure 6.8**). However, in the region of shear stress below 5.0Pa, UV Carbon ink was more likely to be solid-like as its phase angle was smaller than 45^o. When the shear stress increased beyond approximately 7.0Pa, it transformed to be liquid-like. The phase angle increased when its elastic modulus decreased and became smaller than its viscous modulus. The swift decrease of elastic modulus was due to its structure breakdown to become more liquid-like as the shear stress increased. This indicates the yield stress characteristic of UV Carbon ink. It would require minimum shear stress of approximately 7.0Pa to make UV Carbon ink flowed.

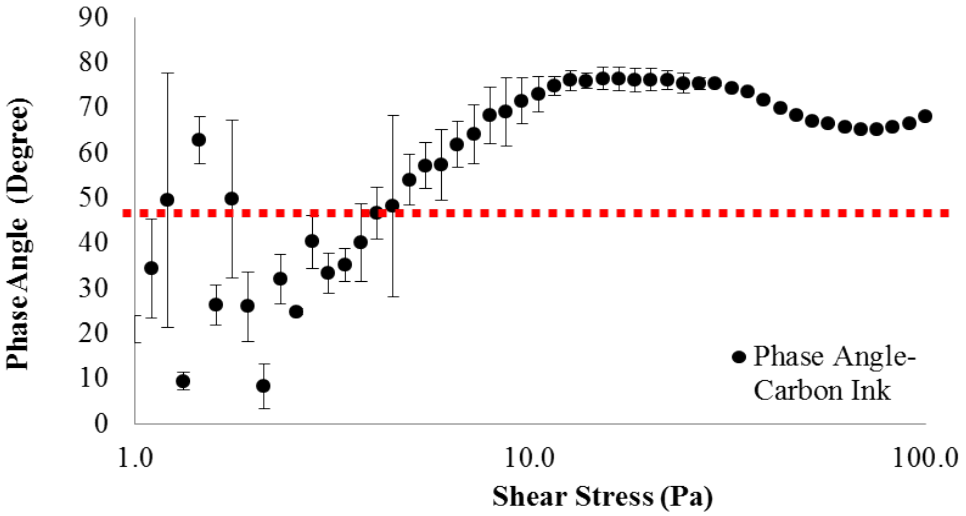

Figure 6.8: Phase angle of UV Carbon ink

The significant fluctuation of the data in the low region of shear stress was due to its high particulate content. Although the information of ink content was not given by the ink manufacturer, the ink was in paste form indicating a high content of particles. The high content of particles caused the instability of measurement in the low region of shear stress. The rearrangement of particle during low shear stress caused the measurement to fluctuate. As the shear continued, the arrangement of the particles became stable and less fluctuation occurred.

Similarly, to UV Carbon ink, in the region of shear stress below 5.0Pa, there was a significant fluctuation of the measurement for both viscous (G") and elastic (G') modulus (**Figure 6.9**). UV Silver ink had minimum content of Silver of 72%. The fluctuation occurred as particles rearranged during shear. However, when the shear stress increased, the measurement stabilised. Contrary to UV Carbon ink, the viscous modulus of UV Silver ink was dominant and greater than its elastic modulus independent of shear stress, indicating the UV Silver was liquid-like at any shear stress. Its liquid-like behaviour should encourage ink flow; however, its filament breakup time was large. The comparison of the ink release would reveal whether the large filament breakup time hindered the release of UV Silver ink from the anilox cells. Its linear viscoelastic region (LVR) was in the region of shear stress below approximately 10.0Pa. Beyond the shear stress of 10.0Pa, its viscous and elastic modulus started decreasing. The viscous and elastic modulus decreased to approximately 90 and 10Pa respectively and plateaued when the shear stress reached approximately 80.0Pa.

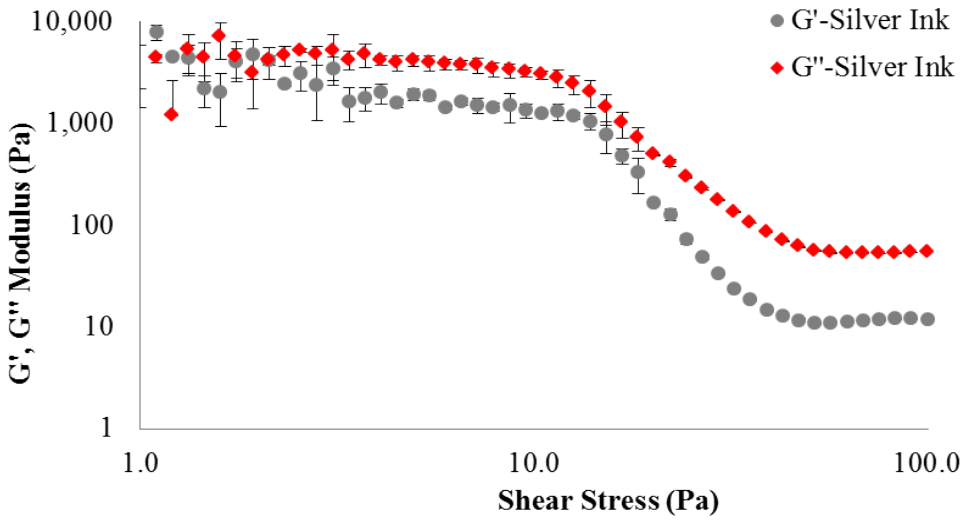

Figure 6.9: Viscoelastic characteristic of UV Silver ink

The elastic modulus of UV Cyan was small compared to the other two inks (**Figure 6.10**). Its elastic modulus was approximately 0.5Pa. Whilst the elastic modulus of UV Carbon and Silver was approximately equal at 3,000Pa initially. The elastic modulus of the UV Carbon started decreasing at approximately 7Pa, whilst the elastic modulus of the UV Silver ink started decreasing at approximately 20Pa, and then plateau at approximately 100Pa.

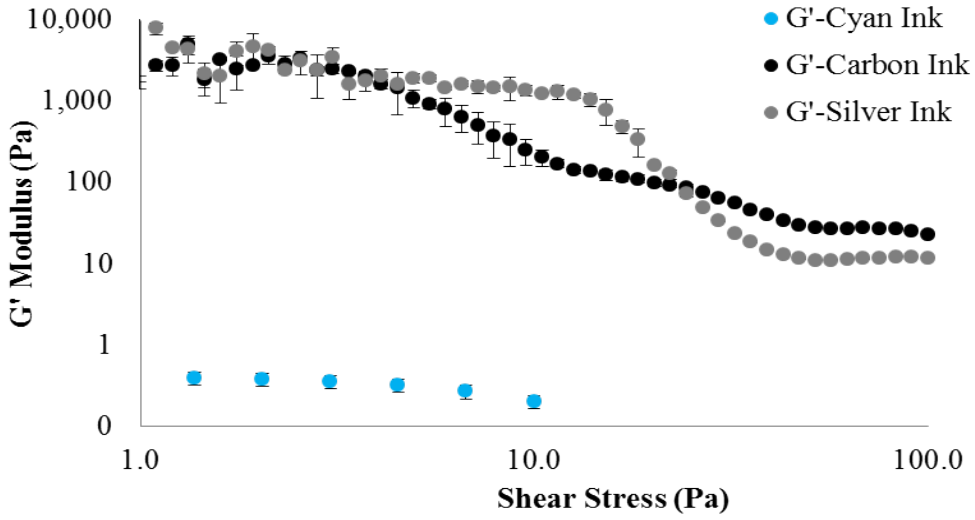

Figure 6.10: The comparison of elastic modulus of UV Cyan, Carbon, and Silver inks

When the shear stress increased beyond 7Pa, the elastic modulus of UV Carbon decrease to be smaller than that of UV Silver ink. The elastic modulus of UV Carbon ink was smaller than that of UV Silver ink until shear stress increased up to approximately 40.0Pa. In the region of shear stress greater than 7.0Pa and smaller than 40.0Pa, the UV Silver ink had a greater elastic modulus and

should be pulled out more than UV Carbon ink. However, when the shear stress increased to be greater than 40.0Pa, the elastic modulus of UV Carbon ink became greater; therefore, UV Silver ink should then be pulled out less than UV Carbon ink.

The shear viscosity, filament breakup, and elastic modulus suggest the UV Cyan ink, which had smallest viscosity would flow better than UV Carbon and Silver inks, which had much greater viscosity. Additionally, it should be released out of the anilox cells better than the other two ink as it had smallest filament breakup time. However, UV Carbon and Silver inks could have more pulled out than UV Cyan ink because their elastic modulus were much greater. The filament breakup time was another parameter to determine if the greater pull-out of the UV Carbon and Silver inks would be release to the printing plate or recoil back to the anilox cells.

The ink release out of the anilox cells were then examined to determine which attributes of inks; shear viscosity (ink flow), filament breakup (ink split), elastic modulus (ink pull-out) is more critical to the ink release out of the anilox cells to the plate.

6.3 Results of the Experiments

6.3.1 Effect of anilox cell geometry on ink release

The anilox cells (**Figure 6.11**) were measured dry to determine the inked volume (**Table 6.2**). The inked, and after-print anilox cells were measured by Alicona InfiniteFocus microscope to determine the ink volume released to the printing plate. The method of the characterisation of the anilox cells, inks, and the ink volume during the printing process has already been described in 3.2.2. These results are summarised in Appendix A – Measurements of anilox and ink release. The following sections include exemplar direct comparison of anilox with similar parameters where appropriate as well as where the combined results identify overall generic trends. A full set of direct comparisons is included in Appendix B – Direct comparisons of ink release from anilox.

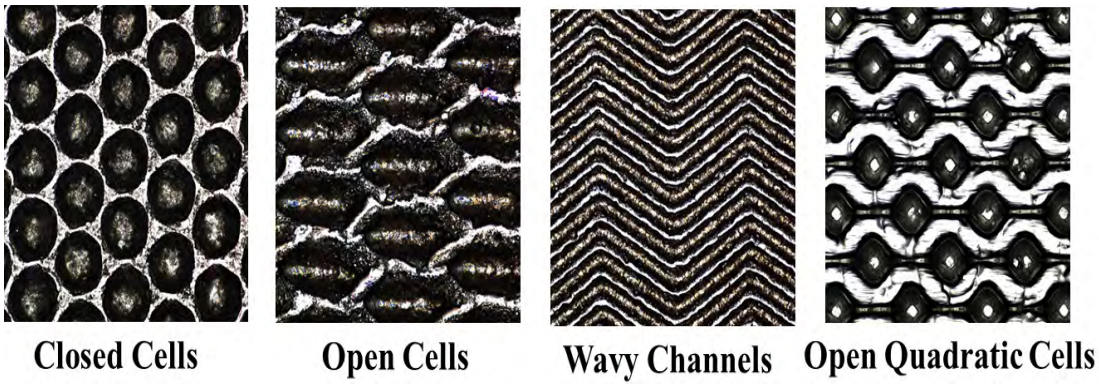

Figure 6.11: Anilox cell geometries

Table 6.2: Summary of anilox measurement

Anilox Cell Shapes	**Anilox Reference**	**Anilox Cell Volume (cc/m^2)**	**Anilox Cell Width (μm)**	**Anilox Cell Depth (μm)**	**Depth to Width Ratio**	**Engraving**
Print Speed of 50m/min						
Conventional Closed Cell	A	6.45	73	16	0.22	Laser
	B	2.76	38	7	0.18	Laser
Hexagonal Closed Cell	C	2.67	39	12	0.31	Laser
	D	2.94	39	14	0.36	Laser
	E	5.10	56	15	0.27	Laser
	F	6.00	71	17	0.24	Laser
	G	7.42	71	21	0.30	Laser
Elongated Hexagonal Open Cell	H	4.84	58	16	0.28	Laser
	I	5.68	70	18	0.26	Laser
	J	8.62	70	26	0.37	Laser
Wavy Channels	K	6.86	56	17	0.30	Laser
	L	7.28	71	17	0.24	Laser
	M	11.10	71	31	0.44	Laser
Open Quadractic Cell	O	6.46	70	22	31	Mechanical
Print Speed of 90m/min						
Conventional Closed Cell	B	2.76	38	7	0.18	Laser
Hexagonal Closed Cell	F	6.00	71	17	0.24	Laser
Elongated Hexagonal Open Cell	I	5.68	70	18	0.26	Laser
Wavy Channels	L	7.28	71	17	0.24	Laser

6.3.1.1 Closed Anilox cells

The conventional closed cells and hexagonal closed cells (anilox A to G) represent the cell patterns currently most commonly in use on flexible packaging. The greater anilox cell volume with much larger cell size should make the ink flow out more easily so a greater proportion is released than with the smaller cell size. Additionally, the anilox cell with wider cell width had already been found to release greater proportion of graphic ink (chapter 4).

The total ink release from anilox A and B were compared for all three inks (**Figure 6.12**). A large volume of ink was released from the larger volume anilox cell. The results agreed with the studies of Damroth et al (1996), Hamblyn (2004), Cherry (2007), and Beynon (2007) who showed the anilox cell volume was the greatest dominant parameter of the volume of the ink transferred to the plate. The degree of increase of ink release due to the increase of anilox cell volume was different for each ink. The differences could be attributed to the ink properties. UV Cyan and Carbon inks, which had small filament breakup time, had greater portion of increase comparing to UV Silver ink, which had large filament breakup time. The cell volume and ink properties had an effect on the ink release but the effect of anilox cell volume appeared to be dominant.

The wider anilox cell released greater ink but the deeper anilox cell hindered the ink release. This direct comparison of cells made by the same process should highlight the effect of the depth-to-width ratio in which the greater depth-to-width ratio had the contrary attributes of wider and deeper cells. If the anilox cells with the greater depth-to-width ratio better release ink, it would indicate that the width of the anilox cell would have greater impact than the depth of the anilox cell. However, if the anilox cells with smaller depth-to-width ratio released better ink, it would indicate that the depth of the anilox cell would have greater impact than the width of the anilox cell.

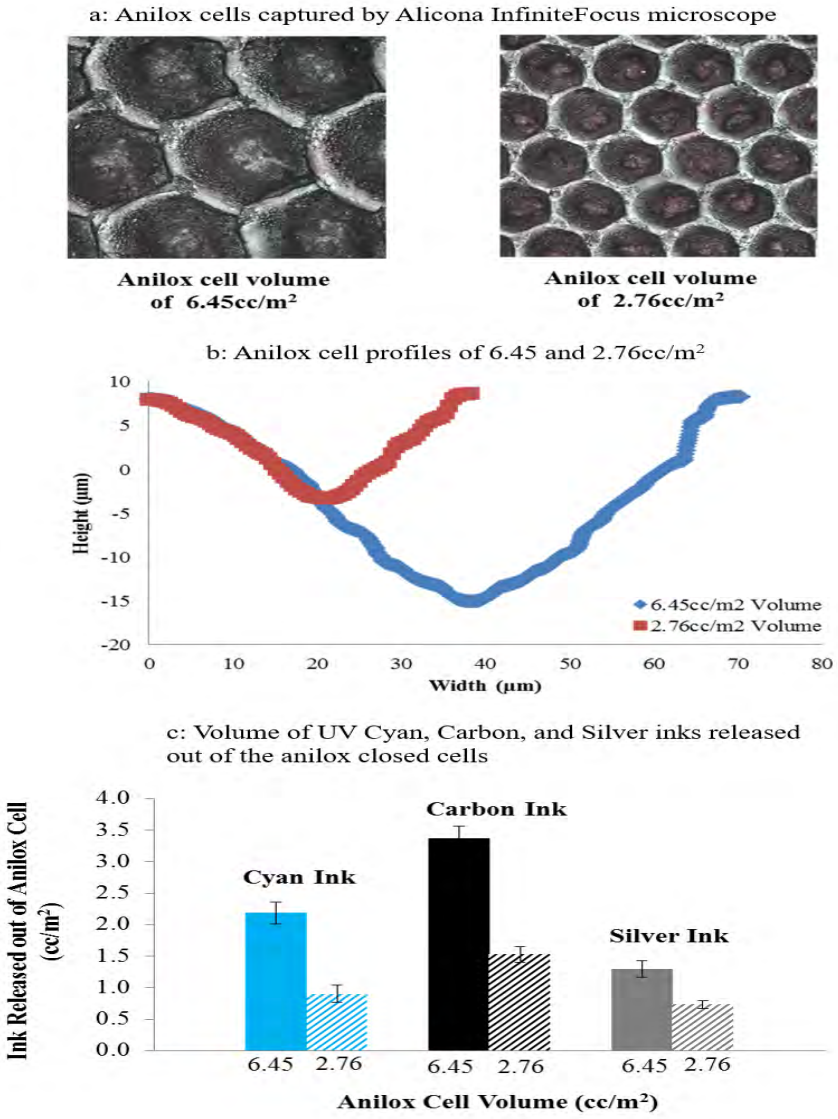

Figure 6.12: Anilox cells (a) and the cell profiles (b) and Volume of inks release (c) of 6.45 (A) and 2.76 (B) cc/m^2

The anilox cells with the smaller depth- to-width ratio should release greater ink because the shallower cells required less force to pull out and the wider cells had the bigger opening for the ink to be released. As the depth-to-width ratio decrease, the ink release increased for all the inks (**Figure 6.13a**). However, the increase depended on the ink characteristics as the degree of increase varied for each ink. The increase of UV Cyan and Silver inks was not significant of 1% compared to the increase of UV Carbon ink of 12%. The UV Carbon ink had large viscosity but small filament breakup time. The anilox cell with smaller depth-to-width ratio coupled with the ink, which had large viscosity but small filament breakup time, would improve the ink release out of the anilox cells.

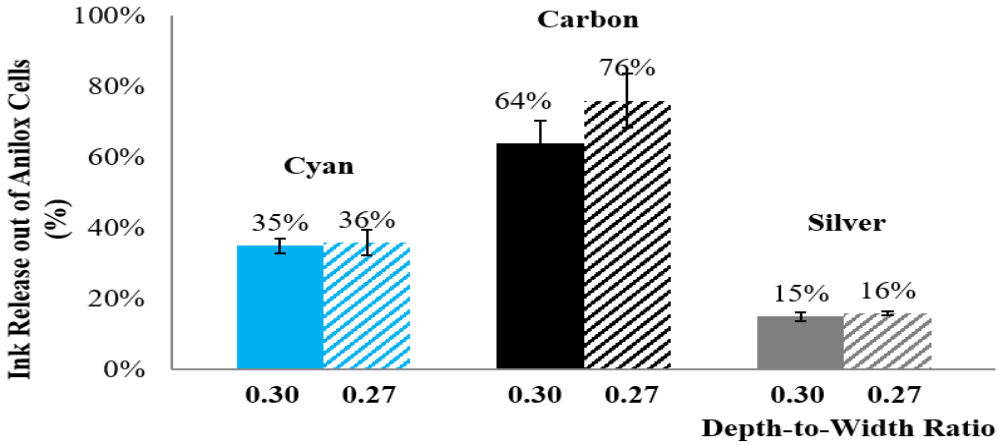

a: The ink release out of anilox closed cells using UV Cyan, Carbon, and Silver inks with anilox cell depth-to-width ratio of 0.27 (E) and 0.30 (G)

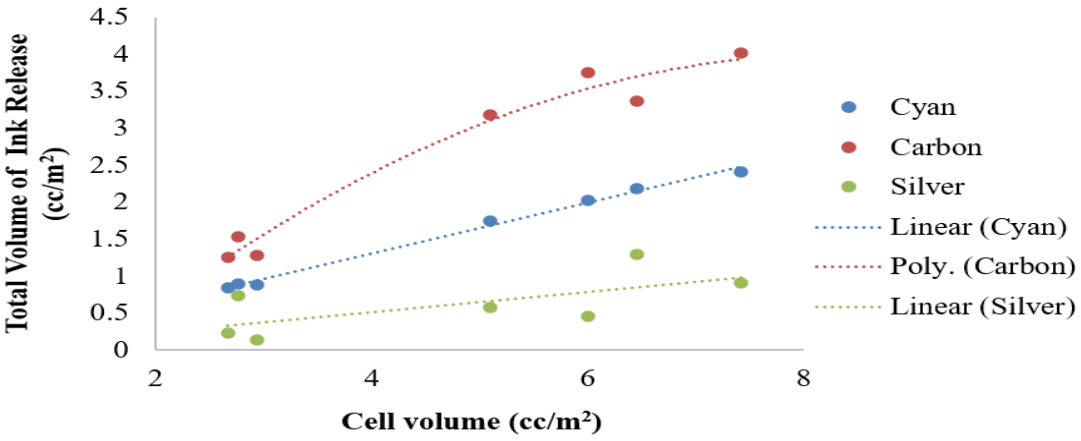

b: Total volume of ink release vs cell volume for anilox closed cells

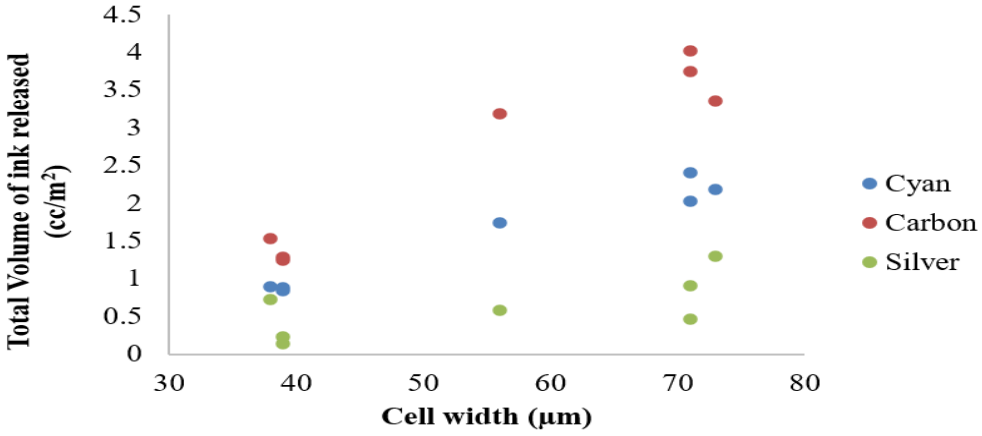

c: Total volume of ink release vs cell width for anilox closed cells

Figure 6.13: a: The ink release out of anilox closed cells using UV Cyan, Carbon, and Silver inks with anilox cell depth-to-width ratio of 0.27 (E) and 0.30 (G), b: Total volume of ink release vs cell volume for anilox closed cells, c: Total volume of ink release vs cell width for anilox closed cells

The cell geometries are similar for anilox rolls A to G, allowing the total volume of ink released to be compared to the anilox volume (**Figure 6.13b**). The UV Cyan graphics ink exhibits a linear relationship with the volume of the anilox cells. The UV Carbon ink over the range of anilox tested shows an increasing 2^{nd} order polynomial curve, with a steadily decreasing gradient. It appears to be approaching a direct relationship with the cell volume as the proportion of ink released approaches 100%. 2^{nd} order polynomial relationship of UV Carbon ink gives better fit than linear relationship and reflects greater proportion of UV Carbon ink release. UV Carbon ink has high viscosity but small filament breakup time, which aid in ink being pulled out and easily released from the anilox cells. In contrast, UV Cyan ink has low viscosity which does not aid in ink being pulled out. UV Silver ink has high filament breakup time, which hinders the ink to split and be released from the anilox cells.

The cell width gives more opportunity for the ink to be released and there is a general trend for the amount of ink released to increase with width (**Figure 6.13c**). However, this is unsurprising as the width of the cell would have a direct relationship with the volume of the cells.

Figure 6.14a shows the cell profiles of the closed anilox cells of 2.94 and 5.10cc/m^2. These two anilox bands had similar cell depth, but approximately 44% difference in cell width. The difference in cell width made the anilox cells with the cell width of 56μm greater of approximately 74% in volume comparing to the anilox cells with the cell width of 39μm. Due to its wider cell (greater opening for the ink to be released) and much greater cell volume, the anilox cells with the cell width of 56μm would be expected to release greater amount of ink out of the cells. A critical aspect is the slope of the walls.

Figure 6.14b shows the cell profiles of the anilox cell with the depth-to-width ratio of 0.27 and 0.30. These similar depth to width ratio results in a similar slope of the cell walls.

Figure 6.14c shows the cell profiles of the closed anilox cells of 2.67 and 2.94cc/m^2. These two anilox bands had approximately same cell width, but approximately 16% difference in cell depth; the anilox cell with volume of 2.94cc/m^2 has the deeper cell depth, but with similar slopes to the cell walls. This indicated that the depth of the anilox cells was critical to the ink release. The studies of Hewson, Kapur and Gaskell (2011) showed that the gravure with shallower cells had greater degree of the ink release. Therefore, the anilox cells with the cell depth of 12μm would be expected to release greater ink out of the cells.

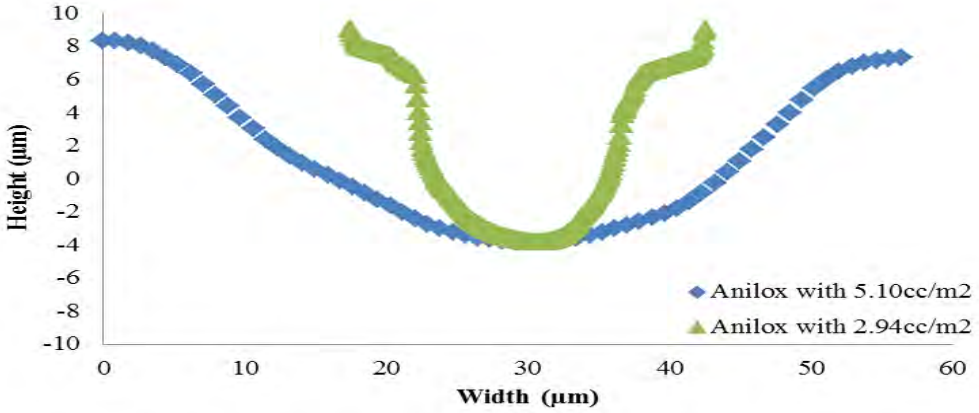

a: The cell profiles of the closed anilox cells of 2.94 (D) and 5.10 (E) cc/m^2

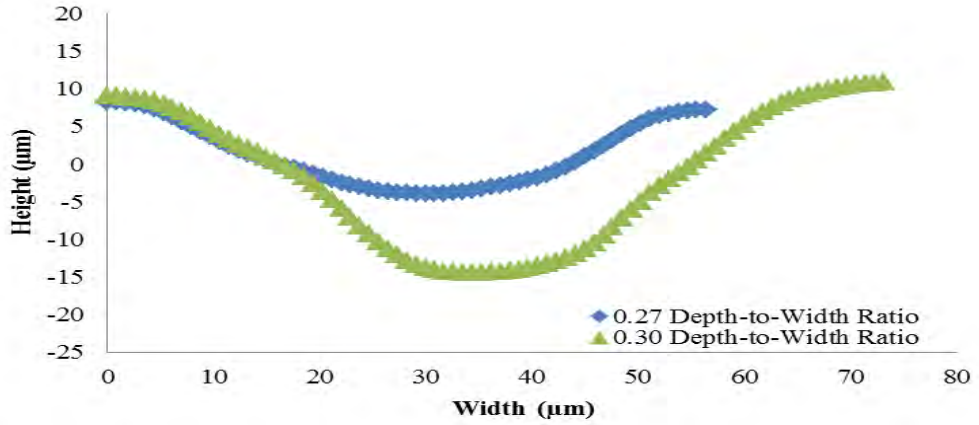

b: The cell profiles of the closed anilox cells with the depth-to-width ratio of 0.27 (E) and 0.30 (G)

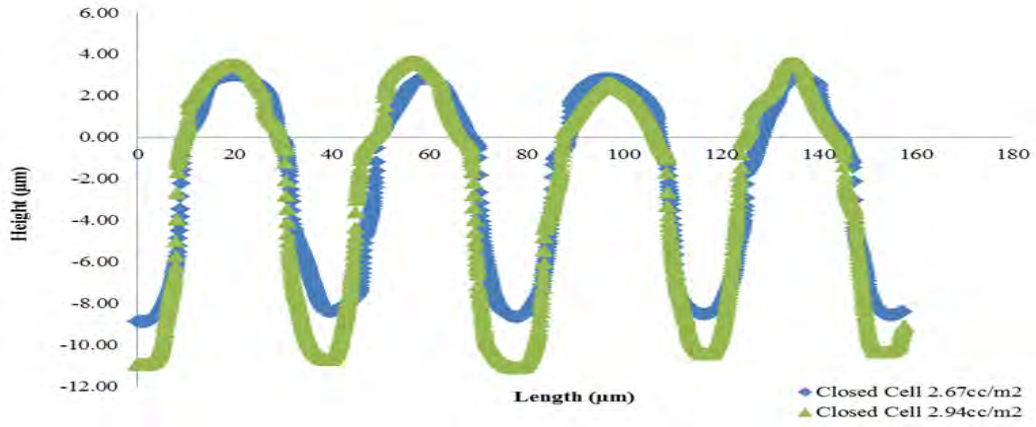

c: The cell profiles of the closed anilox cells of 2.67 (C) and 2.94cc/m^2 (D)

Figure 6.14: a: The cell profiles of the closed anilox cells of 2.94 (D) and 5.10 (E) cc/m^2, b: The cell profiles of the closed anilox cells with the depth-to-width ratio of 0.27 (E) and 0.30 (G), c: The cell profiles of the closed anilox cells of 2.67 (C) and 2.94cc/m^2 (D)

The anilox B cell volume of 2.76cc/m^2 had greater percentage of the ink transfer from the anilox cells to the plate for all the inks especially in the higher viscosity UV Carbon and Silver inks (**Figure 6.15**). The anilox A cell volume of 6.45cc/m^2 had the wider cell width of 73μm (approximately double) compared to 38μm of the anilox cell volume of 2.76cc/m^2. The wider cell width would be expected to have greater release of the ink. Dodds (2011) showed that the wider cavities made it easier to empty the cavity. Similarly, Cherry (2007) showed that the wider anilox opening the more ink transferred to the plate. Considering the cell depth and the depth-to-width ratio of these two anilox cell geometries, the anilox cell volume of 6.45cc/m^2 had deeper cell depth of 16μm (more than double in depth) comparing to the shallower cell depth of 7μm for the anilox cell volume of 2.76cc/m^2. The anilox cell volume of 2.76cc/m^2 had lower depth-to-width ratio of 18% comparing to 22% for the anilox cell volume of 6.45cc/m^2. Kapur (2003) studied the ink release of the different gravure cells. Gravure cells with smaller volume gave better ink release when the ratio of the cell width-to-depth was greater. Hewson, Kapur and Gaskell (2011) also showed that the gravure with shallower cells had greater degree of the ink release. Sankaran and Rothstein (2012) studies showed similar trend that the percentage of ink transferred out of the gravure cells, which had lower aspect ratio of depth and radius, was significantly larger than the gravure cells with higher aspect ratio.

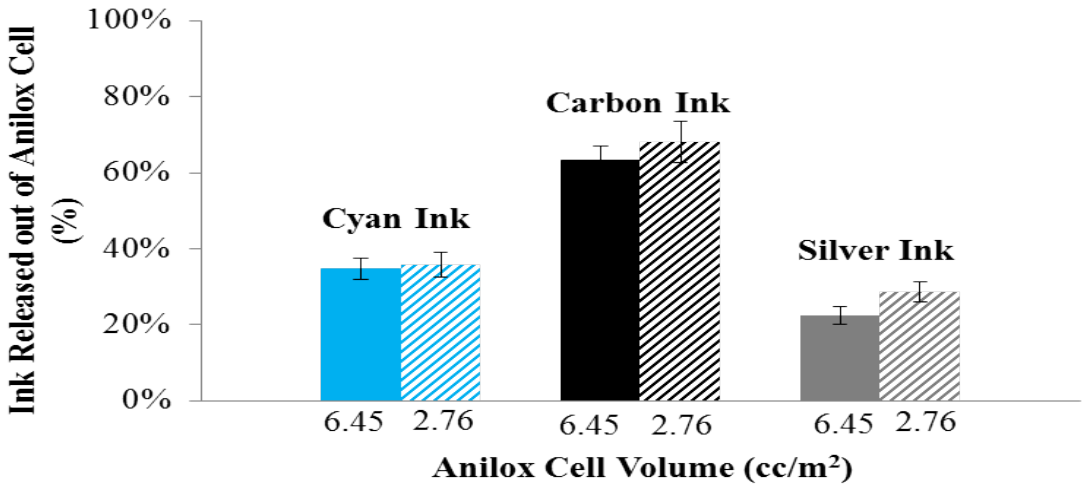

Figure 6.15: Percentage volume of ink released from the anilox cells to the plate

The anilox cells, which had greater cell volume, released greater amount of ink out of its cells; however as a percentage of the initial ink volume filled before print, the proportion was significantly smaller than the ink released out of the anilox cells with smaller cell volume because the anilox cells with smaller cell volume had shallower cell depth and smaller depth-to-width ratio. The depth of the anilox cells was more critical to the ink release than the width. To improve the ink release to the plate, the anilox cells should be shallow and wide; the ink

would be released more to the plate and eventually to the substrate, the thicker ink layer would give the stronger colour for the image print or improve the ink lay-down for functional print.

If the cell depth were the most critical aspect, then one would expect the percentage of ink released to be related to depth. However, this appears to be approximately constant for the graphic inks, falling for the silver ink and random for the carbon ink (**Figure 6.16**).

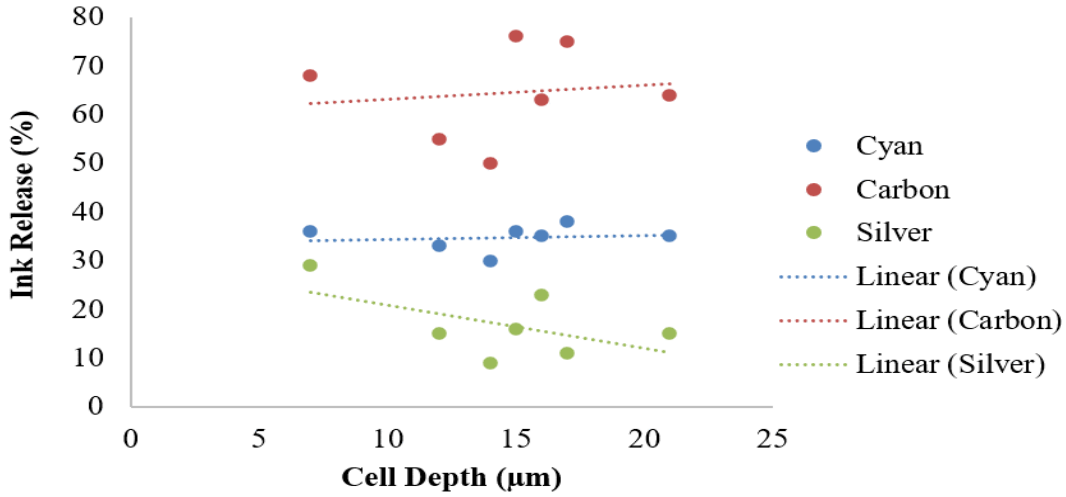

Figure 6.16: Percentage of ink release vs cell depth

6.3.1.2 Engraving Techniques

The mechanically engraving open quadratic anilox was chosen because its attributes were similar to the laser engraving anilox cells, except it had a deeper cell but its open-wall should mitigate the effect of deeper cells; the engraving technique should be comparable. Anilox L and O were used to investigate the anilox cell engraving techniques (**Table 6.3**), which includes the surface roughness.

Table 6.3: The anilox cells used to investigate the effect of anilox cell engraving techniques

Anilox Cell Volume (cc/m^2)	**Anilox Cell Width (μm)**	**Anilox Cell Depth (μm)**	**Anilox Cell Shapes**	**Surface Roughness (μm)**	**Engraving Techniques**
6.00	71	17	Hexagonal Closed cells	436	Laser
6.46	70	22	Open Quadratic cells	2,555	Mechanically

There are some cracks on the surface of the mechanically engraved anilox (**Figure 6.17**). Producing a high surface roughness of approximately 6 times greater than the laser engraved anilox. The rough surface was expected to hinder the release of the ink because the ink is trapped in the rough surface.

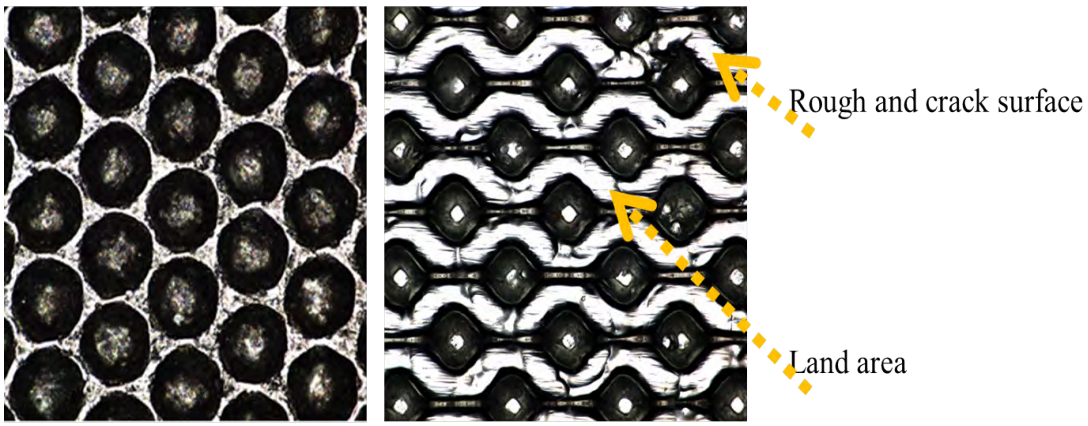

Figure 6.17: Anilox cells engraved by laser and mechanically engraving techniques

The removal of the wall along the open quadratic anilox cells, the additional channel on the edge of the cell profile may mitigate the effect of the ink trap in the rough surface (**Figure 6.18**).

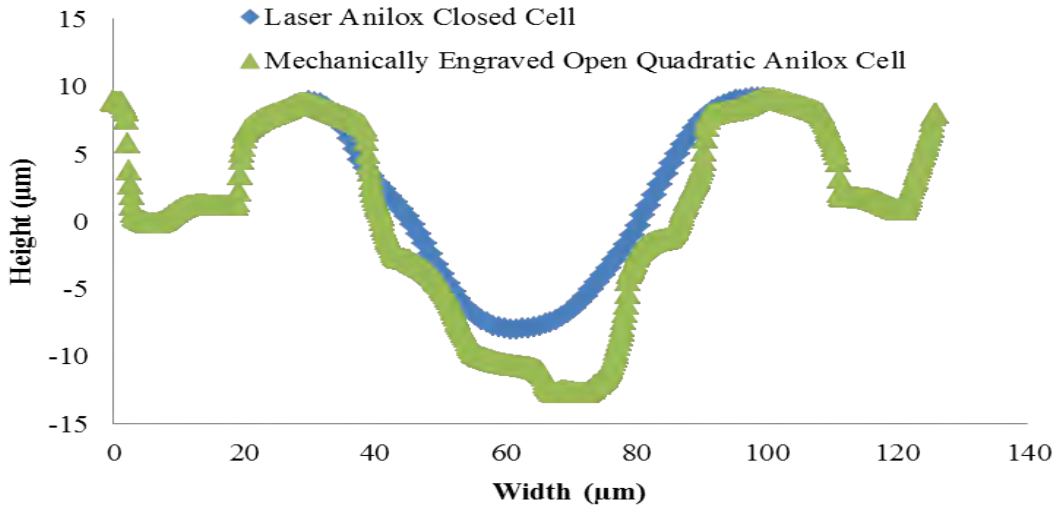

Figure 6.18: The cell profiles of the laser engraving of the anilox closed cells and the mechanically engraving open quadratic anilox cells

The laser engraving anilox released greater ink than the mechanically engraving anilox for all inks (**Figure 6.19**). The mechanically engraving anilox had deeper cell depth and rougher surface. The greater cell volume of the mechanically engraving anilox did not enable it to release more ink. As found previously the cell depth was critical to the ink release, its deeper cells would require greater force to release the inks to the plate.

The surface roughness of the mechanically engraving anilox was approximately 6 times greater than the laser engraving anilox. Additionally, the land area of the top surface of the mechanically engraving anilox in which the roughness and cracks could be seen was greater than the land area of the top surface of the laser engraving anilox. Some of the ink would adhered to the roughness of the cell wall instead of being released to the plate reducing the ink release. Kapur (2003) showed similar trend in that the pickout of the laser engraving anilox cells was greater comparing to the pickout of the mechanically engraving quadrangular anilox cells with similar cell volume and width-to-depth ratio. The laser engraving anilox cells had much smoother surface, which reduced the resistance for the liquid to be released.

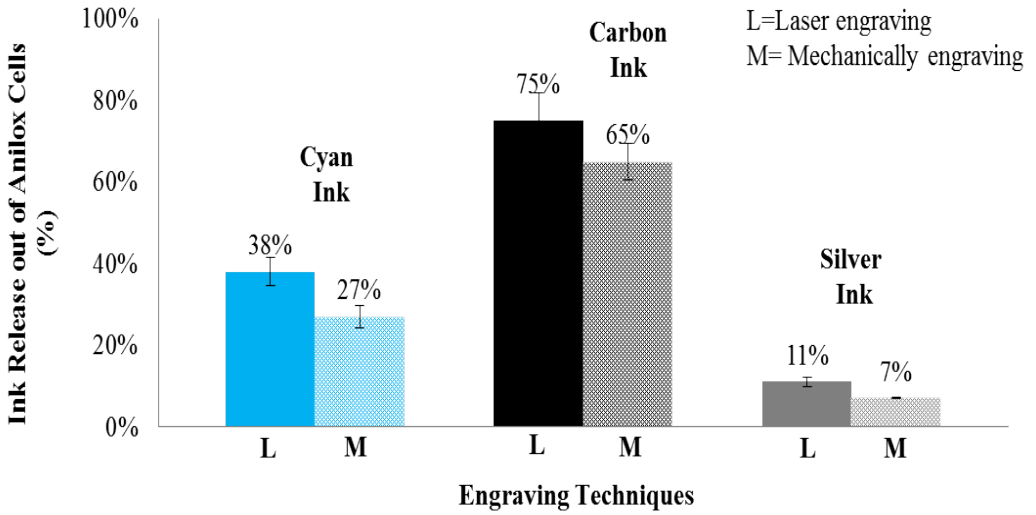

Figure 6.19: Ink release out of laser and mechanically engraved anilox cells

Comparison of ink release with ink type

The percentage of ink released does appear to be related to the depth-to-width ratio as discussion in section **6.3.1.1**, the proportion of ink falling with increasing depth-to-width (**Figure 6.20**). This trend encompasses the production method for the cylinders as it included the mechanically engraved cylinder as well as cylinders laser engraved with two different machines.

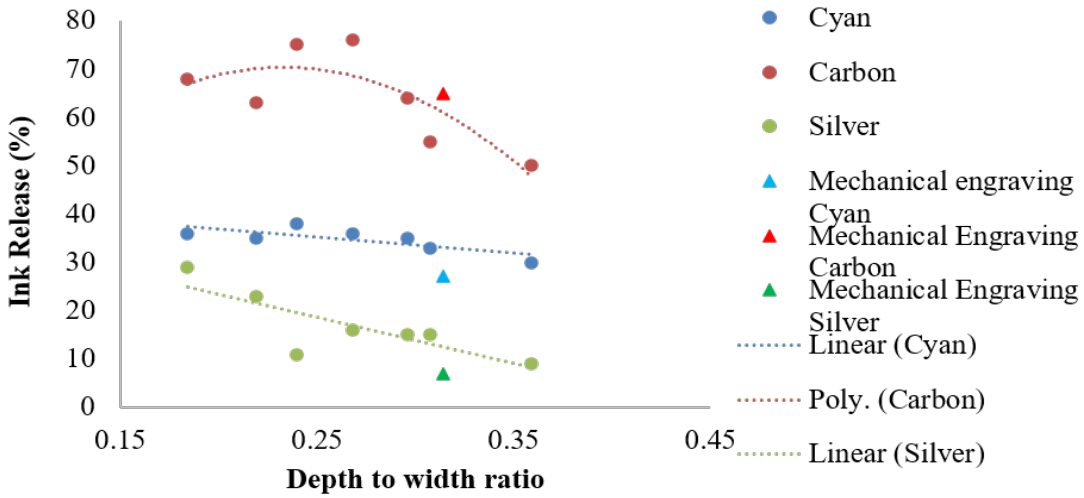

Figure 6.20: Percentage of ink release vs depth-to-width ratio

The proportion of ink released is highly dependent on the viscosity of the inks. The proportion of ink released falls with increasing depth to width ratio. Although the Carbon and Silver ink have similar shear viscosity and viscoelasticity, there is a significant difference between the proportion of ink released. The silver ink had the longest separation time for the ink filament, so

there would have been more opportunity for ink to be drawn back into the cell. This highlights the importance of understanding extensional viscosity and it implications for ink flow and separation.

6.3.1.3 Open Elongated Hexagonal Cells

The cell profile with the depth-to-width ratio of 0.37 was wider and deeper cell (**Figure 6.21**). The anilox open cells with the smaller depth-to-width ratio had greater release for all three inks. The degree of increase was greatest for UV Carbon ink of approximately 25%. However, the increase of the ink release due to the decrease of depth-to-width ratio of UV Cyan ink of approximately 22% was much greater than UV Silver ink, which increased by approximately 1%. The change of the anilox shape affected the ink release. Opening up the wall between the anilox cells, allowed the ink to flow and be more easily released to the printing plate, especially the ink with small filament breakup time such as the UV Cyan and Carbon inks. The much greater filament breakup time of the UV Silver ink still hindered the flow and ink release along the track of the anilox open cells.

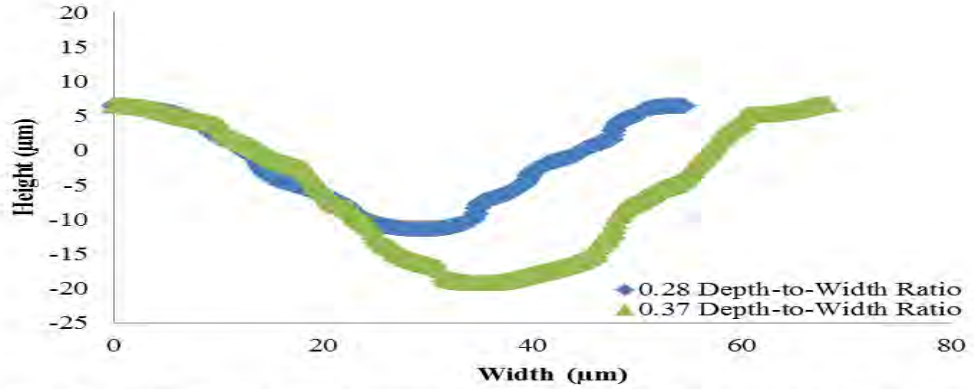

a: Cell profiles of the elongated open anilox cells with the depth to width ratio of 0.28 (H) and 0.37 (J)

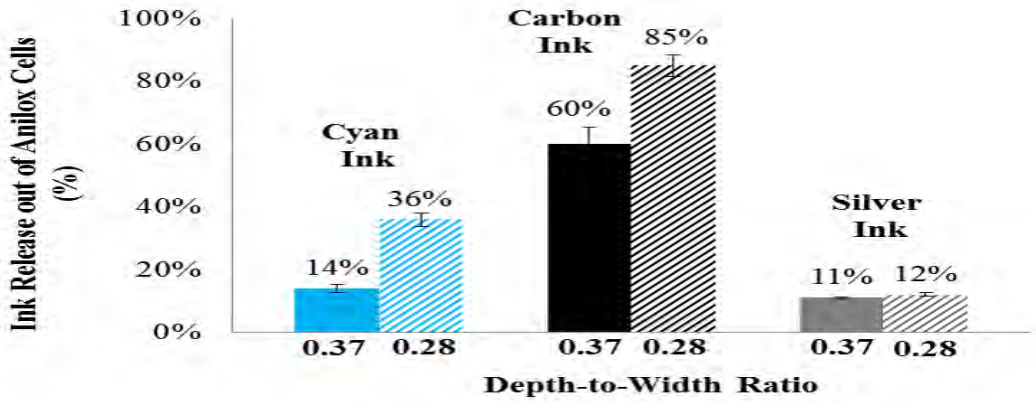

b: Ink release

Figure 6.21: Cell profiles and ink release of the elongated open anilox cells with the depth to width ratio of 0.28 (H) and 0.37 (J)

Similar to the trend seen in the anilox closed cells, the ink release of the anilox open cells increased as the depth-to-width ratio decreased (**Figure 6.22**).

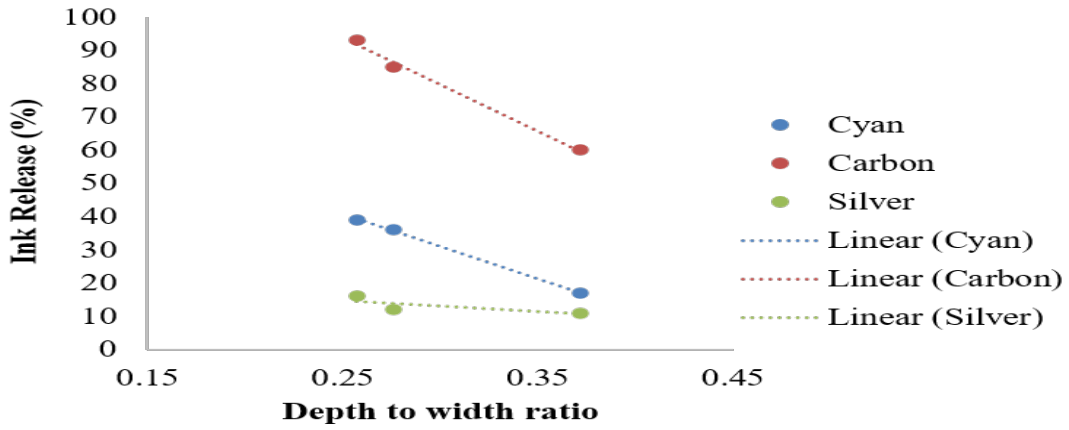

Figure 6.22: Ink release vs depth-to-width ratio of anilox open cells

6.3.1.4 Wavy Channels

The anilox wavy channels had completely different cell shape (**Figure 6.23**). The removal of the walls removed the boundary traditionally used to determined the anilox cell volume; therefore the boundary to determine its volume had to be defined. The empty cells profile is longer as the empty cell volume measured as the air filled the anilox cell. The inked cell is shallowest as the air is replaced by the ink. The after-print cell shows the length between the empty cell and the inked cell; it indicates that there is some ink released out of the anilox cells. The volume of ink release can then be quantified.

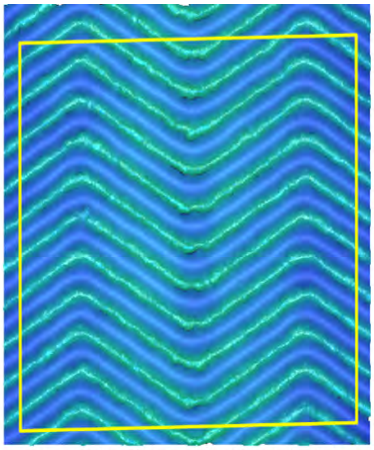

a: Area of volume measurement of wavy anilox cells

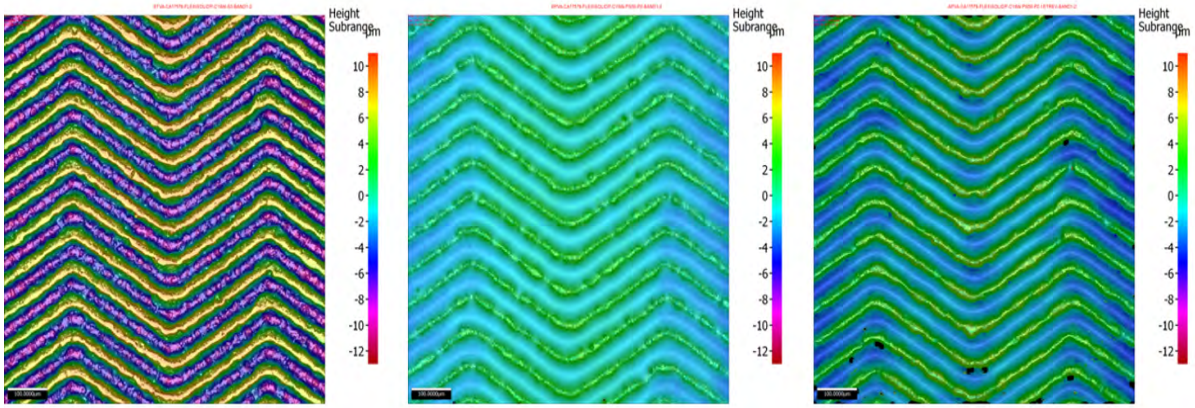

b: Image of the empty dry, inked, and after print

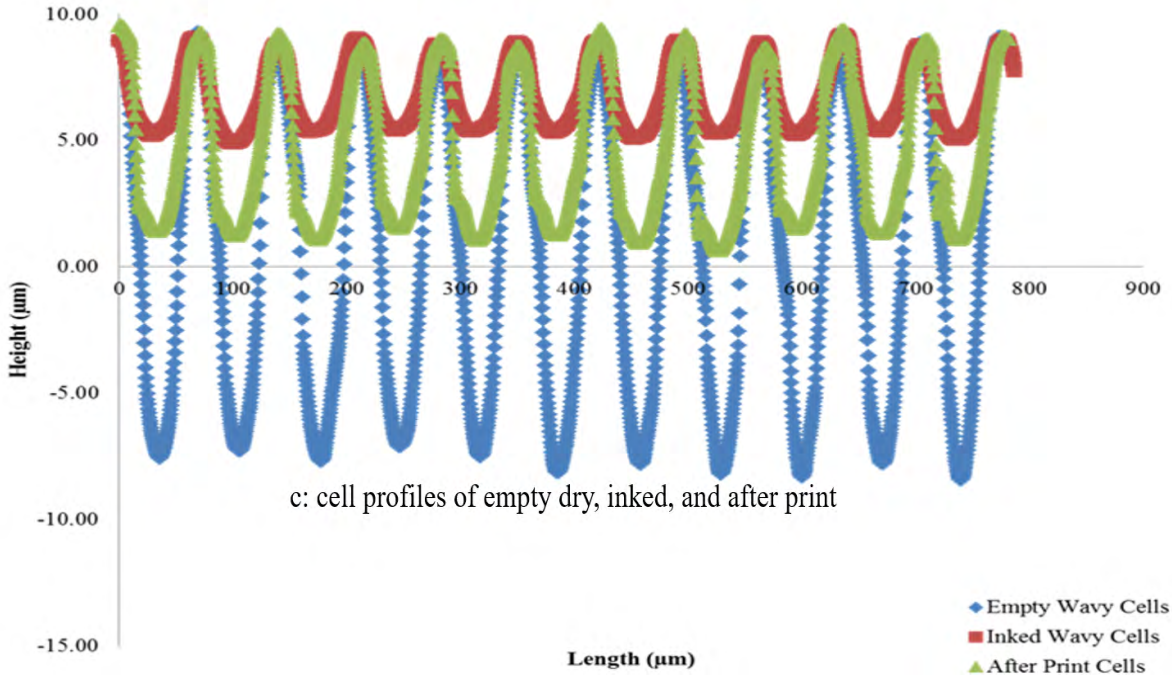

c: cell profiles of empty dry, inked, and after print

Figure 6.23: Area of volume measurement and profile of the empty dry, inked, and after print of wavy anilox cells

The cell profile with the depth-to-width ratio of 0.44 was wider and deeper cell (**Figure 6.24**). Similar trend was found for the anilox wavy channels with the smaller depth-to-width ratio released more of all three inks. The greatest increase was found in UV Carbon ink with the increase of approximately 41%, following by UV Cyan ink with the increase of approximately 11%, and the least was UV Silver ink with the increase of approximately 3%. Completely removing the anilox wall along the track had greatly improved the ink release of the ink with the large viscosity but small filament breakup time (UV Carbon ink). Similarly, to UV Carbon ink, the wavy channel anilox cell slightly improved the ink release of UV Silver; the large filament breakup time mitigated the improvement of the ink release.

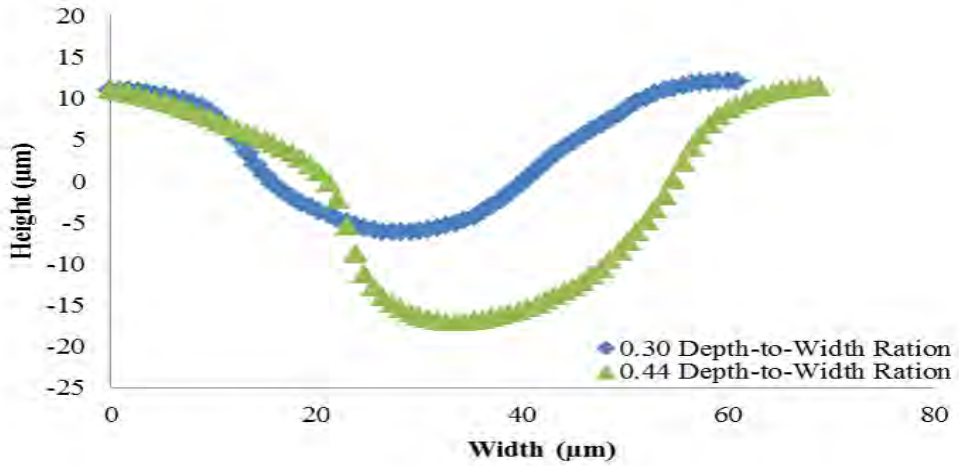

a: Cell profiles

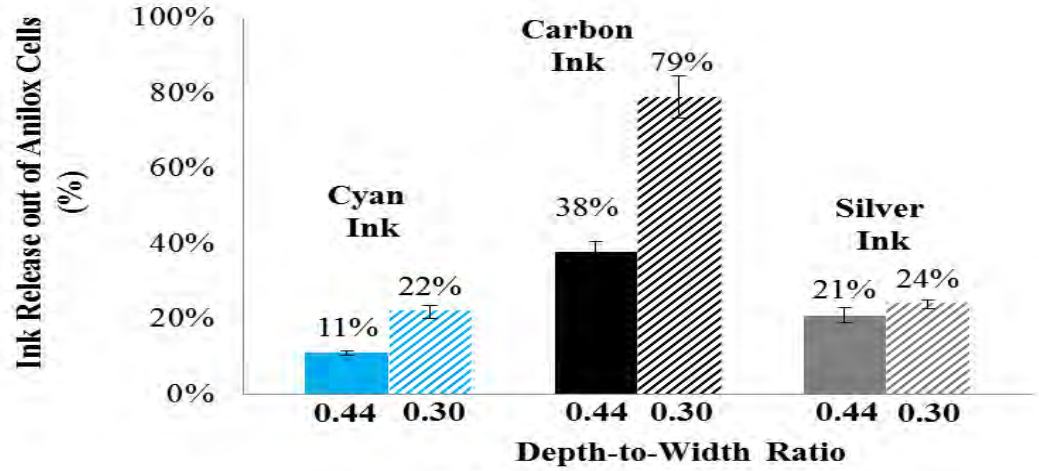

b: Ink release

Figure 6.24: Cell profiles and ink release of the wavy channel with the depth-to-width ratio of 0.30 (K) and 0.44 (M)

Similar to the trend seen in the anilox closed cells, the ink release of the anilox wavy channels increased as the depth-to-width ratio decreased (**Figure 6.25**) .

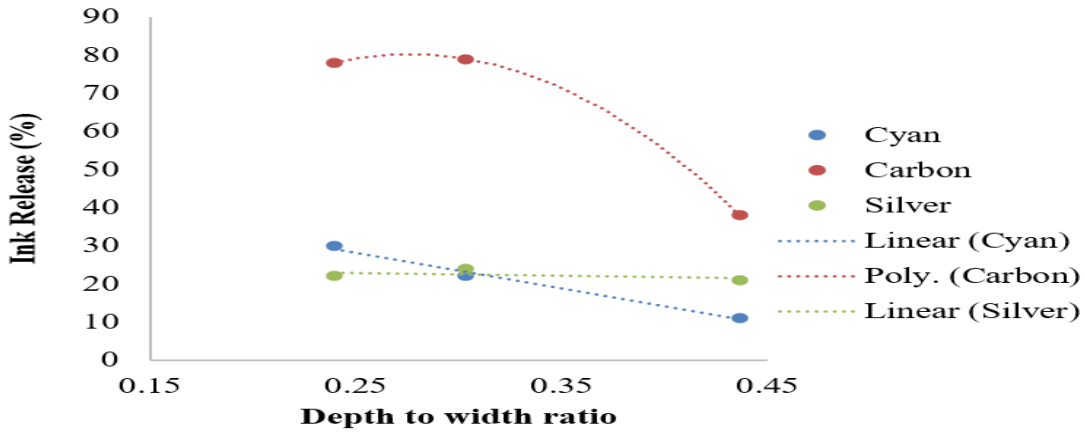

Figure 6.25: Ink release vs depth-to-width ratio of anilox wavy channels

6.3.2 Effect of Anilox Cell Shapes

This comparison was carried out using three anilox cell shapes of each anilox cell shapes; hexagonal closed cells (Anilox F), elongated hexagonal open cells (Anilox I), and wavy channels (Anilox L).

These three anilox bands had approximately same cell width, but the elongated anilox open cell had slightly deeper cell depth (**Figure 6.26**). The difference in shapes made the difference in cell volume especially with the wavy channels, which had much greater cell volume comparing to the other shapes.

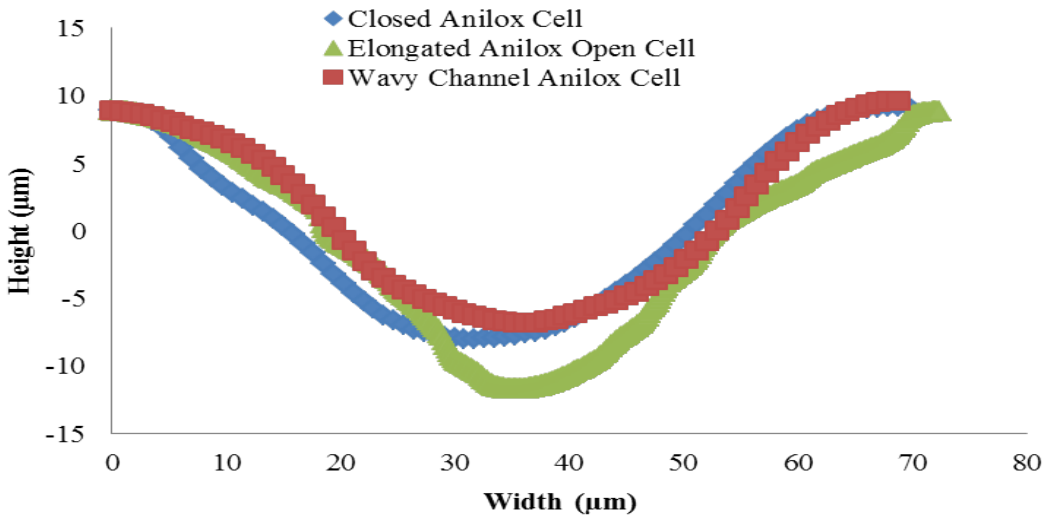

Figure 6.26: The cell profiles of anilox cells with closed, elongated, and wavy channel shapes

The wavy channel anilox cells had the longest track for the ink to flow comparing to the closed and elongated anilox cells (**Figure 6.27**). Additionally, its wall was smallest. The closed anilox cells had smallest track and widest wall along the flow direction of the ink. The wavy channel anilox cells would be expected to give the greatest ink release as its shape gave more opening for the ink to flow, and its wall was smallest; the ink should be left least on the wall. The closed anilox cells should release ink to the printing plate the least because its least opening for the ink to flow and its widest wall would let ink adhere to instead of being released to the printing plate.

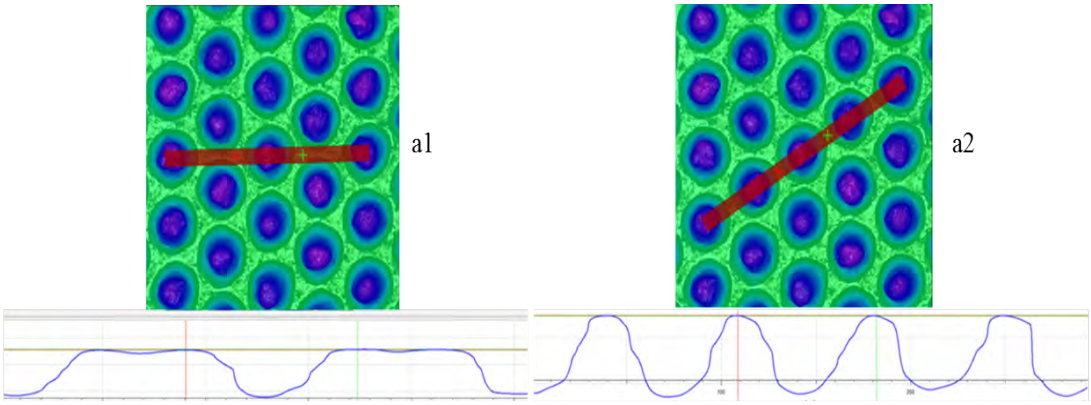

a: The cell profiles along the direction of ink flow (a1) and the cross- section of the anilox closed cells (a2)

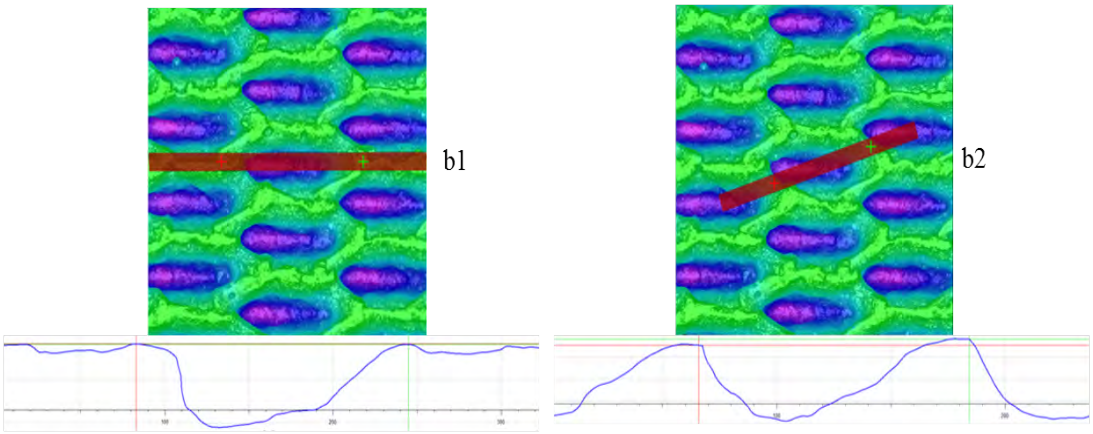

b: The cell profiles along the direction of ink flow (b1) and the cross- section of the anilox open cells (b2)

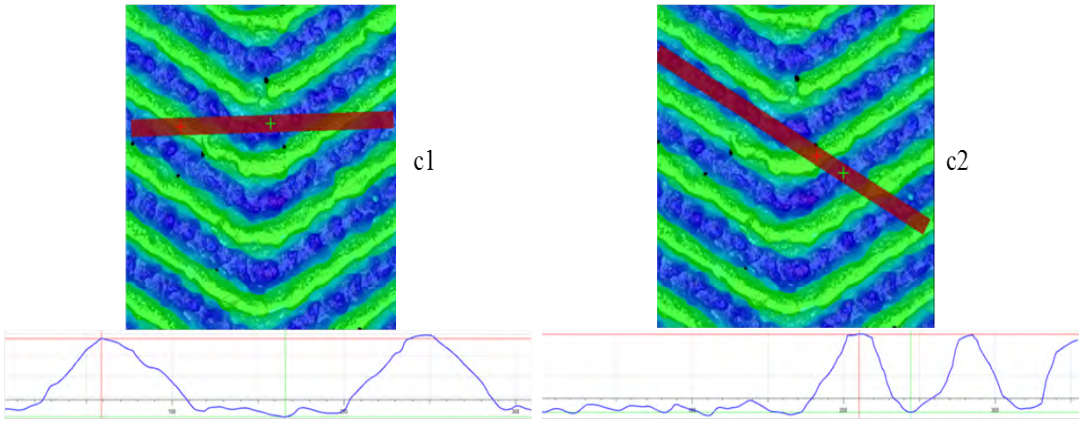

c: The cell profiles along the direction of ink flow (c1) and the cross- section of the anilox wavy channels (c2)

Figure 6.27: a: The cell profiles along the direction of ink flow (a1) and the cross section of the anilox closed cells (a2), b: The cell profiles along the direction of ink flow (b1) and the cross-section of the elongated anilox open cells (b2), c: The cell profiles along the direction of ink flow (c1) and the cross-section of the wavy channel anilox cells (c2)

The ink release of UV Cyan ink out of the elongated anilox open cells was the greatest (**Figure 6.28**). However, it was only 1% different to the anilox closed cells. The ink release of anilox open cells was approximately 9% greater than the ink release of anilox wavy channels.

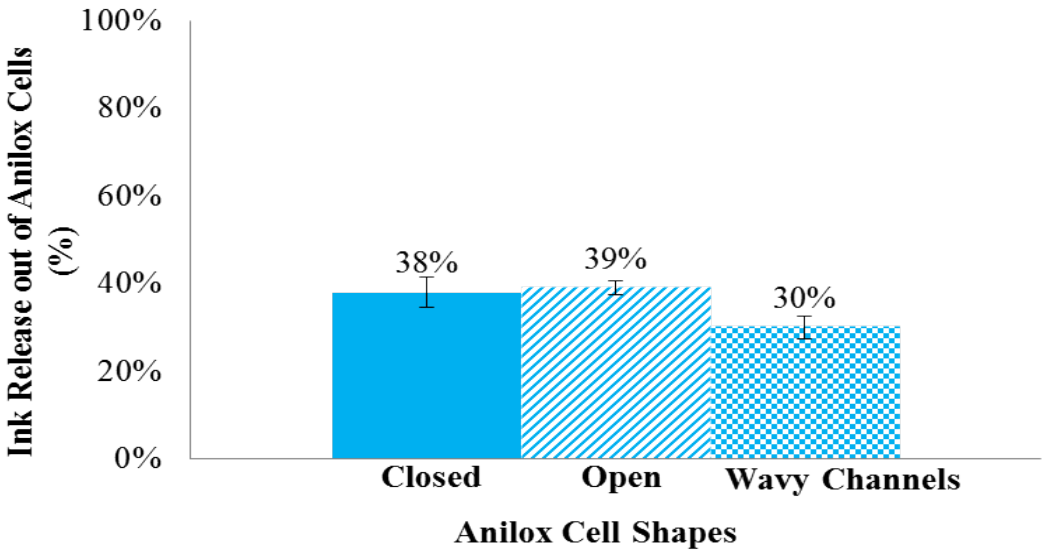

Figure 6.28: Ink release out of anilox cell shapes of hexagonal closed cells, elongated hexagonal open cells, and wavy channels using UV Cyan ink

As the anilox cell shape started evolving; the elongated anilox open cells to the wavy channels the ink release decreased. Eventually, the wavy channels released the least of the ink. This was not expected as anilox wavy channels appeared to release greater ink than the anilox closed cells with commercial press in chapter 5. However, the anilox wavy channels were much shallower on the commercial press approximately 40% compared to the anilox closed cells; the anilox cell depth was more critical to the ink release than the anilox cell width. Its shallower cell depth made the anilox wavy channels released greater ink in chapter 5.

The three anilox cells used in this investigation had similar cell width and depth, therefore the difference in shapes should be the dominant factor affected the ink release. Since UV Cyan ink had low viscosity and filament breakup time, the small viscosity helped it freely flowing but reducing the ink tack (attachment) to the plate. Its release would be more dependent on how much it could flow out of the anilox cells, not on being pulled out.

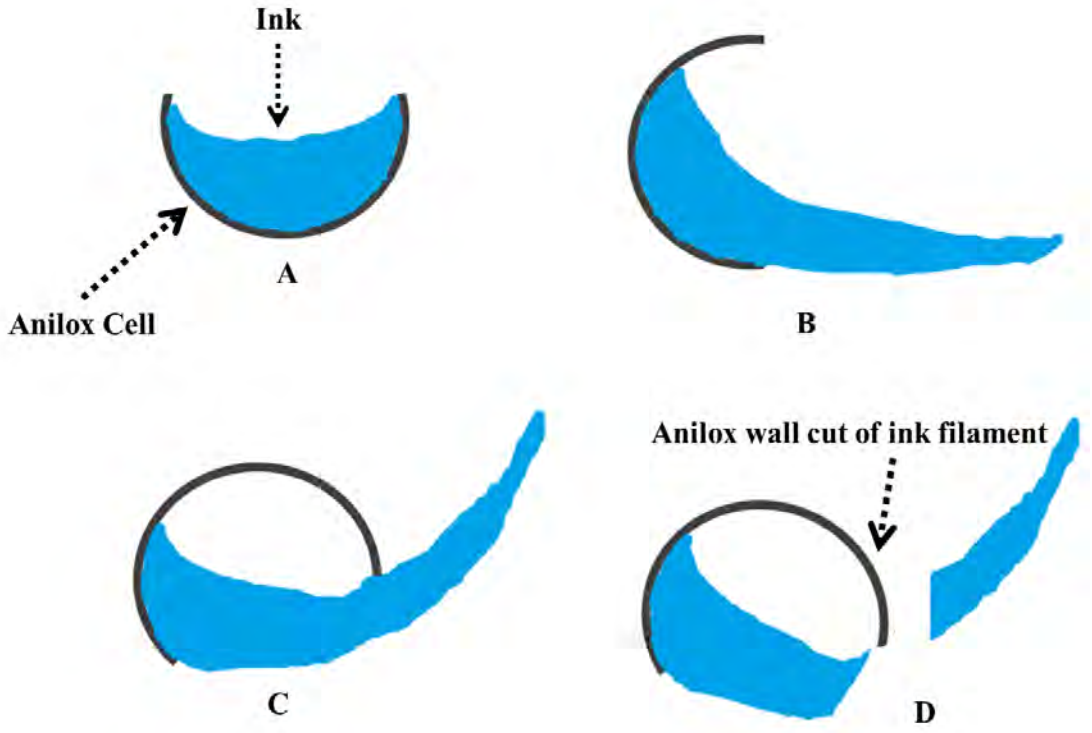

Figure 6.29: The schematic of UV Cyan ink released out of the anilox closed cells during the printing process

During the printing process, the anilox roll turns. This causes the anilox closed cell to turn. changing position from **Figure 6.29 A** to **Figure 6.29 B** and causing the UV Cyan ink to elongate. As the anilox closed cell keeps turning, the other side of anilox cell wall contacts the elongated ink filament (**Figure 6.29 C**) and eventually cuts the ink filament (**Figure 6.29 D**): causing the ink split from the plate.

For the anilox open cells, the reduction of the height of its wall opens up as a track (**Figure 6.30**); allowing the ink to flow more freely. However, UV Cyan ink filament broke up instantly; the open-up track did not add further benefit for the ink to be pulled out along the track. Additionally, the small wall along the track cut off the ink filament as the anilox roll rotated. These resulted in only a slight increase in ink release.

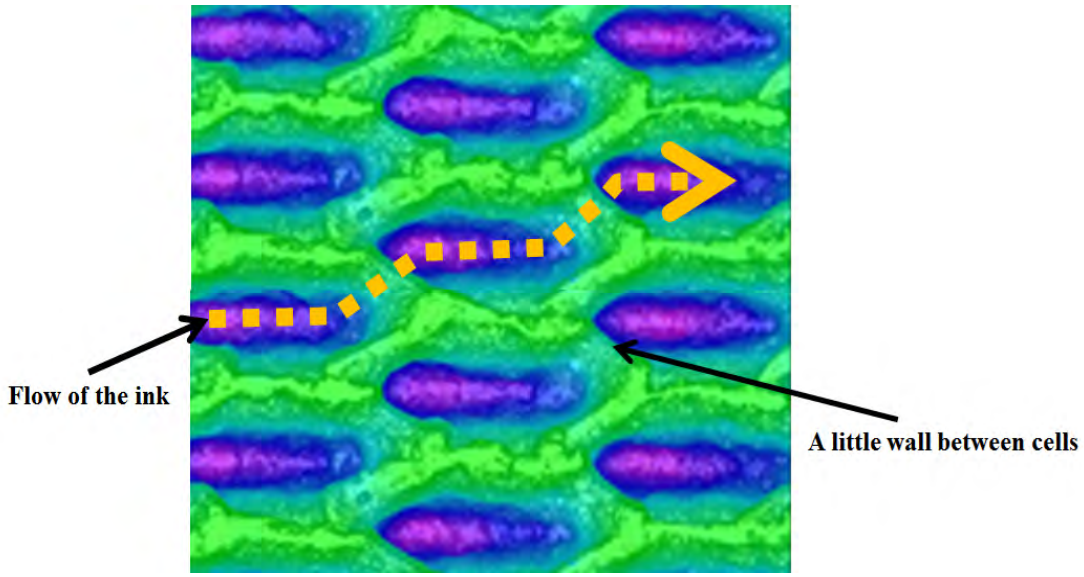

Figure 6.30: Schematic of UV Cyan ink released out of the the anilox open cells during the printing process

The anilox cell wall was completely removed in the anilox wavy channels, allowing UV Cyan ink to keep flowing along the track without any interruption from the anilox cell wall (**Figure 6.31**). The UV Cyan ink released the least out of the anilox wavy channels.

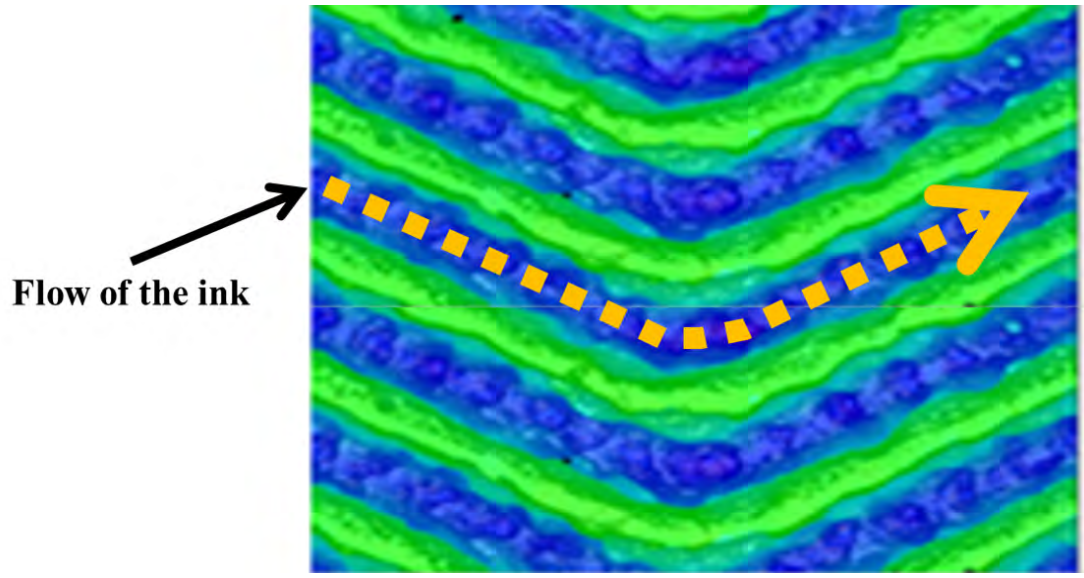

Figure 6.31: Schematic of UV Cyan ink released out of the the anilox wavy channels during the printing process

The UV Silver ink showed contrasting results compared to UV Cyan ink (**Figure 6.32**). These two inks had completely different characteristics; UV Cyan ink had low viscosity and filament breakup time whilst UV Silver ink had the high viscosity and filament breakup time. Because of its large viscosity and

filament breakup time, UV Silver ink could not freely flow as UV Cyan ink. The high viscosity made the pull-out factor dominant, assisting in pulling ink out of the anilox cells. The large filament breakup time of UV Silver ink would require longer time to break and depart to the plate. The anilox open and wavy channels released more UV Silver ink as their tracks or channels allowed the ink to flow while being pulled out. The anilox open cells and wavy channels released greater UV Silver ink than the anilox closed cells. The anilox wavy channels released the greatest proportion of ink. As the wall was completely removed in the anilox wavy channels, there was no restriction in the anilox open cells, this improved the flow of UV Silver ink as its filament dragged along the tracks and allowed the pull-out to happen for longer.

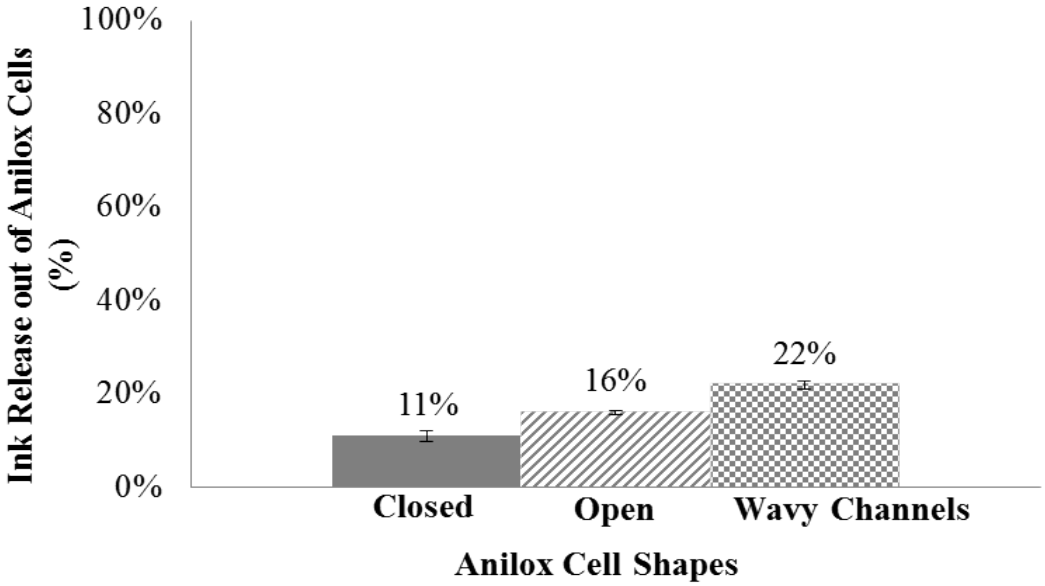

Figure 6.32: The ink release from hexagonal closed cells, elongated hexagonal open cells,and wavy channels using UV Silver ink

However, the high viscosity of UV Silver ink hindered the flow out of the anilox closed cells; small amount of the ink was attached to the plate and pulled out. Additionally, the anilox wall cut off the ink filament reducing the amount available to pulled out.

The anilox open cells and wavy channels were expected to release more of UV Carbon ink because they allowed the ink to flow along the tracks (**Figure 6.33**); The anilox open cells and the wavy channels released greater ink than the anilox closed cells. However, the anilox open cells released greater ink than the anilox wavy channels.

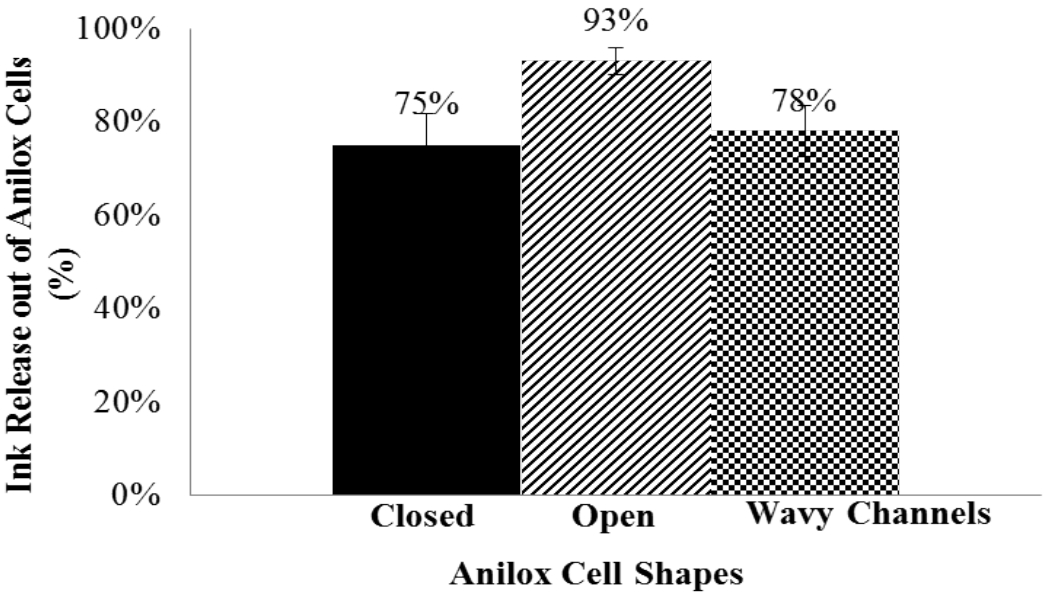

Figure 6.33: Release of UV Carbon ink from hexagonal closed cells, elongated hexagonal open cells, and wavy channels

As the anilox cells evolved from closed to open cells, it allowed the ink to flow along the track and more be pulled out. However, because UV Carbon ink had the small filament breakup time, by removing the cell wall completely as the anilox wavy channels did not allow further ink to be pulled out but merely allowed the ink to flow along the track. Opening up the wall between the neighbouring cells of the anilox open cells allowed the ink to flow and more to be pulled out, the small wall in the track created turbulence in the flow, which further improved ink release.

The ink release was most influenced by the ink characteristics. The performance of the anilox cell shape depended on the attributes of the ink. The UV Cyan ink, which had low shear viscosity, small filament breakup time, and behaved more like Newtonian material. The greatest proportion of the Cyan ink, was released from either anilox closed or open cells. The UV Silver ink, which had high shear viscosity and filament breakup time had the greatest proportion released using the anilox wavy channels. The UV Carbon ink, which had high shear viscosity but small filament breakup time, had the greatest portion released using the anilox open cells.

The UV Carbon ink released comparing to UV Cyan and Silver inks for all anilox cell shapes (**Figure 6.34**). The UV Cyan ink came second and the least one was UV Silver ink. The degree of the effect of the change of anilox cell shape was influenced by the ink characteristic. UV Carbon ink release increased by 18% when the anilox cell shape changed from closed cell to open cell, whilst UV Cyan ink release increased by 1%. The UV Carbon ink with large viscosity but small filament breakup time would have the greatest proportion released for

all anilox shapes.

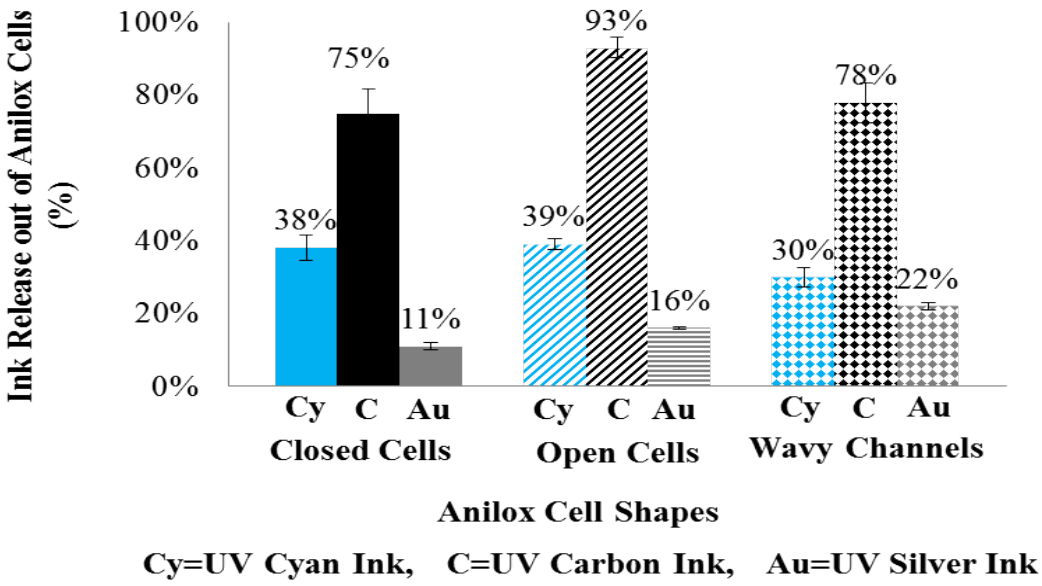

Figure 6.34: Ink release using UV Cyan, Carbon, and Silver inks with 3 shapes of anilox cells; closed cells, open cells, and wavy channels

This information would help the printer select the ink, which would increase the amount of ink released on the substrates without changing the anilox cells which would be more costly, or using the right anilox shape according to the ink characteristics.

The following section examines the effect of ink characteristics on the ink release from the anilox cells.

6.3.3 Effect of Ink Characteristics

There is a general trend of decreasing ink release with increasing depth to width ratio (**Figure 6.35**). The inks form three separate bands as the proportion of ink released is highly dependent on the viscoelastic properties of the ink. The shear viscosity, filament breakup time, and elastic modulus of UV Cyan was much smaller than those of UV Silver ink. More UV Cyan ink was released out of the anilox cells. Low shear viscosity of UV Cyan ink made the ink flow out of the cell, and its small filament breakup time allowed it to split and be released to the plate. The much greater elastic modulus of UV Silver ink increased the stretching and pull-out of ink filament; however, its filament breakup time of 10s is over 20 times greater than that of UV Cyan ink (0.45s) hindering the ink split and release to the plate. As the engagement between the anilox cells to the plate happened instantly, with the print speed set at approximately 80cm/s (50m/min) and the circumference of anilox roll was approximately 20cm, the anilox would be engaged with the plate for approximately 0.24s. Therefore,

most of UV Silver ink, which was pulled out, would not have time to split and would recoil back into the anilox cells during disengagement.

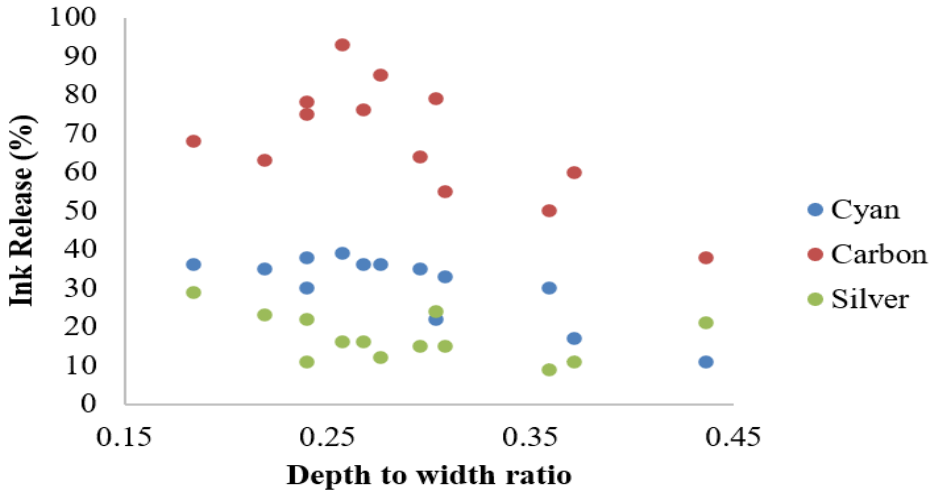

Figure 6.35: Percentage ink release compared to depth to width ratio for all inks

UV Carbon ink, which had similar attributes to the UV Silver ink but its filament breakup time was much smaller; approximately 1.41s, which was comparable to the UV Cyan ink. The small filament breakup time with much greater elastic modulus should make more UV Carbon ink be released than UV Cyan ink as more ink could be pulled out and its filament could be split much easier than UV Silver ink.

Approximately double the amount of UV Carbon ink was released out of the anilox cells compared to UV Cyan ink. More ink having small filament breakup time, would be released than the ink which had large filament breakup time. The small shear viscosity, which made the ink flow more freely, had less effect on the ink release out of the anilox cells compared to the elastic modulus and filament breakup attributes. The combination of having large elastic modulus and small filament breakup time in UV Carbon ink increased the amount of ink pull-out, and made it more readily released out of the anilox cells and transferred to the plate.

The proportion of ink released with the three inks can now be examined in more detail for the various cell engravings. There appears to be some interaction with viscosity which is more easily distinguished when they are separated into ink types (**Figure 6.36**). The proportion of the high viscosity carbon ink released decreases with increasing depth to width ratio for all cell geometries. There is more of a spread of results for the lower ratios which suggest other interactions are occurring.

There is a high proportion of UV Cyan graphics ink released with the conventional closed anilox than with the wavy or the open channel elongated hexagonal at high width to aspect ratio. The proportion of ink release falls with aspect ratio for the wavy channel. Whereas with traditionally engraved graphics cylinders increasing the volume of the cylinder would increase the amount of ink released, this result suggests that it would not be as straight forward with some of these new designs. This could require tighter process control on behalf of the printer.

The proportion of the UV Silver ink released, which had the longest time to separation in the CaBER test, falls with depth to width ratio for the conventional, hexagonal and extended hexagonal cells. However, it remains roughly constant for the wavy channel. This suggests there is an interaction with the high viscosity of the ink. UV Silver and Carbon inks had similar high viscosity. As seen in the ink release of UV Carbon ink, the ink release decreased as the depth to width ratio increased. However, UV Silver ink had greater filament breakup time. Additionally, the wavy channel allowed the ink filament to keep flowing along the track instead of splitting to the plate.

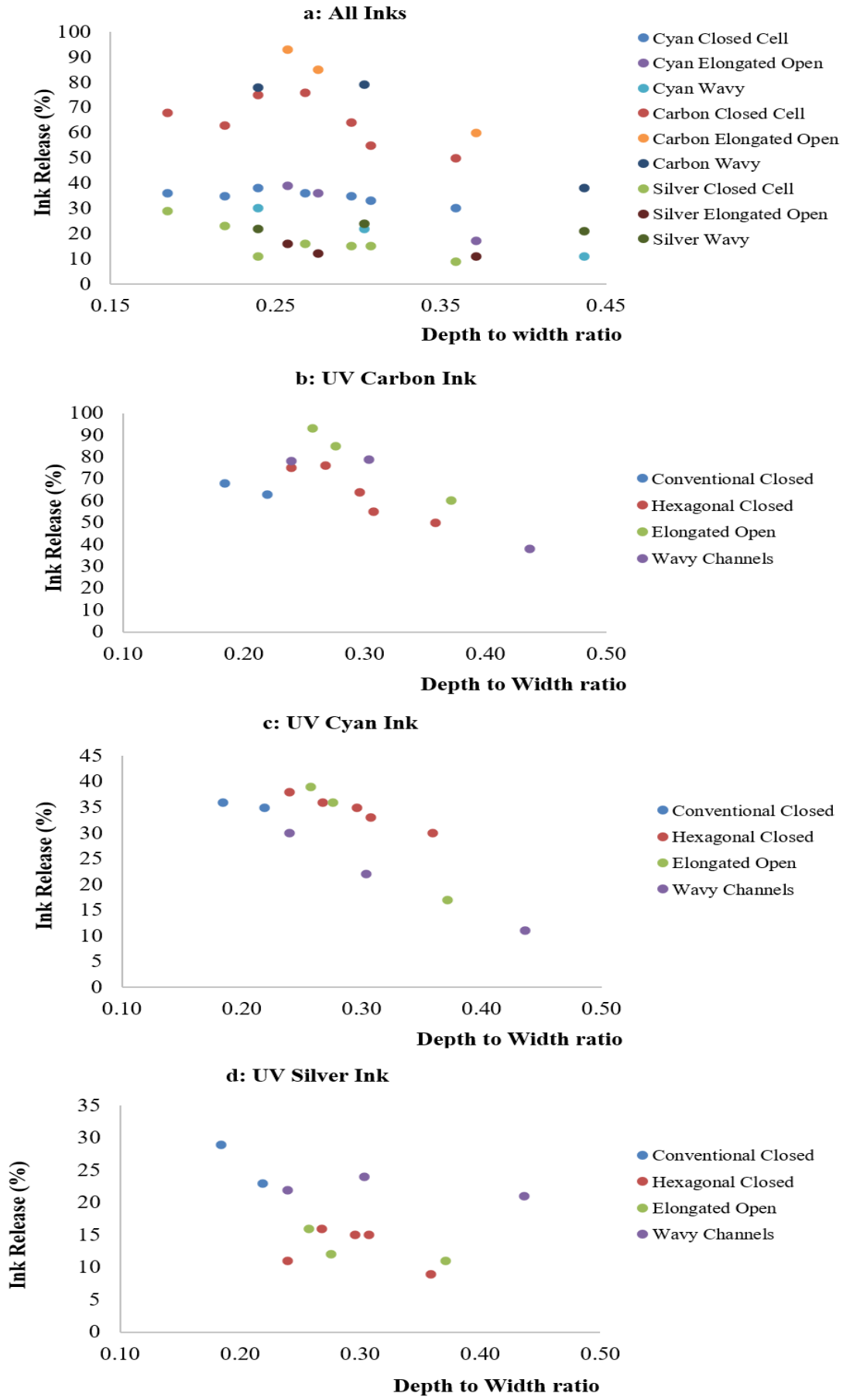

Figure 6.36: Percentage Ink release vs Depth-to-width ratio for all ink types and cell geometries

6.3.4 Effect of Print Speed

In printing, it is normal practice to adjust speed to meet demand. Therefore, the effect of increase the printing speed on the release of ink out of the anilox cells was examined.

Anilox B, F, I and L were chosen because they had similar attributes of width and depth but different cell shapes. This enabled any interaction between anilox shape and ink characteristic with speed to be examined.

The prints were carried out at the printing speed of 90m/min, and then compared to the printing speed at 50m/min. Only two printing speeds were considered due to the limitation of time. A wider range of printing speeds would give better information of how the printing speed affected the ink release. These two printing speeds gave the similar trend for all the inks and anilox shapes.

When the printing speed is increased, it reduces the ink release from the anilox cells to the plate due to two factors; the reduction of the engagement time of the anilox cells with the plate and the increase of filament extension rate, which made the ink filament thinner during the printing process; reducing the amount of ink pulled out of the anilox cells. The expectation was to see a reduction ink release when the printing speed is increased.

The results showed similar trends using UV Cyan ink; when the printing speed increased, the ink release out of the anilox cells reduced for all the anilox cell shapes (**Figure 6.37b**). However, the impact was much greater in the anilox open cells and wavy channels. The increase of the printing speed caused the anilox closed cells to release less ink by approximately 4%, whilst 12% and 19% reduction could be observed for the anilox open cells and wavy channels respectively.

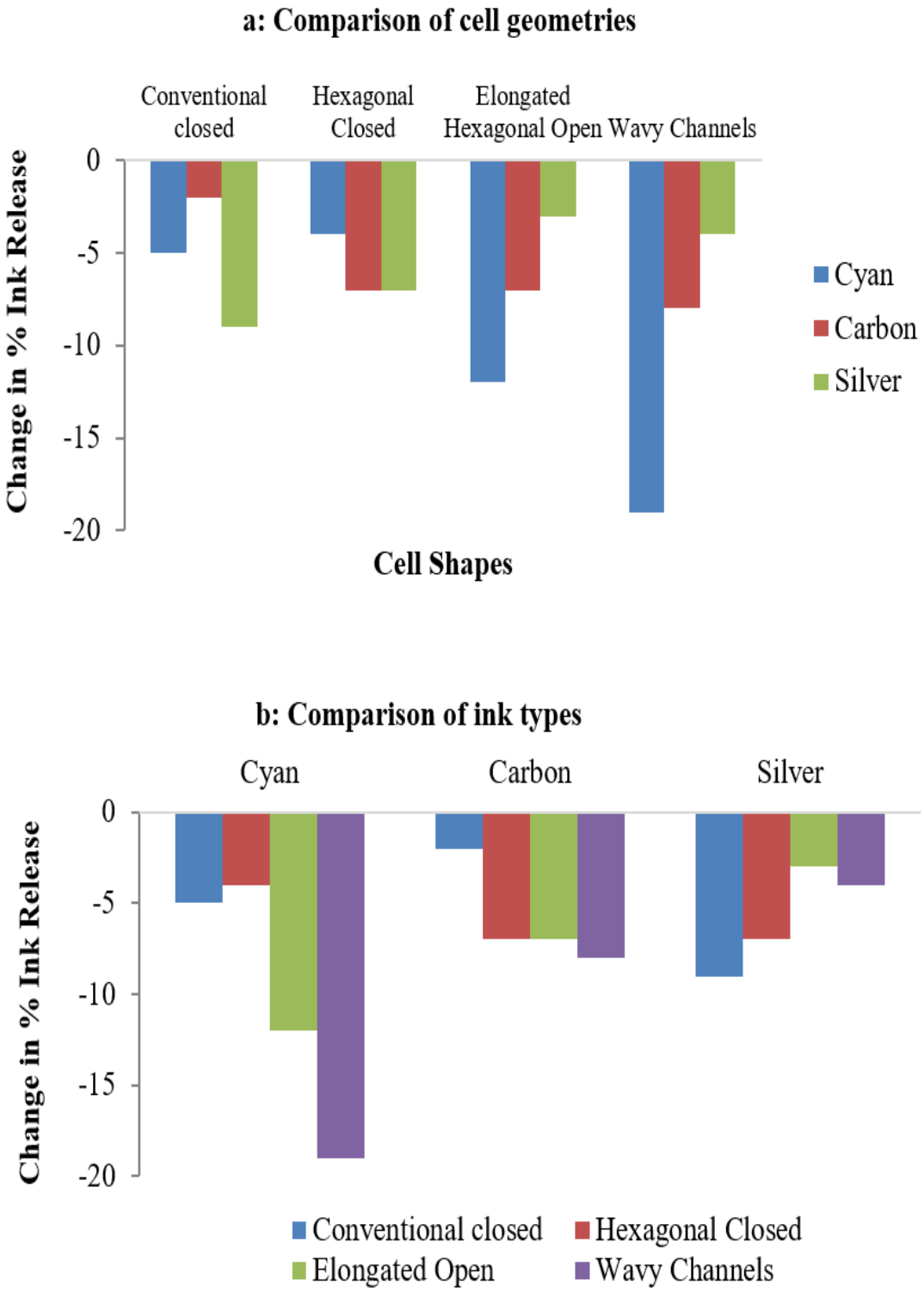

Figure 6.37: Effect of changing speed from 50 to 90m/min

The results using UV Carbon ink showed similar trends, the increase in printing speed decreased the ink release. However, the anilox cell shape did not have a significant effect as seen in UV Cyan ink. The increase of the printing speed caused the anilox closed cells to release less ink by approximately 7%, which was similar to the anilox open cells and wavy channels, which had the reduction by approximately 7% and 8% respectively.

The UV Silver showed similar trends to the UV Carbon ink; the increase of printing speed decreased the ink release, but not significantly as seen in UV Cyan ink. The increase of the printing speed caused the anilox closed cells to release less ink by approximately 7%, with further small reduction for the anilox open cells and wavy channels, which reduced by approximately 3% and 4% respectively.

The increase of the printing speed gave a general trend of a reduction in the ink release when the same anilox shape and ink were used. However, the degree of effect depended on the ink characteristics; as the anilox cell shape evolved from closed cell to open channel, the increase of the printing speed produced a larger decrease in the ink release with the thin UV Cyan ink with small shear viscosity and filament breakup time. The evolving of the anilox cell shape did not have the significant effect on the UV Carbon and Silver inks.

UV Cyan ink had low viscosity, which mitigated the pull-out factor during the engagement with the plate. The anilox open cells and wavy channels allowed the UV Cyan ink to flow along the tracks instead of being pulled out to the plate. The increase of the printing speed reduced the time for the ink to flow to the plate and the increase of the rotation force, kept UV Cyan ink flowing along the tracks; whilst UV Carbon and Silver inks had much greater pull-out factor because of their large viscosity. Even though the engagement time with the plate reduced, their higher viscosity mitigated this. Additionally, the tracks provided by their open cells and wavy channels still allowed the ink to be pulled out as the anilox rotated.

When the printing speed increased from 50m/min to 90m/min, the amount of ink released out of the anilox cells decreased for all inks (**Figure 6.37**). This is a similar trend to the studies of; Damroth et al (1996), Hamblyn (2004), and Cherry (2007) which all showed that the optical density decreased when the print speed increased, Additionally, Elsayad et al (2002) found that increasing the print speed decreased the ink transfer. The studies of Khandavalli and Rothstein (2017) showed similar trend that when the speed increased, it enlarged the extension rates. This caused the severe thinning extensional viscosity reducing the pulling and hence the inks transfer.

When the printing speed increased, the engagement time between the anilox cells and the plate decreased. Additionally, it enlarged the extension rate, which made the ink filament thinner during the printing process; reducing the amount of ink pulled out of the anilox cells. The reduction in time of the engagement between the anilox cells and the plate resulted in decreasing time for ink transfer to the plate; reducing the ink transfer. However, the degree of reduction was different for all three inks.

UV Cyan ink had the greatest reduction of the ink release with the combination change of shape and increase of speed. This was due to its low viscosity, which allowed it to easily flow but not to be pulled out, keeping it flowing in the channel instead of being split to the plate.

UV Carbon and Silver inks had a large elastic modulus. Having large elastic modulus reduced the effect of filament-thinning; the ink could be pulled out. Additionally, the small filament breakup time of UV Carbon ink mitigated the effect of time reduction of the engagement between the anilox cells and plate. The small impact of the increase printing speed to the UV Silver ink when it was used with the anilox open cells and wavy channels was because it had more time to be dragged out along the tracks and be able to split to the plate.

6.4 Closure

Total Cell Volume: The amount of ink available to be released is a function of the total cell volume. The total ink transfer is fundamentally driven by this parameter. However most critical in the assessment of the efficiency of the anilox roll is the proportion of ink which is released.

The Effect of Anilox Cell Geometries: The wider, shallower, and smaller depth-to-width ratio anilox cells released the greatest proportion of the ink. The wider cells gave more of an opening for the ink to be released. The shallower cells required less forced to be pulled out. The depth of the cells was more critical than the width as the anilox cells with greater cell volume and width released less proportion than the anilox cells with smaller cell volume and shallower cells.

The ink characteristics influenced the ink release out of the different cell shapes. The ink with small viscosity and filament breakup time i.e. UV Cyan ink was released with the greatest proportion using the anilox closed cells. Whilst the ink with large viscosity and filament breakup time i.e. UV Silver ink was released with the greatest proportion using the anilox wavy channels. The ink with large viscosity but small filament breakup time i.e. UV Carbon ink could

be released with the greatest proportion using any shapes of the anilox cells.

The Effect of Anilox Cell Engraving: The anilox cells, which were engraved by the laser technique, released greater proportion of ink than the anilox cells engraved by the mechanically engraving technique. The mechanically engraving technique produced anilox cells with much greater surface roughness. There were cracks and holes on the rough surface. These cracks and holes caused the ink to be trapped instead of being released. This reduced the amount of ink transferred to the plate.

The Effect of Ink Characteristics: Ink characteristics were critical to the ink release out of the anilox cells. UV Carbon ink, which had high shear viscosity, large elastic modulus, and small filament breakup time, was release out of the anilox cells with the greatest proportion of approximately 70% comparing to approximately 40 and 20% for UV Cyan and Silver inks respectively. Even though it had initial high shear viscosity, which could hinder the flow, its shear viscosity decreased to very low at high shear rate. This meant under the high speed of printing process, its shear viscosity would decrease and allow it to flow to the plate more freely. Its large elastic modulus made it pulled out in the greater proportion. Its small filament breakup time allowed ease release of the ink to the plate.

The elastic modulus and the filament breakup time were critical to the ink release. The large elastic modulus increased the pull-out. The small filament breakup made it easier to split to the plate with greatest pull-out.

By comparison, the UV Black and HD yellow graphics inks used in chapters 4 and 5 respectively, had a similar initial viscosity at $1s^{-1}$ but were shear thinning. The HD Black in chapter 5 had a viscosity below 0.1 and was Newtonian. Only the HD yellow had a similar filament breakup time of 0.928s, whilst the UV Black and the HD Black was 0.255s & 0.169s respectively.

The Effect of Printing Speed: When the printing speed increased, the engagement time between the anilox cells and the plate decreased. Additionally, it increased the extension rate, which made the ink filament thinner during the printing process; reducing the amount of ink pulled out of the anilox cells. These two factors decrease the amount of ink transferred to the plate. The degree of reduction in the ink transfer was severe for the UV silver ink which had high shear viscosity, large elastic modulus, and long filament breakup time. The printing speed would need to be adjusted during the printing process dependent on the characteristics of ink to optimize the ink release out of the anilox cells.

The critical anilox cell geometries for ink release depended on the ink characteristics. The combination of selecting the right anilox cell geometry and ink characteristics would aid printing quality. The anilox cell geometry was not critical for graphic prints because the inks used for this type of print had characteristics typical of UV Cyan ink. However, the anilox cell geometry was critical to the functional print because the inks used had characteristics typical of UV Carbon and Silver ink. The use of anilox cells with shallower and small depth-to-width ratio would offer better ink release to improve the ink film thickness on the substrates.

Chapter 7

Ink Transfer with Tonal Patches

7.1 Introduction

This chapter explores the ink release with the printing plate with tonal patches, which are used in graphic printing. The experiments used the same methodology and equipment as in chapter 6, with the same UV Cyan, Carbon, and Silver inks. The ink transfer from closed cells (Laser and Mechanically engraved) and elongated hexagonal open cells were studied using anilox cylinders F, I and O. These engravings all had similar width, whilst the laser engraved closed and open cells had similar depth. The anilox open cells were chosen because it gave the best ink release for the graphic and functional inks. The mechanically engraving open quadratic cells were chosen to examine the effect of mechanically engraving on ink transfer of half tones.

7.2 Experimental Method

The dot area is the raised area to contact with the anilox cells during the printing process (**Figure 7.1**) . The floor of the dot should not contact with the anilox cells.

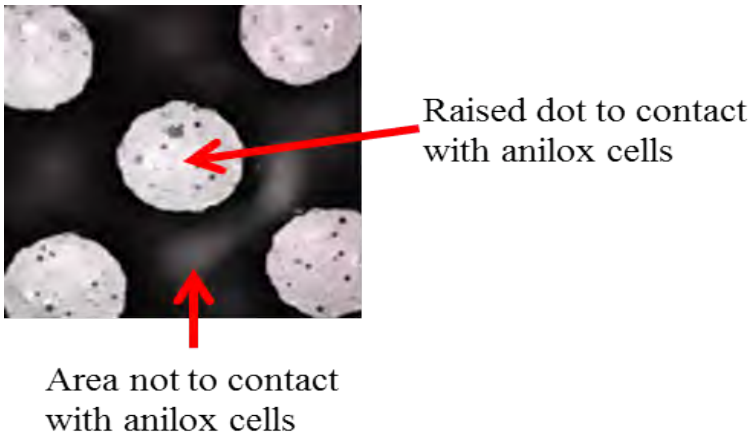

Figure 7.1: The tonal patch plate with the dot coverage of 70%

There are two mechanism of the ink release from the anilox cells to the tonal patch plate; the ink split over the non-contact area, and the pull-out over the contact area. The majority of the ink release is due to the pull-out fraction over the contact-area because the dot area is designed to be approximately 6 times larger than the anilox cell (**Figure 7.2**).

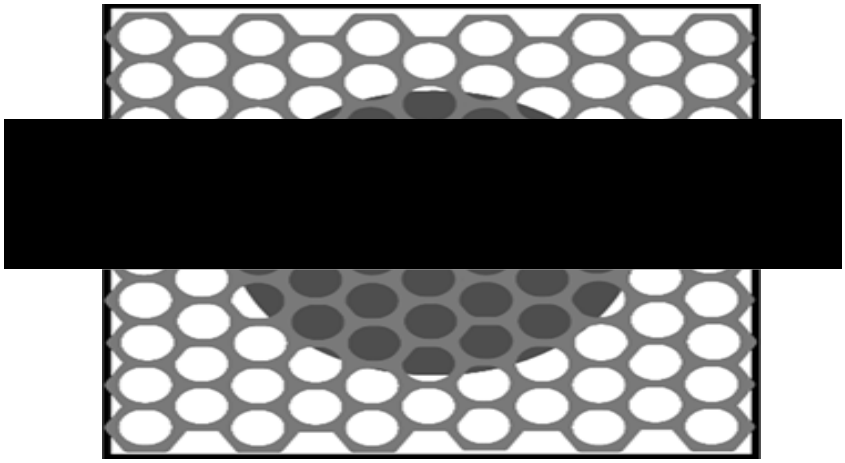

Figure 7.2: The contact between the anilox cells and dot on the tonal patch plate [Bould, 2010]

To establish the ink release out of the anilox cells after printing with the tonal patch, Alicona InfiniteFocus microscope was used to distinguish the contact area from non-contact area of anilox cells and the dot on the plate (**Figure 7.3**). The contrast of the light (shallower ink in the anilox cells) and dark (deeper ink in the anilox cells) area on the anilox cells indicated that the lighter area had no contact with the dot on the plate. As the dot size increased the darker area increased as expected as more anilox cells contacted the dot. The ink volume of these two area were examined (**Table 7.1**). The ink volume of Non-contact area expected to be greater than the contact area as no ink release out of the anilox cells. The volume of the ink release was determined from the contact area.

The wavy channel could not be included as the flow of ink in the channel would not allow this type of analysis to be performed.

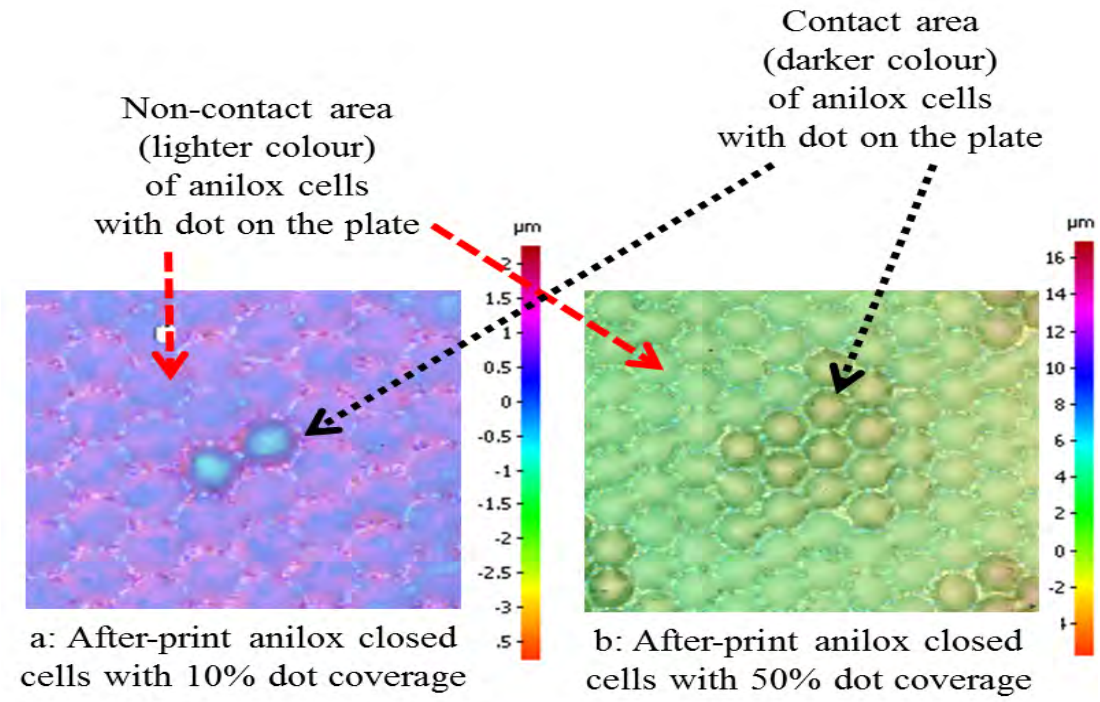

Figure 7.3: Image of after print anilox cells showing the contact and non-contact area of anilox cells with dot on the plate

Table 7.1: Exemplar comparison of the ink left in the anilox cells between the contact and non-contact area of the anilox cells with the dot on the plate during the printing process

Measurement	**Ink of Contact Area (cc/m^2)**	**Ink of Non-Contact Area (cc/m^2)**
1	3.90	4.46
2	3.30	4.42
3	3.49	4.29
4	3.56	4.59
5	3.41	4.46
6	3.92	4.42
7	3.83	4.65
8	4.00	4.46
9	4.00	4.74
Average	3.71	4.50
Standard Deviation	0.27	0.14
Standard Deviation (%)	7	3

7.3 Results of the Experiments

7.3.1 Effect of Anilox Cell Geometries

The UV Cyan ink release increased as the dot area increased (**Figure 7.4**). The increase surface area of dot increased the receiving area and made more ink transfer from the anilox cells to pass to the plate dot.

Compared to the ink release in the closed cells, the open cell improved the ink release by approximately 7% but it reduced by approximately 8% with the mechanically quadratic open cells. Removing the cell wall and creating the track encouraged the ink release to the plate. The rough surface together with deeper cell of the anilox mechanically quadratic open cells hindered the ink flow.

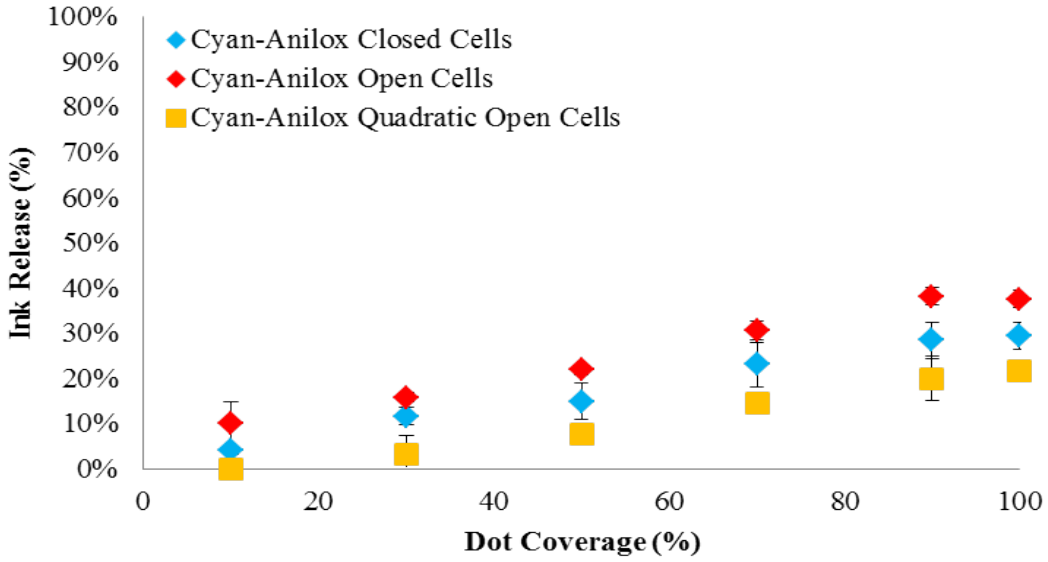

Figure 7.4: UV Cyan ink release with the anilox closed, open, and mechanically quadratic open cells

As the dot area increased, the receiving area increased. The high viscosity of the UV Carbon ink together with the increase of the dot area improved the pull-out effect; more ink could be pulled out to the plate (**Figure 7.5**). Contrary to the UV Cyan ink, where the pull-out effect did not have significant role because of the low viscosity of the UV Cyan ink.

A similar trend is seen to the UV Cyan ink, but there is a greater increase of the ink release of up to 30% in the high dot coverage of 90% using the anilox open cells. But the ink release was lower at 10% when the mechanically quadratic was used.

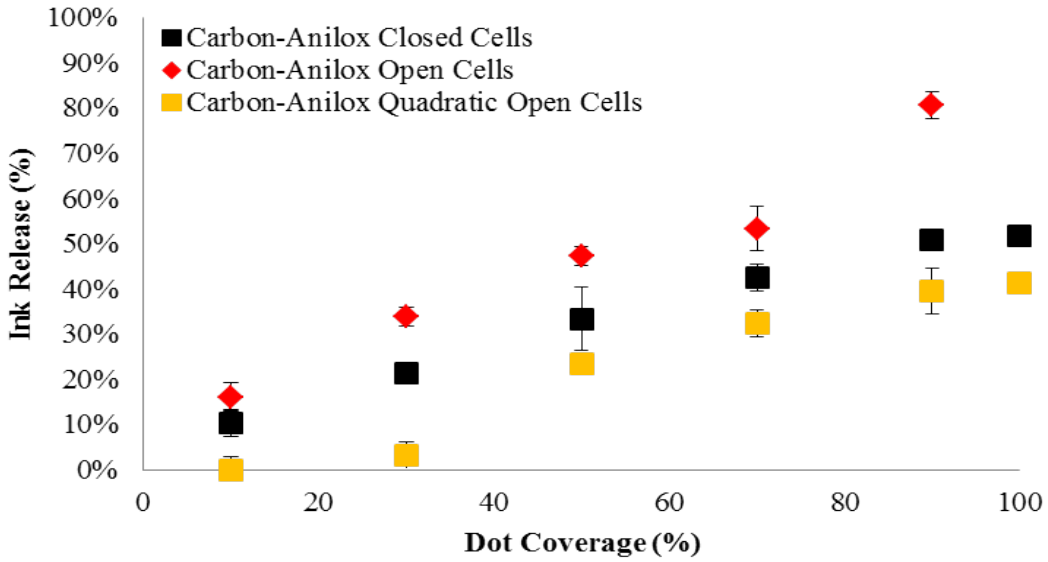

Figure 7.5: UV Carbon ink release with the anilox closed, open, and mechanically quadratic open cells

Contrary to the previous results of using the UV Cyan and Carbon inks, there is not a significant increase of the ink release with UV Silver ink when the anilox open cell was used (**Figure 7.6**). The large filament breakup time of the UV Silver ink mitigate the benefit of having the wall open up. The ink release was worse at approximately 8% when the mechanically engraved quadratic open cells was used.

When the prints were carried out using the tonal patch plate, the ink release increased as the dot coverage area increase. When the dot coverage area increased, it increased the receiving area which the ink could be pull out. However, the increase of the ink release plateaued from the dot coverage at approximately 50% for the UV Silver ink. Because of its large filament breakup time made its ink filament not to split even though the receiving area increased. The inks with small filament breakup time could easily split to the increase receiving area of the dot coverage.

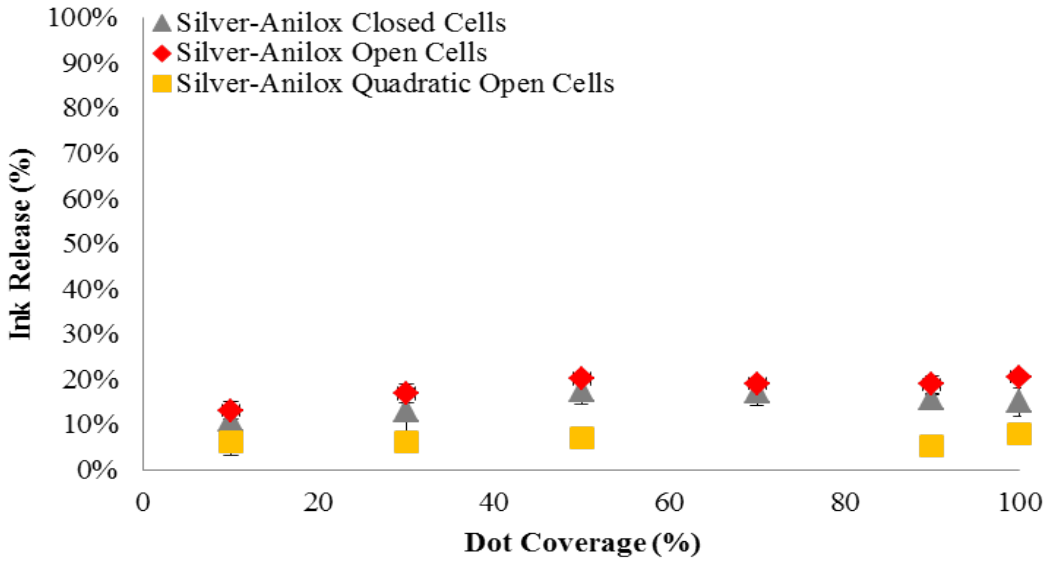

Figure 7.6: UV Silver ink release with the anilox closed, open, and mechanically quadratic open cells

The after-print images of the anilox closed and open cells with UV Cyan and Carbon inks were examined (**Figure 7.7**). With a small dot coverage such as 30%, the inflow of the low viscosity ink (UV Cyan) happened during the test and measurement when the ink was used with the anilox open cells. The track of the anilox open cells allowed the inflow to happen because there was no wall to stop the flow especially when the ink behaved as Newtonian liquid (**Figure 7.7 b & c**). However, the inflow effect did not happen when the UV Carbon was used. The large viscosity of the UV Carbon ink resisted the inflow. When the dot area increased, the inflow effect was mitigated.

Opening up the wall between the anilox cells improved the ink release for the UV Cyan and Carbon inks with small filament breakup time. However, it did not affect the UV Silver ink, which had large filament breakup time; making it difficult to split. The roughness of surface and deeper cells made the ink release worse than the anilox cells with smoother surface using the laser engraving technique and shallower cells.

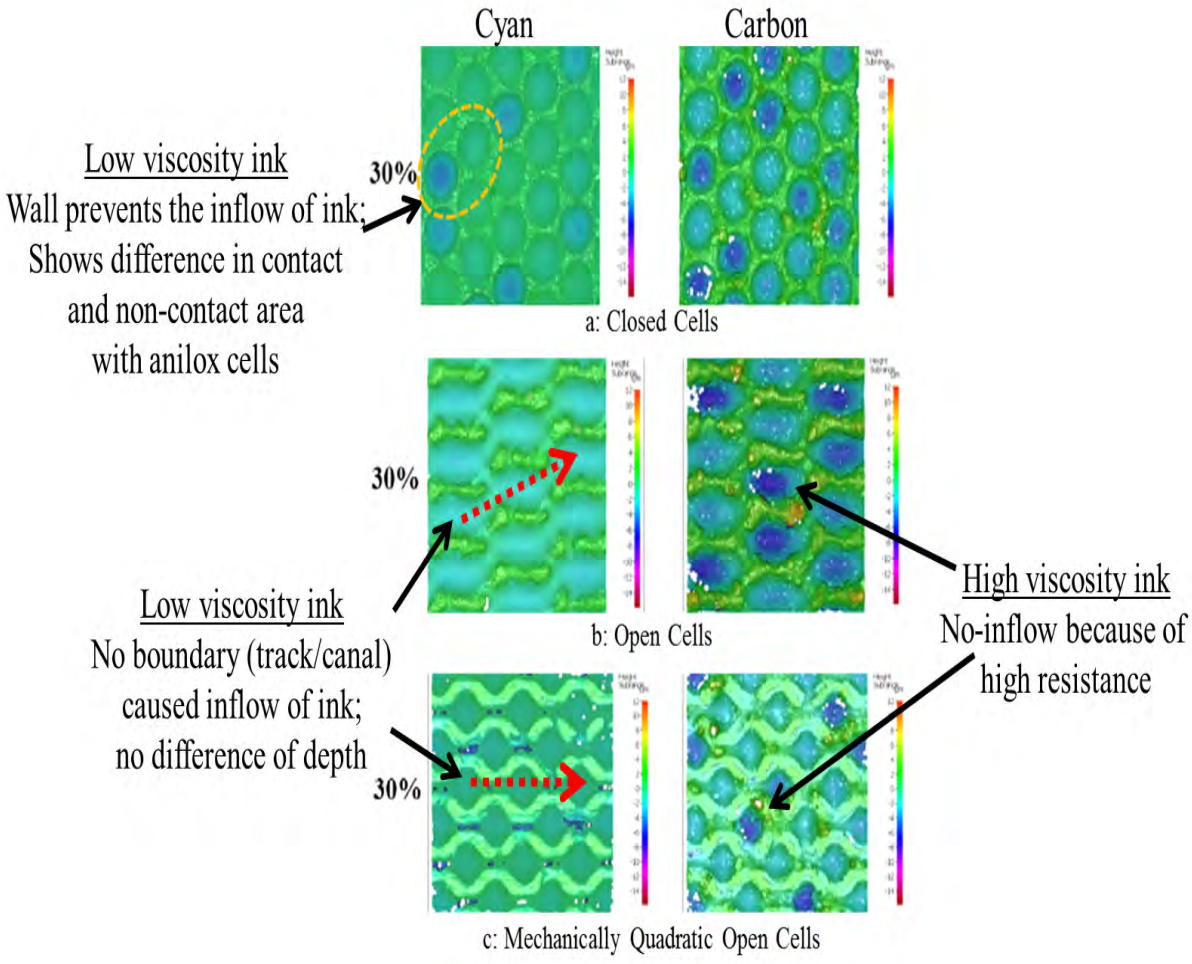

Figure 7.7: Ink release with UV Cyan and Carbon inks

7.3.2 Effect of Ink Characterisation

The images of the anilox closed cells after print with the dot coverage area of 10, 50, and 100% using the UV Cyan, Carbon, and Silver inks (**Figure 7.8**). There are some areas darker than the surrounding, indicating contact with the plate dot during the print. The darker the area indicates greater ink pull out. The dark area increased as the dot coverage increased because when the dot coverage increased, the dot size increased, increasing the contact area with the anilox cells. The print using the UV Carbon showed the darkest area comparing to the other two inks. The print using the UV Cyan showed the darker area comparing to the print using the UV Silver; indicating the UV Cyan ink had the greater ink release. The print using the UV Silver ink showed to be constant in colour from dot coverage 50% to 10%; indicated that no significant change when the dot coverage increased, indicated that the ink was not significantly released.

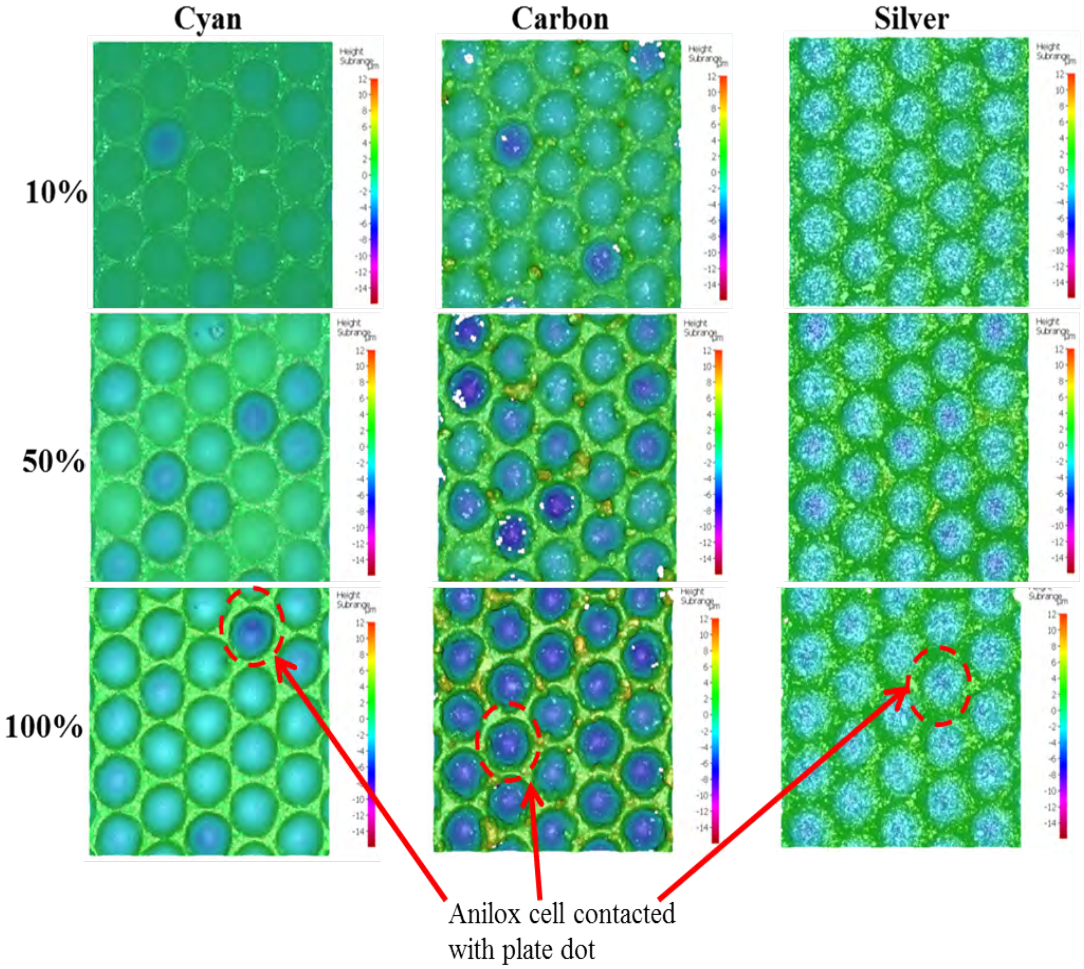

Figure 7.8: The images of the anilox closed cells after print with the dot coverage area of 10, 50, and 100% using the UV Cyan, Carbon, and Silver inks

The ink release increased as the dot coverage increased for the UV Carbon and Cyan inks (**Figure 7.9**). The ink release of the UV Silver ink was constant from dot coverage of 50%. Similar to the trend seen in the prints using the solid plate, the UV Carbon ink has the most pull-out, then UV Cyan, and the least was the UV Silver. The ink with the large viscosity but having the small filament breakup time; UV Carbon gave the best ink release out of the anilox cells. Having the large viscosity and filament breakup time; UV Silver hindered the ink release.

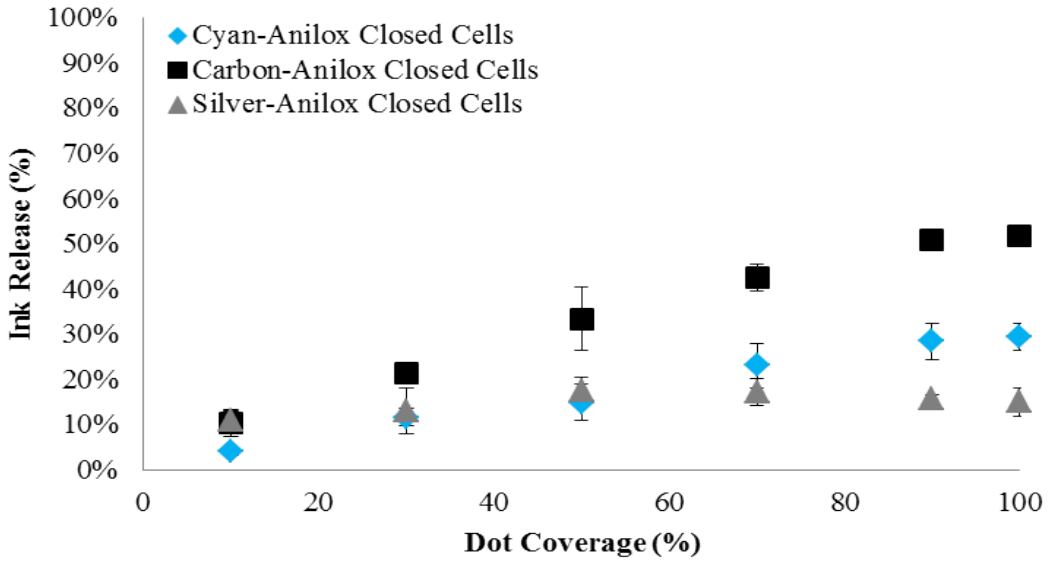

Figure 7.9: The results of the anilox closed cells after print with the dot coverage area of 10 to 100% using the UV Cyan, Carbon, and Silver inks

The images of the anilox open cells after print with the dot coverage area of 10, 50, and 100% using the UV Cyan, Carbon, and Silver inks (**Figure 7.10**). Similar to the images seen using the anilox closed cells, there are some areas darker than the surrounding. The dark area increased as the dot coverage increased. The print using the UV Carbon showed the darkest area comparing to the other two inks. However, the print using the UV Silver ink was constant in colour; no significant change when the dot coverage increased, indicated that only a small amount of ink was being released. The UV Cyan ink was slightly darker when the dot coverage increased; indicated a slight increase in the release of the ink. The low viscosity of UV Cyan ink caused the reflow of the ink along the open track between the test and the measurement time especially in the low dot coverage; 10%, where the printing dot size was very small; resulted in there being no discernible difference between the area of contact or non-contact with the printing dot. However, the reflow did not affect the UV Carbon and Silver inks because of their higher viscosity.

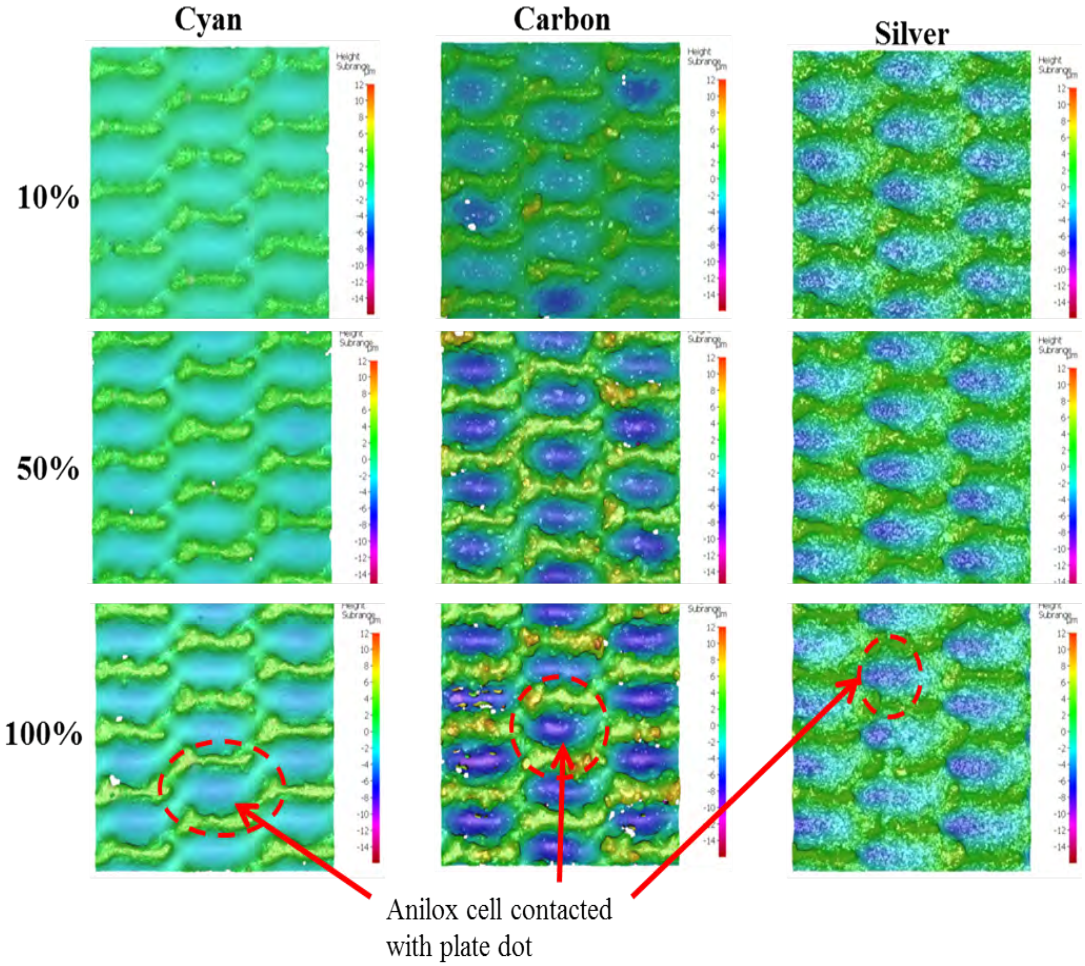

Figure 7.10: Anilox open cells after print with the dot coverage area of 10, 50, and 100% using the UV Cyan, Carbon, and Silver inks

The UV Cyan, Carbon, and Silver inks were printed using open cells with dot coverage area of 10 to 100% (**Figure 7.11**). Similar to the closed cells, the ink release increased as the dot coverage increased for all the inks. The UV Carbon ink had the most pull-out, then the UV Cyan, and the least was the UV Silver. There was a slightly increase with the UV Silver ink for coverage from 10% to 50%, and then approximately constant ink release, whilst the UV Cyan ink release increased as the dot coverage area increased. The large filament breakup time of the UV Silver ink hindered the breaking of the ink filament, increased contact area did not improve its ink release.

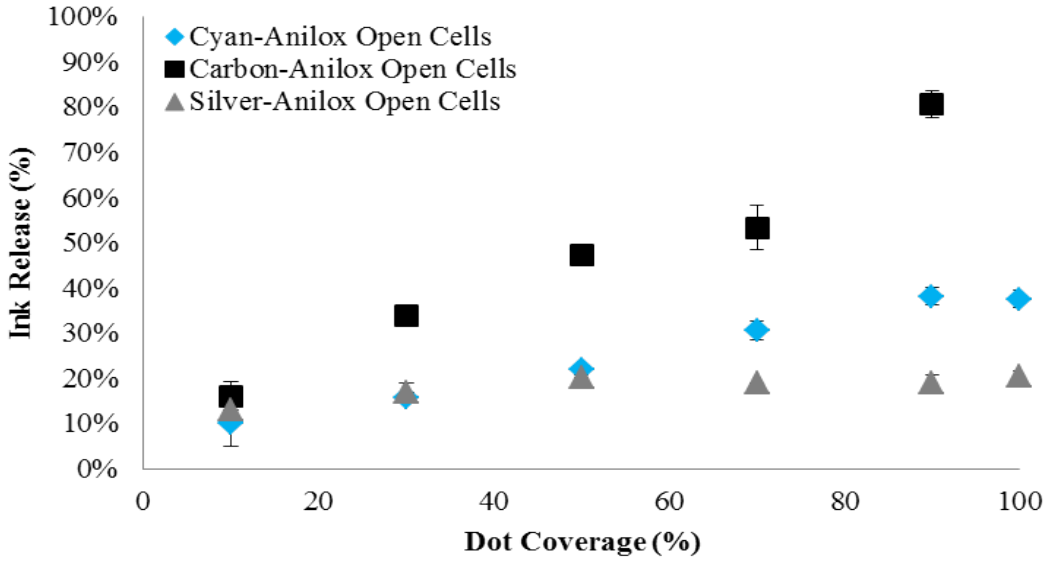

Figure 7.11: Anilox open cells after print with the dot coverage area of 10 to 100% using the UV Cyan, Carbon, and Silver inks

As with the previous cases, the more UV Carbon ink was transferred compared to the other two inks (**Figure 7.12**). The image did not include the 10% dot coverage because this area of UV Cyan and Carbon was contaminated during printing. The print using the UV Silver ink showed little change when the dot coverage increased, indicated that the ink was not significantly released to the plate. The print using the UV Cyan ink was constant in colour; however, it was slightly darker at the dot coverage of 100%; indicating a slight increase in ink transfer when the dot coverage increased. Additionally, the low viscosity of UV Cyan ink caused the flow of the ink along the open track between the test and the measurement time especially in the low dot coverage; 30%, where the printing dot size was very small; resulted in no significant different of the area of contact or non-contact with the printing dot. However, the reflow was not affected the UV Carbon and Silver inks because of their high viscosity.

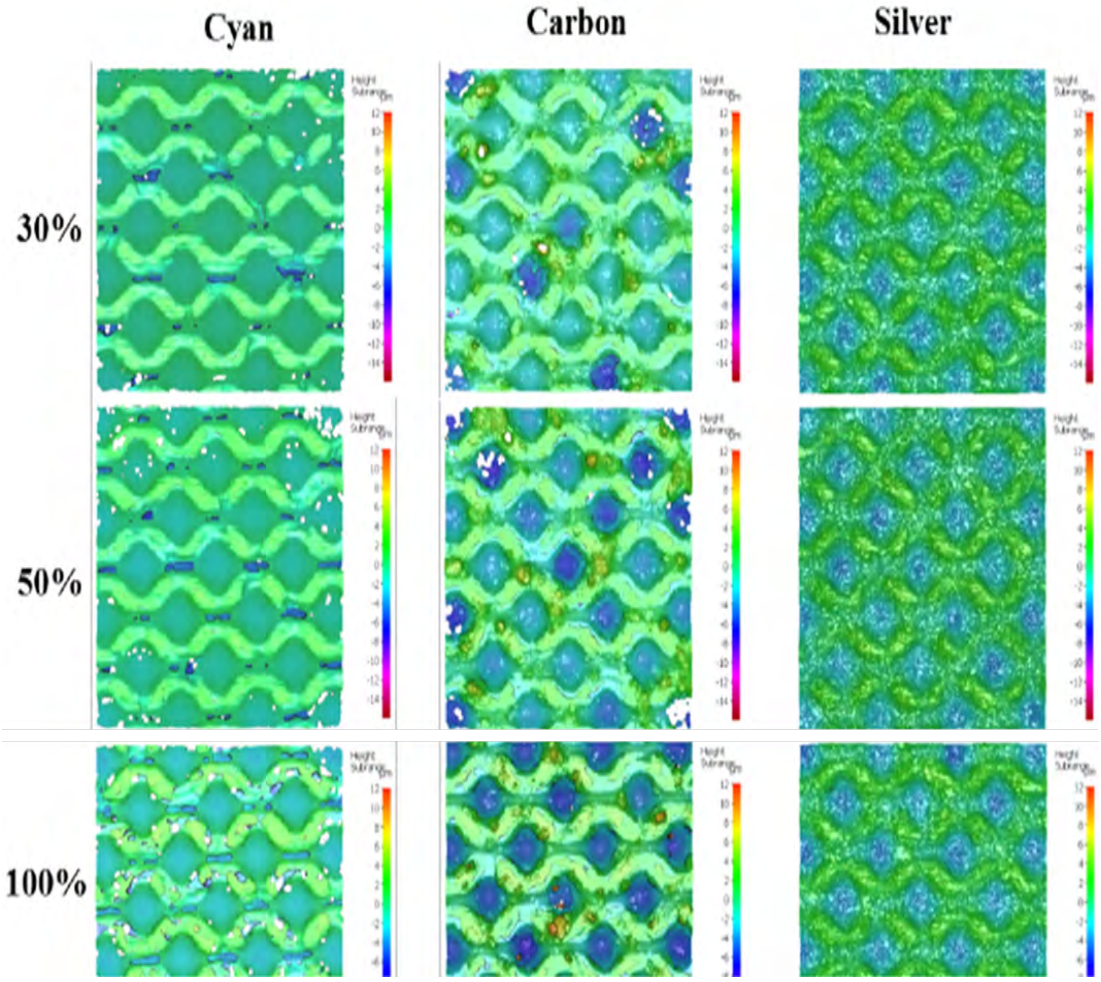

Figure 7.12: The anilox mechanically quadratic open cells after print with the dot coverage area of 30, 50, and 100% using the UV Cyan, Carbon, and Silver inks

The results of after print with the dot coverage area of 10 to 100% using the UV Cyan, Carbon, and Silver inks (**Figure 7.13**). Similarly, the ink release with the mechanically engraved quadratic open cells increased as the dot coverage increased for the UV Cyan and Carbon inks, but with no significant increase for the UV Silver ink. The UV Carbon ink had the most pull-out, then the UV Cyan, whilst the UV Silver inks had the least.

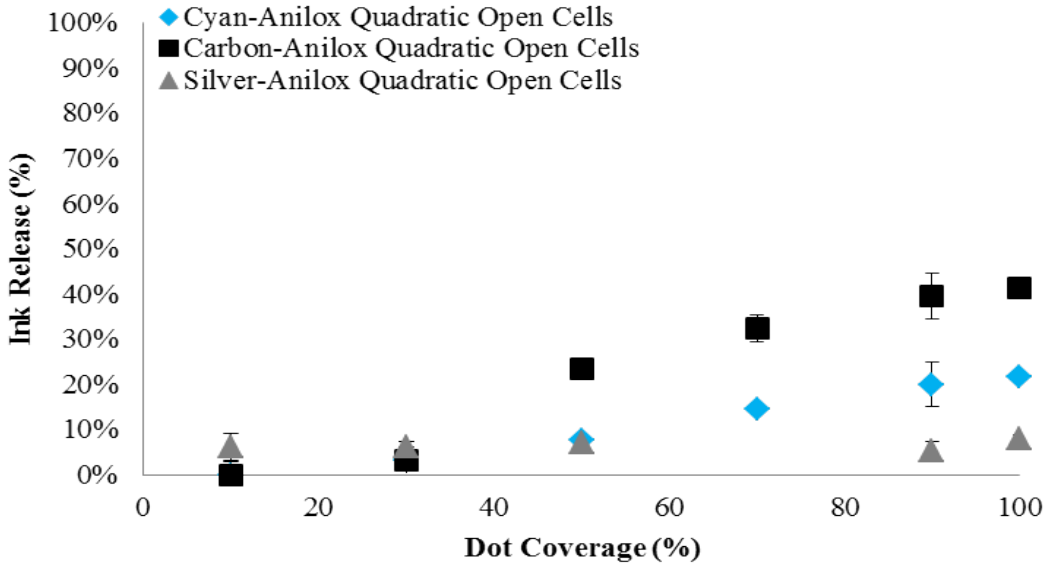

Figure 7.13: The results of the anilox mechanically quadratic open cells after print with the dot coverage area of 10 to 100% using the UV Cyan, Carbon, and Silver inks

7.4 Closure

Using the tonal patch plate gave similar trends to those seen using the solid printing plate; the UV Carbon released the most and using the anilox open cells improved the ink release. The increase of the dot coverage area increased the contact and receiving area, which increased the ink release for the UV Cyan and Carbon inks. However, there was a limited increase of the ink release when the dot coverage area increased with the UV Silver ink. The limitation was at the dot coverage area of approximately 50% after this dot coverage the ink release was plateaued. The opening up of the wall did not improve the ink release of this ink.

Chapter 8

Conclusions and Future Work

8.1 Introduction

There have been many claims for the benefits of the engraving patterns which have been enabled by the advent of laser technology. The objective of this project was to study the effect of the anilox engraved geometries on the ink release from the anilox to the plate.

Initial studies were performed on full scale presses to enable the research to be set in practical context. The Cooper flexo press was used to print a UV flexo Black ink onto a non-absorbent substrate, glass, to enable a perspective to be gained on ink release without the complication of absorption by the substrate. Two anilox cell bands with the closed range of cell volume but different in cell width and depth were used to investigate the ink release out of the anilox cells. The features on the printing plate were the tonal patch of 1-100% dot area coverage, and the track width of 20-600μm. The measured parameters were the optical density for the tonal patch prints, and the track ink volume and width for the track prints as these parameters could indicate the ink release of the anilox cells.

A second series of experiments were on a commercial central impression (CI) press with two bands of the anilox cells; elongated closed cells and wavy cells, two inks with low and high viscosity, the tonal patches and thin PET substrate. The ink release of those two anilox bands were compared for the two ink types.

Informed by these studies, a series of laboratory experiments were performed using a flexographic proofing press; RK flexiproof press. The initial studies had focused on traditional low viscosity graphic inks. However, the developments in ink technology, particularly for functional applications such as printed electronics and sensors, are leading to inks which are more viscous, non-Newtonian and with varying extensional viscosity. Three inks; UV Cyan, Carbon, and Silver, were printed onto a PET substrate. The experiments were carried out to establish the ink release from the closed anilox cells traditionally

used in flexography, open and wavy anilox cells (new concepts) to study the effect of the cell geometries, ink and print speed. Mechanically engraving quadratic channel anilox cells were used to compare its ink release against the laser engraving closed anilox cells.

The measurement of the ink release was done directly by measuring the anilox cells before and after prints. This approach was different from most of the previous studies in which the printed substrate was measured instead of the anilox cells themselves.

8.2 Effect of the Anilox Cell Geometries

Generally for the anilox cells with the same shape but different in width and depth, the anilox cells with the wider or greater opening could release ink better than those with smaller opening because there was more space for the ink to get out. However, the greater cell width did not always release greater ink. The cell depth was more critical to the ink release than the width of the anilox cells. The anilox cells which were shallower and with the smaller depth-to-width ratio released a greater proportion of ink out of the anilox cells.

For the anilox cells with difference cell shapes, the characteristics of ink influenced the ink release. The anilox hexagonal closed cells (typically used in the flexographic printing process) was the best used with the ink, which had a low ink viscosity and elastic modulus, and small filament breakup time (typically used for graphic prints). This might be the reason why the graphic prints using the flexographic printing process rarely switched the anilox hexagonal closed cells to the other shapes. When the ink had high ink viscosity, elastic modulus, and filament breakup time such as UV Silver ink, then the wavy channel released the greatest proportion of ink from the cell. Additionally, the wavy channel gave better ink lay-down. It gave the ink film with smoother and more consistency layer; reduced the fluctuation or inconsistency around the edge and surface.

The anilox cells, which were engraved by laser, gave greater ink release comparing to the anilox cells, which were engraved by mechanically engraving. The mechanically engraving generated anilox cells with much greater surface roughness. There were cracks and holes on the rough surface. These cracks and holes caused the ink to be trapped instead of being released, reducing the amount of ink transferred to the plate.

8.3 Effect of the Ink Viscosity

The characteristics of ink influenced the release from the anilox cells. Previous studies examined the effect of ink viscosity in which the results showed that the greater ink viscosity increased the ink release. Unlike previous studies, the ink elastic modulus and filament breakup established via the CaBER test were included as well measurement of the visco-eleastic properties using small amplitude oscillatory shear on a rotational rheometer The ink with high viscosity and elastic modulus, but small filament breakup time gave greatest ink release for all anilox shapes. The high viscosity and elastic modulus increased the ink pull-out fraction, and the small filament breakup time made this greater pull-out fraction readily separated from the anilox cells. The filament breakup time and elastic modulus were critical to the ink release. The large elastic modulus increased the pull-out portion and with the small filament breakup time, the pull-out portion could easily separate.

8.4 Effect of the Print Speed

Generally, when the printing speed increased, it decreased the ink release due to two factors; reduction of engagement time between the anilox cells and the plate (reducing time for ink to transfer), enlargement of the filament extension rate, which made the ink filament thinner during the printing process; reducing the amount of ink pulled out of the anilox cells. However, the decrease of ink release was affected by the ink characteristics and the anilox cells shapes. The decrease of ink release was significant when UV Cyan ink (small viscosity and elastic modulus) was used with the anilox open cells and wavy channels. This liquid-like ink flowed along the track instead of being pulled out. In contrast, the decrease of ink release was insignificant when UV Carbon and Silver inks (large viscosity and elastic modulus) was used with the open cells and wavy channels. Their large viscosity and elastic modulus mitigated the effect of enlargement of the filament extension rate; maintaining the pull-out fraction.

8.5 Print Using the Tonal Patch Plate

The tonal patch plate gave similar trend to those seen using the solid printing plate; the UV Carbon released the most and the anilox open cells improved the ink release. The increase of the dot coverage area increased the contact and receiving area, which increased the ink release for the UV Cyan and Carbon inks. However, there was limited ink release when the dot coverage area increased with the UV Silver ink. The limitation was at approximately a dot coverage area of 50% after which the ink release plateaued. Additionally, the opening in the wall did not improve the ink release.

The information gained from these investigation will aid the selection or

development of anilox cell geometries and inks appropriate for different printing applications; the anilox hexagonal closed cells was the best for the graphic prints, however high ink viscosity and elastic modulus could increase the ink release and make the image more vibrant. The anilox open and channels were more suitable with the functional prints as they released more of paste-like inks, which could increase the efficiency of printable electronics, such as by increasing the conductivity.

8.6 Future Work

The wavy channel improved the flow of ink such as UV Silver, which had large filament breakup time. Changing the wavy angle would affect the flow. For example, if the wavy angle decrease; it would make the ink flow better as the wall around the curve is like a blockage hindering the flow of ink. The improvement of anilox cell geometries for UV Silver, which is widely used in the printed electronics, would make the flexographic printing more competitive in the printable electronic industry.

This research focused on the ink release from the anilox cells to the printing plate, there could be further investigation of how the anilox cell geometries affect the print on the substrate. It would be of interest to establish how the anilox cell geometries affected the ink lay-down on the substrates. The results could aid in the design of anilox cell geometry which improve print quality of the final products for both graphic and functional prints.

The printing speed between 50 to 90m/min (for example, 50, 60, 70, 80, 90) should be examined to fully understand the trend of ink release. Additionally, the high-speed camera can be used to capture the ink filament breakup during the printing process. This will enable more understanding of ink release mechanism during printing process.

The surface tension of paste-like inks; UV Carbon and Silver should be determined. The ink may need to be diluted in order to be measured. However, it should be done with caution that the dilution did not alter the outcome and may not represent the paste-like behaviour. When the surface tension is determined, the relationship of printing speed and ink release should be explored possibly through the dimensionless number such as capillary number.

The phase angle of the ink should be considered as a better indicate of ink release. Because phase angle relates to the elastic and viscous moduli and its value can indicate the shift of the ink from solid-like to liquid-like, which informs when the ink may start flowing. Additionally, as the value of phase angle is clearly defined (between 0 to 90), then comparison will be simpler.

The development of ink characteristic to improve the ink release by creating the ink formula to increase the ink viscosity but having small filament breakup. This improves the print quality; for example, graphic prints would benefit from this type of ink because it increases the ink film thickness; improving the vibrant colour. The functional print can increase the conductivity due to the greater amount of ink on the substrate.

These would help improve the anilox design and ink improvement in the flexographic printing process. Ultimately, to increase the print quality so flexography becomes the preferred choice for the printer.

References

Ascanio, G., Carreau, P., Brito-De La Fuente, E. and Tanguy, P. (2004). Forward Deformable Roll Coating at High Speed with Newtonian Fluids. Chemical Engineering Research and Design, 82(3), pp.390-397.

Barnes, H.A., Hutton, J.E., K. Walters F. R. S. (1989) An Introduction to Rheology, 3rd edn., The Netherlands: Elsevier Science.

Beynon, D. (2007). Plate to Substrate Ink Transfer in the Flexographic Printing Process. Swansea: Swansea University.

Bould, D. C. (2001). An Investigation into Quality Improvement in Flexographic Printing. PhD. University of Wales Swansea.

Bould, D., Claypole, T. and Bohan, M. (2004). An investigation into plate deformation in flexographic printing. Proceedings of the Institution of Mechanical Engineers, Part B: Journal of Engineering Manufacture, 218(11), pp.1499-1511.

Castrejón-Pita, A., Castrejón-Pita, J. and Hutchings, I. (2012). Breakup of Liquid Filaments. Physical Review Letters, 108(7)

Chang, G., Koo, J. and Song, K. (2003). Wall slip of vaseline in steady shear rheometry. Korea-Australia Rheology Journal, 15(2), pp.55-61.

Cherry, J. (2007). Ink release characteristics of anilox rolls. Swansea: Swansea University.

Cooperprint.co.uk. 2020. Cooper Printing Machinery LTD. [online] Available at: ¡https://www.cooperprint.co.uk/cooper_flexopress.html¿ [Accessed 15 April 2020].

Correct-Touch Graphic Arts. (2017). Anilox Rolls - Correct-Touch Graphic Arts. [online] Available at: http://ctgraphicarts.com/anilox-rolls/ [Accessed 28 Aug. 2017].

Coyle, D., Macosko, C. and Scriven, L. (1986). Film-splitting flows in forward roll coating. Journal of Fluid Mechanics, 171(-1), p.183.

Damroth, G., DiPiassa, J., Hausman, G., Hines, M., Rivas, M., Rose, B. Shaffer, L., Wald, J. and Ziegler, R. "The Effect of UV Flexo Ink Viscosity, Anilox Cell Volume and Press Speed on Print Density and Dot Gain". TAGA, 1996, pp86-101

Deganello, D. (2007). Study of Ink Release from Gravure Cells Using Neural Networks and CFD Simulations. Swansea: Swansea University

De Grke, Y. H., Dalphond, J. E., Mangin, P. J., "A Mechanistic Approach to Ink Transfer, Part 111: Properties of Ink Filaments in Printing Nips", Advances in Printing Science and Technology, 21,312, 1992

Dodds, S. (2011). Stretching and Slipping Liquid Bridges:Liquid Transfer in Industrial Printing. 1st ed. Minnesota, USA: The University of Minnesota

Dycotecmaterials.com. 2020. DM-AS-10000. [online] Available at: ¡ https://www.dycotecmaterials.com/product/dm-as-10000/¿ [Accessed 4 May 2020].

Elsayad, S., Morsy, F., El-Sherbiny, S. and Abdou, E. (2002). Some factors affecting ink transfer in gravure printing. Pigment Resin Technology, 31(4), pp.234-240

Ercan, S. (2001). THE INFLUENCE OF PROCESS PARAMETERS ON FILAMENT SIZE DISTRIBUTION. Maine, USA: The University of Maine

Flexoexchange.com. 2014. Laser Engraving of Anilox Rolls. [online] Available at: http://www.flexoexchange.com/gorilla/tofcarticle.html [Accessed: 7 Feb 2014]

Flexographic Technical Association. (2018). Flexography Forecasts for 2017: Economical, Versatile, Budget Friendly; Scientifically Proven Predictable - Page 2 of 5 - Flexographic Technical Association. [online] Flexographic Technical Association. Available at: https://www.flexography.org/flexo-prepress/flexography-forecasts-for-2017-economical-versatile-budget-friendly-scientifically-proven-predictable/15290/2/ [Accessed 26 Mar. 2018].

Franck, A. (n.d.) 'Understanding Rheology of Structured Fluids', TA Instruments, (), pp. 1-11

Hamblyn, S. (2004). The Role of the Plate in the Ink Transfer Process in Flexographic Printing. Swansea: Swansea University.

Harperimage.com. 2014. Harper Corporation - Manufacturer of Anilox Rollers for Flexographic Printers. [online] Available at: http://www.harperimage.com/ [Accessed: 21 Jan 2014]

Hewson, R., Kapur, N. and Gaskell, P. (2011). A two-scale model for discrete cell gravure roll coating. Chemical Engineering Science, 66(16), pp.3666-3674

Johnson, M. (2003). VISCOELASTIC ROLL COATING FLOWS. (1ST ed.). Maine, USA: The University of Maine.

Kapur, N. (2003). A parametric study of direct gravure coating. Chemical Engineering Science, 58(13), pp.2875-2882

Khandavalli, S. and Rothstein, J. (2017). Ink transfer of non-Newtonian fluids from an idealized gravure cell: The effect of shear and extensional deformation. Journal of Non-Newtonian Fluid Mechanics, 243, pp.16-26

Kipphan, H. (2001). Handbook of Print Media. Berlin, Heidelberg: Springer Berlin Heidelberg

Koenig-bauer.com. 2020. Evo XG, Koenig & Bauer, We're On It.. [online] Available at: ¡https://www.koenig-bauer.com/en/products/flexo/ci-flexo-presses/evo-xg/¿ [Accessed 1 May 2020].

Krebs, F. (2009). Fabrication and processing of polymer solar cells: A review of printing and coating techniques. Solar Energy Materials and Solar Cells, 93(4), pp.394-412.

Lamer, Tunde F. (2018) Large Amplitude Oscillatory Shear (LAOS) studies of fibrin and whole blood clots. Doctoral thesis, Swansea University, pp.30, 51.

Lécuyer, H., Mmbaga, J., Hayes, R., Bertrand, F. and Tanguy, P. (2009). Modelling of forward roll coating flows with a deformable roll: Application to non-Newtonian industrial coating formulations. Computers and Chemical Engineering, 33(9), pp.1427-1437.

Lee, S. and Na, Y. (2010). Analysis on the ink transfer mechanism in R2R application. Journal of Mechanical Science and Technology, 24(1), pp.293-296

Lychock, G. (1995). Dot Area, Dot Gain, and n-Factors. [ebook] X-Rite World Headquarters. Available at: https://www.xritephoto.com/documents/apps/public/whitepapers/Ga00005a.pdf [Accessed 8 Aug. 2018]

Mackley, M., Butler, S., Huxley, S., Reis, N., Barbosa, A. and Tembely, M. (2017). The observation and evaluation of extensional filament deformation and breakup profiles for Non Newtonian fluids using a high strain rate double piston apparatus. Journal of Non-Newtonian Fluid Mechanics, 239, pp.13-27

Mai, R., Pekarovicova, A. and Fleming, P. (2007). Correlation between Ink Rheology and Press Performance of Water-based Flexographic Inks. Flexo.

Mallik, S., Ekere, N., Durairaj, R., Marks, A. and Seman, A. (2009). Wall-slip effects in SnAgCu solder pastes used in electronics assembly applications. Materials and Design, 30(10), pp.4502-4506.

Malvernpanalytical.com. (2019). A Basic Introduction to Rheology. [online] Available at: https://www.malvernpanalytical.com/en/learn/knowledge-center/whitepapers/WP160620BasicIntroRheology [Accessed 19 Aug. 2019].

Mariani, P., Vesce, L. and Di Carlo, A. (2015). The role of printing techniques for large-area dye sensitized solar cells. Semiconductor Science and Technology, 30(10), p.104003

Morgan, M., Holder, A., Curtis, D. and Deganello, D. (2017). Formulation, characterisation and flexographic printing of novel Boger fluids to assess the effects of ink elasticity on print uniformity. Rheologica Acta, 57(2), pp.105-112.

Novakovic et al., IEEE Indus. Appl. Mag., 22(5), 73, 2016.

https://nzic.org.nz. (2018). PRINTING INK TECHNOLOGY AND MANUFACTURE. [online] Available at: https://nzic.org.nz/ChemProcesses/polymers/10E.pdf [Accessed 26 Mar. 2018].

Oroian, M. (2013). Measurement, prediction and correlation of density, viscosity, surface tension and ultrasonic velocity of different honey types at different temperatures. Journal of Food Engineering, 119(1), pp.167-172.

Owens, M., Vinjamur, M., Scriven, L. and Macosko, C. (2011). Misting of non-Newtonian liquids in forward roll coating. Journal of Non-Newtonian Fluid Mechanics, 166(19-20), pp.1123-1128

Pritchard, G. (2017). All about Dot Gain/TVI (Tone Value Increase). [online] The-print-guide.blogspot.com. Available at: http://the-print-guide.blogspot.com/2009/06/all-about-dot-gaintvi-tone-value.html [Accessed 30 Sep. 2017].

Sachdev, S., Muralidharan, A. and Boukany, P. (2016). Molecular Processes Leading to "Necking" in Extensional Flow of Polymer Solutions: Using Microfluidics and Single DNA Imaging. Macromolecules, 49(24), pp.9578-9585

Sankaran, A. and Rothstein, J. (2012). Effect of viscoelasticity on liquid transfer during gravure printing. Journal of Non-Newtonian Fluid Mechanics, 175-176, pp.64-75.

Scrimgeour, J. (2017). Back-to-basics. Part 6. Plates and screens — AJS Labels Blog. [online] Ajslabels.com. Available at: http://www.ajslabels.com/blog/b-t-b-part-6-printing-plates-screens 2320 [Accessed 2 Sep. 2017].

Shukla, A., Sudhakar, K. and Baredar, P. (2016). A comprehensive review on design of building integrated photovoltaic system. Energy and Buildings, 128, pp.99-110.

SMOLKA, L., BELMONTE, A., HENDERSON, D. and WITELSKI, T. (2004). Exact solution for the extensional flow of a viscoelastic filament. European Journal of Applied Mathematics, 15(6), pp.679-712

Turkoz, E., Deike, L. and Arnold, C. (2017). Comparison of jets from Newtonian and non-Newtonian fluids induced by blister-actuated laser-induced forward transfer (BA-LIFT). Applied Physics A, 123(10)

Understand Building Construction. (2017). Glass as a Building Material. [online] Available at: http://www.understandconstruction.com/glass.html [Accessed 15 Sep. 2017].

Woodward, R. (2018). Surface Tension Measurements Using the Drop Shape Method. [Document] Portsmouth, VA, USA

Wu, J., Carvalho, M. and Kumar, S. (2019). Emptying of gravure cavities containing shear-thinning and shear-thickening liquids. Journal of Non-Newtonian Fluid Mechanics, 268, pp.46-55.

Yao, M. and McKinley, G. (1998). Numerical simulation of extensional deformations of viscoelastic liquid bridges in filament stretching devices. Journal of Non-Newtonian Fluid Mechanics, 74(1-3), pp.47-88.

Zevallos, G., Carvalho, M. and Pasquali, M. (2005). Forward roll coating flows of viscoelastic liquids. Journal of Non-Newtonian Fluid Mechanics, 130(2-3), pp.96-109.

Appendix A-Measurements of anilox and ink release

A1-Summary of anilox measurement

Anilox Cell Shapes	**Anilox Reference**	**Anilox Cell Volume (cc/m^2)**	**Anilox Cell Width (μm)**	**Anilox Cell Depth (μm)**	**Depth to Width Ratio**	**Engraving**
Print Speed of 50m/min						
Conventional Closed Cell	A	6.45	73	16	0.22	Laser
	B	2.76	38	7	0.18	Laser
Hexagonal Closed Cell	C	2.67	39	12	0.31	Laser
	D	2.94	39	14	0.36	Laser
	E	5.10	56	15	0.27	Laser
	F	6.00	71	17	0.24	Laser
	G	7.42	71	21	0.30	Laser
Elongated Hexagonal Open Cell	H	4.84	58	16	0.28	Laser
	I	5.68	70	18	0.26	Laser
	J	8.62	70	26	0.37	Laser
Wavy Channels	K	6.86	56	17	0.30	Laser
	L	7.28	71	17	0.24	Laser
	M	11.10	71	31	0.44	Laser
Open Quadractic Cell	O	6.46	70	22	31	Mechanical
Print Speed of 90m/min						
Conventional Closed Cell	B	2.76	38	7	0.18	Laser
Hexagonal Closed Cell	F	6.00	71	17	0.24	Laser
Elongated Hexagonal Open Cell	I	5.68	70	18	0.26	Laser
Wavy Channels	L	7.28	71	17	0.24	Laser

A2-Total of ink release (cc/m^2)

	Ink Release (cc/m^2)			Standard Deviation (%)		
Anilox Reference	**Cyan**	**Carbon**	**Silver**	**Cyan**	**Carbon**	**Silver**
Print Speed of 50m/min						
A	2.18	3.36	1.30	8	6	10
B	0.90	1.53	0.73	9	8	9
C	0.84	1.25	0.23	9	9	6
D	0.88	1.28	0.14	9	8	9
E	1.74	3.18	0.58	10	10	4
F	2.03	3.75	0.46	9	9	8
G	2.41	4.02	0.91	6	10	9
H	1.30	3.33	0.36	6	4	5
I	1.91	3.55	0.51	4	3	3
J	1.00	4.27	0.54	10	9	2
K	1.23	3.90	0.90	9	9	5
L	1.67	4.41	0.99	9	7	4
M	0.93	3.56	1.71	6	7	10
O	1.30	3.15	0.46	10	7	3
Print Speed of 90m/min						
B	0.78	1.47	0.52	7	5	14
F	1.89	3.42	0.17	4	8	9
I	1.30	3.10	0.43	8	6	5
L	0.58	4.06	0.81	5	7	5

A3-Ink release (%)

	Ink Release (%)			Standard Deviation (%)		
Anilox Reference	**Cyan**	**Carbon**	**Silver**	**Cyan**	**Carbon**	**Silver**
Print Speed of 50m/min						
A	35	63	23	3	4	2
B	36	68	29	3	5	3
C	33	55	15	3	5	1
D	30	50	9	3	4	1
E	36	76	16	4	8	1
F	38	75	11	3	7	1
G	35	64	15	2	6	1
H	36	85	12	2	3	1
I	39	93	16	2	3	0
J	14	60	11	1	5	0
K	22	79	24	2	6	1
L	30	78	22	3	5	1
M	11	38	21	1	3	2
O	27	65	7	3	5	0
Print Speed of 90m/min						
B	31	66	20	2	3	3
F	34	68	4	1	5	0
I	27	86	13	2	5	1
L	11	70	18	1	5	1

Appendix B-Direct comparisons of ink release from anilox

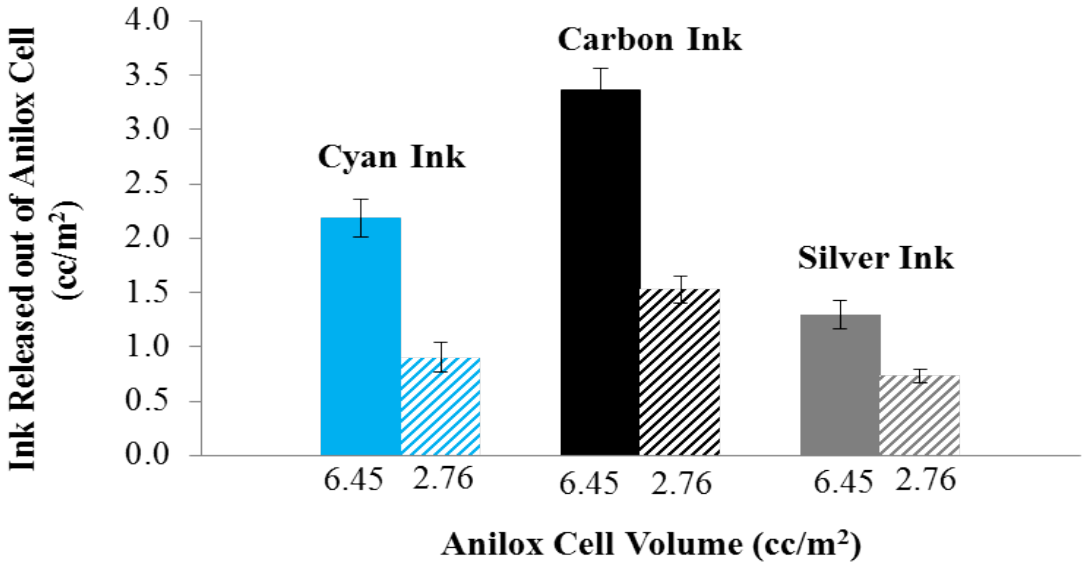

Figure B1: Ink released from the anilox closed cells to the plate

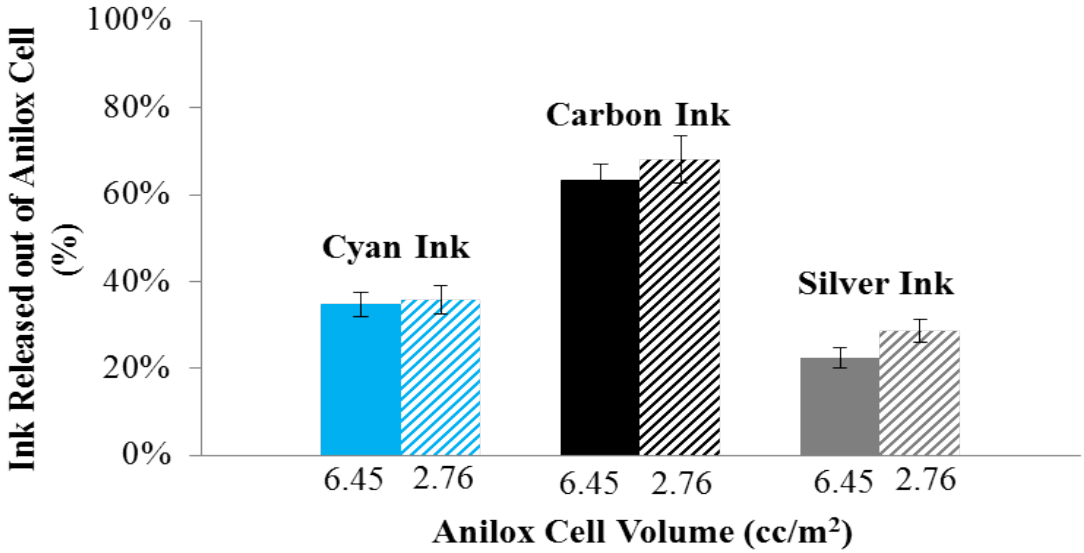

Figure B2: Percentage volume of ink released from the anilox closed cells to the plate

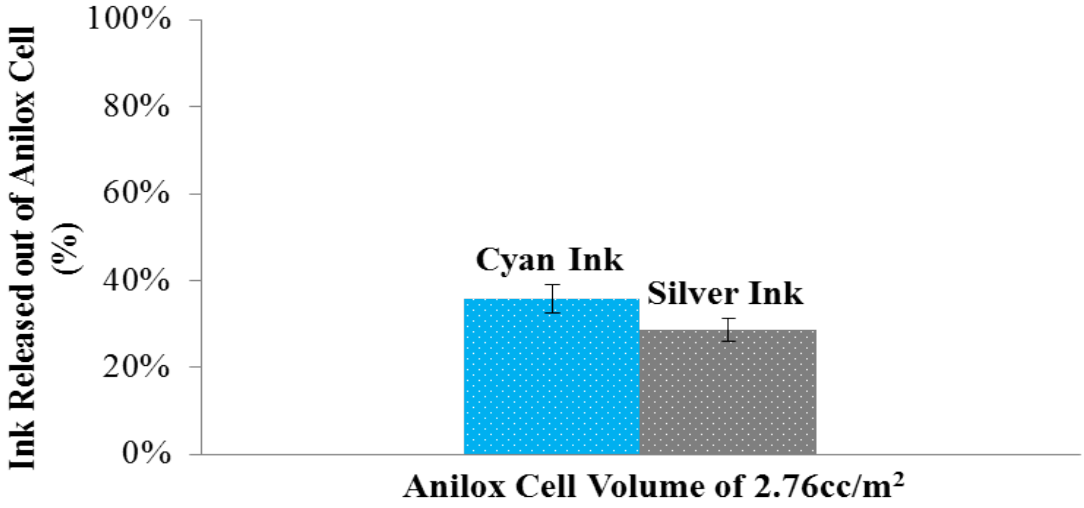

Figure B3: Percentage volume of UV Cyan and Silver inks released out of the anilox cells to the plate using the anilox closed cells with the volume of 2.76cc/m^2

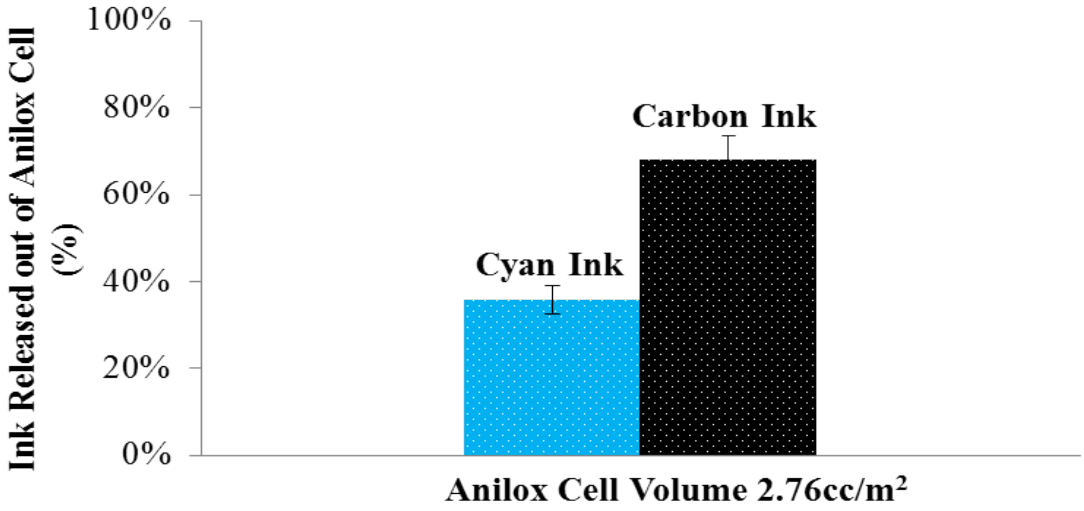

Figure B4: Percentage volume of UV Cyan and Carbon inks released out of the anilox cells to the plate using the anilox closed cells with the volume of 2.76cc/m^2

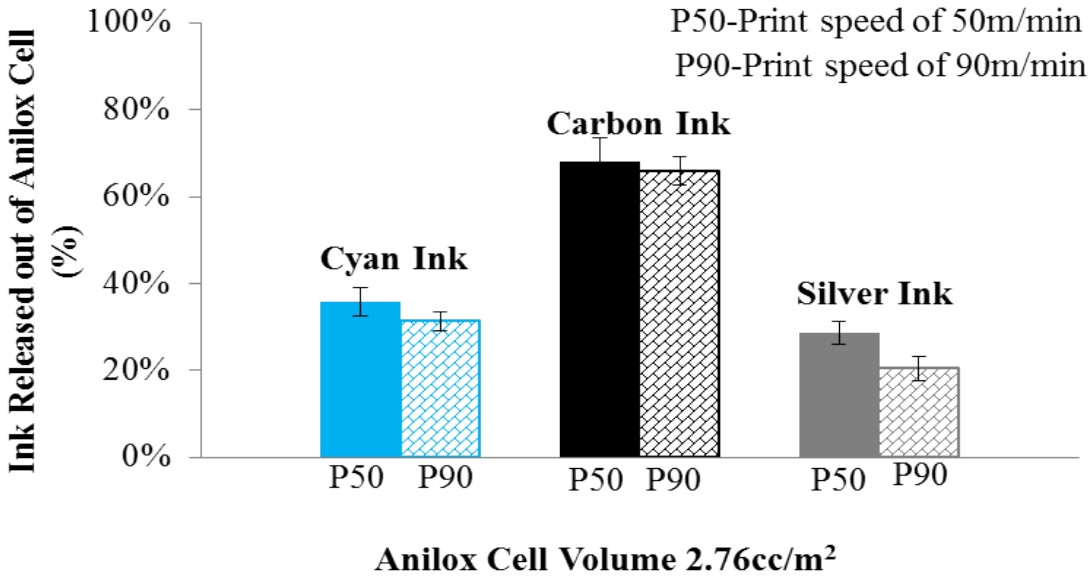

Figure B5: Effect of speed on the percentage ink volume released out of the anilox cells to the plate with the volume of 2.76cc/m^2

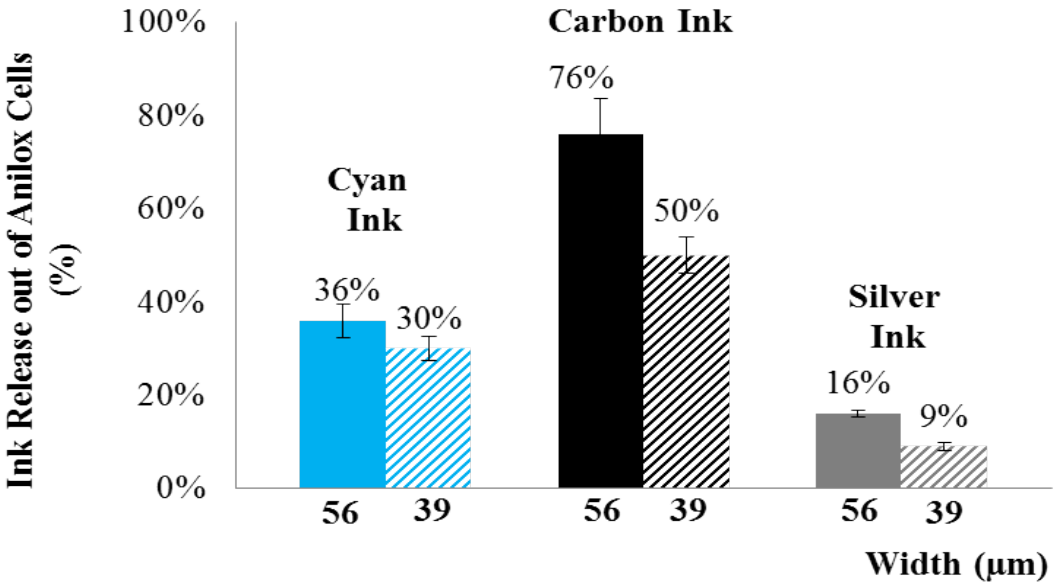

Figure B6: The ink release out of anilox cells using UV Cyan, Carbon, and Silver inks with anilox cell depth of 39 and 56μm

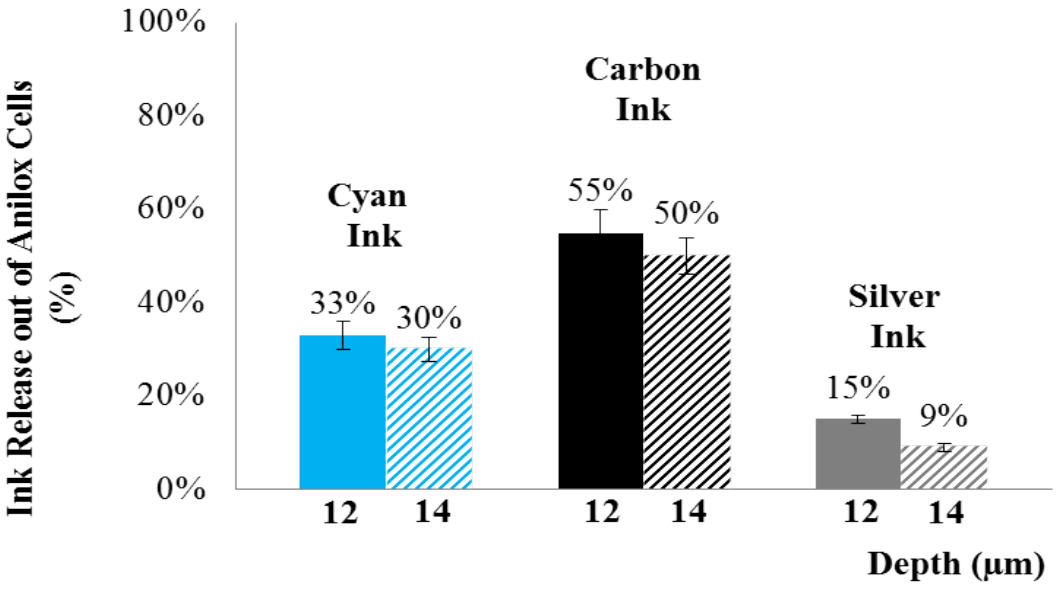

Figure B7: The ink release out of anilox cells using UV Cyan, Carbon, and Silver inks with anilox cell depth of 12 and 14μm

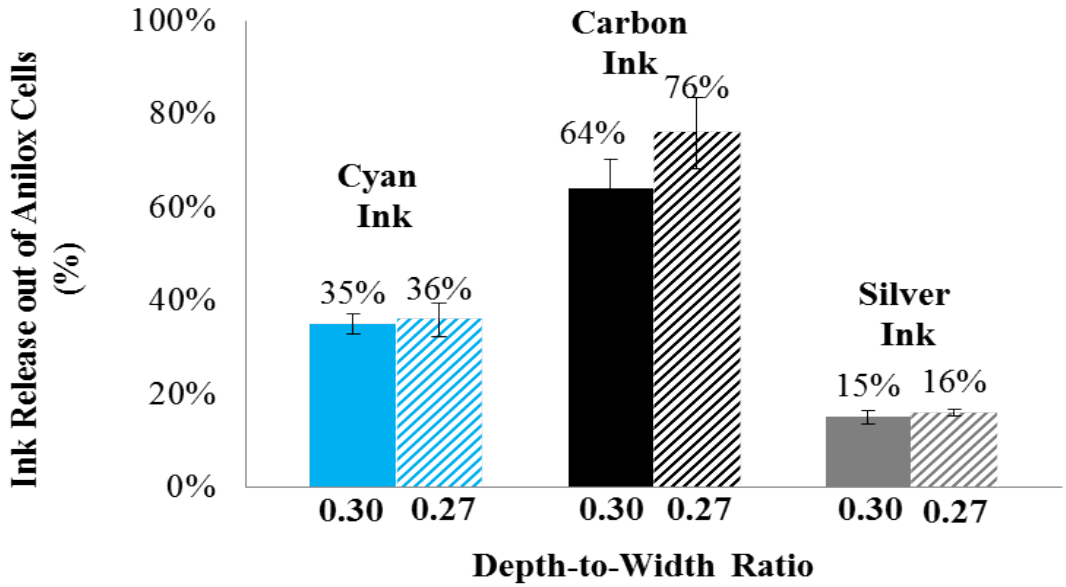

Figure B8: The ink release out of anilox closed cells using UV Cyan, Carbon, and Silver inks with anilox cell depth-to-width ratio of 0.27 and 0.30

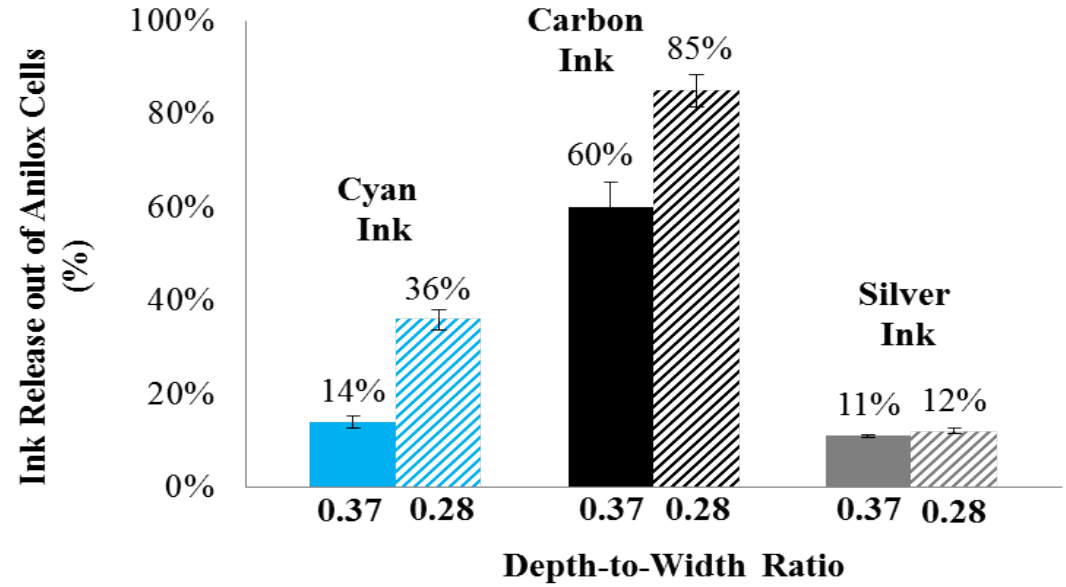

Figure B9: Ink release out of anilox open cells

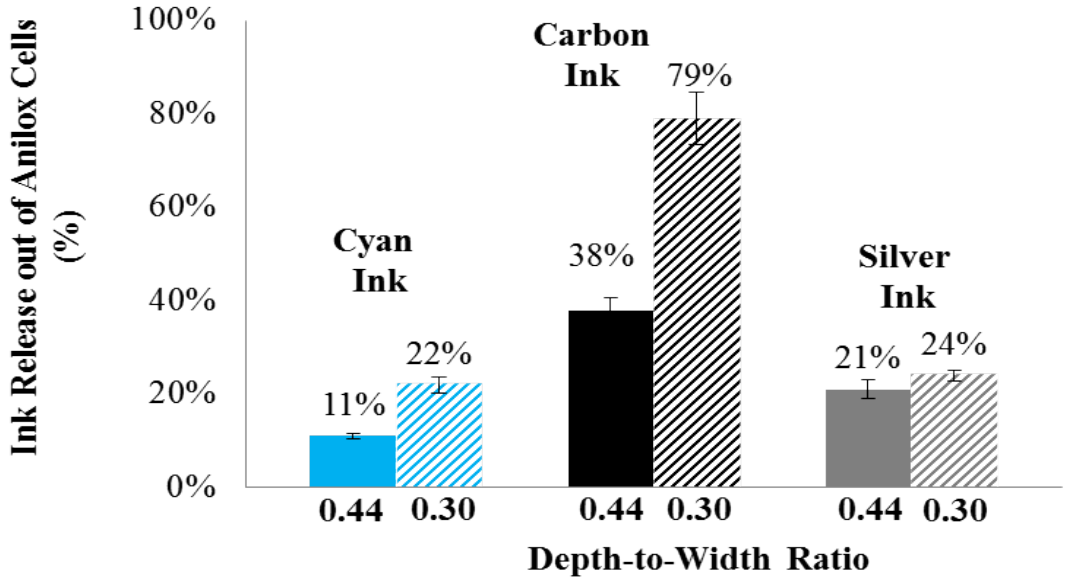

Figure B10: Ink release out of anilox wavy channels

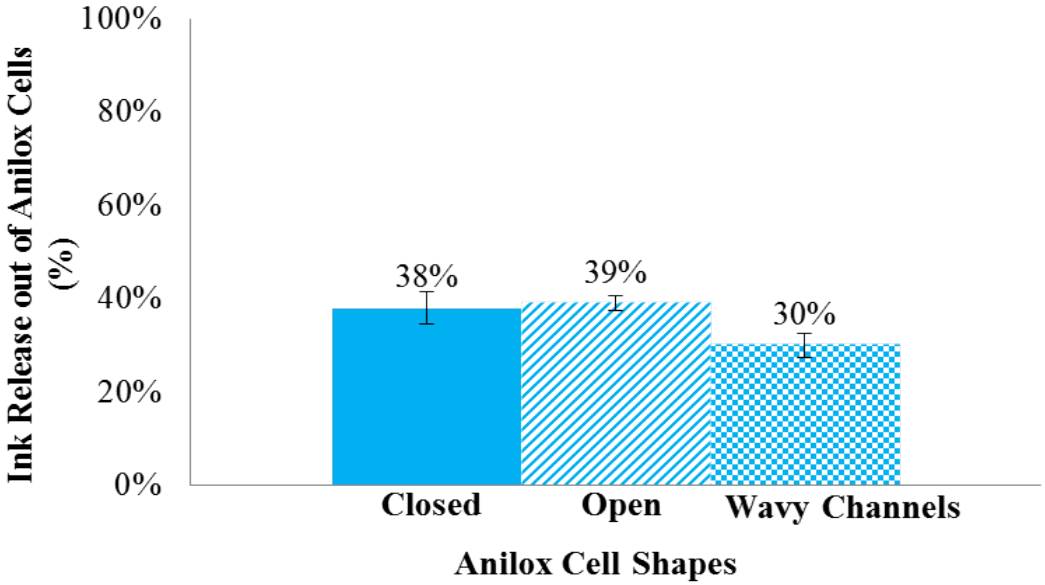

Figure B11: Ink release out of anilox cell shapes of hexagonal closed cells, elongated hexagonal open cells, and wavy channels using UV Cyan ink

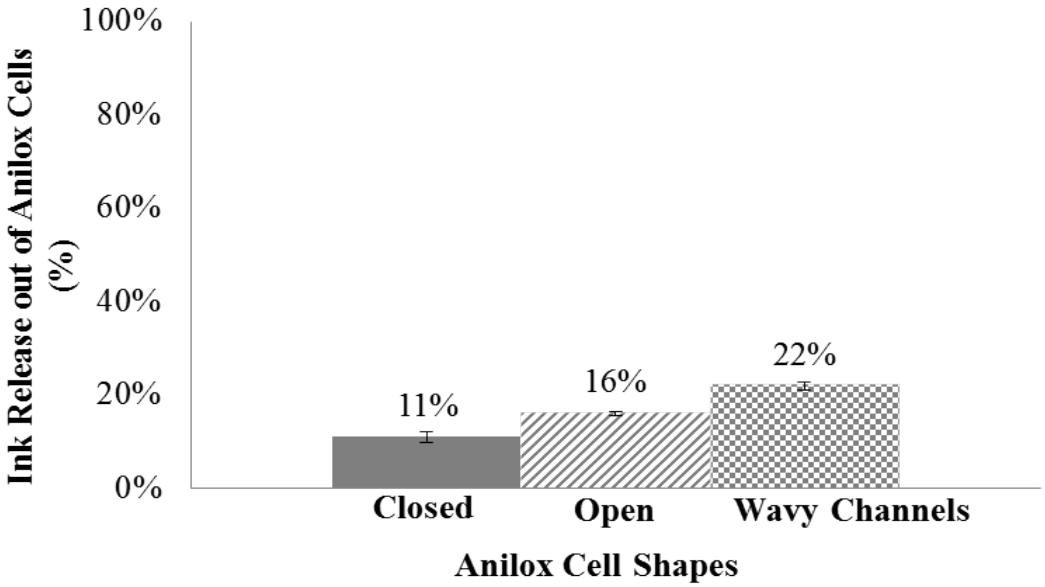

Figure B12: The ink release out of anilox cell shapes of hexagonal closed cells, elongated hexagonal open cells, and wavy channels using UV Silver ink

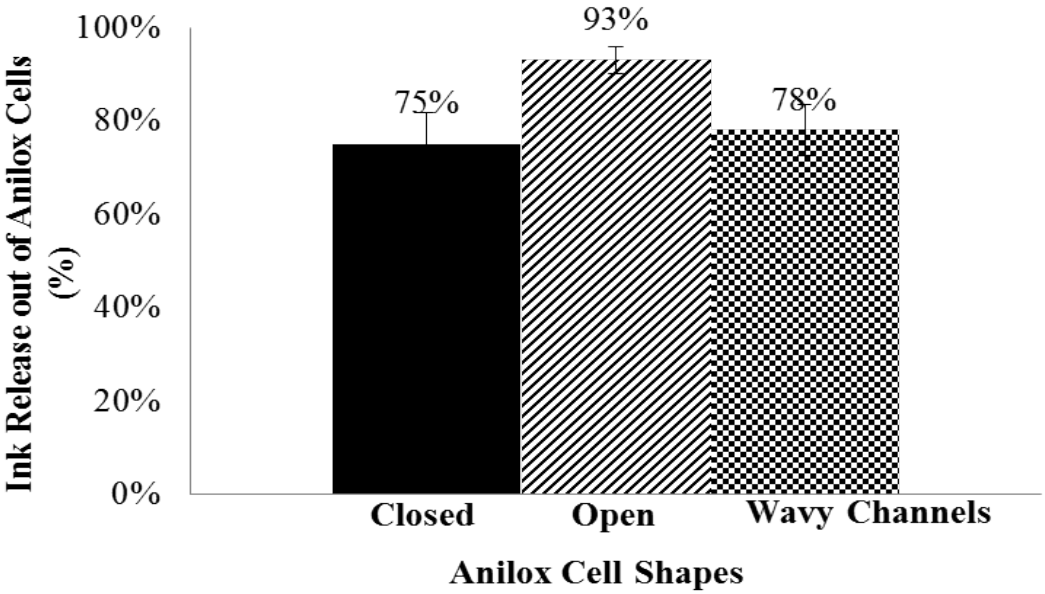

Figure B13: Ink release out of hexagonal closed cells, elongated hexagonal open cells, and wavy channels using UV Carbon ink

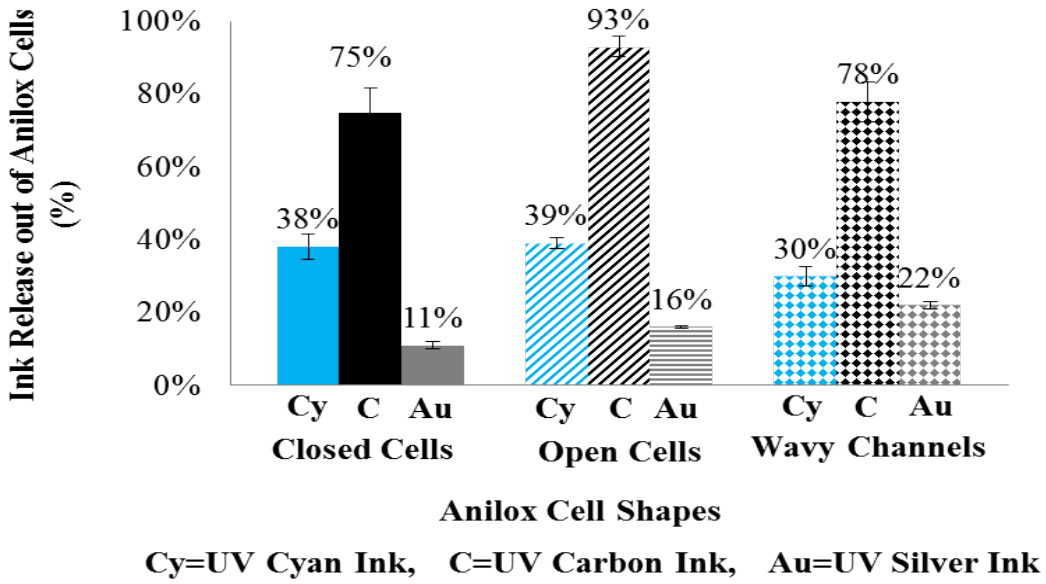

Figure B14: The ink release using UV Cyan, Carbon, and Silver inks with 3 shapes of anilox cells; closed cells, open cells, and wavy channels

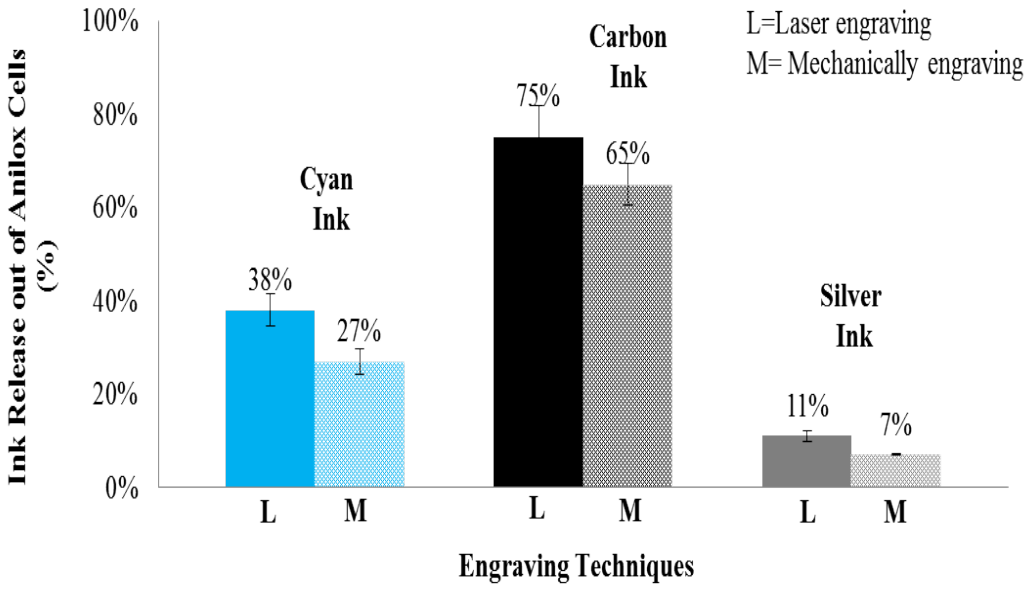

Figure B15: Ink release out of laser and mechanically engraved anilox cells

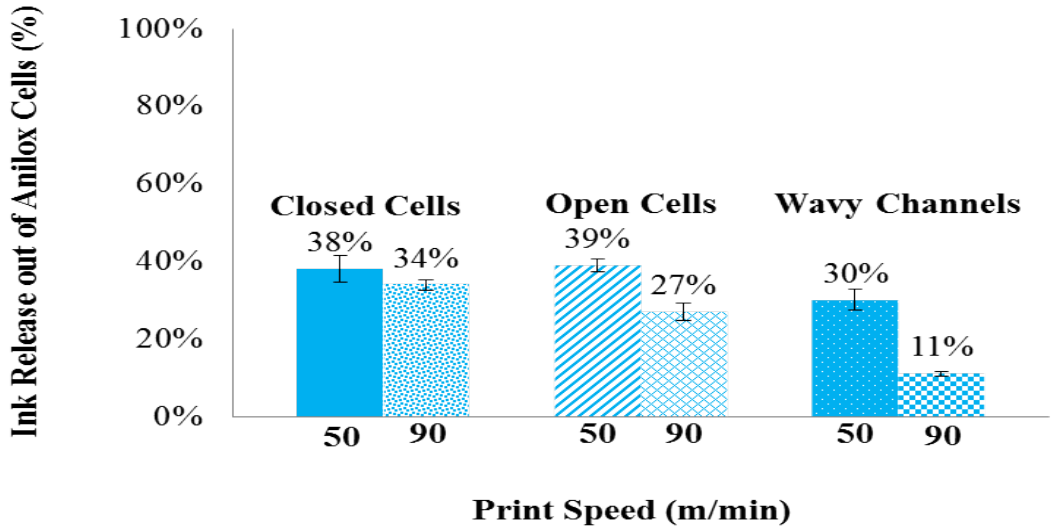

Figure B16: The ink release out of three anilox cell shapes using UV Cyan ink to investigate the effect of printing speed

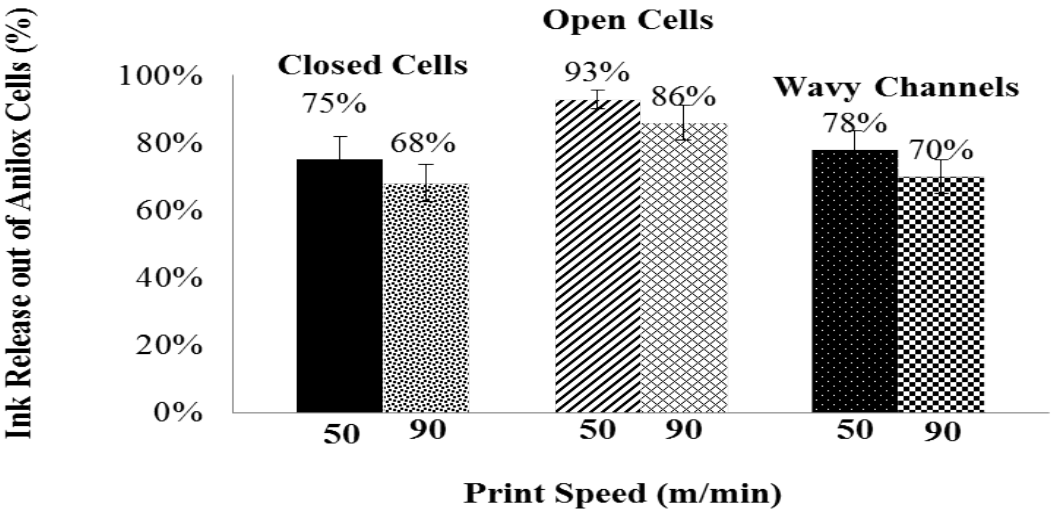

Figure B17: The ink release out of three anilox cell shapes using UV Carbon ink to investigate the effect of printing speed

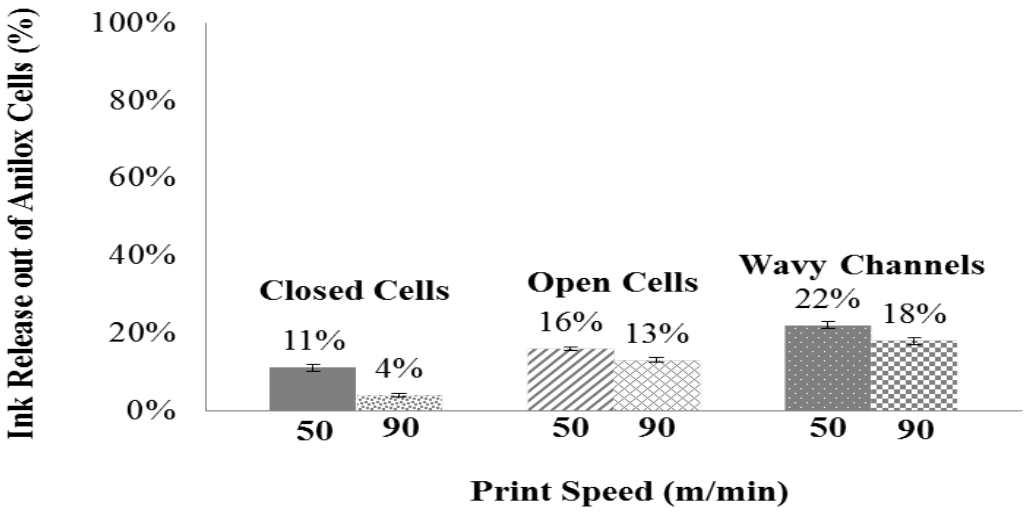

Figure B18: The ink release out of three anilox cell shapes using UV Silver ink to investigate the effect of printing speed